“Cutting-edge” technology for oncological oral surgery

S.G. Brouwer de Koning

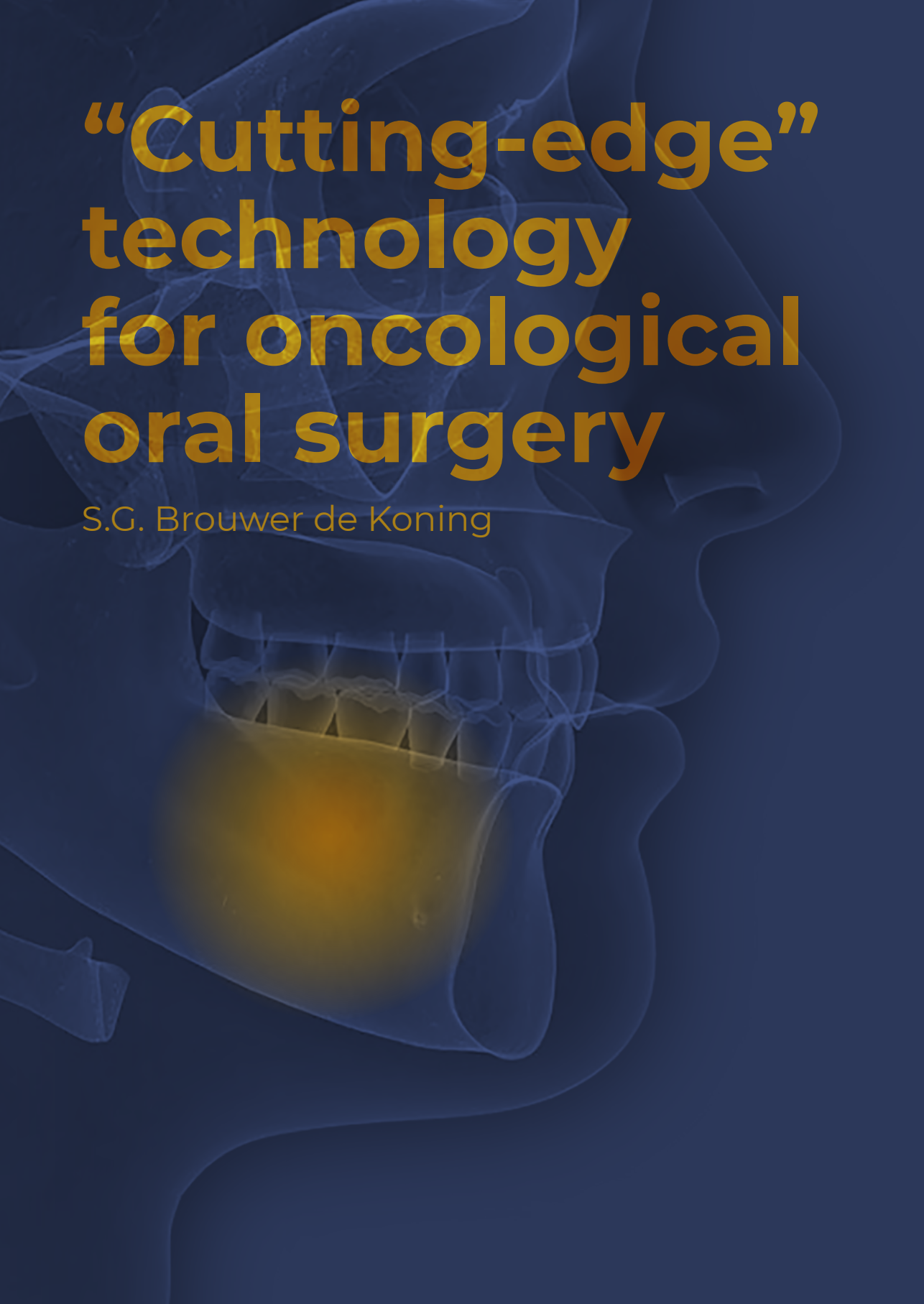

“Cutting-edge” technology for oncological oral surgery

S.G. Brouwer de Koning

Cutting-edge technology refers to technology that employs the most current and high-level developments. It stands for innovation and aims to optimize the current workflow and outcome. *Cutting edge* technology in oncologic surgery refers to technology that evaluates the *cutting edge* (Dutch: 'snijrand') of the surgically removed specimen. The status of the cutting edge is essential to determine the success of oncological surgery: if tumor cells are present at the *cutting edge*, additional therapy is indicated.

“Cutting-edge” technology for oncological oral surgery

Proefschrift

ter verkrijging van
de graad van doctor aan de Universiteit Twente,
op gezag van de rector magnificus,
prof.dr.ir. A. Veldkamp,
volgens besluit van het College voor Promoties
in het openbaar te verdedigen
op vrijdag 23 april 2021 om 14.45 uur

door

Susan Gijsbertje Brouwer de Koning

geboren op 17 februari 1991 te Gouda, Nederland

Dit proefschrift is goedgekeurd door:

Promotor prof. dr. T.J.M. Ruers
Copromotor dr. M.B. Karakullukçu

Colofon

Cover design Hester Koers en Susan Brouwer de Koning
Layout Hester Koers
Printed by Drukwerkdeal
ISBN 978-90-365-5130-4
DOI 10.3990/1.9789036551304

The research described in this thesis was performed at the Netherlands Cancer Institute – Antoni van Leeuwenhoek, Amsterdam, The Netherlands

Promotiecommissie

Voorzitter / secretaris	prof. dr. J.L. Herek
Promotor	prof. dr. T.J.M. Ruers, Universiteit Twente
Copromotor	dr. M.B. Karakullukçu, Antoni van Leeuwenhoek
Leden	prof. dr. S. Manohar, Universiteit Twente
	prof. dr. ir. R.M. Verdaasdonk, Universiteit Twente
	prof. dr. I.B. Tan, Universiteit Maastricht
	prof. dr. L.E. Smeele, Universiteit van Amsterdam
	prof. dr. ir. H.J.C.M. Sterenborg, Universiteit van Amsterdam

Table of contents

Chapter 1

General introduction

Oral cavity cancer

Cancer of the oral cavity or lip was diagnosed in 354,864 patients and accounted for the death of 177,384 patients, worldwide, in 2018 (1, 2). In the Netherlands, 902 patients were diagnosed with oral cavity cancer, and 307 patients died from this disease, in 2017 (3). Cancer of the oral cavity generally comprises cancer of the tongue, floor of mouth, alveolar process, retromolar trigone or cheek (4). Etiological factors most frequently associated with oral cavity cancer include alcohol consumption, tobacco smoking, human papillomavirus (HPV) infection, Epstein-Barr virus (EBV) infection, dental hygiene and irritation, betel nut or tobacco chewing, or an occupation with exposure to pollutes, chemicals, wood or metal dust (4, 5). Patients may present with mouth pain or nonhealing mouth ulcers, loosening of teeth, dysphagia, odynophagia, weight loss, bleeding, or referred otalgia.

When diagnosed, the severity of the disease is established according to the AJCC/UICC cancer staging system (6). The system describes the anatomical extent of the disease based on three components: T for the extent of the primary tumor, N for the involvement of regional lymph node metastasis and M for the presence of distant metastasis. The TNM stage of the cancer affects planning of treatment and gives an indication of prognosis and survival. Five-year survival rates are 84% for early-staged (localized), 66% for intermediate-staged (regional) and 39% for advanced-staged (distant) disease in the United States (7).

Surgical resection is the foundation of any approach with curative intent in the management of oral cavity cancer: 77.5% of the patients with oral cavity cancer in the Netherlands is treated surgically (surgery only or surgery combined with radiotherapy and/or chemotherapy) (8). For early-staged disease, surgery alone may be adequate initial treatment, while for most patients with intermediate-staged to advanced-staged disease, adjuvant radiation alone or combined with chemotherapy is indicated to reduce the risks of local and regional recurrence (9, 10). For the management of the primary tumor, surgical interventions range from simple wide local excision and primary closure in small tumors, to composite resections of the tongue/floor of mouth/mandible in advanced tumors with the need for locoregional flaps or microvascular free flap reconstruction (11).

Need for intra-operative guidance

The trade-off in oncological surgery is to remove enough tissue to ensure entire tumor removal, while as much healthy tissue as possible is conserved to provide good functional and aesthetic outcome. In order to achieve an optimal result, the exact localization of tumor borders during surgery is key. This remains a challenge: only in a few cases, visible and palpable aspects of the tumor are present. For the rest of the cases, the surgeon keeps the diagnostic imaging in mind to determine where to cut. There is no guidance on where to cut exactly in order to ensure that the tumor is removed completely, and that healthy tissue is conserved. Guidance can be considered in two ways: to determine whether the complete tumor has been removed *after* the resection (resection margin assessment) or to indicate where to cut *during* the resection (surgical guidance). The relevance of each of these is discussed separately below.

Part I: Resection margin assessment

The resection margin is the margin of healthy tissue that is resected around the tumor. The resection margin can be considered positive, close or negative: when tumor cells are close to, or present at the resection surface, the resection margin is found close or *positive*, respectively, suggesting that the tumor is not entirely resected; a *negative* or *clear* resection margin implies that the whole tumor is resected (Figure 1a). Two types of margins are defined: the mucosal margin (surface, epithelial) and the deep margin (submucosa, muscle and deep tissue at the side of or underneath the tumor) (Figure 1b). While the mucosal margin is often easy to estimate due to visible aspects of the tumor at the surface, the extent of tumor growth below the mucosa, and thus the deep margin, is difficult to identify.

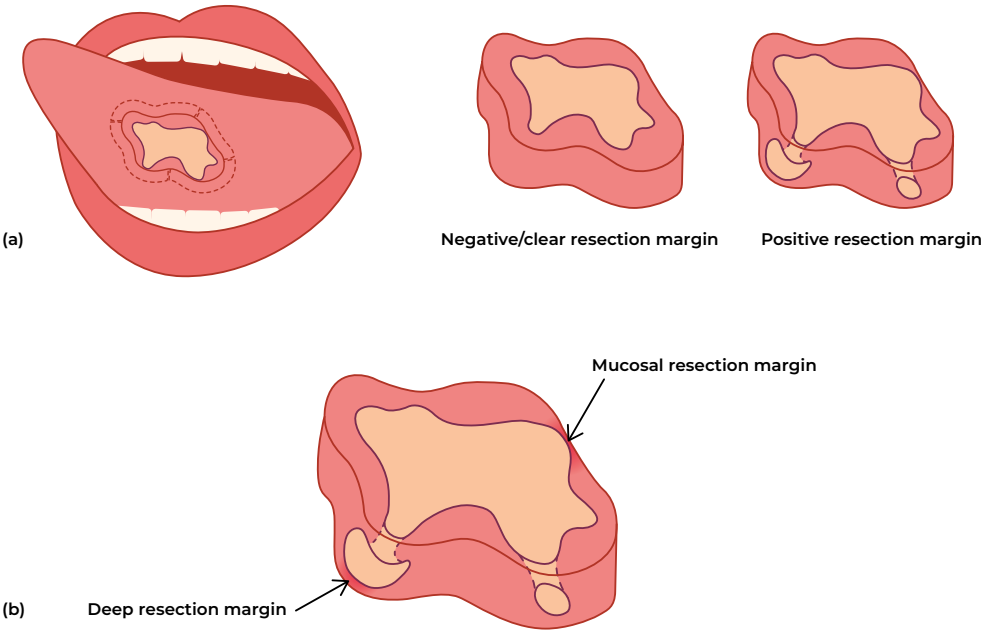

Figure 1 (a) a negative or clear resection margin implies that the whole tumor is resected, a positive resection margin suggests that the tumor is not entirely resected; (b) the mucosal margin (surface, epithelial) and the deep margin (submucosa, muscle and deep tissue at the side of or underneath the tumor)

Impact of resection margin status

Despite the surgical removal of the tumor, the disease is likely to recur locally or regionally, affecting the survival of these patients. There are multiple factors predicting recurrence and/or overall survival: tumor characteristics (tumor site, pattern of invasion, perineural invasion, lymphovascular invasion, lymphocytic response, extracapsular spread), TNM classification, patient age and margin status (especially involvement of posterior and deep margins) (12-20). Models have been constructed to accurately predict the chance for recurrence using a combination of the factors above, e.g., with

a resection margin of 2.5 mm, the presence of perineural invasion decreases the 3-year local recurrence free survival probability from 93% to 86% (21). Of all the factors affecting prognosis, the resection margin is the only factor that can be controlled by surgeons and pathologists. This is the reason that resection margin assessment is subject of research for many years now.

As a result of its significant prognostic value, a positive resection margin is the decisive factor when considering further therapy after surgery. Guidelines recommend re-resection, and if re-resection is not feasible, radiotherapy with or without chemotherapy (10, 22-25). In literature, there is no consensus on whether this approach guarantees disease control equal to that achieved in patients with clear resection margins, while the approach does increase the overall costs of treatment and the morbidity experienced by the patient (26).

Although the significant predictive value of the margin has been widely studied (14, 26-29), it has been argued that the positive margin should not be the only decisive factor for adjuvant therapy (28, 30). Some studies suggest deciding on adjuvant treatment based on more than the status of the resection margin alone, basically, the presence of adverse tumor characteristics (12, 31, 32).

Margin guidelines

In the Netherlands, a clear resection margin is defined as >5 mm healthy tissue between the tumor and the resection surface, according to the guidelines of the Royal College of Pathologists (Table 1). However, there is no consensus on what constitutes an adequate resection margin: a recent survey among members of the American Head and Neck Society (AHNS) showed that 56.5% of the respondents define a clear margin as >5 mm between resection plane and tumor cells on microscopic evaluation (33). Other definitions used were 3 mm, 2 mm, >1 mm, no ink on tumor on microscopic evaluation or 1-1.5 cm gross margin.

Guidelines on the definition differ and seem arbitrarily chosen at the time (Table 1). As a result, the optimal definition of a clear margin in association with local recurrence or overall survival has been evaluated extensively in literature (Table 2). However, it is not possible to use the current literature for robust scientific evidence on the association between margin extent and local recurrence, since the heterogeneity among the different studies is too large (e.g., in anatomical tumor site, discrimination between local recurrence and second primary tumor, margin reported as continuous variable or as positive/negative, specimen or tumor bed evaluation and the retrospective design of the studies) (34, 35).

A clear definition of an adequate resection margin is clinically important because of its large contribution to the decision on adjuvant therapy. Furthermore, the definition of the margin determines the required sampling depth that a feasible intra-operative margin assessment technology should be able to evaluate.

Table 1 Guidelines on the definition of a positive, close or a clear margin

Guideline	Positive margin	Close margin	Clear margin	Relevant evidence
The Royal College of Pathologists (36)	< 1 mm	1 to 5 mm	> 5 mm	Higher rate of local recurrence in patients with 'tumor at the margin' (37)
National Comprehensive Cancer Network Guidelines (10)	Carcinoma *in situ* or carcinoma at the margin	< 5 mm	≥ 5 mm	Higher rate of local recurrence in patients with a 'close margin of < 5mm' and '(*in situ*) carcinoma at the margin' (38)

Table 2 Studies reporting on significant association of margin definition and local recurrence or overall survival

	Primary tumor site; number of patients	Recommended definition of		Significant difference compared to clear margin group in
		Positive margin	Close margin	
Jain, 2020 (27)	Tongue and gingi-va-buccal complex; *n* = 612	< 2 mm		Disease free survival ($p = 0.0281$)
Buchakjian, 2018 (15)		<1 mm		Local recurrence
Zanoni, 2017 (30)	Tongue; *n* = 381		< 2.2 mm	Local recurrence (HR = 9.03 for positive margin vs HR = 2.81 for 0.01-2.0 mm margin)
Lee, 2017 (17)	Tongue; *n* = 151	Deep margin, early vs advanced tumor stage: 2.5 mm vs 8.0 mm		Overall recurrence ($p = 0.046$)
Tasche, 2017 (39)	Tongue, alveolus, FOM; n = 432		< 1mm	Local recurrence
Yamada, 2016 (40)	Oral cavity; *n* = 127		< 4 mm	Local recurrence ($p = 0.037$)
Dillon, 2015 (13)	Oral cavity; *n* = 54		1 to 5 mm	Disease free survival ($p = 0.014$)
Varvares, 2015 (26)	Oral cavity; *n* = 108		< 5mm	Local recurrence ($p = 0.004$), disease free ($p = 0.004$) and overall survival (p = 0.03)
Wong, 2012 (28)	Oral cavity; *n* = 192	≤ 1 mm	< 2 mm	Positive margin: local recurrence ($p = 0.03$) Close margin: Disease specific survival ($p = 0.03$) and overall survival ($p = 0.03$)
Nason, 2009 (41)	Oral cavity; *n* = 277		≤ 3 mm	Recurrence ($p = 0.01$) and 5-year survival (HR = 2.5 for positive margin vs HR = 1.5 for 0.01-3.0 mm margin)
Binahmed, 2007 (14)	Tongue, FOM, other; *n* = 425		< 2 mm	Local recurrence ($p = 0.005$)
Sutton, 2003 (42)	Oral cavity; *n* = 200		< 5 mm	Local recurrence ($p = 0.0002$), disease free survival ($p = 0.004$)

Positive margin rates

Positive resection margin rates range between 5-43% (20). In addition, close margin rates are reported over a range of 11-45%. Thus, about 85% of the patients have their tumor resected with an inadequate resection margin. This also applies to patients treated in the Netherlands (20, 31). These numbers cannot be used as a factor to compare institutes on quality of surgery. For example, an institute reporting on a higher positive margin rate does not necessarily mean that the surgeon in that institute performs worse. The definition of the positive margin might have been very strict, or the protocol for margin sampling is very accurate and extensive, resulting in a higher number of positive margins. This mainly has consequences for the decision on adjuvant therapy: the patient receives adjuvant therapy depending on the margin definition and histopathological protocol followed by the institute of treatment, while the same patient in a different institute would not.

The deep resection margin is significantly more often found close or positive when compared to the mucosal margin (43, 44). This can be explained by, among others, anatomical constraints that could limit the extent of the resection. In addition, on the mucosal surface, the tumor is visible, whereas during resection of the tumor in the soft tissue, the tumor is not visible, but only palpable. Furthermore, tumor characteristics as perineural and lymphovascular invasion are unrecognizable during resection and due to the infiltrative growth pattern more likely to be present at the cut edge of the deep margin (45, 46).

Thus, in the attempt to lower the positive margin rates significantly, the technology should provide intraoperative feedback on the deep resection margin predominantly: the technology should be able to distinguish tumor cells from healthy soft tissue, rather than from healthy mucosal tissue.

Factors associated with resection margin assessment

The golden standard to assess resection margins is post-operative microscopic evaluation by the histopathologist. There are different methods for dissection, sampling, and estimating the resection margin, affecting the number of positive margins that are reported (20).

The status of the margins can be estimated based on the resected specimen or additional samples that are taken from the resulting defect (tumor bed) (Figure 2a). With the specimen-driven approach, the resection margin can be measured as a continuous variable, and the margin can be categorized as a positive, close or negative margin. While in the patient-driven approach, the tumor bed samples can only confirm the presence or absence of tumor cells, and close margins will be underestimated as clear margins. Due to the categorization into positive, close or negative margins, the specimen-driven approach results in a more accurate prediction of local recurrence (15, 26, 29, 47-50). Although many surgeons still take tumor bed samples for intraoperative margin assessment, the AJCC has recommended specimen-driven intraoperative assessment as standard of care (6).

The specimen margin can be determined by perpendicular sectioning or by *en face* (shave) flat peripheral tissue sections that are parallel to the margin (Figure 2b) (34, 51, 52). The advantage of the latter method is that a greater surface of the entire margin can be evaluated. However (comparable with tumor bed samples), the margin can only be classified as positive or negative for the presence of tumor cells, and close margins cannot be measured. Perpendicular sectioning does provide a quantifiable distance between the tumor and the cut edge of the specimen, but the evaluation of the entire margin is limited to the location of the cross sections only, with the possibility of missing gross tumor extending to the margin between the sections. Most often, these techniques are utilized together.

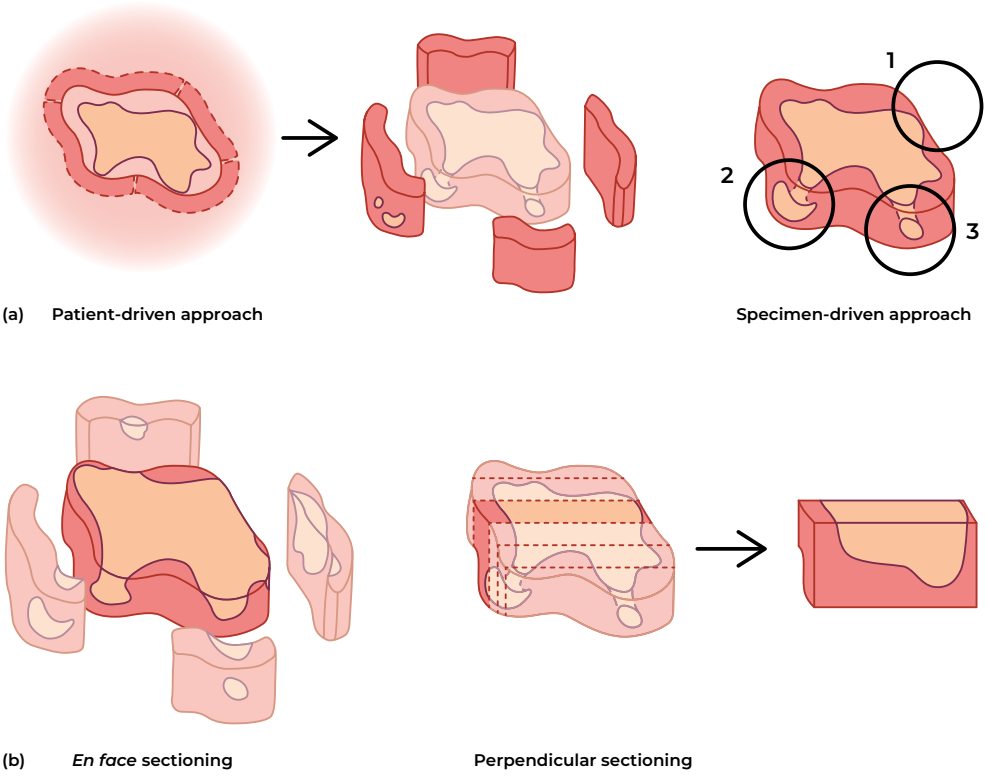

Figure 2 Approaches to estimate the status of the resection margin: (a) the status of the margin is determined from additional samples taken from the defect (patient-driven approach, left) or the status of the margin is determined from the specimen (specimen-driven approach, right); (b) using the specimen-driven approach the margins can be estimated en face (shave) by taking flat peripheral tissue parallel to the margin (left) or by perpendicular sectioning (right)

Besides the sampling technique, a close collaboration between surgeon and histopathologist is required. Specifically, clear communication is needed on the main specimen orientation (which is often multi-interpretable and resulting in localization issues during re-resection after a positive margin), and on the areas that are suspected for involvement of tumor cells (35).

Thus, for a technique to provide assessment of the margin during surgery, it is warranted to allow evaluation of the complete surface and to measure the distance between the cut edge of the specimen and the tumor border.

Other factors affecting the estimation of the resection margin are tissue shrinkage of the specimen and the process of field cancerization.

Tissue shrinks the moment it is resected. This may cause resection margins to move closer to the tumor. The total tissue shrinkage depends on the tumor site, the method of resection and fixation technique (53-55). The largest percentages of shrinkage are reported for buccal mucosa and tongue

specimens (48%-71.9% and 33%-42%, respectively) (53, 54). Only 5-10% of tissue shrinkage depends on the resection technique and formalin fixation (55). Accounting for this multi-factorial process of tissue shrinkage, an *in situ* resection margin of at least 8-10 mm is recommended to obtain pathological clear margins of 5 mm (56). The majority of shrinkage occurs post-resection or prefixation, due to muscle contraction (53, 57). This means that most of the shrinkage already has occurred at the time of intraoperative margin assessment. Thus, in the comparison between the margin measured by intraoperative margin assessment and final histopathological examination, tissue shrinkage is not expected to cause significant discrepancies.

The value of the resection margin is also affected by the process of field cancerization, which suggests that in patients with oral squamous cell carcinoma, multiple, unrelated, precancerous lesions may exist as a result of carcinogens that altered an area of epithelium, rather than one cell (58). As a result, a resection with microscopically adequate resection margins may not result in local disease control, due to microscopic islands of cancer distant from the resection that were left behind.

Surgery is the foundation of any approach with curative intent in the management of oral cavity cancer. Surgeons aim to remove the tumor with an adequate margin of healthy tissue. However, clear resection margins are only reported in 15% of the surgeries. Since the status of the resection margin is an important prognosticator of local recurrence and decreased survival, it is a decisive factor when considering adjuvant therapy. In order to improve treatment and outcome of patients with oral cavity cancer, there is an urgent need for a technology that is able to assess the resection margin for the presence of tumor cells during surgery. By providing real-time feedback on whether the tumor is removed completely, the surgeon is able to act directly to improve the outcome of the surgery. In a survey among American Head and Neck surgeons, 86.5% of the respondents indicated to utilize such intraoperative guidance if it were cost-effective and could accurately allow visualization of the tumor border (33).

Whether the technology is cost- and time-efficient depends on several factors. Firstly, the sampling depth needs to correspond with the desired margin clearance. The current guidelines on what considers an adequate margin are inconsistent and there is no statistical agreement between studies for an optimal margin width that decreases the rate of local recurrence. Furthermore, factors associated with margin assessment confound the meaning of a millimetre accurate margin extent, e.g., inconsistency in dissection and sampling methods, but also the effect of specimen shrinkage and field cancerization. Secondly, the technology should be able to evaluate the resected specimen, rather than tumor bed samples, as this approach has shown to predict local recurrences with higher accuracy. The whole resection surface should be evaluated in an acceptable amount of time. Lastly, the technology should perform ultimately in the evaluation of deep resection margins, since these margins are reported positive in the majority of the cases. In this thesis, technologies that are currently available or under development for intraoperative resection margin assessment are discussed, followed by several technologies that were evaluated for feasibility on this application.

Part II: Surgical guidance for mandibular osteotomies

While resection margin assessment occurs *after* the resection, surgical guidance indicates where to cut *during* the resection. This is amongst others relevant in patients with malignant disease abutting or invading the mandible. These patients often undergo segmental resection of the mandible. To restore continuity of the mandible, and associated function and aesthetics, reconstruction with a titanium plate in combination with an osseous free flap is performed in the majority of cases (e.g., osteomyocutaneous free fibular flap (FFF)) (59). The osteotomies (i.e., the resection through bone) of the involved part of the mandible must be determined accurately to ensure clear resection margins, but also to allow precise placement of bone segments, enabling the contour of the fibular graft to match the native resected mandible.

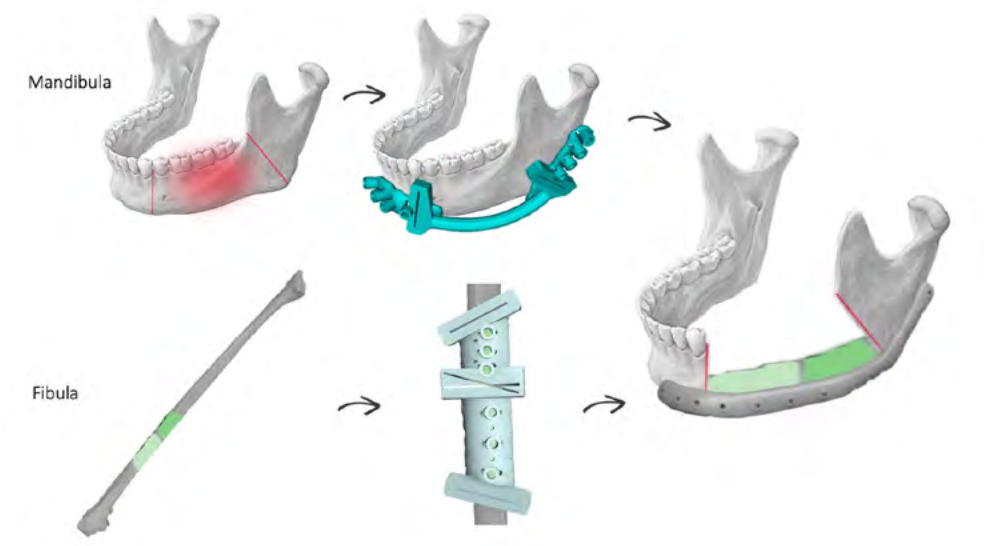

Figure 3 A patient-specific cutting guide is used on the mandibular bone to guide the osteotomy according to the virtual surgery planning. a second patient-specific cutting guide is used on the fibular bone to prepare two bone segments for reconstruction of the mandible. The bone segments are fixated with a titanium plate.

To ensure complete tumor resection with adequate resection margins, the location of the osteotomies is usually planned with a 10-mm margin between the tumor and the osteotomy. The histopathological guidelines of the Royal College of Pathologists specify for bone resection margins 'if bone invasion is present, the presence or absence of carcinoma at the bone margins should be recorded' (36). Tumor positive bone resection margins are reported in 21% of the patients and these patients have a significantly lower 5-year overall survival (60).

The location of the osteotomies is also relevant for accurate reconstruction of the mandible. With an accurate reconstruction, the aesthetics of the face can be re-established, the ability of mastication and occlusion can be restored, and speech can be maintained. To allow accurate reconstruction of the mandible, the reconstruction segments need to fit the mandibular defect as precisely as possible. When less or more mandibular bone is resected than planned, the graft segments used for reconstruction will not fit as precisely and the graft segments have to be adjusted manually during surgery. This increases the operation time and affects the accuracy of the reconstruction.

The exact location of the osteotomy, as well as the reconstruction after resection, is prepared through virtual surgical planning (VSP) (61). Three-dimensional (3D) rendered models of the mandible and graft are constructed from a preoperative computed tomography (CT) scan. The 3D models are used to perform a virtual (segmental) mandibulectomy and to virtually segment the fibular graft to match the defect. To translate the position of the osteotomy from the virtual surgical plan to the clinical situation in the operating room, patient-specific cutting guides and fixation plates are designed and manufactured using computer-aided design/computer-aided manufacturing (CAD/CAM) techniques (Figure 3). This procedure is costly and time-consuming. In the meantime, there is a change in the tumor size, for which the cutting guide cannot account for during surgery. Therefore, there is a need for a technology that saves preparation time, money and provides flexibility during surgery.

Surgical navigation

Surgical navigation provides real-time visual feedback on the position of surgical instruments in relation to the patient's anatomy. In advance of the surgery, a 3D model is constructed for each patient specifically, using pre-operative imaging (e.g., CT scan). This model represents the anatomy of the patient, i.e., the tumor, together with adjacent critical anatomical structures. During surgery, this 3D virtual model is registered with the patient. a tracking system, e.g., optical tracking or electromagnetic tracking, localizes sensors that are attached to the patient, and implemented in surgical instruments. This way, the position of surgical instruments can be tracked in relation to the patient, and this is visualized simultaneously on the virtual 3D model (Figure 4). Surgical navigation is used routinely in neurosurgery and craniomaxillofacial surgery, in which the registration of the 3D virtual model with the patient is done on the skull. This is not feasible for mandibular surgery due to the fact that the mandible is mobile in relation to the skull: during surgery, the position of the mandible in relation to the skull differs from its position during preoperative imaging (that was used to create the virtual model) (62). Thus, new methods are needed to perform the registration on the mandible itself.

Since surgical navigation could facilitate precise localization of tumor borders, this technology holds potential to provide guidance for mandibular osteotomies. To prepare surgery, still the surgical plan will be constructed using VSP. However, instead of using cutting guides to determine where to place the osteotomy during surgery, the surgical navigation would indicate where to cut. The virtual model for surgical navigation can be prepared one day prior to surgery and only depends on the date of the preoperative CT scan. Thus, if radiology planning allows, VSP can be performed near the day of surgery. This procedure eliminates the factor of tumor growth in the time between virtual surgery planning, printing of the patient specific cutting guides, and the surgery. As a result, the virtual model provides a more accurate representation of the real-time situation. This can affect the number of positive bone resection margins and the number of cases in which reconstruction segments have to be adjusted manually to fit the mandibular defect.

In patients undergoing surgery for malignant disease invading the mandible, osteotomies must be determined accurately to ensure clear resection margins, but also to allow precise placement of bone segments for accurate reconstruction of the mandible. The precise location of the osteotomy is carefully planned on a virtual 3D model, in advance of the surgery. At the moment, patient-specific cutting guides are used to translate the virtually planned osteotomy to the surgery. In this thesis, the accuracy of the current procedure is evaluated and surgical navigation is studied as an alternative to the use of patient-specific cutting guides.

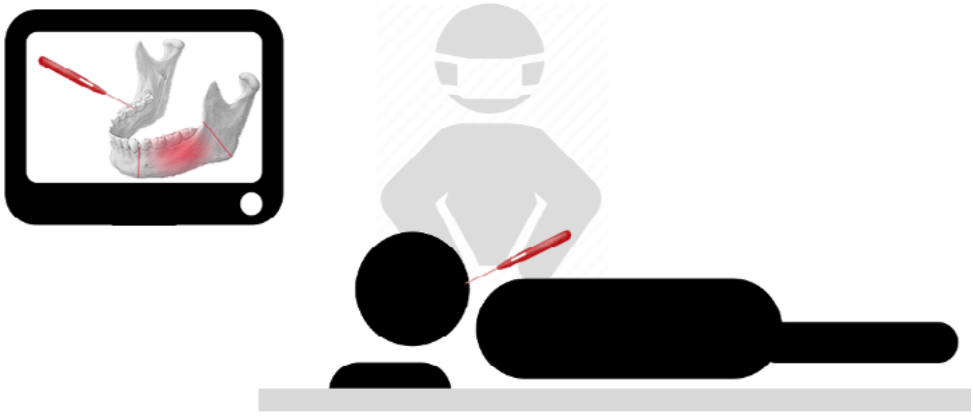

Figure 4 Surgical navigation provides real-time visual feedback on the position of the surgical instruments in relation to the patient's anatomy.

Outline of this thesis

In this thesis, different technologies are evaluated on their feasibility to provide guidance during oncological oral surgery in order to ensure radical tumor resection and to facilitate accurate reconstruction. Technologies to assess resection margins in oral squamous cell carcinoma will be discussed first, followed by technologies that provide surgical guidance on the exact localization of mandibular osteotomies.

Part I: Resection margin assessment

To determine whether the tumor is completely excised during surgery, there is a need for technologies that provide intra-operative feedback on the status of the resection margin. **Chapter 2** presents an overview of the technologies that are currently used and investigated for intra-operative resection margin assessment in head and neck surgery.

In order to be feasible for intra-operative resection margin assessment, the technology should be able to distinguish tumor from healthy tissue. This discrimination is known from diagnostic imaging: tumor dimensions are reported from ultrasound (US) and magnetic resonance imaging (MRI). In **Chapter 3**, a retrospective study was conducted to estimate how accurate these tumor dimensions could be measured on preoperative imaging techniques. The contrast found between tumor and healthy tissue on US images was reason to conduct a study to evaluate whether US could be used for intra-operative resection margin assessment (**Chapter 4**).

US is an imaging technique that could be used for macroscopic evaluation of the margin. To evaluate the resection margin on a microscopic scale, the feasibility of optical technologies was studied. First, the performance of a hand-held diffuse reflectance spectroscopy probe was evaluated, with the aim to develop a surgical instrument that could acquire point-measurements at a suspicious location at the margin (**Chapter 5**). Further, hyperspectral imaging was evaluated as a diffuse reflectance imaging technique that may have the advantage over a point-based technique by giving an overview of the resection margin in one view (**Chapter 6**).

Part II: Surgical guidance for mandibular osteotomies

The osteotomies of the involved part of the mandible must be determined accurately to ensure adequate resection margins, but also to allow precise placement of bone segments for reconstructive surgery. To translate the position of the osteotomies from the virtual surgical plan to the clinical situation in the operating room, patient-specific cutting guides and fixation plates are designed and manufactured using computer-aided design/computer-aided manufacturing (CAD/CAM) techniques. In **Chapter 7** the accuracy of this currently used methodology is evaluated.

As an alternative for the patient-specific cutting guides to translate the virtual surgery plan to the operating room, surgical navigation can be used. **Chapter 8** describes a study investigating the accuracy of electromagnetic (EM) navigation in eleven patients undergoing mandibular surgery. In order to improve the accuracy of EM navigation further, the registration procedure could be optimized: the method on how the virtual three-dimensional rendered model is registered to the actual patient's mandible at the operating room table. **Chapter 9** describes a study in which a dental splint was designed to improve the accuracy of registration. Finally, to achieve both guidance in localization of the osteotomy as well

as guidance during sawing, a navigated cutting guide was developed. In **Chapter 10**, this concept was introduced as an alternative to a navigated surgical pointer or a navigated surgical saw and the efficacy was evaluated in multiple navigated osteotomies on mandible models.

In **Chapter 11** the topics and results described in this thesis are discussed and future perspectives are given.

References

1. Bray, F., et al., Global cancer statistics 2018: GLOBOCAN estimates of incidence and mortality worldwide for 36 cancers in 185 countries. CA Cancer J Clin, 2018. 68(6): p. 394-424.
2. Ferlay, J., et al., Estimating the global cancer incidence and mortality in 2018: GLOBOCAN sources and methods. Int J Cancer, 2019. 144(8): p. 1941-1953.
3. Nederlandse Kankerregistratie (NKR), IKNL. Verkregen via iknl.nl/nkr-cijfers, op (1 oktober 2020).
4. hoofdhalskanker.info Verkregen op 14 oktober 2020.
5. Sankaranarayanan R, et al., Head and neck cancer: a global perspective on epidemiology and prognosis. Anticancer Res, 1998 Nov-Dec;. 18(6B):4779-86.
6. Brierley, J.D., et al., Union for International Cancer Control (UICC) TNM Classification of Malignant Tumours 8th edition. 2017: John Wiley & Sons, Ltd., The Atrium, Southern Gate, Chichester, West Sussex.
7. Siegel, R.L., K.D. Miller, and A. Jemal, Cancer statistics, 2020. CA Cancer J Clin, 2020. 70(1): p. 7-30.
8. van Dijk, B.A., et al., Trends in oral cavity cancer incidence, mortality, survival and treatment in the Netherlands. Int J Cancer, 2016. 139(3): p. 574-83.
9. Ettinger, K.S., L. Ganry, and R.P. Fernandes, Oral Cavity Cancer. Oral Maxillofac Surg Clin North Am, 2019. 31(1): p. 13-29.
10. National Comprehensive Cancer Network. Head and neck cancers (Version 1.2018). NCCN clinical practice guidelines in oncology. Available at: https://www.nccn.org/professionals/physician_gls/pdf/head-and-neck.pdf. Accessed April 1, 2018.
11. Gonzalez, M. and A. Riera, Tongue Cancer. (Updated 2020 Sep 15). In: StatPearls (Internet). Treasure Island (FL): StatPearls Publishing; 2020 Jan-. Available from: https://www.ncbi.nlm.nih.gov/books/NBK562324/?report=classic.
12. Brandwein-Gensler, M., et al., Oral squamous cell carcinoma: histologic risk assessment, but not margin status, is strongly predictive of local disease-free and overall survival. Am J Surg Pathol, 2005. 29(2): p. 167-78.
13. Dillon, J.K., et al., How does the close surgical margin impact recurrence and survival when treating oral squamous cell carcinoma? J Oral Maxillofac Surg, 2015. 73(6): p. 1182-8.
14. Binahmed, A., R.W. Nason, and A.A. Abdoh, The clinical significance of the positive surgical margin in oral cancer. Oral Oncol, 2007. 43(8): p. 780-4.
15. Buchakjian, M.R., et al., Independent Predictors of Prognosis Based on Oral Cavity Squamous Cell Carcinoma Surgical Margins. Otolaryngol Head Neck Surg, 2018. 159(4): p. 675-682.
16. Szewczyk, M., et al., Positive fresh frozen section margins as an adverse independent prognostic factor for local recurrence in oral cancer patients. Laryngoscope, 2018. 128(5): p. 1093-1098.
17. Lee, D.Y., et al., Survival and recurrence of resectable tongue cancer: Resection margin cutoff value by T classification. Head Neck, 2018. 40(2): p. 283-291.
18. Barry, C.P., et al., Influence of surgical margins on local recurrence in T1/T2 oral squamous cell carcinoma. Head Neck, 2015. 37(8): p. 1176-80.
19. Kurita, H., et al., Impact of different surgical margin conditions on local recurrence of oral squamous cell carcinoma. Oral Oncol, 2010. 46(11): p. 814-7.
20. Smits, R.W., et al., Resection margins in oral cancer surgery: Room for improvement. Head Neck, 2016. 38 Suppl 1: p. E2197-203.
21. Sridharan, S., et al., Early squamous cell carcinoma of the oral tongue with histologically benign lymph nodes: a model predicting local control and vetting of the eighth edition of the American Joint Committee on Cancer pathologic T stage. Cancer, 2019. 125(18): p. 3198-3207.
22. Bernier, J., et al., Defining risk levels in locally advanced head and neck cancers: a comparative analysis of concurrent postoperative radiation plus chemotherapy trials of the EORTC (#22931) and RTOG (# 9501). Head Neck, 2005. 27(10): p. 843-50.
23. Bernier, J., et al., Postoperative Irradiation with or without Concomitant Chemotherapy for Locally Advanced Head and Neck Cancer. The New England Journal of Medicine, 2004. 350;19.
24. Cooper, J.S., et al., Postoperative Concurrent Radiotherapy and Chemotherapy for High-Risk Squamous-Cell Carcinoma of the Head and Neck. The New England Journal of Medicine, 2004. 350.

25. Cooper, J.S., et al., Long-term follow-up of the RTOG 9501/intergroup phase III trial: postoperative concurrent radiation therapy and chemotherapy in high-risk squamous cell carcinoma of the head and neck. Int J Radiat Oncol Biol Phys, 2012. 84(5): p. 1198-205.
26. Varvares, M.A., et al., Surgical margins and primary site resection in achieving local control in oral cancer resections. Laryngoscope, 2015. 125(10): p. 2298-307.
27. Jain, P.V., et al., Redefining adequate margins in oral squamous cell carcinoma: outcomes from close and positive margins. Eur Arch Otorhinolaryngol, 2020. 277(4): p. 1155-1165.
28. Wong, L.S., et al., Influence of close resection margins on local recurrence and disease-specific survival in oral and oropharyngeal carcinoma. Br J Oral Maxillofac Surg, 2012. 50(2): p. 102-8.
29. Buchakjian, M.R., et al., Association of Main Specimen and Tumor Bed Margin Status With Local Recurrence and Survival in Oral Cancer Surgery. JAMA Otolaryngol Head Neck Surg, 2016. 142(12): p. 1191-1198.
30. Zanoni, D.K., et al., a Proposal to Redefine Close Surgical Margins in Squamous Cell Carcinoma of the Oral Tongue. JAMA Otolaryngol Head Neck Surg, 2017. 143(6): p. 555-560.
31. Dik, E.A., et al., Resection of early oral squamous cell carcinoma with positive or close margins: relevance of adjuvant treatment in relation to local recurrence: margins of 3 mm as safe as 5 mm. Oral Oncol, 2014. 50(6): p. 611-5.
32. Ch'ng, S., et al., Close margin alone does not warrant postoperative adjuvant radiotherapy in oral squamous cell carcinoma. Cancer, 2013. 119(13): p. 2427-37.
33. Bulbul, M.G., et al., Margin Practices in Oral Cavity Cancer Resections: Survey of American Head and Neck Society Members. Laryngoscope, 2020.
34. Baddour, H.M., Jr., K.R. Magliocca, and A.Y. Chen, The importance of margins in head and neck cancer. J Surg Oncol, 2016. 113(3): p. 248-55.
35. Kubik, M.W., et al., Intraoperative Margin Assessment in Head and Neck Cancer: a Case of Misuse and Abuse? Head Neck Pathol, 2020. 14(2): p. 291-302.
36. Helliwell, T. and J.A. Woolgar, Standards and datasets for reporting cancers. Dataset for histopathology reporting of mucosal malignancies of the oral cavity London, UK: The Royal College of Pathologists 2013.
37. Slootweg, P.J., et al., Treatment failure and margin status in head and neck cancer. a critical view on the potential value of molecular pathology. Oral oncology 2002. 38: p. 500-503.
38. Looser, K.G., J.P. Shah, and E.W. Strong, The significance of 'positive' margins in surgically resected epidermoid carcinomas. Head & Neck Surgery, 1978. 1: p. 107-111.
39. Tasche, K.K., et al., Definition of "Close Margin" in Oral Cancer Surgery and Association of Margin Distance With Local Recurrence Rate. JAMA Otolaryngol Head Neck Surg, 2017. 143(12): p. 1166-1172.
40. Yamada, S., et al., Estimation of the width of free margin with a significant impact on local recurrence in surgical resection of oral squamous cell carcinoma. Int J Oral Maxillofac Surg, 2016. 45(2): p. 147-52.
41. Nason, R.W., et al., What is the adequate margin of surgical resection in oral cancer? Oral Surg Oral Med Oral Pathol Oral Radiol Endod, 2009. 107(5): p. 625-9.
42. Sutton, D.N., et al., The prognostic implications of the surgical margin in oral squamous cell carcinoma. Int J Oral Maxillofac Surg, 2003. 32(1): p. 30-4.
43. Woolgar, J.A. and A. Triantafyllou, a histopathological appraisal of surgical margins in oral and oropharyngeal cancer resection specimens. Oral Oncol, 2005. 41(10): p. 1034-43.
44. Lawaetz, M. and P. Homoe, Risk factors for and consequences of inadequate surgical margins in oral squamous cell carcinoma. Oral Surg Oral Med Oral Pathol Oral Radiol, 2014. 118(6): p. 642-6.
45. Hinni, M.L., et al., Surgical margins in head and neck cancer: a contemporary review. Head Neck, 2013. 35(9): p. 1362-70.
46. Li, M.M., et al., Margin Analysis in Head and Neck Cancer: State of the Art and Future Directions. Ann Surg Oncol, 2019. 26(12): p. 4070-4080.
47. Chang, A.M., et al., Early squamous cell carcinoma of the oral tongue: comparing margins obtained from the glossectomy specimen to margins from the tumor bed. Oral Oncol, 2013. 49(11): p. 1077-82.
48. Yahalom, R., et al., a prospective study of surgical margin status in oral squamous cell carcinoma: a preliminary report. J Surg Oncol, 2008. 98(8): p. 572-8.
49. Maxwell, J.H., et al., Early Oral Tongue Squamous Cell Carcinoma: Sampling of Margins From Tumor Bed and Worse Local Control. JAMA Otolaryngol Head Neck Surg, 2015. 141(12): p. 1104-10.
50. Thomas Robbins, K., et al., Surgical margins in head and neck cancer: Intra- and postoperative considerations. Auris Nasus Larynx, 2019. 46(1): p. 10-17.

51. Williams, M.D., Determining Adequate Margins in Head and Neck Cancers: Practice and Continued Challenges. Curr Oncol Rep, 2016. 18(9): p. 54.
52. Chiosea, S.I., Intraoperative Margin Assessment in Early Oral Squamous Cell Carcinoma. Surg Pathol Clin, 2017. 10(1): p. 1-14.
53. Cheng, A., D. Cox, and B.L. Schmidt, Oral squamous cell carcinoma margin discrepancy after resection and pathologic processing. J Oral Maxillofac Surg, 2008. 66(3): p. 523-9.
54. El-Fol, H.A., et al., Significance of post-resection tissue shrinkage on surgical margins of oral squamous cell carcinoma. J Craniomaxillofac Surg, 2015. 43(4): p. 475-82.
55. George, K.S., et al., Does the method of resection affect the margins of tumours in the oral cavity? Prospective controlled study in pigs. Br J Oral Maxillofac Surg, 2013. 51(7): p. 600-3.
56. Johnson, R.E., et al., Quantification of surgical margin shrinkage in the oral cavity. Head & Neck, 1997.
57. Umstattd, L.A., et al., Shrinkage in oral squamous cell carcinoma: An analysis of tumor and margin measurements in vivo, post-resection, and post-formalin fixation. Am J Otolaryngol, 2017. 38(6): p. 660-662.
58. Slaughter, D.P., H.W. Southwick, and W. Smejkal, 'Field cancerization' in oral stratified squamous epithelium - Clinical Implications of Multicentric Origin. Cancer, 1953.
59. Brown, J.S., et al., Mandibular reconstruction with vascularised bone flaps: a systematic review over 25 years. Br J Oral Maxillofac Surg, 2017. 55(2): p. 113-126.
60. Smits, R.W.H., et al., Evaluation of bone resection margins of segmental mandibulectomy for oral squamous cell carcinoma. Int J Oral Maxillofac Surg, 2018. 47(8): p. 959-964.
61. Rodby, K.A., et al., Advances in oncologic head and neck reconstruction: systematic review and future considerations of virtual surgical planning and computer aided design/computer aided modeling. J Plast Reconstr Aesthet Surg, 2014. 67(9): p. 1171-85.
62. Sukegawa, S., T. Kanno, and Y. Furuki, Application of computer-assisted navigation systems in oral and maxillofacial surgery. Jpn Dent Sci Rev, 2018. 54(3): p. 139-149.

Part I

Resection margin assessment

Chapter 2

Assessment of the deep resection margin during oral cancer surgery: a systematic review

S.G. Brouwer de Koning[1]

A.W.M.A. Schaeffers[1]

W. Schats

M.W.M. van den Brekel

T.J.M. Ruers

M.B. Karakullukcu

1 Equal contribution

Submitted for publication in European Journal of Surgical Oncology (March 2021)

Abstract

The main challenge for radical resection in oral cancer surgery is to obtain adequate resection margins. Especially the deep margin, which can only be estimated based on palpation during surgery, is often reported inadequate. To increase the percentage of radical resections, there is an urgent need for a quick, easy, minimal invasive method, which assesses the deep resection margin without interrupting or prolonging surgery. This systematic review provides an overview of technologies that are currently being studied with the aim of fulfilling this demand.

A literature search was conducted through the databases Medline, Embase and the Cochrane Library. a total of 62 studies were included. The results were categorized according to the type of technique: 'Frozen Section Analysis', 'Fluorescence', 'Optical Imaging', 'Conventional imaging techniques', and 'Cytological assessment'. This systematic review gives for each technique an overview of the reported performance (accuracy, sensitivity, specificity, positive predictive value, negative predictive value, or a different outcome measure), acquisition time, and sampling depth.

At the moment, the most prevailing technique remains frozen section analysis. In the search for other assessment methods to evaluate the deep resection margin, some technologies are very promising for future use when effectiveness has been shown in larger trials, e.g., fluorescence (real-time, sampling depth up to 6 mm) or optical techniques such as hyperspectral imaging (real-time, sampling depth few mm) for microscopic margin assessment and ultrasound (less than 10 min, sampling depth several cm) for assessment on a macroscopic scale.

Keywords

intra-operative margin assessment, deep resection margin, oral squamous cell carcinoma.

Introduction

Patients with early-stage and resectable advanced-stage oral cancer are often treated with surgery (1). Primarily, the goal is to obtain adequate resection margins, since inadequate margins are associated with a higher risk of recurrence and worse prognosis (2).

There is no consensus on what constitutes an adequate resection margin: a recent survey among members of the American Head and Neck Society (AHNS) showed that 56.5% of the respondents define a clear margin as >5 mm (3). Other definitions used were 3 mm, 2 mm, >1mm, no ink on tumor on microscopic evaluation or 1-1.5 cm gross margin. The optimal definition of a clear margin in association with local recurrence or overall survival has been evaluated extensively (2, 4-14). However, it is not possible to use the current literature for robust scientific evidence since the large heterogeneity among the different studies (15, 16). The most commonly used guidelines are defined by The Royal College of Pathologists and the National Comprehensive Cancer Network (NCCN). Both guidelines agree on the definition of an adequate margin, i.e., more than 5 mm of healthy tissue between tumor cells and the resection border. However, a positive margin is defined as tumor cells at the resection margin by the Royal College of Pathologist, while a positive margin can involve tumor cells within the first millimeter according to the NCCN (12, 17, 18). The definitive status of the resection margin is determined by the histopathologist, several days after surgery. In case positive margins are reported, adjuvant treatment is required, e.g., subsequent surgery, radiotherapy or chemoradiotherapy (1, 12, 19-24).

During surgery, estimating the extent of tumor growth into tissue is thought to be the main challenge for a radical resection. The superficial pattern of tumor growth in oral squamous cell carcinoma (OSCC) allows a good estimation of the mucosal margin. However, the deep margin can only be estimated based on palpation and information on tumor thickness obtained by preoperative imaging. Due to this limited intra-operative feedback on tumor margins, resections are inadequate in 30% to 85% of the procedures (25). To reduce the number of inadequate resections, there is an urgent need for technologies that can provide information on the status of the margin during surgery. With intra-operative margin assessment, the resected specimen (specimen-driven) or the tumor bed (patient-driven) is examined and the surgeon is informed on whether the margins are sufficient during the initial surgery. In case inadequate margins are found, the surgeon extends the resection directly when feasible, thereby often preventing the necessity of adjuvant postoperative treatment and possibly improving prognosis (12, 23). Hence, intra-operative margin assessment is useful in pursuing adequate resection margins and decision-making during and after surgery.

Recently a systematic review towards intraoperative margin assessment was published, emphasizing the need for more studies to improve accuracy of techniques to reduce positive margins (26). However, no distinction between mucosal and deep margins was made. Technologies for intra-operative margin assessment have to distinguish healthy tissue from tumor tissue. Healthy mucosal tissue differs from healthy tissue that is found at the deep margin, and therefore requires a different approach. The focus of intra-operative margin assessment should be on the deep margin for two reasons: Woolgar *et al.* showed that the deep margin was involved in 87% of the tissues with inadequate margins, and Weijers *et al.* found that there was no significant difference in recurrence rate between close and clear mucosal margins, suggesting that the deep margin is more important than the mucosal margin (22, 27).

The aim of this systematic review is to provide an overview of all intra-operative techniques that are available or under development to assess the deep tumor resection margin in patients with OSCC.

Methods

A literature search was conducted through the databases Medline, Embase and the Cochrane Library, on the 28th of August 2020 using a combination of indexed search terms and free text terms: 'margins of excision' OR 'depth of invasion' OR 'invasion depth' OR 'deep resection margin' OR 'deep resection' AND 'Head and neck neoplasms' OR 'Mouth neoplasms' AND 'Intraoperative period'.

The study selection was conducted by two researchers who independently screened titles and abstracts for a relevant contribution to this review. Studies were included that examined OSCC, assessed the surgical margin during surgery for immediate feedback on the status of the margin, evaluated the deep resection margin rather than the mucosal margin, were human studies, and were scholarly journal articles with full texts available. Based on the title and abstract, studies were excluded that evaluated phantoms and animals, cancers other than head and neck, technologies that were not intended for intra-operative use and when the outcome measure was not meeting the purpose of this review. Full texts were evaluated on the following exclusion criteria: when the focus of the article was to evaluate the status of the resection margin as a prognostic predictor, the outcome of the intraoperative assessment of the surgical margin was not compared with a verification method, transoral robotic surgery (TORS) was used, the study population consisted of less than three patients, only mucosal/superficial margins were evaluated, the technology was used for pre-operative diagnosis instead of intraoperative assessment, or the study was focused on the presence of specific genes to predict tumor recurrence. Furthermore, the authors believed that studies before the year 1999 could be excluded, because relatively old techniques have been improved and repeatedly studied since. In addition, references of included articles were screened on eligibility for inclusion. Figure 1 shows the process for study selection.

Studies were categorized into different groups according to the type of technology that was used for intra-operative margin evaluation: 'Frozen Section Analysis', 'Fluorescence', 'Optical Imaging', 'Conventional imaging techniques', and 'Cytological assessment'. Data extracted from the included studies were as follows: (1) study methodology, (2) margin assessment technology, (3) whether margins were assessed on the remaining defect after tumor removal, or at the resection surface of the specimen, or if the tumor was evaluated *in situ*, (4) verification method, (5) definition of positive margin, (6) sample size, (7) tumor site, (8) accuracy of the technology, or sensitivity, specificity, positive predictive value (PPV) and negative predictive value (NPV), or a different outcome measure, (9) acquisition time, and (10) sampling depth.

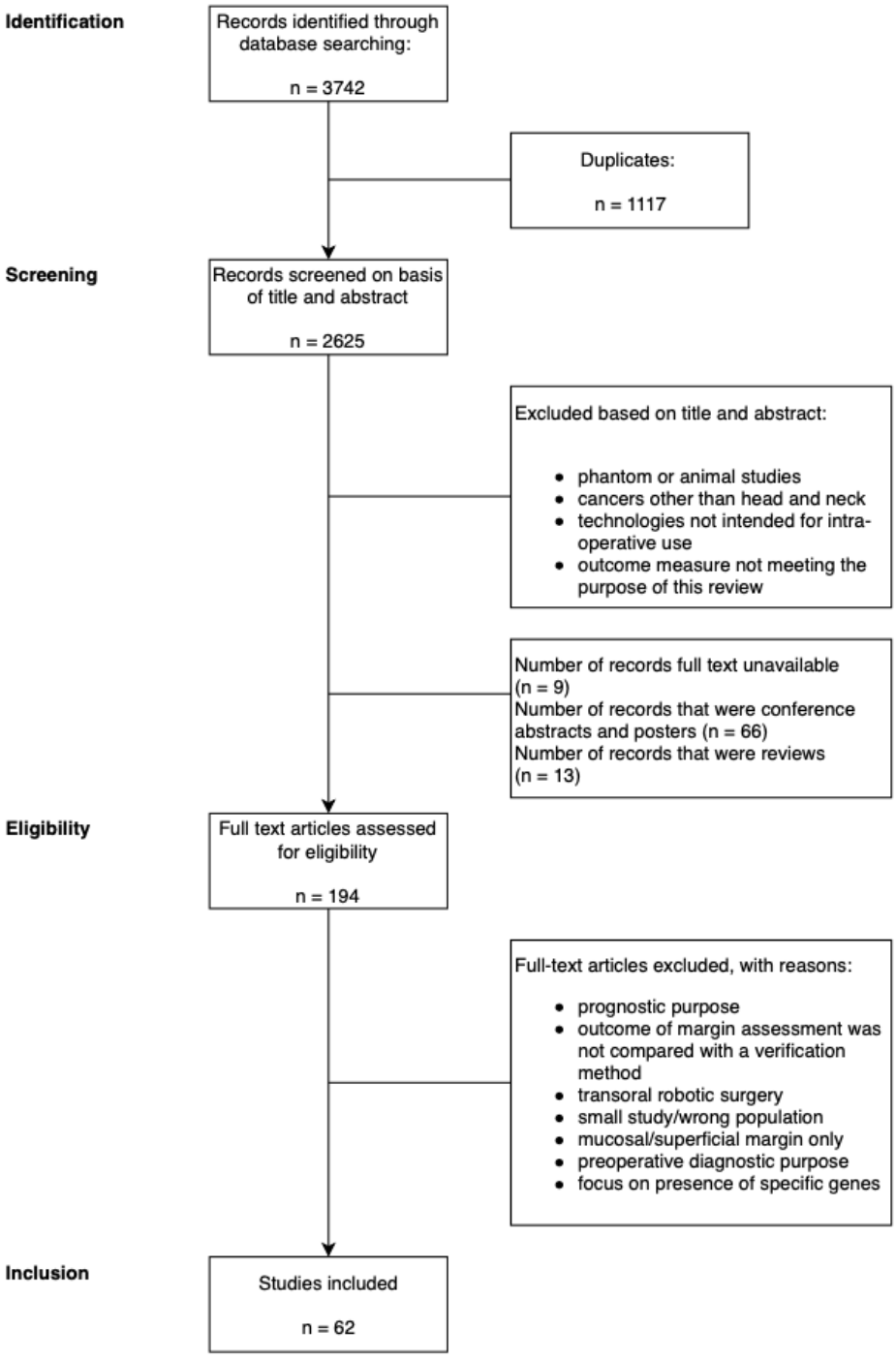

Figure 1 Flow diagram of selection strategy

Results

Frozen section analysis

With frozen section analysis (FSA), the surgeon and the pathologist collaborate to provide a rapid intraoperative evaluation of the surgical margin. The freshly resected tissue is transported to the pathology department, frozen in a cryostat machine, thinly sliced with a razor, affixed to a glass slide and dipped into fixatives and tissue stains for immediate interpretation (28). The diagnostic performance of this methodology has been widely studied in both retrospective and prospective studies (Table 1). Frozen sections were obtained from both the remaining defect after tumor excision, as well as from the resected specimen itself, and the diagnosis that was the result of the FSA was verified with the final histopathological outcome. Number of patients that were included by the studies ranged from 20-435. FSA is mainly applicable for soft tissue specimen; the high density of bone makes routine FSA of cortical bony margins difficult. Few groups have presented methods for bone margin FSA resulting in sensitivities and specificities of 77-88.9% and 90-100%, respectively (29, 30). Despite the high accuracies achieved with FSA, the technique is subject to false negatives due to the complexity of some surgical specimens. With one frozen section, only a small fraction of the specimen can be evaluated, and the time needed to evaluate one frozen section is 15-30 minutes.

Fluorescence

More than 90% of the head and neck tumors express the epidermal growth factor receptor (EGFR), offering a cancer-specific target for contrast agents, like panitumumab or cetuximab. These antibodies can be conjugated with a near-infrared fluorescent dye (e.g. IRDye800CW, indocyanine green) for intra-operative tumor detection (31). The advantage of panitumumab over cetuximab is the higher binding affinity and improved safety profile (32). Acquisition times vary between real time and several minutes (Table 2). In addition, near-infrared fluorescence can penetrate through approximately 5-6 mm tissue, making this a promising technique for detection of positive and close margins (33, 34). However, disadvantages of the use of these conjugated antibodies are the intravenous administration that may lead to adverse reactions, the long plasma half-lives (unbound tracers result in non-specific background fluorescence; administration requires additional planning since it needs to be done several days in advance of the surgery), and the relatively high doses required to have sufficient tracers reach the tumor. Therefore, additional research has been performed to activatable fluorescent tracers that can be applied topically, like γ-glutamyl hydroxymethyl rhodamine green (g-Glu-HMRG) and 5-aminolevulinic acid-induced protoporphyrin IX (5-ALA-induced PPIX) (35-37). These tracers required an incubation period of 10 minutes and 1-2.5 hours respectively, before malignant tissue fluoresced. Also, sampling depth is limited to less than one millimeter.

Focusing on bone resection margins, Nieberler *et al.* evaluated the use of integrin αvβ6-targeting arginylglycylaspartic acid peptides as a marker for fluorescent cytology (38). They reported on high diagnostic values and the technique required 40 minutes to use.
Another type of fluorescence use is fluorescence lifetime imaging, in which endogenous fluorophore lifetime of tissue is probed by illumination with a pulsed, long-wave ultraviolet light source (39). This technique has been evaluated by Tajudeen *et al.*, in combination with dynamic optical contrast imaging (DOCI) so that the fluorophore lifetime can be mapped over a macroscopic field of view. Significant differences ($p<0.05$) were found in fluorescence lifetime in different types of tissue and acquisition time was less than two minutes.

Optical techniques

The most studied optical techniques used for intra-operative margin assessment in oral squamous cell carcinoma are Raman spectroscopy (RM), diffuse reflectance spectroscopy (DRS), hyperspectral imaging (HSI), optical coherence tomography (OCT) and narrow band imaging (NBI) (Table 3).

Raman Spectroscopy

Raman spectroscopy (RS) is an optical technique based on inelastic scattering of light by molecules in tissue and therefore provides detailed information about its molecular composition (40). RS is able to discriminate tumor from healthy tissue by the difference in water concentration in these two tissue types. Barosso *et al.*, Cals *et al.* and Yu *et al.* used a different part of the spectrum (2500-4000 cm^{-1}, 400-1800 cm^{-1} and 300-3950 cm^{-1}, respectively) and obtained comparable results in the discrimination of OSCC and healthy tissue in tongue specimen (sensitivity 99%/100%/99%, specificity 92%/78%/94%, respectively) (41-43). Similar results are also reported for mandibular specimens (40). The technique can be used directly on tissue because it is non-destructive, and there is no need for reagents or labelling (40). RS is fast (measurements in the order of 1 second or less, with real-time signal analysis) and can be applied through the use of hand-held fiber-optic probes at any location. However, the sampling area per measurement is in the order of 300-1000 µm, so multiple measurements are needed to evaluate the whole resection surface (40, 42, 44). Also, the sampling depth is up to 40-50 µm, which challenges the detection of close margins where tumor cells are present within 5 mm from the resection surface. RS is now built into a needle that can be inserted several millimeters into the tissue as an approach to overcome this limited sampling depth. The published results on this are expected soon (Erasmus Medical Center, The Netherlands, project number: 106467).

Diffuse Reflectance Spectroscopy

In diffuse reflectance spectroscopy (DRS), diffusely reflected light is measured after illuminating the tissue with a broadband white light source. The reflectance spectrum contains information about the absorption and scattering properties of the illuminated tissue. Differences in these properties allow for tissue characterization, e.g., to discriminate tumor from healthy tissue. a total of 28 tumor specimens of tongue, oropharynx, floor of mouth and cheek were evaluated and a sensitivity and specificity of 89% and 82%, respectively, was reported (45). The handheld probe has to be positioned directly on the tissue, the technique is non-invasive and does not require the administration of agents. Using DRS, tissue type characterization can be made available real-time. However, the sampling area is limited to a few millimeters, requiring multiple measurements to evaluate a surface. Sampling depth is approximately 1 mm, which will not be enough to detect close margins that have tumor cells within 5 mm from the surface. Also, for intraoperative use, it is required to turn off the light in the operation room, because this will interfere with the technique.

Hyperspectral imaging

The image acquired by hyperspectral imaging (HSI) is constructed of a diffuse reflectance spectrum for each pixel, allowing to evaluate the whole resection surface in one view. Results are reported for the detection of the reflected light in the visual (VIS) part of the wavelength spectrum (400-950 nm) and the near infrared (NIR) part (950-1700 nm) (46-48). The extension of the spectral range toward the infrared spectrum, where absorption of light by blood is negligible, should make the technology more applicable for use during surgery. Results of two different studies reporting on 14 tongue specimens and 21 tongue, larynx, pharynx and mandible specimens using a VIS HSI camera were comparable in the discriminative power of tumor and healthy tissue (sensitivity of 84% and 81%; specificity of 77%

and 80%, respectively) (46, 47). Recently, Halicek *et al.* reported on a larger study on 102 patients using a deep learning model to detect squamous cell carcinoma with VIS HSI in less than 2 minutes with a sampling depth of less than 3 mm (48). a sensitivity of 80% and a specificity of 77% were obtained with the NIR camera on tongue specimens (46).

This technology is non-invasive and does not require the administration of an agent. Image acquisition and tissue type characterization can be achieved within seconds. The field of view is in the order of several centimeters, and the sampling depth of a few millimeters. Challenges are the rough surfaces that create shadows on the imaging field. Also, wet surfaces completely reflect light, creating specular glare. Shadowed and glare pixels do not contain useful information for tissue characterization. Like for DRS, also for HSI darkness is required. It is unknown whether HSI is able to detect small tumor pockets more than 3 mm below the resection surface.

Optical coherence tomography

In optical coherence tomography (OCT), a light beam of a specific wavelength in the near infrared spectrum is projected on the tissue. Tissue type characterization is based on the echo delay time of the reflected light by the different layers of the tissue. With OCT, two-dimensional cross-sectional images can be constructed with a high resolution that is comparable to low resolution histology (49). Images can be acquired non-invasively, without the need for tissue preparation. Hamdoon *et al.* evaluated OCT images for (superior, inferior, lateral and medial) margin assessment of 28 freshly resected specimen of the tongue, floor of mouth, buccal mucosa and retromolar trigone (50). Sensitivity and specificity were 81.5% and 87%, respectively. Maximum image width used was 6 mm, and the resulting image could be on the screen instantly. The major limitation of OCT lies into the sampling depth: a loss of tissue accuracy and definition occurred beyond 2 mm. Recently, De Leeuw *et al.* evaluated full-field OCT, that is able to produce en-face images with both large fields of view and a µm resolution, but a limited sampling depth of 50 µm. Five minutes are required to acquire and interpret OCT images of one square cm. a sensitivity and specificity of 90% and 87% were found, respectively, from OCT images of 32 specimens.

Narrow Band Imaging

Narrow band imaging (NBI) uses two specific wavelengths of the visible spectrum, that correspond to the absorption peak of hemoglobin, so that the microvascular abnormalities can be visualized. It is mostly used to determine the mucosal margins, however Tirelli *et al.* evaluated both mucosal and deep margins (51). Although the technique seemed to achieve a precise definition of the superficial tumor extension, the authors concluded that NBI is ineffective in defining deep margins.

Conventional imaging techniques

Ultrasound

In radiology, ultrasound (US) is used to measure the tumor thickness for diagnostic purposes, indicating that the border of the tumor can be imaged on an US image (52). Several studies have looked into the use of US for tumor margin assessment as well, both during the resection as well as directly on the resected specimen. US can evaluate the tissue up to several centimeters in depth, depending on the frequency used, it is a cheap, fast and harmless technology that is widely available. In the largest study, evaluating tongue specimens of 31 patients, the mean (SD) difference between the deep resection margin measured on US and histopathology was 1.1 (0.9), with a Pearson's correlation coefficient of 0.79 ($p < 0.01$) (53).

Songra *et al.* reported on sensitivity, specificity and correlation coefficient (83%, 63% and 0.0648 respectively) comparing the margin measured on US and histopathology of 14 patients (54). Margins of five tongue specimens measured on US by Helbig *et al.* differed 0-4 mm from the margin measured on histopathology (55). Acquisition time varied between real time and twenty minutes. The review of Tarabichi *et al.* encourages to conduct further research using standardized imaging protocols and well-defined patient populations to evaluate the use of US in therapeutic decision making further (56). Kodama *et al.* reported on a sampling depth of 2 cm, others only mention a few centimeters (Table 4).

Computed Tomography

Ivashchenko *et al.* verified resection margins of maxillary malignancies by cone-beam computed tomography (CBCT) in six patients (57). Preoperatively, the intended resection volume was delineated on the diagnostic CT and this was compared to the actual resection that was imaged by a CBCT at the end of the surgery. They found that an intraoperative CBCT is a promising way to assess surgical margins of maxillary tumors. Their method required ten minutes intraoperatively, however, an intraoperative sterile cone-beam CT is required in the OR, artefacts from dental fillings hamper accurate image acquisition and this method is limited to the evaluation of bone margins only due to the poor soft tissue contrast on CT.

Specimen radiography

Radiography on mandible specimens can be useful in evaluating the completeness of excision (58, 59). The method is cheap, easy to perform, widely available and requires 20 minutes. However, convex structures, such as the mandible are difficult to interpret on a two-dimensional plane. The researchers also found a loss of accuracy when images were taken in the anterior-posterior direction, due to compact structure of the cortical bone in the mandible (58). They encourage further studies to determine whether the technique is able to detect small bone infiltrations in the different sizes and shapes of the specimens.

Magnetic Resonance Imaging

Magnetic resonance imaging (MRI) was evaluated for resection margin status of tongue specimens with OSCC in two studies: 10 tongue specimens imaged with an ex-vivo 7 Tesla MRI and 10 tongue specimens imaged with a 3 Tesla clinical whole-body MRI (60, 61).

The tumor could be recognized on the ex-vivo 7 Tesla MRI when invasion depth >3 mm (60). The study suggested that it will be difficult to detect small tumors with MRI and the inability to visualize microscopic invasive growth patterns will hamper the prediction of the resection margin. To be feasible for clinical application, the scan time needs to be decreased (total time in this study was 1.5 hours), the resolution needs to be increased, and larger study populations have to be evaluated. An MRI would lead to extra costs; however, the authors expect that this would outweigh the costs from subsequent surgeries and additional radiotherapy. The 3 Tesla clinical whole-body MRI was logistically more favorable, and after optimization of the method for an envisioned clinical application, this imaging technology was evaluated for margin identification (61). However, the identification of margins less than 5 mm was very poor and requires improvement to allow use of MRI for clinical practice.

Image guided surgery

Feichtinger *et al.* used 3D-navigation based on positron emission tomography/computed tomography (PET/CT) image fusion to evaluate the resection margins during surgery in six patients with maxillary sinus or oral cavity tumors (62). After setting up the navigation system and ablation of the tumor, the defect was navigated with the pointer and the distance between the resection plane and the 3D image of the tumor image on the PET/CT was measured in every direction. Additional resection was performed when the distance was not sufficient. The technique was evaluated in six patients and inadequate resection margins were confirmed by histopathological examination. This technique requires a navigation system, pre-operative preparation of the virtual tumor model and edentate patients receive screws in the supraorbital region for registration purposes one day before surgery. However, the results on deep margin assessment are promising and larger study populations are necessary to confirm the effectiveness of this technique. However, in soft tissues like the tongue, navigation remains very difficult and this can only be done in tumors in or attached to bony structures.

Cytological assessment

In this review, intraoperative cytological assessment (ICA) covers the range of methodologies that discriminate tumor from healthy tissue on a cytological level from obtaining tissue with scrape, bench or imprint smears that are stained by e.g. hematoxylin and eosin or toluidine (Table 5). All studies verified their results with the final histopathological outcome. Both soft tissue margins and bony resection margins were studied. One study evaluated the surgical defect, the rest of the studies focused on the resected specimen. Table 5 shows the high performance of the methodologies in differentiating between tumor and healthy tissue. The number of patients included by the studies ranged from 15-154. All studies included for this review reported on the low costs of ICA, on the fact that no training is required, that the time needed is limited to only several minutes, cellular details are preserved and that a wider area of the resection margin can be assessed at once (63-66). However, the main limitation of ICA is the fact that it can only assess the superficial layer of the resection margin and cannot assess whether the tumor is in close proximity to that margin. Nieberler *et al.* developed a method to isolate cells from up to a cm for evaluation so that even close bone margins could be found (67-69). However, this increased the processing time significantly.

Discussion

Surgery is the first choice of treatment of OSCC and radical tumor resection is crucial for recurrence-free, disease-free and overall survival (2, 17). a range of 30% to 85% of the surgeries results in resection margins that are inadequate, in predominantly deep margins (25, 27, 70). This shows the urgent need for a technique to evaluate the deep resection margin during surgery. To gain insight into which technologies are being studied for this purpose, 3742 articles were systematically reviewed and 62 articles were included. An overview was provided on the reported performance (accuracy, sensitivity, specificity, positive predictive value, negative predictive value, or a different outcome measure), acquisition time, and sampling depth of each technique.

Margin assessment is challenging, since the accuracy is affected by communication between surgeon and pathologist, accurate tumor localization, technique and type of margin sampling and the influence

of tumor cut-through (71). After resection, the tissue is subject to tissue shrinkage, leading to a smaller margin than the margin that was accounted for during the resection (72). To be applicable in the operating room, the technique should be fast and easy enough so that the surgical procedure does not need to be extended or interrupted too long. Ideally, the technique should be able to identify deep, mucosal and bone margins simultaneously. a recent survey of Bulbul *et al.* showed that 86% of the American Head and Neck surgeons are willing to use such a technique to assess margins intraoperatively (3).

FSA is the most commonly used intra-operative margin assessment method: 97% of American Head and Neck surgeons reported to use FSA in current practice (3). However, FSA has disadvantages concerning the use in bone margins, high rates of false negatives and required time (29, 30, 73). Interestingly, overall survival of margin revisions after positive FSA is not equal to initial negative margin resection and does not lead to better local control (74). Moreover, specimen driven FSA leads to improved sensitivity compared to patient driven FSA, although sampling techniques differed between studies (4, 73). Relocating the sample site after a reported positive margin is challenging after resection: Kerawala *et al.* showed a mean error of 12 mm for relocating the deep margin (75). To overcome the relocation issue, Van Lanschot *et al.* recently proposed a method for accurate relocation of inadequate tumor resection margins in the wound bed: the surgeon places numbered tags on both sides of the resection line in a pair-wise manner, so that after the resection, one tag of each pair remains on the specimen and the corresponding tag remains on the wound bed (76). Cost-effectiveness analysis has been performed for FSA, showing a cost-benefit ratio of 20:1. However, a reoperation compared to re-resection in case of positive margins on FSA during the initial operation leads to higher expenses (77). Concluding, FSA is an acceptable, yet not optimal, intra-operative technique.

In the search for other margin assessment methods than FSA, some techniques are very promising for future use after proven effectiveness in larger trials. For example, fluorescence techniques could be useful assessing deep margins to a maximum of 6.3 mm deep and lead to high sensitivities and specificities (33). Real time assessment, with high sensitivities and specificities is possible using Raman spectroscopy and needle insertion with this technology is promising to reach sufficient sampling depth. Other optical imaging techniques perform accurately but have the same disadvantage regarding sampling depth and the need to dim theater lights (49, 50).

Ultrasound is promising, although standardized imaging protocols need to be developed and evaluated on well-defined patient populations (56). Radiography might work for bone margins, but is difficult to interpret in convex structures (58, 59). Computed tomography (CT) and magnetic resonance imaging (MRI) of the specimen provide encouraging results, but these imaging technologies are challenging for real-time feedback on tumor margins in the operation room itself. Image guided surgery using positron emission tomography/CT showed promising results on deep margin assessment in maxillary tumors but larger study populations are necessary. Cytological assessment is a low-cost, widely available and quick alternative, but margin assessment is limited to the surface of the specimen (67-69).

This review is limited by the inability to equally compare the different techniques directly, because different selection criteria and outcome measures were used in the reviewed studies. Furthermore, only studies on techniques that are feasible for theatre are reviewed, excluding techniques that might be superior in discriminating tumor from healthy tissue in the future, e.g. Jakobsohn *et al.* showed that gold nanorods could properly differentiate tumor from normal cells *in vitro* with real-time photothermal molecular imaging (78). Optical molecular imaging utilizing pH responsive peptide combined with

fluorescence showed a more intense signal in cancerous than normal tissue (79). Goldenberg *et al.* found that a quantitative methylation-specific polymerase chain reaction could intra-operatively detect cancerous cells (80). However, all of these studies are still in either the pre-clinical phase or not yet feasible for clinical use.

Lastly, the margin discussion still raises the question on how to handle initially positive margins that become negative after re-resection: should patients receive adjuvant treatment as a result of their initially positive margin? There are studies available that show worse local control in the patient group with initial positive margins that were converted into negative margins, when compared to the patients with initially negative margins (4). Also, the fact that there is no consensus on the optimal margin definition, limits the development of techniques for intra-operative margin evaluation, since the sampling depth is a critical requirement for the technique to meet.

Conclusion

In this review, we systematically analyzed literature on intraoperative deep margin assessment methods for oral squamous cell carcinoma. At the moment, the most prevailing technique remains frozen section analysis. In the search for other assessment methods to evaluate the deep resection margin, some technologies are very promising for future use when effectiveness has been shown in larger trials, e.g., fluorescence (real-time, sampling depth up to 6 mm) or optical techniques such as hyperspectral imaging (real-time, sampling depth few mm) for microscopic margin assessment and ultrasound (less than 10 min, sampling depth several cm) for assessment on a macroscopic scale.

Table 1 Included studies reporting on frozen section analysis for intra-operative margin assessment

Frozen section															
Author, year	**Study methodology**	**Margin assessment technology**	**Specimen/ defect driven/ in situ**	**Verification method**	**optimal margin (mm)**	**Sample size (number of patients)**	**Tumor site**	**Sensitivity (%)**	**Specificity (%)**	**Accuracy (%)**	**PPV (%)**	**NPV (%)**	**Acquisition time**	**Sampling depth**	**Other outcome measures/ remarks**
Abbas, 2017 (81)	Retrospective	FS	defect	histology	10	77	variable: oral soft tissue	72.7	95.3	90.9	66.6	93.9			
Amit, 2015 (73)	Prospective	FS	specimen and defect	histology	5	71	variable: oral soft tissue	91 vs 22	93 vs 100						FP: 9% vs 0%; FN: 17% vs 44%
De Visscher, 2002 (82)	Prospective	FS	specimen	histology	3	72	lip						20 min		8 of the 9 patients who had a positive margin on FS was confirmed by histopathology; FP: 1.4%
DiNardo, 2000 (77)	Retrospective	FS	defect	histology	5	80	variable: oral soft tissue	34.3	100	71.3	100	66.2	15 min		
Du, 2016 (83)	Retrospective	FS	specimen	histology	5	253	variable: oral soft tissue	78	97	93	89	94			
Gooris, 2003 (84)	Retrospective	FS	unknown	histology	5	131	lip			99					
Layfield, 2018 (85)	Retrospective	FS	specimen	histology		288	variable: oral soft tissue	88.9	98.6		93.3	97.6			
Moe, 2019 (86)	Prospective	FS	specimen	histology		30	variable: oral soft tissue	90.9	100	96.8	100	95.2			Correlation coefficient FS and histopathology: >0.95
Mair, 2017 (87)	Retrospective	FS vs GE	specimen (FS) vs in situ (GE)	histology	5	435	variable: oral soft tissue	45.45 vs 61.9	98.8 vs 88.3	92.9 vs 83.7	93.5 vs 91.6	83.3 vs 53.1			
Nayanar, 2019 (88)	Retrospective	FS	specimen	histology	no tumor at margin	265	variable: oral soft tissue	82.05	96.46				20 min		
Oxford, 2006 (29)	Retrospective	FS	unknown	histology		25	mandible and maxilla	88.9	100					superficial	
Pandey, 2010 (89)	Retrospective	FS	specimen	histology	5	104	unknown	78.57	99.55	98.32					
Ribeiro, 2003 (90)	Retrospective	FS	specimen	histology	10	82	variable: oral soft tissue	92.8	99.8						99.5% concordance
Sharma, 2008 (91)	Prospective	FS	specimen	histology		47	variable: oral soft tissue	72	99.4	96.74	94.7	96			FP: 0.59; FN: 28%
Tirelli, 2019 (92)	Prospective	FS	defect	histology	3	42	variable: oral soft tissue	93.6	96.8		90.7	96.8			
Varvares, 2015 (10)	Retrospective	FS	specimen vs defect	histology	5	91 vs 8	variable: oral soft tissue								Agreement FS and histopathology: 95%
Wysluch, 2010 (30)	Prospective	FS	specimen	histology	10	20	mandible	77	90				30 min		

FS = frozen section analysis; GE = general examination

Table 2 Included studies reporting on fluorescence for intra-operative margin assessment

Fluorescence														
Author, year	**Study methodology**	**Margin assessment technology**	**Specimen/ defect driven/ in situ**	**Verification method**	**optimal margin (mm)**	**Sample size (number of patients)**	**Tumor site**	**Sensitivity (%)**	**Specificity (%)**	**PPV (%)**	**NPV (%)**	**Acquisition time**	**Sampling depth**	**Other outcome measures/ remarks**
Gao, 2018 (32)	Prospective	FLUO (panitumumab-IR-Dye800CW, 800 nm)	specimen	histology	5	21	variable	91	88	80	93	real time	1 mm and 2 mm	
Leunig, 2000 (37)	Prospective	FLUO (5-ALA, 375-440 nm)	specimen and defect	histology		58	tongue and gingiva	99	60	77	98	up to 2.5 hours		
Nieberler, 2018 (38)	Prospective	FLUO (integrin αvβ6-targeting RGD peptides)	specimen	cytology		122	mandible and maxilla	100	98.3	92	100	40 min		
Pan, 2020 (93)	Prospective	FLUO (indocyanine green, 785 nm)	specimen, defect and in situ	histology		20	variable: oral soft tissue					real time		
Rosenthal, 2015 (94)	Prospective	FLUO (cetuximab-IR-Dye800)	specimen, defect and in situ	histology		12	variable: oral soft tissue					real time (video 30 seconds)		Tumor to background ratio *in vivo* 1.56; *in vitro* 1.43
Shimane, 2016 (36)	Prospective	FLUO (g-Glu-HMRG)	specimen and in situ	histology		10	variable: oral soft tissue					10 min		Tumor to background ratio of 5.2
Slooter, 2018 (35)	Prospective	FLUO (g-Glu-HMRG, 525nm)	specimen	histology		15	variable: oral soft tissue	80	87			10 min		OSCC tissue fluoresced 4 times brighter than normal tissue
Tajudeen, 2016 (39)	Prospective	FLUO (autofluorescence, 400-500 nm)	specimen	histology		15	variable: oral soft tissue					<2 min	> 1mm	
Van Keulen, 2018 (33)	Prospective	FLUO (panitumumab-IR-Dye800CW, 800 nm)	specimen, defect and in situ	histology	5	14	variable: oral soft and hard tissue					real time		Significant difference between fluorescence lifetime of different tissue types (tumor, muscle, collagen, fat) ($p<0.05$).
Van Keulen, 2019 (95)	Prospective	FLUO (panitumumab-IR-Dye800CW, 800 nm)	specimen	histology	5	8	variable: oral soft tissue	95	89			7 min	< 6.3 mm	Improved surgical decision making in 3 cases (21.4%): identification of a close margin (n=1) and unanticipated regions of primary disease (n=2).
Van Keulen, 2020 (34)	Prospective	FLUO (panitumumab-IR-Dye800CW, 800 nm)	specimen	histology	5	12	variable: oral soft tissue					2.5 min	5 mm	To detect tumor within 2 mm of the specimen surface, sensitivity was 100%.
Voskuil, 2020 (96)	Prospective	FLUO (cetuximab-800CW, 778-795 nm)	specimen	histology	1	15	variable	100	91			10 min	5 mm	The highest intensity peak consistently detected the closest margin to the tumor.
Warram, 2015 (97)	Prospective	FLUO (cetuximab-IR-Dye800)	specimen	histology		11	variable: oral soft tissue	90.5	78.6	80.9	89.2	real time		Fluorescence intensities were significantly higher in tumor tissue compared to normal tissue.

FLUO = fluorescence

Table 3 Included studies reporting on optical techniques for intra-operative margin assessment

Optical techniques															
Author, year	**Study methodology**	**Margin assessment technology**	**Specimen/ defect driven/ in situ**	**Verification method**	**optimal margin (mm)**	**Sample size (number of patients)**	**Tumor site**	**Sensitivity (%)**	**Specificity (%)**	**Accuracy (%)**	**PPV (%)**	**NPV (%)**	**Acquisition time**	**Sampling depth**	**Other outcome measures/ remarks**
Barroso, 2015 (41)	Prospective	RS (2500-4000 cm-1)	specimen	histology		14	tongue	99	92				< 30 min		
Barroso, 2018 (40)	Prospective	RS (2500-4000 cm-1)	specimen	histology		22	mandible	95	87	95			< 60 min	40 um	
Yu, 2019 (43)	Prospective	RS (300-3950 cm-1)	specimen	histology		12	tongue	99.31	94.44	96.9					
Brouwer de Koning, 2018 (45)	Prospective	DRS (400-1600 nm)	specimen	histology	5	28	variable: oral soft tissue	89	82	86			Real time	>1 mm	
Cals, 2016 (42)	Prospective	RS (400-1800 cm-1)	specimen	histology	5	10	tongue	100	78	91					
Brouwer de Koning, 2019 (46)	Prospective	HSI (400-950 nm)	specimen	histology		14	tongue	84	77	82			Real time	few mm	also HSI NIR (950-1700nm): sensitivity 80%, specificity 77%
Halicek, 2018 (47)	Prospective	HSI (450-900 nm)	specimen	histology		21	variable: oral soft tissue	81	80	81					
Halicek, 2019 (48)	Prospective	HSI (450-900 nm)	specimen	histology		102	variable: oral soft tissue						1 min/ image	< 3 mm	AUC's upwards of 0.80-0.90
De Leeuw, 2020 (98)	Prospective	OCT	specimen	histology	5	32	variable: oral soft tissue	90	87				5 min/ cm^2	50 µm	
Hamdoon, 2016 (50)	Prospective	OCT (1310 nm)	specimen	histology	5	28	variable: oral soft tissue	81.5	87	88	61.5	95	Real time	2 mm	Surgeon 2 achieved accuracy 84%
Tirelli, 2018 (51)	Prospective	NBI (415 nm and 540 nm)	in situ	histology	3	61	variable: oral soft tissue						5 min		Conclusion: NBI only works for mucosal margin, not for deep margin

RS = Raman Spectroscopy; DRS = Diffuse Reflectance Spectroscopy; HSI = Hyperspectral Imaging; OCT = Optical Coherence Tomography; NBI = Narrow Band Imaging

Table 4 Included studies reporting on conventional imaging techniques for intra-operative margin assessment

Conventional imaging techniques														
Author, year	**Study methodology**	**Margin assessment technology**	**Specimen/ defect driven/ in situ**	**Verification method**	**optimal margin (mm)**	**Sample size (number of patients)**	**Tumor site**	**Sensitivity (%)**	**Specificity (%)**	**PPV (%)**	**NPV (%)**	**Acquisition time**	**Sampling depth**	**Other outcome measures/ remarks**
Brouwer de Koning, 2020 (53)	Prospective	US, 5-10 MHz probe	specimen	histology	5	31	tongue					5 min		Mean (SD) deep resection margins measured on US images differed by 1.1 (0.9) mm from those reported by the histopathologist (Pearson's correlation coefficient: 0.79, p < 0.01).
Helbig, 2001 (55)	Prospective	US, 8-12 MHz probe	in situ	histology	2	5	tongue					<10 min		Difference between margin measured on US and histopathology varied between 0-4 mm.
Kodama, 2010 (99)	Prospective	US, 7.5 MHz probe	specimen and in situ	histology	10	4	tongue						>2cm	
Songra, 2006 (54)	Prospective	US, 5-10 MHz probe	specimen and in situ	histology	5	14	variable: oral soft tissue	83	63	63	83	real time	up to a few cm	Pearson correlation coefficient US and histopathology: 0.648 (P < 0.01).
Tarabichi, 2018 (100)	Unclear	US, 7-15 MHz probe	specimen and in situ	histology	5	12	tongue						several cm	Preliminary results that suggest that ultrasound has the potential to improve our ability to obtain a clear, deep margin based on more objective assessment.
Tominaga, 2007 (101)	Prospective	US, 7.5 MHz probe	specimen	histology	5	3	tongue					>20 min	several cm	Quick and eficient method to confirm surgical clearance.
Ivashchenko, 2019 (57)	Prospective	CT	defect	histology and preoperative planning	10	6	maxilla					<10 min	3D view	Two resections were reported pathologically as less than radical, each of which was detected by intraoperative CT. The mean (SD) distance between the planned and the actual resection was 1.49 (2.78) mm.
Ntomouchtsis, 2013 (58)	Prospective	RADIOGR	specimen	histology	5	16	mandible	100	100			20 min	3D view	
Shan, 2019 (59)	Prospective	RADIOGR	specimen	histology	10	10	mandible					'fast'		
Heidkamp, 2020 (61)	Prospective	MRI	specimen	histology	5	10	tongue	36	92	38	91	< 30 min		
Steens, 2017 (60)	Prospective	MRI	specimen	histology		10	tongue					>1,5 hour	3D view	Tumor can be recognized on MR when invasion depth >3 mm. Difference between margin measured on MR and histopathology varied between 0.1-1.8 mm.
Feichtinger, 2010 (62)	Prospective	nav	defect	histology	5	6	variable: oral soft and hard tissue						3D view	Intraoperative navigation showed an unsafe resection margin in 4 patients. This was confirmed by the histopathological examination.

US = ultrasound; CT = computed tomography; RADIOGR = radiography; MRI = magnetic resonance imaging; nav = navigation

Table 5 Included studies reporting on cytological assessment for intra-operative margin assessment

Cytological techniques															
Author, year	**Study methodology**	**Margin assessment technology**	**Specimen/ defect driven/ in situ**	**Verification method**	**optimal margin (mm)**	**Sample size (number of patients)**	**Tumor site**	**Sensitivity (%)**	**Specificity (%)**	**Accuracy (%)**	**PPV (%)**	**NPV (%)**	**Acquisition time**	**Sampling depth**	**Other outcome measures/ remarks**
Junaid, 2013 (63)	Prospective	Staining (toluiniunm chloride)	defect	histology		56	variable: oral soft tissue	100	84.9	85.71	27.2	100	5 min		
Kurita, 2008 (64)	Prospective	Staining (indigo carmine and Congo red)	specimen	histology		15	variable: oral soft tissue						several minutes		No significant difference in the tumor-margin distance between histopathological and digital microscopic examination (Wilcoxon signed-ranks test, P > 0.63). The deviation ranged from 0.4 to 4.1 mm with a median absolute difference of 1.7 mm.
Cariati, 2019 (102)	Prospective	Cyto	unclear	histology	no tumor at margin	17	variable	33.3	85.7		33.3	85.7	<35 min		
Namin, 2015 (103)	Retrospective	Cyto	specimen	histology	10	51	mandible and maxilla			100					
Nieberler, 2016 (67)	Prospective	Cyto	specimen	histology	10	102	variable: hard tissue	94.4	97.4	97	85	99.1	20 min	a few mm	
Nieberler, 2020 (69)	Prospective	Cyto	specimen	histology		107	variable: hard tissue	78.6	95.7	93.5	73.3	96.7	<20 min		
Nieberler, 2017 (68)	Prospective	Cell isolation	specimen	histology		154	variable: hard tissue	92.3	100		100	97.4	1 hour	1 cm^3	
Ojha, 2018 (65)	Prospective	Staining (Field staining)	specimen	histology		23	variable: oral soft tissue						5 min		100% concordance
Yadav, 2013 (66)	Prospective	Touch imprint	specimen	histology	no tumor at margin	30	variable: oral soft tissue	91.1	74.4	83	97.2	88.6		up to 1 cm	

Cyto = cytological assessment

References

1. Colevas, A.D., et al., NCCN Guidelines Insights: Head and Neck Cancers, Version 1.2018. J Natl Compr Canc Netw, 2018. 16(5): p. 479-490.
2. Jain, P.V., et al., Redefining adequate margins in oral squamous cell carcinoma: outcomes from close and positive margins. Eur Arch Otorhinolaryngol, 2020. 277(4): p. 1155-1165.
3. Bulbul, M.G., et al., Margin Practices in Oral Cavity Cancer Resections: Survey of American Head and Neck Society Members. Laryngoscope, 2020.
4. Buchakjian, M.R., et al., Association of Main Specimen and Tumor Bed Margin Status With Local Recurrence and Survival in Oral Cancer Surgery. JAMA Otolaryngol Head Neck Surg, 2016. 142(12): p. 1191-1198.
5. Zanoni, D.K., et al., a Proposal to Redefine Close Surgical Margins in Squamous Cell Carcinoma of the Oral Tongue. JAMA Otolaryngol Head Neck Surg, 2017. 143(6): p. 555-560.
6. Lee, D.Y., et al., Survival and recurrence of resectable tongue cancer: Resection margin cutoff value by T classification. Head Neck, 2018. 40(2): p. 283-291.
7. Tasche, K.K., et al., Definition of "Close Margin" in Oral Cancer Surgery and Association of Margin Distance With Local Recurrence Rate. JAMA Otolaryngol Head Neck Surg, 2017. 143(12): p. 1166-1172.
8. Yamada, S., et al., Estimation of the width of free margin with a significant impact on local recurrence in surgical resection of oral squamous cell carcinoma. Int J Oral Maxillofac Surg, 2016. 45(2): p. 147-52.
9. Dillon, J.K., et al., How does the close surgical margin impact recurrence and survival when treating oral squamous cell carcinoma? J Oral Maxillofac Surg, 2015. 73(6): p. 1182-8.
10. Varvares, M.A., et al., Surgical margins and primary site resection in achieving local control in oral cancer resections. Laryngoscope, 2015. 125(10): p. 2298-307.
11. Wong, L.S., et al., Influence of close resection margins on local recurrence and disease-specific survival in oral and oropharyngeal carcinoma. Br J Oral Maxillofac Surg, 2012. 50(2): p. 102-8.
12. Nason, R.W., et al., What is the adequate margin of surgical resection in oral cancer? Oral Surg Oral Med Oral Pathol Oral Radiol Endod, 2009. 107(5): p. 625-9.
13. Binahmed, A., R.W. Nason, and A.A. Abdoh, The clinical significance of the positive surgical margin in oral cancer. Oral Oncol, 2007. 43(8): p. 780-4.
14. Sutton, D.N., et al., The prognostic implications of the surgical margin in oral squamous cell carcinoma. Int J Oral Maxillofac Surg, 2003. 32(1): p. 30-4.
15. Baddour, H.M., Jr., K.R. Magliocca, and A.Y. Chen, The importance of margins in head and neck cancer. J Surg Oncol, 2016. 113(3): p. 248-55.
16. Kubik, M.W., et al., Intraoperative Margin Assessment in Head and Neck Cancer: a Case of Misuse and Abuse? Head Neck Pathol, 2020. 14(2): p. 291-302.
17. NCCN Guidelines- Head and Neck Cancers (Internet). Version 1.2018. 2018
18. Helliwell, T. and J.A. Woolgar, Standards and datasets for reporting cancers. Dataset for histopathology reporting of nodal excisions and neck dissection specimens associated with head and neck carcinomas. London, UK. The Royal College of Pathologists. 2013.
19. Loree, T.R. and E.W. Strong, Significance of Positive Margins in Oral Cavity Squamous Carcinoma. The American Journal of surgery, 1990. 160.
20. Slootweg, P.J., et al., Treatment failure and margin status in head and neck cancer. a critical view on the potential value of molecular pathology. Oral Oncology, 2002. 38: p. 500-503.
21. Weijers, M., et al., The clinical relevance of epithelial dysplasia in the surgical margins of tongue and floor of mouth squamous cell carcinoma: an analysis of 37 patients. J Oral Pathol Med, 2002. 31(11-5).
22. Weijers, M., et al., The status of the deep surgical margins in tongue and floor of mouth squamous cell carcinoma and risk of local recurrence; an analysis of 68 patients. Int J Oral Maxillofac Surg, 2004. 33(2): p. 146-9.
23. Bernier, J., et al., Defining risk levels in locally advanced head and neck cancers: a comparative analysis of concurrent postoperative radiation plus chemotherapy trials of the EORTC (#22931) and RTOG (# 9501). Head Neck, 2005. 27(10): p. 843-50.
24. Eckardt, A., et al., Recurrent carcinoma of the head and neck: treatment strategies and survival analysis in a 20-year period. Oral Oncol, 2004. 40(4): p. 427-32.
25. Smits, R.W., et al., Resection margins in oral cancer surgery: Room for improvement. Head Neck, 2016. 38 Suppl 1: p. E2197-203.

26. Kain, J.J., et al., Surgical margins in oral cavity squamous cell carcinoma: Current practices and future directions. Laryngoscope, 2020. 130(1): p. 128-138.
27. Woolgar, J.A. and A. Triantafyllou, a histopathological appraisal of surgical margins in oral and oropharyngeal cancer resection specimens. Oral Oncol, 2005. 41(10): p. 1034-43.
28. Black, C., et al., Critical evaluation of frozen section margins in head and neck cancer resections. Cancer, 2006. 107(12): p. 2792-800.
29. Oxford, L.E. and Y. Ducic, Intraoperative evaluation of cortical bony margins with frozen-section analysis. Otolaryngol Head Neck Surg, 2006. 134(1): p. 138-41.
30. Wysluch, A., et al., Intraoperative evaluation of bony margins with frozen-section analysis and trephine drill extraction technique: a preliminary study. Head Neck, 2010. 32(11): p. 1473-8.
31. Lee, Y.J., et al., Intraoperative Fluorescence-Guided Surgery in Head and Neck Squamous Cell Carcinoma. Laryngoscope, 2020.
32. Gao, R.W., et al., Determination of Tumor Margins with Surgical Specimen Mapping Using Near-Infrared Fluorescence. Cancer Res, 2018. 78(17): p. 5144-5154.
33. van Keulen, S., et al., The Clinical Application of Fluorescence-Guided Surgery in Head and Neck Cancer. J Nucl Med, 2019. 60(6): p. 758-763.
34. van Keulen, S., et al., The Sentinel Margin: Intraoperative Ex Vivo Specimen Mapping Using Relative Fluorescence Intensity. Clinical Cancer Research, 2019. 25(15): p. 4656-4662.
35. Slooter, M.D., et al., Detecting tumour-positive resection margins after oral cancer surgery by spraying a fluorescent tracer activated by gamma-glutamyltranspeptidase. Oral Oncol, 2018. 78: p. 1-7.
36. Shimane, T., et al., Oral cancer intraoperative detection by topically spraying a gamma-glutamyl transpeptidase-activated fluorescent probe. Oral Oncol, 2016. 54: p. e16-8.
37. Leunig, A., et al., Detection of squamous cell carcinoma of the oral cavity by imaging 5-aminolevulinic acid-induced protoporphyrin IX fluorescence. Laryngoscope, 2000. 110(1): p. 78-83.
38. Nieberler, M., et al., Fluorescence imaging of invasive head and neck carcinoma cells with integrin alphavbeta6-targeting RGD-peptides: an approach to a fluorescence-assisted intraoperative cytological assessment of bony resection margins. Br J Oral Maxillofac Surg, 2018. 56(10): p. 972-978.
39. Tajudeen, B.A., et al., Dynamic optical contrast imaging as a novel modality for rapidly distinguishing head and neck squamous cell carcinoma from surrounding normal tissue. Cancer, 2017. 123(5): p. 879-886.
40. Barroso, E.M., et al., Raman spectroscopy for assessment of bone resection margins in mandibulectomy for oral cavity squamous cell carcinoma. Eur J Cancer, 2018. 92: p. 77-87.
41. Barroso, E.M., et al., Discrimination between oral cancer and healthy tissue based on water content determined by Raman spectroscopy. Anal Chem, 2015. 87(4): p. 2419-26.
42. Cals, F.L., et al., Development and validation of Raman spectroscopic classification models to discriminate tongue squamous cell carcinoma from non-tumorous tissue. Oral Oncol, 2016. 60: p. 41-7.
43. Yu, M., et al., Deep convolutional neural networks for tongue squamous cell carcinoma classification using Raman spectroscopy. Photodiagnosis Photodyn Ther, 2019. 26: p. 430-435.
44. Barroso, E.M., et al., Water Concentration Analysis by Raman Spectroscopy to Determine the Location of the Tumor Border in Oral Cancer Surgery. Cancer Res, 2016. 76(20): p. 5945-5953.
45. Brouwer de Koning, S.G., et al., Toward complete oral cavity cancer resection using a handheld diffuse reflectance spectroscopy probe. J Biomed Opt, 2018. 23(12): p. 1-8.
46. Brouwer de Koning, S.G., et al., Toward assessment of resection margins using hyperspectral diffuse reflection imaging (400-1,700 nm) during tongue cancer surgery. Lasers in Surgery & Medicine, 2020. 52(6): p. 496-502.
47. Halicek, M., et al., Optical Biopsy of Head and Neck Cancer Using Hyperspectral Imaging and Convolutional Neural Networks. Proc SPIE Int Soc Opt Eng, 2018. 10469.
48. Halicek, M., et al., Hyperspectral Imaging of Head and Neck Squamous Cell Carcinoma for Cancer Margin Detection in Surgical Specimens from 102 Patients Using Deep Learning. Cancers, 2019. 11(9): p. 14.
49. van Manen, L., et al., The clinical usefulness of optical coherence tomography during cancer interventions. J Cancer Res Clin Oncol, 2018. 144(10): p. 1967-1990.
50. Hamdoon, Z., et al., Optical coherence tomography in the assessment of oral squamous cell carcinoma resection margins. Photodiagnosis Photodyn Ther, 2016. 13: p. 211-217.
51. Tirelli, G., et al., Tailored resections in oral and oropharyngeal cancer using narrow band imaging. Am J Otolaryngol, 2018. 39(2): p. 197-203.
52. Lodder, W.L., et al., Tumour thickness in oral cancer using an intra-oral ultrasound probe. Eur Radiol, 2011. 21(1): p. 98-106.

53. Brouwer de Koning, S.G., et al., Ultrasound aids in intraoperative assessment of deep resection margins of squamous cell carcinoma of the tongue. British Journal of Oral & Maxillofacial Surgery, 2020. 58(3): p. 285-290.
54. Songra, A.K., et al., Observation of tumour thickness and resection margin at surgical excision of primary oral squamous cell carcinoma--assessment by ultrasound. Int J Oral Maxillofac Surg, 2006. 35(4): p. 324-31.
55. Helbig, M., et al., Intraoperative B-mode endosonography of tongue carcinoma. Head Neck, 2001. 23(3): p. 233-7.
56. Tarabichi, O., et al., Utility of intraoral ultrasound in managing oral tongue squamous cell carcinoma: Systematic review. Laryngoscope, 2019. 129(3): p. 662-670.
57. Ivashchenko, O., et al., Intraoperative verification of resection margins of maxillary malignancies by cone-beam computed tomography. Br J Oral Maxillofac Surg, 2019. 57(2): p. 174-181.
58. Ntomouchtsis, A., et al., Pilot study of intraoperative digital imaging with the use of a mammograph for assessment of bone surgical margins in the head and neck region. Clin Radiol, 2013. 68(3): p. e136-42.
59. Shan, A., et al., Intraoperative Radiographic Assessment of Bone Resection Margins During Mandibulectomy: a Case Series. Ear, Nose, & Throat Journal, 2019: p. 145561319888034.
60. Steens, S., et al., Evaluation of tongue squamous cell carcinoma resection margins using ex vivo MR. 1: p. S24.
61. Heidkamp, J., et al., Assessment of surgical tumor-free resection margins in fresh squamous-cell carcinoma resection specimens of the tongue using a clinical MRI system. Head & Neck, 2020. 42(8): p. 2039-2049.
62. Feichtinger, M., et al., Intraoperative control of resection margins in advanced head and neck cancer using a 3D-navigation system based on PET/CT image fusion. J Craniomaxillofac Surg, 2010. 38(8): p. 589-94.
63. Junaid, M., et al., Toluidine blue: yet another low cost method for screening oral cavity tumour margins in third world countries. J Pak Med Assoc, 2013. 63(7): p. 835-7.
64. Kurita, H., et al., Accuracy of intraoperative tissue staining in delineating deep surgical margins in oral carcinoma surgery. Oral Oncol, 2008. 44(10): p. 935-40.
65. Ojha, S.S., et al., Role of Field Staining in the Cytological Assessment of Intraoperative Surgical Specimens. Acta Cytol, 2018. 62(5-6): p. 327-332.
66. Yadav, G.S., et al., Intraoperative imprint evaluation of surgical margins in oral squamous cell carcinoma. Acta Cytol, 2013. 57(1): p. 75-83.
67. Nieberler, M., et al., Clinical Impact of Intraoperative Cytological Assessment of Bone Resection Margins in Patients with Head and Neck Carcinoma. Ann Surg Oncol, 2016. 23(11): p. 3579-3586.
68. Nieberler, M., et al., Intraoperative cell isolation for a cytological assessment of bone resection margins in patients with head and neck cancer. Br J Oral Maxillofac Surg, 2017. 55(5): p. 510-516.
69. Nieberler, M., et al., Defining secure surgical bone margins in head and neck squamous cell carcinomas: The diagnostic impact of intraoperative cytological assessment of bone resection margins compared with preoperative imaging. Oral Oncology, 2020. 102: p. 104579.
70. Lawaetz, M. and P. Homoe, Risk factors for and consequences of inadequate surgical margins in oral squamous cell carcinoma. Oral Surg Oral Med Oral Pathol Oral Radiol, 2014. 118(6): p. 642-6.
71. Williams, M.D., Determining Adequate Margins in Head and Neck Cancers: Practice and Continued Challenges. Curr Oncol Rep, 2016. 18(9): p. 54.
72. El-Fol, H.A., et al., Significance of post-resection tissue shrinkage on surgical margins of oral squamous cell carcinoma. J Craniomaxillofac Surg, 2015. 43(4): p. 475-82.
73. Amit, M., et al., Improving the rate of negative margins after surgery for oral cavity squamous cell carcinoma: a prospective randomized controlled study. Head Neck, 2016. 38 Suppl 1: p. E1803-9.
74. Bulbul, M.G., et al., Does Clearance of Positive Margins Improve Local Control in Oral Cavity Cancer? a Meta-analysis. Otolaryngol Head Neck Surg, 2019. 161(2): p. 235-244.
75. Kerawala, C. and K.W. Ong, Relocating the site of frozen sections-- is there room for improvement? Head & Neck, 2000. 23: p. 230-232.
76. van Lanschot, C.G.F., et al., Relocation of inadequate resection margins in the wound bed during oral cavity oncological surgery: a feasibility study. Head Neck, 2019. 41(7): p. 2159-2166.
77. DiNardo, L.J., et al., Accuracy, utility, and cost of frozen section margins in head and neck cancer surgery. Laryngoscope, 2000. 110(10 Pt 1): p. 1773-6.
78. Jakobsohn, K., et al., Towards real-time detection of tumor margins using photothermal imaging of immune-targeted gold nanoparticles. Int J Nanomedicine, 2012. 7: p. 4707-13.
79. Loja, M.N., et al., Optical molecular imaging detects changes in extracellular pH with the development of head and neck cancer. Int J Cancer, 2013. 132(7): p. 1613-23.
80. Goldenberg, D., et al., Intraoperative molecular margin analysis in head and neck cancer. Arch Otolaryngol Head Neck Surg, 2004. 130(1): p. 39-44.

81. Abbas, S.A., et al., Accuracy of frozen sections in oral cancer resections, an experience of a tertiary care hospital. J Pak Med Assoc, 2017. 67(5): p. 806-809.
82. de Visscher, J.G., et al., Surgical margins for resection of squamous cell carcinoma of the lower lip. Int J Oral Maxillofac Surg, 2002. 31(2): p. 154-7.
83. Du, E., et al., Refining the utility and role of Frozen section in head and neck squamous cell carcinoma resection. Laryngoscope, 2016. 126(8): p. 1768-75.
84. Gooris, P.J., et al., Frozen section examination of the margins for resection of squamous cell carcinoma of the lower lip. J Oral Maxillofac Surg, 2003. 61(8): p. 890-4; discussion 895-7.
85. Layfield, E.M., et al., Frozen Section Evaluation of Margin Status in Primary Squamous Cell Carcinomas of the Head and Neck: a Correlation Study of Frozen Section and Final Diagnoses. Head Neck Pathol, 2018. 12(2): p. 175-180.
86. Moe, J., et al., Intraoperative Depth of Invasion Is Accurate in Early-Stage Oral Cavity Squamous Cell Carcinoma.
87. Mair, M., et al., Intraoperative gross examination vs frozen section for achievement of adequate margin in oral cancer surgery. Oral Surg Oral Med Oral Pathol Oral Radiol, 2017. 123(5): p. 544-549.
88. Nayanar, S.K., et al., Frozen Section Evaluation in Head and Neck Oncosurgery: An Initial Experience in a Tertiary Cancer Center. Turk Patoloji Derg, 2019. 35(1): p. 46-51.
89. Pandey, S., S. Bhamra, and A. Singh, Accuracy of intraoperative frozen section in assessing margins in oral cancers: a tertiary care hospital based study. Indian Journal of Pathology and Oncology, 2020. 7(3): p. 415-419.
90. Ribeiro, N.F.F., et al., De frozen sections help achieve adequate surgical margins in the resection of oral carcinoma? J Oral Maxillofac Surg, 2003. 32(2): p. 152-158.
91. Sharma, S.M., et al., Accuracy of intraoperative frozensection in assessing margins in oral cancer resection. J Maxillofac Oral Surg, 2009. 8(4): p. 357-61.
92. Tirelli, G., et al., Frozen sections and complete resection in oral cancer surgery. Oral Dis, 2019. 25(5): p. 1309-1317.
93. Pan, J., et al., Real-time surveillance of surgical margins via ICG-based near-infrared fluorescence imaging in patients with OSCC. World Journal of Surgical Oncology, 2020. 18(1): p. 96.
94. Rosenthal, E.L., et al., Safety and Tumor Specificity of Cetuximab-IRDye800 for Surgical Navigation in Head and Neck Cancer. Clin Cancer Res, 2015. 21(16): p. 3658-66.
95. van Keulen, S., et al., Rapid, non-invasive fluorescence margin assessment: Optical specimen mapping in oral squamous cell carcinoma. Oral Oncol, 2019. 88: p. 58-65.
96. Voskuil, F.J., et al., Fluorescence-guided imaging for resection margin evaluation in head and neck cancer patients using cetuximab-800CW: a quantitative dose-escalation study. Theranostics, 2020. 10(9): p. 3994-4005.
97. Warram, J.M., et al., a ratiometric threshold for determining presence of cancer during fluorescence-guided surgery. J Surg Oncol, 2015. 112(1): p. 2-8.
98. De Leeuw, F., et al., Value of Full-Field Optical Coherence Tomography Imaging for the Histological Assessment of Head and Neck Cancer. Lasers in Surgery & Medicine, 2020. 18: p. 18.
99. Kodama, M., et al., Ultrasonography for intraoperative determination of tumor thickness and resection margin in tongue carcinomas. J Oral Maxillofac Surg, 2010. 68(8): p. 1746-52.
100. Tarabichi, O., et al., Intraoperative Ultrasound in Oral Tongue Cancer Resection: Feasibility Study and Early Outcomes. Otolaryngol Head Neck Surg, 2018. 158(4): p. 645-648.
101. Tominaga, K., et al., Intraoperative surgical clearance confirmation of tongue carcinomas using ultrasound. Dentomaxillofac Radiol, 2007. 36(7): p. 409-11.
102. Cariati, P., et al., Intraoperative cytological examination of bone medullary. a useful technique to predict the extension of bone invasion in segmental mandibulectomy. American Journal of Otolaryngology, 2019. 40(5): p. 743-746.
103. Namin, A.W., et al., Efficacy of bone marrow cytologic evaluations in detecting occult cancellous invasion. Laryngoscope, 2015. 125(5): p. E173-9.

Chapter 3

The oral cavity tumor thickness: measurement accuracy and consequences for tumor staging

S.G. Brouwer de Koning

M.B. Karakullukcu

C.A.H. Lange

T.J.M. Ruers

European Journal of Surgical Oncology (2019) https://doi.org/10.1016/j.ejso.2019.06.005

Abstract

Introduction

In the 8th edition of the AJCC/UICC cancer staging system (AJCC8), the depth of invasion (DOI) of the oral cavity tumor is the discriminative factor in tumor staging over the previously used greatest dimension (GD). In order to obtain a complete representation of how accurate we stage oral cavity cancer clinically, we evaluated the accuracy of measurements of the tumor dimensions on ultrasound (US) and magnetic resonance (MR) imaging by comparing this with the histopathology as the "golden standard". Secondly, we compared the pathological tumor staging of these tumors according to the AJCC7 and AJCC8, to evaluate the effect of the incorporation of the DOI in the AJCC8.

Materials and Methods

In a retrospective analysis, including 85 oral cavity tumors, the GD and tumor thickness (TT) measured on US and MR, were compared to histopathology with a Pearson correlation coefficient (R) and a Bland-Altman plot. The tumors were staged according to both the AJCC7 and AJCC8.

Results

TT was more reliably measured with US (R=0.67, limits of agreement=10.7mm), whereas GD was more reliably measured with MR (R=0.69, limits of agreement = 25.7mm). The AJCC8 staging resulted into a higher tumor stage in 21% of the cases, compared to the AJCC7.

Conclusion

For preoperative tumor staging, the TT is best estimated by the use of US. The incorporation of DOI in the AJCC8 can result in a higher tumor stage in more than twenty percent of the patients, with an associated worse prognosis for the patient.

Keywords

oral cavity tumor; tumor depth of invasion; ultrasound; MR imaging; histopathology; 8th edition of the AJCC/UICC cancer staging system.

Introduction

The AJCC/UICC cancer staging system is established to stage cancer according to the severity of the disease. The system describes the anatomical extent of the disease based on three components: T for the extent of the primary tumor, N for the involvement of regional lymph node metastasis and M for the presence of distant metastasis. The TNM stage of the cancer affects the planning of the treatment and gives an indication of prognosis and survival (1). In the previously used T classification for oral cavity cancer, the tumor's greatest dimension (GD) was the discriminating factor to stage the tumor in the different T categories (2). Because this measure has a suboptimal prognostic performance (3), the tumor's depth of invasion (DOI) has been evaluated for prognostic performance instead (4). The DOI reflects the proximity to underlying lymph-vascular structures and thus, can be considered as a predictor of the presence of pathologic lymph nodes (5, 6). Ebrahimi *et al.* showed in a retrospective analysis including 3,149 patients with oral squamous cell carcinoma, that the tumor's DOI is significantly associated with disease specific survival ($p<0.001$) (4). This analysis was reason for the Union for International Cancer Control to implement the DOI into the new AJCC8 (Table 1).

Table 1 Primary tumor staging (T) in 7th and 8th editions of the AJCC/UICC cancer staging system.

Tumor stage primary tumor	AJCC7†, 2009	AJCC8‡, 2017	
	Greatest dimension	**Greatest dimension**	**Depth of invasion**
T1	≤ 2 cm	≤ 2 cm	≤ 5 mm
T2	>2 - 4 cm	≤ 2 cm 2-4 cm	5 - 10 mm <10 mm
T3	> 4 cm	> 4 cm	> 10 mm

† 7th edition of the AJCC/UICC cancer staging system, ‡ 8th edition of the AJCC/UICC cancer staging system

GD and tumor thickness (TT) can be measured on pre-operative imaging, and can be very different from each other in e.g. large superficial tumors. Both the magnetic resonance imaging (MR) or ultrasound (US) have difficulties to overcome in accurate imaging of oral cavity cancer. Especially the imaging of small primary tumors can be challenging. The acquisition of an intra-oral US image can be hampered by the limited space in the oral cavity or in case the tumor is located too distant, making it difficult to reach (e.g. palate tumors). Artefacts due to tooth prostheses and movement from the swallowing reflexes make interpretation of the MR images difficult. Still, when comparing TT measured with US or MR and histopathology, Pearson correlation coefficients of up to 0.98 are reported in literature (7-10).

GD and DOI can be measured on the histopathology sections. Before the introduction of the AJCC8, TT and DOI measures were often incorrectly used interchangeably, while these two measures can be very different in an ulcerative tumor, for example. With the AJCC8, the definitions of the terms TT and DOI have become more specific (11). The TT is solely the thickness of the tumor, while the DOI is measured specifically from the basement membrane to the closest intact squamous mucosa. The latter is measured specifically on histopathological sections.

In order to obtain a complete representation of how accurate we measured oral cavity cancer, we conducted a retrospective study including all oral cavity cancer patients treated in our institute during the last 5 years. Our oral cavity tumor diagnostic protocol includes US and MRI of the oral cavity and neck. We compared GD and TT measurements from US and MR with the histopathology as the "gold standard". Secondly, we compared the pathological T staging of these patients according to the 7th and 8th edition of the AJCC/UICC cancer staging system to evaluate the effect of incorporating the DOI in the new T staging.

Materials and methods

Patient population

We selected all oral cavity cancer patients with a tumor that was clinically staged as T1 or T2, and of which US or MR images were acquired in our institute between 2011 and 2016. The tumor dimensions were measured with three modalities: US, MR and histopathology (Figure 1).

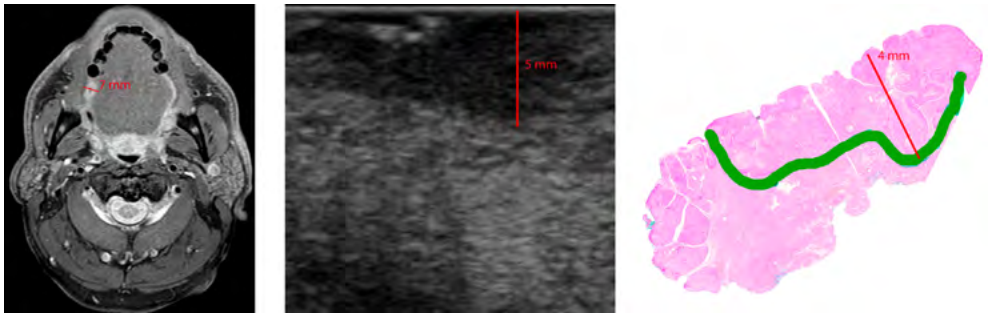

Figure 1 TT measured on MR, US and histopathology, respectively.

GD and TT measurements on US and MR

US images were acquired by the radiologist, with the Hitachi, EUB-900, and a 13-7 MHz transducer (EUP-O54J). The probe was positioned directly on the lesion, so that the TT and GD could be measured along the length and width axes. This is the standard way our radiologists use to describe the tumor with US.

MR examinations were performed on a Philips Achieva 3T scanner using a dedicated 16-channel SENSE neurovascular coil (Philips Medical Systems, Best, The Netherlands). The following MR sequences were used to measure GD and DOI: T1W TSE TRA, TR (repetition time), TE (echo time) 538/10 ms, flip angle 90, matrix 288/248, slice thickness 4 mm; STIR TSE COR, TR/TE 2500/60 ms, flip angle 90, matrix 216/170, slice thickness 4 mm; T1 3D Thrive fat-saturation, after intravenous injection of 15 cc gadoterate meglumine, TR/TE 9.86/4.59 ms, flip angle 10, matrix 200/179, slice thickness 1 mm. According to the standard protocol, the tumor dimensions were measured in 3D: the length and width axes were measured on all axial, sagittal and coronal slices. The radiologist reported on

the tumor dimensions, thereby suggesting the T stage for diagnosis discussions at the tumor board. These reported measurements were used for this study rather than renewing the measurements in a second read of the scan. We believe that these values represent the day to day practice better than careful re-measurements. The tumor dimensions were measured on the histopathology sections by the pathologist and recorded in the pathological report.

TT and GD were used for the correlation and agreement analysis with histopathology.

Correlation and agreement US and MR with histopathology

To compare GD and TT measured on US and MR, with the histopathology as a "gold standard", two different statistical methods were used. First the correlation between US/MR and histopathology was evaluated with Pearson's correlation coefficient. Two modalities were considered significantly correlated when $p<0.05$. The use of Pearson's correlation coefficient allows us to compare our results with that of other studies in this field. Pearson correlation coefficient and its p-value were calculated using SPSS statistical package version 22 (SPSS Inc, Chicago, IL).

Although Pearson's correlation coefficient gives insight in whether data of two data sets are correlated, it does not indicate agreement between two data sets (12). To evaluate the agreement between US/MR and histopathology, we analyzed the data with a Bland-Altman plot. a Bland-Altman plot shows the mean difference of two modalities with 95% confidence intervals as 'limits of agreement'. This allows easy interpretation of whether the difference of the two modalities is clinically relevant. The Bland-Altman plot measures the variation between the observations on US/MR and histopathology.

T staging according to the 7th and 8th editions of the AJCC/UICC cancer staging system

GD and DOI were used in comparing T stage according to AJCC7 and AJCC8. Using the GD measured on histopathology, the tumors were classified into T stage according to AJCC7. Taking also the DOI into account, the same cases were classified into T stage according to the AJCC8. Agreement between the classifications according to AJCC7 and AJCC8 was evaluated and rates of over/under staging using AJCC8 were calculated.

Results

Patient population

A total of 142 patients with oral cavity cancer were treated in our institute between 2011 and 2016. In 32 cases, tumor dimensions were reported by only one modality. Histopathology data was not available for 11 patients, because of their treatment with photodynamic therapy (PDT) instead of surgery. In 5 cases, US was acquired after the excision and in one patient, histopathology showed scar tissue instead of tumor tissue. In addition, the tumor was not assessable on US in 10 cases. Thus, the study population consisted of 83 patients, for whom at least one of the measures (GD/TT/DOI) was reported on histopathology and US or MR.

The mean age of the 83 included patients was 61 (ranging from 31 to 88). The population consisted of 45 men and 38 women. Two patients had two tumors, so that 85 tumors were included in the study.

The site of disease within the oral cavity was at the tongue (n=58), floor of the mouth (n=24), the palate (n=2) and the lip (n=1). All tumors were squamous cell carcinoma.

GD and TT data on US, MR and histopathology

US and MR measures were not reported for all included tumors (Table 2). TT was measured on US and histopathology in 76 of the 85 tumors. TT was measured on 46 of the 85 tumors using MR.

The GD was measured on US and histopathology for 44 of the 85 tumors, and on MR and histopathology for 47 of the 85 tumors.

Table 2 Number of tumors where TT and GD was measured on US and MR. Total number of tumors included in the study was 85.

	US and pathology	MR and pathology
Number of tumors where TT was measured on:	76	46
Number of tumors where GD was measured on:	44	47

Tumor thickness

Mean TT measured on US images was 5.1 mm (standard deviation STD: 3.1 mm) and the mean TT on the associated histopathology sections was 5.1 mm (STD: 3.5 mm). The TT measures for the MR dataset, using different data (see section 3.2), showed a mean TT of 7.4 mm (STD: 3.5 mm) that was found on MR and a mean TT of 6.1 mm (STD: 3.2 mm) that was reported on the histopathology sections.

There was a significant relationship between the TT measured on both US and MR with histopathology. US and histopathology measures of the TT were correlated with a Pearson's correlation coefficient of $r(76)=0.67$, $p<0.001$. MR and histopathology measures of the TT were correlated with a Pearson's correlation coefficient of $r(46)=0.38$, $p=0.009$.

The 95% limits of agreement (1.96*STD) comparing US and histopathology measurements were-5.3 mm to 5.4 mm (Figure 2). Mean difference between TT measured on US and histopathology was 0.05 mm (STD 2.7 mm). For MR and histopathology, the 95% limits of agreement were-6.1 mm to 8.6 mm (Figure 2). The mean difference between measurements on MR and histopathology was 1.3 mm (STD 3.7 mm).

In all, compared to MR, the TT measured on US showed a higher correlation and agreement with histopathology.

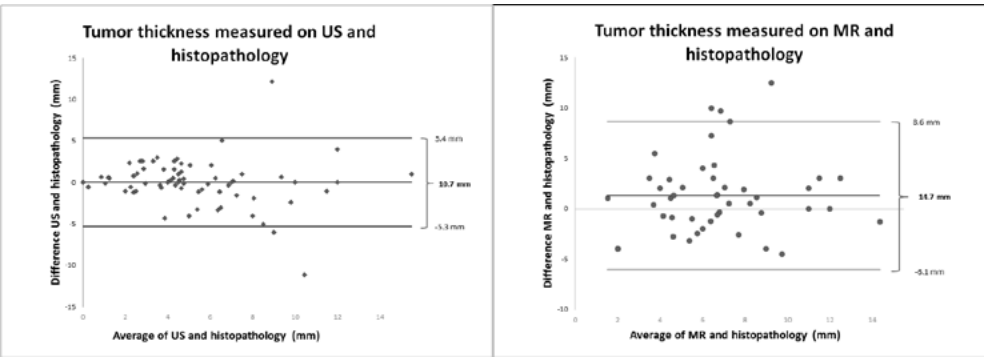

Figure 2 Bland Altman plot of TT measured on US (a, n = 76) and MR images (b, n = 46) compared to the TT measured on histopathological sections. Mean difference between the TT measured on US and histopathology was 0.05 mm, 95% limits of agreement -5.3 to 5.4 mm. Mean difference between the TT measured on MR images and histopathology was 1.3 mm, 95% limits of agreement -6.1 to 8.6 mm.

Greatest dimension

The GD was reported on US images (mean GD: 14.3 mm, STD: 5.1 mm) with associated histopathology sections (mean GD: 15.9 mm, STD: 8.6 mm). Similarly, but using a different data set (see section 3.2), the GD was reported from MR images (mean GD: 18.8 mm, STD: 7.6 mm) and associated histopathology sections (mean GD: 17.6 mm, STD: 8.8 mm).

There was a significant relationship between the GD measured on both US and MR with histopathology. US and histopathology measures of the GD were correlated with a Pearson's correlation coefficient of $r(44)=0.61$, $p<0.001$. MR and histopathology measures of the GD were correlated with a Pearson's correlation coefficient of $r(47)=0.69$, $p<0.001$.

The 95% limits of agreement of US and histopathology measurements of the GD were -14.9 mm to 11.7 mm (Figure 3). Mean difference between US and histopathology was 1.6 mm (STD 6.8 mm). The 95% limits of agreement of MR and histopathology measurements of the GD were –11.7 mm to 14 mm (Figure 3). Mean difference between MR and histopathology was 1.1 mm (STD 6.6 mm).

Compared to US, the GD measured on MR showed a higher correlation and agreement with histopathology.

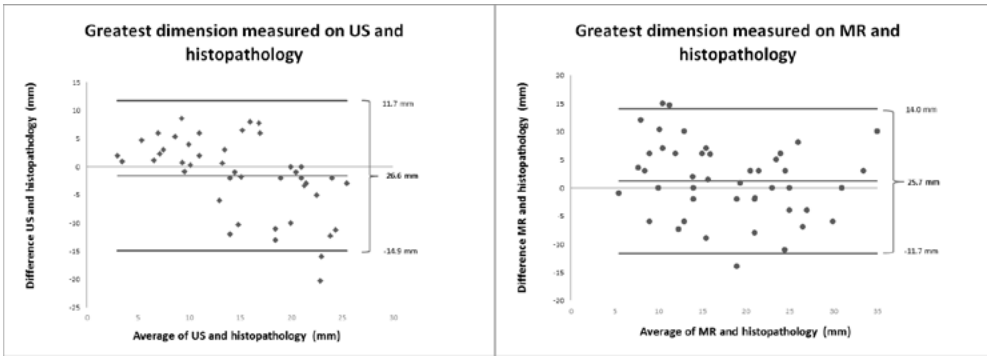

Figure 3 Bland Altman plot of GD of the tumor measured on US (a, n = 44) and MR images (b, n = 47) compared to the GD measured on histopathological sections. Mean difference between the GD measured on US and histopathology was -1.6 mm, 95% limits of agreement -14.9 to 11.7 mm. Mean difference between the GD measured on MR images and histopathology was 1.1 mm, 95% limits of agreement -11.7 to 14.0 mm.

T staging according to the 7th and 8th editions of the AJCC/UICC cancer staging system

Using the GD and DOI measured on the histopathology sections, AJCC7 and AJCC8 agreed in 67 out of 85 tumors (79%): 48 tumors were classified as T1 according to both staging systems, and 19 as T2 (Table 3). However, 18 out of 85 tumors (21%) were classified into a higher T class when staging with AJCC8. No tumors were classified in a lower category with AJCC8.

Discussion

In the AJCC8, DOI of the oral cavity tumor is the discriminative factor in tumor staging over the previously used GD. In this study, we have evaluated the accuracy of the tumor dimensions, measured preoperatively on US and MR images, that were performed before the introduction of AJCC8. This was done by comparing them with the histopathology as the "gold standard". With two different statistical analyses, we found that TT is more reliably measured with US (R=0.67, limits of agreement = 10.7 mm) and GD is more reliably measured with MR (R=0.69, limits of agreement = 25.7 mm). Secondly, we evaluated the pathological T staging of patients in our hospital according to both the AJCC7 and AJCC8, to assess the effect of incorporating the DOI in the new T staging. When staging according to the 8th edition, 21% of the tumors would have been classified into a higher T class.

One explanation for the difference in tumor thickness measurements based on MR- and US images might be the difference in indication of the two imaging modalities. US is performed with the focus on the TT. This is important for the decision on further treatment. On the contrary, the MR is indicated for staging of the disease, e.g. tumor dimension and tumor extension towards the neck. The MR was not indicated to measure TT specifically, because this was not required for tumor staging according to the AJCC7.

The Pearson correlation coefficient has often been used to compare tumor dimensions measured on US/MR with histopathology (Table 4). In literature, the correlation coefficient ranges between R=0.80-0.99 for US and histopathology, and between R=0.54-0.99 for MR and histopathology. In contrast to our retrospective analysis, most of these studies were prospective and did set up very specific selection criteria (e.g. specific tumor size and site). Alsaffar *et al.* argues that the correlation between MR and histopathology is less accurate for tumors smaller than 5 mm (R(9)= -0.211, p=0.56), compared to tumors larger than 5 mm (R(40) = 0.856, p<0.001) (13). Lwin *et al.* shows bad correlation (R(24) = 0.45, p=0.03) between MR and histopathology for tumors located in the floor of the mouth (14). When the latter performs their analysis on tongue tumors only, a much better correlation is found (R(43) = 0.87, p<0.001). Our aim was to give a reflection of the daily clinical situation and thus our analysis includes all types of oral cavity cancers, including tumors located in the floor of the mouth (23/85).

Table 3 T staging based on histopathology according to 7th and 8th editions of the AJCC/UICC cancer staging system. The number of tumors classified into a higher T stage by using the 8th edition over the 7th edition are shown in the aligned cells. The last row of the table shows this number of tumors classified into a higher T stage, as a percentage of the total number of tumors included.

Tumor stage Histopathology		**AJCC7†**	
		T1	**T2**
AJCC8‡	**T1**	48	0
	T2	10	19
	T3	1	7
		21%	

† 7th edition of the AJCC/UICC cancer staging system, ‡ 8th edition of the AJCC/UICC cancer staging system

Similar to our analysis, Yesuratnam *et al.* evaluated the US and MR agreement with histopathology also by using Bland-Altman plots. For US and histopathology, they found a mean difference of 1.28 mm (STD 3.55 mm, 79 patients) (15). Similarly, for MR and histopathology, they report on a mean difference of 2.99 mm (STD 4.41 mm) (78 patients). The associated measures in our findings were a difference of 0.05 mm (STD 2.7 mm, 76 patients) for US and histopathology and 1.3 mm (STD 3.7 mm, 44 patients) for MR and histopathology. Thus, for both US and MR, the agreement with histopathology was more accurate in our studies.

Many institutions use computerized tomography (CT) to stage patients preoperatively. Madana *et al.* compared the TT measured on preoperative CT scan and histopathology (16). Their retrospective study included 116 patients with a diagnosis of oral tongue squamous cell carcinoma, and they found a highly significant correlation between the TT measured on CT and histopathology. They suggest that although MRI may be superior to CT in the evaluation of soft tissue lesions, that their results support the use of CT in measuring TT.

Overall, it can be argued whether the histopathology is the best measurement to use as a “gold standard”, due to the pathological processing of the resected specimen. This process can result in specimen shrinkage (14). Also, the direction of the sliced histopathology sections is not the same as the slicing direction of MR slices, or the same angle of the US probe positioning.

According to our comparison between T staging according to the AJCC7 and AJCC8, more than twenty percent of the tumors will be classified into a higher T stage, due to the incorporation of the DOI in the T staging system. Clinically, this will mean that patients will receive radiotherapy and chemotherapy more often.

Conclusion

This retrospective analysis has shown that the oral cavity tumor thickness is more accurately measured with US than MR for preoperatively tumor staging. More value should be acknowledged to the TT measured by US when staging the tumor during tumor board. We predict that with the incorporation of the DOI in the AJCC8, more than twenty percent of the oral cavity tumors will be classified into a higher T stage, with an associated worse prognosis for the patient.

References

1. O'Sullivan B, Brierley J, Gospodarowicz M, Wittekind C. UICC TNM classification of Malignant Tumours. Eighth ed. Wiley. 2017.
2. Sobin L, Gospodarowicz M, Wittekind C. UICC TNM classification of Malignant Tumours. Seventh ed. Wiley. 2009.
3. Kreppel M, Drebber U, Rothamel D, Eich HT, Kubler A, Scheer M, et al. Prognostic impact of different TNM-based stage groupings for oral squamous cell carcinoma. Head Neck. 2011;33(10):1467-75.
4. International Consortium for Outcome Research in Head and Neck Cancer, Ebrahimi A, Gil Z, Amit M, Yen TC, Liao CT, et al. Primary tumor staging for oral cancer and a proposed modification incorporating depth of invasion: an international multicenter retrospective study. JAMA Otolaryngol Head Neck Surg. 2014;140(12):1138-48.
5. Pinto FR, de Matos LL, Palermo FC, Kulcsar MA, Cavalheiro BG, de Mello ES, et al. Tumor thickness as an independent risk factor of early recurrence in oral cavity squamous cell carcinoma. Eur Arch Otorhinolaryngol. 2014;271(6):1747-54.
6. Mucke T, Kanatas A, Ritschl LM, Koerdt S, Tannapfel A, Wolff KD, et al. Tumor thickness and risk of lymph node metastasis in patients with squamous cell carcinoma of the tongue. Oral Oncol. 2016;53:80-4.
7. Goel V, Parihar PS, Parihar A, Goel AK, Waghwani K, Gupta R, et al. Accuracy of MRI in Prediction of Tumour Thickness and Nodal Stage in Oral Tongue and Gingivobuccal Cancer With Clinical Correlation and Staging. J Clin Diagn Res. 2016;10(6):TC01-5.
8. Kodama M, Khanal A, Habu M, Iwanaga K, Yoshioka I, Tanaka T, et al. Ultrasonography for intraoperative determination of tumor thickness and resection margin in tongue carcinomas. J Oral Maxillofac Surg. 2010;68(8):1746-52.
9. Mark Taylor S, Drover C, Maceachern R, Bullock M, Hart R, Psooy B, et al. Is preoperative ultrasonography accurate in measuring tumor thickness and predicting the incidence of cervical metastasis in oral cancer? Oral Oncol. 2010;46(1):38-41.
10. Yamane M, Ishii J, Izumo T, Nagasawa T, Amagasa T. Noninvasive quantitative assessment of oral tongue cancer by intraoral ultrasonography. Head Neck. 2007;29(4):307-14.
11. Lydiatt WM, Patel SG, O'Sullivan B, Brandwein MS, Ridge JA, Migliacci JC, et al. Head and Neck cancers-major changes in the American Joint Committee on cancer eighth edition cancer staging manual. CA Cancer J Clin. 2017;67(2):122-37.
12. Khan K, Chien P. Evaluation of a clinical test. I: Assessment of reliability. British Journal of Obstetrics and Gynaecology. 2001;108:562-7.
13. Alsaffar HA, Goldstein DP, King EV, de Almeida JR, Brown DH, Gilbert RW, et al. Correlation between clinical and MRI assessment of depth of invasion in oral tongue squamous cell carcinoma. J Otolaryngol Head Neck Surg. 2016;45(1):61.
14. Lwin CT, Hanlon R, Lowe D, Brown JS, Woolgar JA, Triantafyllou A, et al. Accuracy of MRI in prediction of tumour thickness and nodal stage in oral squamous cell carcinoma. Oral Oncol. 2012;48(2):149-54.
15. Yesuratnam A, Wiesenfeld D, Tsui A, Iseli TA, Hoorn SV, Ang MT, et al. Preoperative evaluation of oral tongue squamous cell carcinoma with intraoral ultrasound and magnetic resonance imaging-comparison with histopathological tumour thickness and accuracy in guiding patient management. Int J Oral Maxillofac Surg. 2014;43(7):787-94.
16. Madana J, Laliberte F, Morand GB, Yolmo D, Black MJ, Mlynarek AM, et al. Computerized tomography based tumor-thickness measurement is useful to predict postoperative pathological tumor thickness in oral tongue squamous cell carcinoma. J Otolaryngol Head Neck Surg. 2015;44:49.
17. Lodder WL, Teertstra HJ, Tan IB, Pameijer FA, Smeele LE, van Velthuysen ML, et al. Tumour thickness in oral cancer using an intra-oral ultrasound probe. Eur Radiol. 2011;21(1):98-106.
18. Park JO, Jung SL, Joo YH, Jung CK, Cho KJ, Kim MS. Diagnostic accuracy of magnetic resonance imaging (MRI) in the assessment of tumor invasion depth in oral/oropharyngeal cancer. Oral Oncol. 2011;47(5):381-6.
19. Songra AK, Ng SY, Farthing P, Hutchison IL, Bradley PF. Observation of tumour thickness and resection margin at surgical excision of primary oral squamous cell carcinoma--assessment by ultrasound. Int J Oral Maxillofac Surg. 2006;35(4):324-31.
20. Yuen AP, Ng RW, Lam PK, Ho A. Preoperative measurement of tumor thickness of oral tongue carcinoma with intraoral ultrasonography. Head Neck. 2008;30(2):230-4.
21. Lam P, Au-Yeung K, Cheng P, Wei W, Yuen A, Smith N, et al. Correlating MRI and Histologic Tumor Thickness in the Assessment of Oral Tongue Cancer. American Journal of Roentgenology. 2004;182:803-8.

Chapter 4

Ultrasound aids in intraoperative assessment of deep resection margins of squamous cell carcinoma of the tongue

S.G. Brouwer de Koning

M.B. Karakullukcu

C.A.H. Lange

W.H. Schreuder

L.H.E. Karssemakers

T.J.M. Ruers

British Journal of Oral & Maxillofacial Surgery (2020) https://doi.org/10.1016/j.bjoms.2019.11.013

Abstract

Introduction

We wanted to find out whether ultrasound (US) can be used to assess the deep resection margins after excision of squamous cell carcinoma (SCC) of the tongue, as intraoperative feedback on their condition might help to prevent them being too close. Resected specimens of cancers of the tongue from 31 patients with SCC of the tongue were suspended in US gel and scanned with a small 5-10 MHz US probe. The tumour was readily visible and US could differentiate it from muscle tissue. The margin of normal tongue musculature surrounding the tumour was measured on the US images, and the minimal resection margin was noted and compared with that reported by the histopathologist. The mean (SD) deep resection margins measured on the US images differed by 1.1 (0.9) mm from those reported by the histopathologist (Pearson's correlation coefficient: 0.79, $p < 0.01$). The US measurements took a maximum of five minutes. It is feasible to use US to assess resection specimens of SCC of the tongue as an adjunct to existing strategies (such as frozen section analysis) to help achieve the desired deep surgical margins. The method is easy to incorporate into surgical routine as it does not take long.

Keywords

squamous cell carcinoma of the tongue; deep resection margin; ultrasound; intraoperative resection margin assessment; histopathology.

Introduction

Up to 80% of patients diagnosed with a tumour of the oral cavity stage 1 or 2, have it resected as the primary treatment (1) and there is considerable discussion about how wide the surgical margin should be to be considered adequate. Many national guidelines follow the norms set by the UK Royal College of Pathologists, and accept a minimum of 5 mm as an adequate margin (2,3) so surgeons aim to remove the tumour with at least a 5 mm margin of healthy tissue. We know of no standard intraoperative methods other than frozen section analysis to provide information about the involvement of these margins by tumour cells. As this method prevents involved margins, it provides no information about the extentof achieved clear margins, especially the soft tissue margins. The tumour resections are reported to be less than radical (tumour cells found at the resection surface) or with closemargins (tumour cells found within 1-5 mm from the resection surface) in up to 85% of the patients (4). As patients need to have a successive operation to remove residual disease, or need to be given adjuvant radiotherapy, technology that provides intraoperative feedback on the condition of the margins would be indispensable.

Recently, Tarabichi et al published a systematic review on the use of intraoral ultrasound in the management of squamous cell carcinoma (SCC) of the tongue (5). From the 19 papers included in their analysis, they concluded that ultrasound (US) is useful in the evaluation of cancers of the tongue. Several studies show that intraoral US can accurately show the thickness of the tumour: Pearson's correlation coefficients of up to 98% have been reported when comparing the thickness of tumour measured on US with the corresponding histopathological measurement. (6–8) US is therefore a technique that can image the border between tumour and healthy tissue accurately, and this encourages us to investigate using US for intraoperative assessment of the margins of the freshly-excised specimen (9).

We know of six studies that have been looking into the use of US to assess the clearance of resection margins in tongue cancer specimens. US has been used to provide guidance when positioning sutures or needles to point out the safety margin during the resection (6,10,11). In those studies, the resection margins were adequate as verified by the histopathological slides. Songra et al (12) used a different intraoperative method, and showed the cut surface on US by placing a metal retractor into the surgical cut, halfway through the resection. They compared the clearance of deep margins measured by US with the histopathological slide, and reported a Pearson's correlation coefficient of 0.648 ($p < 0.01$) based on 14 tumours of the oral cavity (11 that affected the tongue) (12).

As well as using US as guidance *in vivo* during the resection, US can be used to evaluate the margins of the resected specimen *ex vivo*. Tominaga et al immersed the fresh specimen in a gelatin solution to maintain its original shape and orientation, then refrigerated this for 20 minutes so that the gelatin could solidify (13). Trying this approach on three patients with tumours of the lateral tongue, they found that fine images could be obtained easily and with no specialist skills.

Tarabichi et al used US to measure the width of the deep margin of the resected specimens of 12 patients, but as this was not the focus of their study they did not relate the deep margin found on the US to that reported by the histopathologist (14). As far as we know, therefore, there are no studies that have reported the *ex vivo* measurement of the deep resection margins of specimens of tongue cancer using US verified by histopathological examination. Further research using standard imaging protocols

and well-defined groups of patients is to be encouraged (5), and this study can be taken to be a first response to the recommendation. We have evaluated whether US is a feasible technique to measure the deep resection margin of specimens of tongue cancer during routine operations.

Material and methods

Specimens of resected SCC of the tongue from patients that were treated at the Netherlands Cancer Institute-Antoni van Leeuwenhoek hospital, Amsterdam, The Netherlands, were included in the study. All ethical guidelines for *ex vivo* human studies were followed.

The SCC were resected in the conventional way. The freshly resected specimens were suspended in ultrasound gel, orientated with the surface of the tumour at the top. This was done to create a contrast between the deep resection margin and the gel, and to prevent the specimen from being compressed by the ultrasound probe. The small 5-10 MHz probeof the ALOKA ProSound SSD-Alpha 5 (ALOKA Co. Ltd) was placed on the mucosal surface of the specimen, taking care not to apply pressure. Specimens were scanned with the US probe in two axes (coronal and sagittal, or coronal and axial). US images were acquired by three authors (radiologist, surgeon, and research worker). All measurements took less than five minutes, and the minimal deep resection margins were noted.

After the US measurements, the specimen was taken to the histopathology department for standard processing, which comprised inking of the resection margins, placement in formalin, and embedding in paraffin wax. The specimen was subsequently sectioned and stained with haematoxylin and eosin. The slices were analysed by the histopathologist, who reported the closest distance between tumour cells and the inked deep resection surface (soft tissue margin).

Statistical analysis

The minimal resection margin found on US was verified with the minimal resection margin reported by the histopathologist (used as the gold standard, Figure 1). The degree of correlation was expressed using Pearson's correlation coefficient, in which the US and histopathological measurements were considered to be significantly correlated when $p < 0.05$. To evaluate the agreement between US and histopathological measurements, we also analysed the data using a Bland-Altman plot, which shows the mean difference of two techniques with 95% CI as "limits of agreement". This allows for easy interpretation of whether the difference between US and histopathological measurement is clinically relevant.

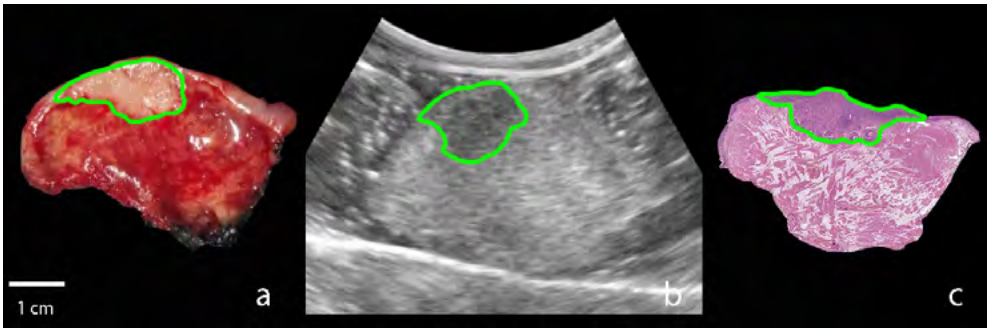

Figure 1 (a) Macroscopic colour image of the cloven tongue specimen with the tumour (green), corresponding with the ultrasound image plane (b) and the histopathological slide (c) (haematoxylin and eosin).

Results

A total of 31 specimens with SCC of the tongue were included in the study, 25 of which were located at the lateral tongue. Two were at the base, two at the dorsal surface, and two at the ventral surface of the tongue. Eleven of the tumours were staged as T1, 16 as T2, one as T3, and three as T4. In all cases, the specimen, surrounded by the gel, could be imaged without compression by the probe, and the tumour was visible as a hypointense mass on the US image (Figure 2). Table 1 gives the details of each tumour and, in 19 of the 31, the minimal resection margin measured on US was within a 1 mm range of the margin measured on the histopathological sections.There was a significant relation between the minimal margin measured on the US images and histopathology sections (Pearson's correlation coefficient $r(31) = 0.79$, $p < 0.01$).

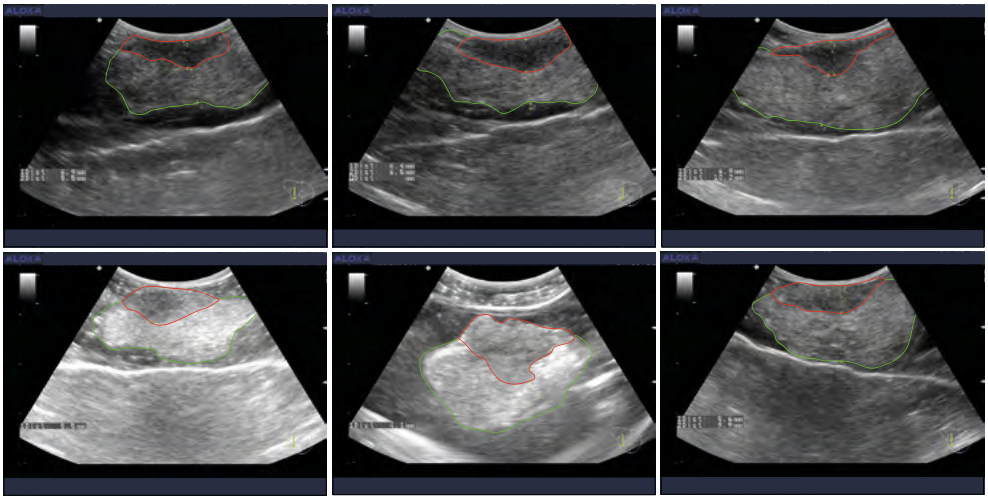

Figure 2 Various examples of resection margins measured with ultrasound (tumour = red, healthy margin = green).

Table 1 Details of tumours on ultrasound (US) and histopathological examination.

Case	TNM stage	Tumor Location	Minimal resection margin measured on US (mm)	Minimal resection margin measured on histopathology (mm)	Absolute difference (mm)
1	T2N2bMx	Lateral tongue	6.9	4.5	2.4
2	T4N1/2b	Tongue base	6	7	1
3	T2N0M0	Lateral tongue	7.5	9	1.5
4	T2N2bM0	Lateral tongue	5.1	6	0.9
5	T2N0Mx	Lateral tongue	4.3	5	0.7
6	T2N0M0	Lateral tongue	7.8	9	1.2
7	T1N0M0	Lateral tongue	8.4	10	1.6
8	T1N0Mx	Lateral tongue	7.1	9	1.9
9	T1N0M0	Lateral tongue	9	6	3
10	T4N0M0	Lateral tongue	3	3	0
11	T1cN0Mx	Dorsal surface of the tongue	6.7	6	0.7
12	T2N0M0	Lateral tongue	4.7	4	0.7
13	T1N0M0	Tongue base	3.7	4	0.3
14	T2N0M0	Lateral tongue	5.1	5	0.1
15	T1N0Mx	Lateral tongue	5.1	7	1.9
16	T2N0M0	Dorsal surface of the tongue	6	4	2
17	T1N0M0	Ventral surface of the tongue	7.2	7	0.2
18	T2N0Mx	Lateral tongue	4	3	1
19	T2N0M0	Lateral tongue	5.5	4.5	1
20	T2N0M0	Lateral tongue	9.9	9	0.9
21	T1N0M0	Lateral tongue	6	6	0
22	T1N0Mx	Lateral tongue	4.4	4	0.4
23	T4N2M0	Lateral tongue	7.4	5	2.4
24	T2N0M0	Lateral tongue	5.2	5	0.2
25	T1N0Mx	Lateral tongue	6.9	8	1.1
26	T2N0Mx	Lateral tongue	5.5	5	0.5
27	T2N0M0	Lateral tongue	4.7	4.5	0.2
28	T3N0M0	Lateral tongue	2,2	1,5	0,7
29	T1N0M0	Lateral tongue	5,5	9	3,5
30	T2N0M0	Lateral tongue	3,9	2	1,9
31	T1N0Mx	Ventral surface of the tongue	9	10	1
				Mean absolute difference (mm)	1.13 ± 0.9

The mean absolute difference was 1.1 (0.9) mm between the US and histopathological measurements, and the difference between them in 95% of the cases was within the range of -2.74 to 2.85 mm (95% limits of agreement, Figure 3).

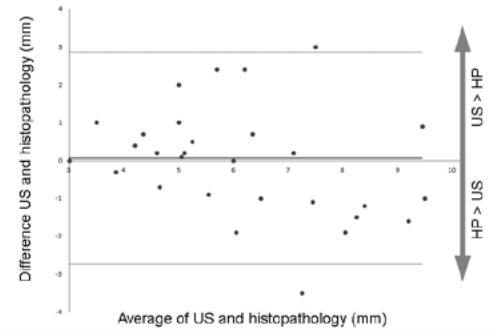

Figure 3 Bland Altman plot of the deep margin measured on ultrasound and histopathology (mean difference =0.05 mm, 95% limits of agreement -2.74 to 2.85 mm). Most of the ultrasound measurements agree with the histopathological ones.

Discussion

We have looked at 31 freshly-resected specimens of tongue cancer, to find out whether it is possible to estimate the minimal resection margin by using US in a simple way that can provide immediate feedback to the surgeon. In 19 of the 31, the minimal resection margin measured on US was within a 1 mm range of the margin measured on the histopathological sections.

In the cases where the margin measured on US was an overestimation, a possible explanation could be shrinkage of the specimen during the time between excision and fixation in the pathology department. El-Fol et al reported a mean discrepancy between margins measured *in situ* and the histopathological margin of up to 33% in 20 specimens of tongue cancer (15). Underestimation of the margin measured on US could be a result of pressure from the US probe, although this pressure was minimised as much as possible by suspending the specimen in US gel. Another explanation could be that microscopic infiltrations were not visible on US images but were found on microscopic histopathological analysis. This could be evaluated with a more accurate slice-by-slice comparison of US and histopathological specimens. We only aimed to evaluate the performance of a simple and quick procedure: US scanning of the whole volume of the tumour.

Intraoperative assessment of resection margins requires a technique that is easy to use by the surgeons themselves, as it is not logistically possible to have a radiologist in the surgical department. We invited a radiologist in this early stage of the research to show us how to acquire optimal US images. However, also during this early stage of the research, we wanted surgeons to make the measurements by themselves as that will be the final aim of the study. The method we used does not require extensive training of the operator and is therefore easy to implement in the surgical routine. However, an operatorindependent technique is preferable. As the current study showed, the potential for using US in measuring the resection margin during operation as a first try, we recommend that future studies should try to find operator- independent ways of acquiring US images of excised specimens.

We have shown that the tumour tissue and healthy tongue(muscle) can be distinguished on US images, which shows potential for operations involving SCC of the tongue. However, it does not guarantee similar results on tumours located at other sites of the oral cavity. We predict that as long as the discrimination between SCC and healthy muscle needs to be made, US could be of potential use. However, when the discrimination between tumour and healthy tissue does not involve SCC and healthy muscle, the technique has to be evaluated with a new validation study.

Consecutive studies will focus on expanding the dataset, so that conclusions can be drawn as to whether the site or the size of the tumour, and the depth of invasion, can affect the US measurement of the margin.

We encourage future research to explore the effect of immediate feedback to the surgeon about the condition of the margins. At present, the only currently available tool for such immediate feedback is frozen section taken from the specimen or the resection bed. Sampling the margins of the specimen seems to be the better option to clear them (16). However, the frozen section sampling does not tell the surgeon what extent of healthy tissue has been removed. Frozen section analysis of the whole volume of the removed specimen is not feasible because of the time it would take, and it would jeopardise further histopathological analysis. a technique such as that used in this study will therefore provide the surgeon with valuable information about the extent of the healthy tissue margin and allow removal of extra resection margins. Steens et al reported on the use of ex-vivo magnetic resonance imaging (MRI) to evaluate the resection margins of specimens of tongue (17). In six of the seven specimens, the resection margin found on MRI was within a 2 mm range of the histopathologist's measurement. However, *ex vivo* MRI needs optimisation to reduce the scanning time and be able to give an outcome on the resection margins during operation.

Measurements with US are not time-consuming and are easy to make. It is available in almost any operation complex and is not expensive to use. Our rather simple approach of suspending the specimen in a lump of gel and evaluating the deep resection margin on the excised specimen allows immediate feedback to the surgeon. This is easier and less time consuming than the workflow described in other studies, where the specimen was fixed in gelatin and refrigerated for 20 minutes, (13) or where the deep resection margin was marked with needles during the resection (11).

So far, Songra et al are the only group that have reported a Pearson's correlation coefficient by using US for assessment of deep resection margins during the resection. However, their approach differs from ours in that they measured the deep resection margin halfway through the resection, by placing a metal retractor into the surgical incision. The orientation of the specimen to the resection bed is an issue that needs to be solved when our technique is used. Now that the correlation of the margins as measured by US and histopathologically has been confirmed by this study, our group will be concentrating on implementing the method by developing techniques to provide the surgeon with the site of the inadequate margins to facilitate extra resections.

Conclusions

US is a feasible technique for intraoperative estimation of the deep resection margins of a tumour specimen from the tongue. The method can be used as an adjunct to standard techniques such as frozen section analysis, and is easy to implement during the surgical operation because of the short measurement time.

References

1. National Cancer Registration and Analysis Service and Cancer Research UK. Chemotherapy, radiotherapy and tumour resections in England: 2013-2015; 2019. Available from URL: https://www.cancerdata.nhs.uk/treatments Last accessed 28 November2019.
2. Woolgar JA, Triantafyllou A. a histopathological appraisal of surgical margins in oral and oropharyngeal cancer resection specimens. Oral Oncol 2005;41:1034–43.
3. Helliwell TWJ, The Royal College of Pathologists, Standards and Minimum Datasets for Reporting Common Cancers. Minimum dataset for head and neck histopathology reports; 1998. Available from URL: https://www.ncbi.nlm.nih.gov/pmc/articles/PMC4873923. Last accessed 14 November 2019.
4. Smits RW, Koljenovic S, Hardillo JA, et al. Resection margins in oral cancer surgery: room for improvement. Head Neck 2016;38(suppl.1):E2197–203.
5. Tarabichi O, Bulbul MG, Kanumuri VV, et al. Utility of intraoral ultrasound in managing oral tongue squamous cell carcinoma: systematic review. Laryngoscope 2018;129:662–70.
6. Kodama M, Khanal A, Habu M, et al. Ultrasonography for intraoperative determination of tumor thickness and resection margin in tongue carcinomas. J Oral Maxillofac Surg 2010;68:1746–52.
7. Mark Taylor S, Drover C, Maceachern R, et al. Is preoperative ultrasonography accurate in measuring tumor thickness and predicting the incidence of cervical metastasis in oral cancer? Oral Oncol 2010;46:38–41.
8. Yamane M, Ishii J, Izumo T, et al. Noninvasive quantitative assessment of oral tongue cancer by intraoral ultrasonography. Head Neck 2007;29:307–14.
9. Klein Nulent TJW, Noorlag R, Van Cann EM, et al. Intraoral ultrasonography to measure tumor thickness of oral cancer: a systematic review and meta-analysis. Oral Oncol 2018;77:29–36.
10. Helbig M, Flechtenmacher C, Hansmann J, et al. Intraoperative B-mode endosonography of tongue carcinoma. Head Neck 2001;23:233–7.
11. Baek CH, Son YI, Jeong HS, et al. Intraoral sonography-assisted resection of T1-2 tongue cancer for adequate deep resection. Otolaryngol Head Neck Surg 2008;139:805–10.
12. Songra AK, Ng SY, Farthing P, et al. Observation of tumour thickness and resection margin at surgical excision of primary oral squamous cell carcinoma—assessment by ultrasound. Int J Oral Maxillofac Surg 2006;35:324–31.
13. Tominaga K, Yamamoto K, Khanal A, et al. Intraoperative surgical clearance confirmation of tongue carcinomas using ultrasound. Dentomaxillofac Radiol 2007;36:409–11.
14. Tarabichi O, Kanumuri V, Juliano AF, et al. Intraoperative ultrasound in oral tongue cancer resection: feasibility study and early outcomes. Otolaryngol Head Neck Surg 2018;158:645–8.
15. El-Fol HA, Noman SA, Beheiri MG, et al. Significance of post-resection tissue shrinkage on surgical margins of oral squamous cell carcinoma. J Craniomaxillofac Surg 2015;43:475–82.
16. Chiosea SI. Intraoperative margin assessment in early oral squamous cell carcinoma. Surg Pathol Clin 2017;10:1-14.
17. Steens SCA, Bekers EM, Weijs WLJ, et al. Evaluation of tongue squamous cell carcinoma resection margins using ex-vivo MR. Int J Comput Assist Radiol Surg 2017;12:821–8.

Chapter 5

Towards complete oral cavity cancer resection using a handheld diffuse reflectance spectroscopy probe

S.G. Brouwer de Koning

E.J.M. Baltussen

M.B. Karakullukcu

B. Dashtbozorg

L. A. Smit

R. Dirven

B.H.W. Hendriks

H.J.C.M. Sterenborg

T.J.M. Ruers

Journal of Biomedical Optics (2018) https://doi.org/10.1117/1.JBO.23.12.121611

Abstract

Introduction

This *ex vivo* study evaluates the feasibility of diffuse reflectance spectroscopy (DRS) for discriminating tumor from healthy tissue, with the aim to develop a technology that can assess resection margins for the presence of tumor cells during oral cavity cancer surgery. Diffuse reflectance spectra were acquired on fresh surgical specimens from 28 patients with oral cavity squamous cell carcinoma. The spectra (400-1600 nm) were detected after illuminating tissue with a source fiber at 0.3, 0.7, 1.0 and 2.0 mm distances from a detection fiber, obtaining spectral information from different sampling depths. The spectra were correlated with histopathology. a total of 76 spectra were obtained from tumor tissue and 110 spectra from healthy muscle tissue. The first-order and second-order derivatives of the spectra were calculated and a classification algorithm was developed using 5-fold cross-validation with a linear support vector machine. The best results were obtained by the reflectance measured with a 1 mm source-detector distance (sensitivity, specificity and accuracy, respectively 89%, 82%, and 86%). DRS can accurately discriminate tumor from healthy tissue in an *ex vivo* setting using a 1 mm source-detector distance. Accurate validation methods are warranted for larger sampling depths to allow for guidance during oral cavity cancer excision.

Keywords

resection margin assessment, diffuse reflectance spectroscopy, oral cavity cancer, tissue recognition, machine learning, linear support vector machine.

Introduction

Patients with early stage oral cavity squamous cell carcinoma are generally treated with surgery. Surgeons aim to remove the tumor with a margin of healthy tissue, to ensure optimal local control and prognosis.

The extent of the margin is a trade-off between removing enough tissue to ensure clear margins, and sparing as much healthy tissue as possible for good functional outcome. During surgery, information about the extent of the tumor is limited to the surgeon's palpation of the tumor and pre-operative radiological assessment with magnetic resonance (MR) and/or ultrasound (US) imaging. Other than palpation, there is no real-time feedback about tumor borders. In general, the deep resection plane is the most challenging location to achieve well clear margins. Hence, in up to 30-85% of the patients, the tumor is removed with an involved or close margin of healthy tissue (i.e. an involved margin, in which tumor cells are present at the resection surface, or a close margin, in which tumor cells are found within 5 mm from the resection surface) (1). The majority of these patients need adjuvant treatment with either additional surgery, radiotherapy or sometimes chemo radiation. To reduce the number of patients needing adjuvant treatment, there is an urgent need for a technology which can provide real-time feedback on the presence of tumor cells at the resection margins.

In diffuse reflectance spectroscopy (DRS), diffusely reflected light is measured after illuminating the tissue with a broadband white light source using fiber optics. The reflectance spectrum contains information about the absorption and scattering properties of the illuminated tissue, representing an 'optical fingerprint' of the tissue. This technology can be incorporated into a handheld probe for intra-operative tissue characterization.

Within our research group, this technology has been investigated for the ability to discriminate tumor from healthy tissue in lung, liver, breast and colorectal cancer specimens (2-5). For example, using the fat and water content obtained from the near infrared (NIR) part of the reflectance spectrum, it was possible to distinguish tumor from healthy fat tissue in breast specimens with a sensitivity and specificity of 100% (4). Similar numbers were obtained in discriminating colorectal cancer from healthy colorectal wall (muscle) using an advanced classification algorithm on both the visual and the NIR part of the spectrum (5).

DRS and related technologies have been investigated for use as non-invasive screening tools for early detection of malignancies in the oral cavity (6-13). These studies focused on the discrimination between (pre-)malignant, benign, and healthy mucosa. The instruments used, measured the reflected light over a wavelength range within 350-1000 nm and translated the measured spectra into tissue components. Amelink *et al.* measured a significant decrease in microvascular oxygenation and scattering amplitude, and an increase in blood content and scattering slopes in tumor tissue, compared to healthy mucosa (7). Likewise, Stephen *et al.* showed that tumor tissue reflects more light of the two wavelengths 545 nm and 575 nm, the wavelengths specifically for the absorption by oxyhemoglobin components, compared to healthy mucosa (12). In various studies, sensitivities of 82-97% and specificities of 87-100% have been reported for discriminating oral cavity tumor from healthy mucosa (9, 11, 12).

In contrast to these studies, which concentrate on early tumor detection on the mucosal surface, we aim to use DRS as an intra-operative tool to evaluate the deep resection plane of oral cavity tumors. Hence we want to differentiate tumor tissue from healthy muscle tissue at the resection plane of the deep resection margin. Furthermore, the main absorber in the visual wavelength range, used by the studies mentioned above, is blood. They showed that the detection of the microvasculature played a significant role for tumor diagnosis. In contrast to those studies, we would like to use the technology intra-operatively, in an environment where blood is present, and where the blood components will not indicate the tissue type that has been measured. Thus, for intra-operative use of the DRS technology, we extended our wavelength range towards the NIR (1000-1700 nm) in which the absorption of light by blood is negligible (2, 4).

With the aim to assess the deep resection margin during oral cavity cancer surgery, we evaluated whether DRS (400-1600 nm) can discriminate tumor from healthy oral muscle tissue, in an *ex vivo* setting.

Materials and methods

Patient population

Patients undergoing surgery for the removal of oral cavity cancer were considered for this study. Despite different locations of the tumors throughout the oral cavity, all measurements were performed on the same tumor type and on healthy oral muscle tissue. All patients were treated in the Netherlands Cancer Institute-Antoni van Leeuwenhoek, Amsterdam. All ethical guidelines for *ex vivo* human studies were followed.

Diffuse Reflectance Spectroscopy

Measurements were obtained with a system consisting of a broad-band Tungsten halogen light for illumination and two different spectrometers to record the diffuse reflectance spectra from the tissue. The first spectrometer contained a silicon detector resolving the visual light between 400 and 1100 nm (Andor Technology, DU420A-BRDD), and the second spectrometer contained an InGaAs detector resolving light in the NIR region from 800 to 1700 nm (Andor Technology, DU492A-1.7) (14). The optical fibers guiding the light from the light source towards the tissue and the light reflected from the tissue towards the spectrometers are in contact with the tissue via a handheld probe. Multiple diffuse reflectance spectra were obtained for different distances between source fiber and detector fiber: 0.3 mm, 0.7 mm, 1 mm and 2 mm (Figure 1). Different source detector distances were used to obtain different sampling depths.

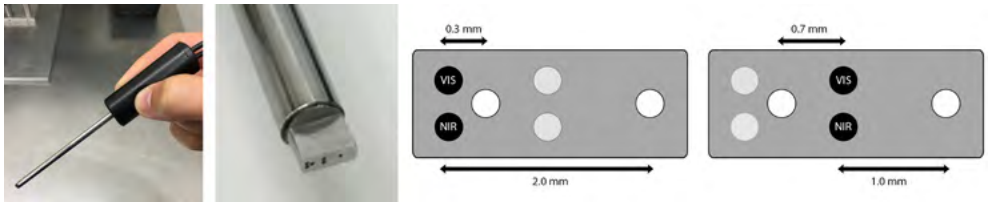

Figure 1 (a) The handheld probe of the DRS system used, with a close up of the tip of the probe (b). Two different fiber configurations (c,d) are used to obtain the diffuse reflectance spectra from four different distances between source and detection fibers.

Measurement workflow

Directly after resection, the specimen was brought to the pathology department, where the resection margins were inked according to standard pathological protocol. The pathologist localized the tumor by palpation, and cut the specimen into two parts, right through the middle of the tumor. At the cut surface, suspected tumor and healthy tissue areas were pointed out by the pathologist. Based on this, the measurement locations were chosen in both tumor tissue and healthy muscle tissue. An RGB (red, green, blue) image was taken from the cut surface for registration purposes. DRS measurements were acquired and the probe's position for each measurement was recorded on an RGB image. The spectroscopy system could only measure on two fibers simultaneously. As a consequence, all measurements were first acquired with the 2 mm and 0.3 mm fiber distance. Subsequently, to acquire the measurements for the 1 mm and 0.7 mm fiber distances, the probe was positioned at the same location on the basis of the RGB images. Thereafter, the specimen was brought back to the pathology department for further routine pathological processing.

Pathology registration

The locations measured with the DRS probe had to be matched with the corresponding locations on the histopathology slide, in order to confirm the tissue type that was measured. For this, a digital scan was made of the histopathological slide taken from the cut surface which was registered to the RGB image (Figure 2). Due to the fact that the specimen was deformed during the histopathological processing, a non-rigid registration algorithm was used for the registration. In this algorithm, obviously matching points in both the histopathological slide and the RGB image were visually selected. On the histopathological slide, the pathologist delineated tumor and healthy muscle tissue. The measurement locations were drawn on the RGB image, based on the images taken from the probe's position during each measurement. An overlay of the delineated registered histopathological slide on the RGB image containing the measurement locations, enabled determination of the measured tissue type for each measurement. Only measurements acquired at locations with an undisputed tissue type were included in the analysis, meaning that the probe was positioned on one tissue type only, and not on a boundary between two different tissue types. For algorithm development, such 'pure' tissue classes are obligatory.

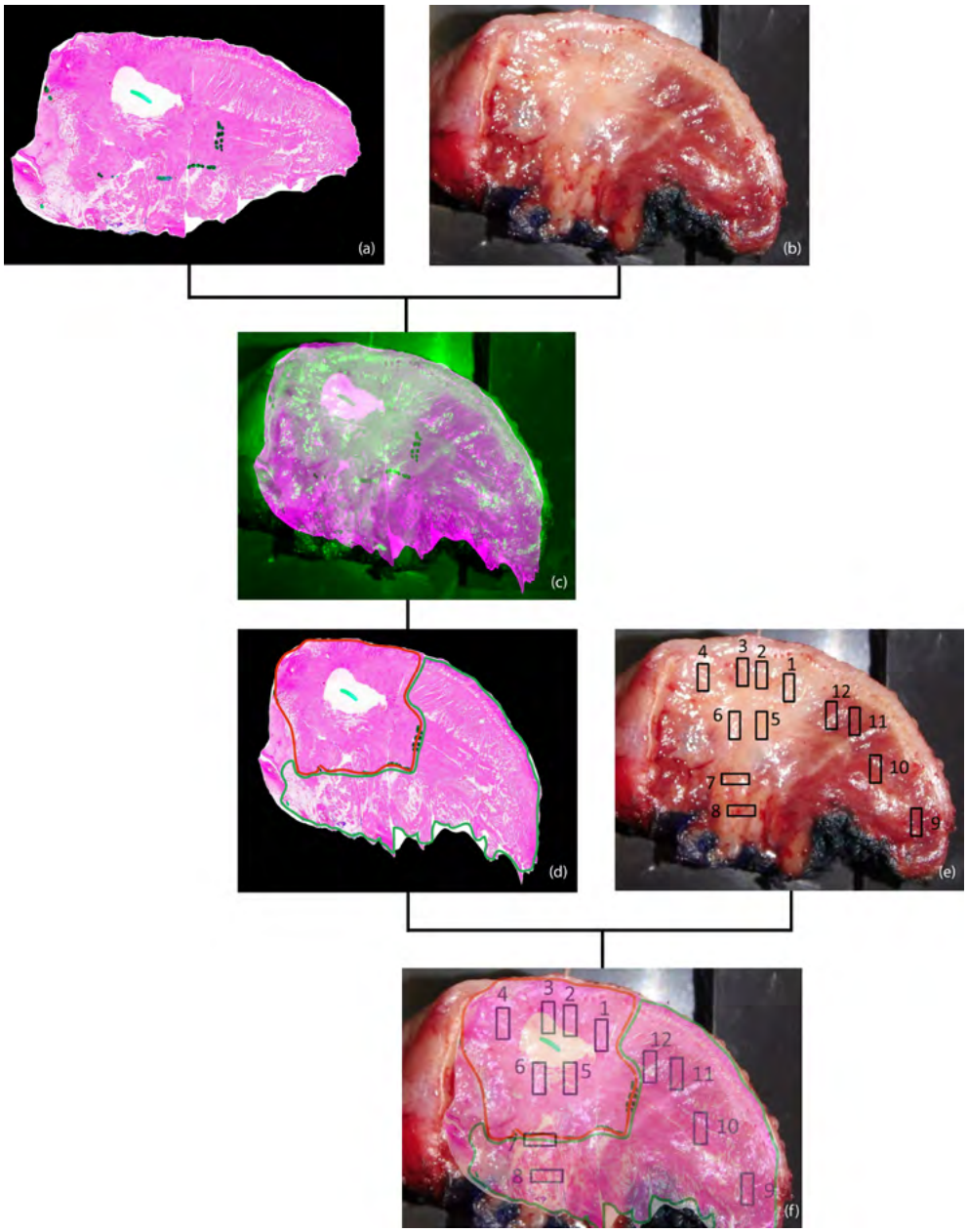

Figure 2 Procedure for finding the histopathological classification of the locations of the DRS measurements. The scanned histopathological slide (a) is registered to the RGB image (b). The result is shown as an overlay (c). The tumor (red) and healhty muscle (green) are then annotated on the registered histopathological slide (d). The measurement locations are drawn onto the RGB image (e). The registered and annotated histopathological slide is shown as an overlay on the RGB with the measurement locations (f).

Data analysis

The diffuse reflectance spectra were acquired from tumor and muscle measurement locations, in the wavelength range of 400-1600 nm at a 1 nm interval. To investigate subtle changes in the shape of the reflectance spectra, the first-order derivative (3) and the second-order derivative were calculated with the following equations:

First-order derivative: $R'(\lambda_i) = \frac{R(\lambda_{i+1}) - R(\lambda_i)}{\lambda_{i+1} - \lambda_i}$

Second-order derivative: $R''(\lambda_i) = \frac{R'(\lambda_{i+1}) - R'(\lambda_i)}{\lambda_{i+1} - \lambda_i}$

Where λ_{i+1} and λ_i are the adjacent wavelengths, and $R(\lambda_i)$, $R'(\lambda_i)$ and $R''(\lambda_i)$ are the original reflectance measurements, the first-order derivative, and the second order derivative, respectively.

The spectral data (the first and second order derivatives) was down sampled with a factor 5 to reduce the number of features and prevent the algorithm from overfitting. For the classification of samples, we performed a repeated 5-fold cross-validation using linear support vector machine (SVM). In this approach, patients were randomly divided into five equally sized partitions. Each partition was used as validation set, while the other four partitions were used to train the classifier.

The cross-validation procedure was repeated ten times, each with a different random distribution of the patients over the five partitions, yielding ten tissue type predictions per measurement location. Of these predictions, mean sensitivity, specificity, accuracy (ACC), area under the curve (AUC) and Matthew's correlation coefficient (MCC) were calculated. The latter gives an indication of the quality of the classification (ranging from-1 to 1, with-1 indicating perfect disagreement, 0 random outcome and 1 perfect agreement between prediction and observation), and corrects for classification problems with an unequal class (tumor/healthy) size.

This analysis was repeated for each of the four data sets, obtained from the different distances between source and detection fiber. Receiver-operating curve (ROC) and MCC's were used to compare results of the different fiber distances.

All data analyses were performed in MATLAB R2018a.

Results

Freshly excised specimens were measured from 28 patients with squamous cell carcinoma in the oral cavity. Nineteen of the tumors were located in the tongue (sixteen lateral tongue, two dorsal tongue, one tongue base), one in the oropharynx, seven in the floor of the mouth (six para medial, one anterior), and one in the left cheek. Table 1 shows the total number of spectra measured from tumor and healthy muscle tissue for each distance between source and detection fiber. In figure 3 the mean original reflectance spectra are shown with the accompanying standard deviations (STD) for both the tumor and healthy muscle measurement locations. Largest differences between the two tissue types are visible in

the wavelength range of 600-1000 nm when measuring with 0.7 mm, 1 mm or 2 mm between source and detection fiber. Especially the slope of the spectra along these wavelengths differs between tumor and healthy. For the 0.3 mm source-detector distance, there is almost a complete overlap between the STD's of both tissue types. For all source-detector distances, the NIR part of the spectrum (1000-1700 nm) does not indicate any difference between measurements acquired on tumor or healthy tissue.

Table 1 Number of measurements for each distance between source and detection fiber.

Distance between source and detection fiber	0.3 mm	0.7 mm	1 mm	2 mm
Number of total measurements (patients)	172 (24)	186 (28)	186 (28)	186 (27)
Number of tumor measurements	70 (20)	76 (23)	76 (23)	77 (22)
Number of muscle measurements	102 (22)	110 (26)	110 (26)	109 (25)

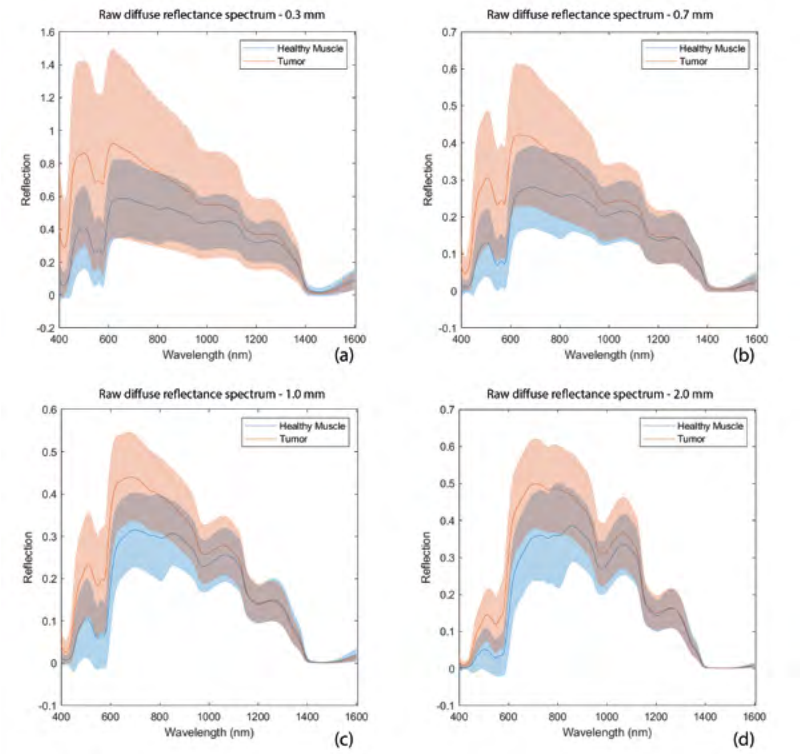

Figure 3 Mean and standard deviation of the raw diffuse reflectance spectra of tumor and healthy muscle for the 0.3 mm (a), 0.7 mm (b), 1 mm (c) and 2 mm (d) distances between source and detection fiber.

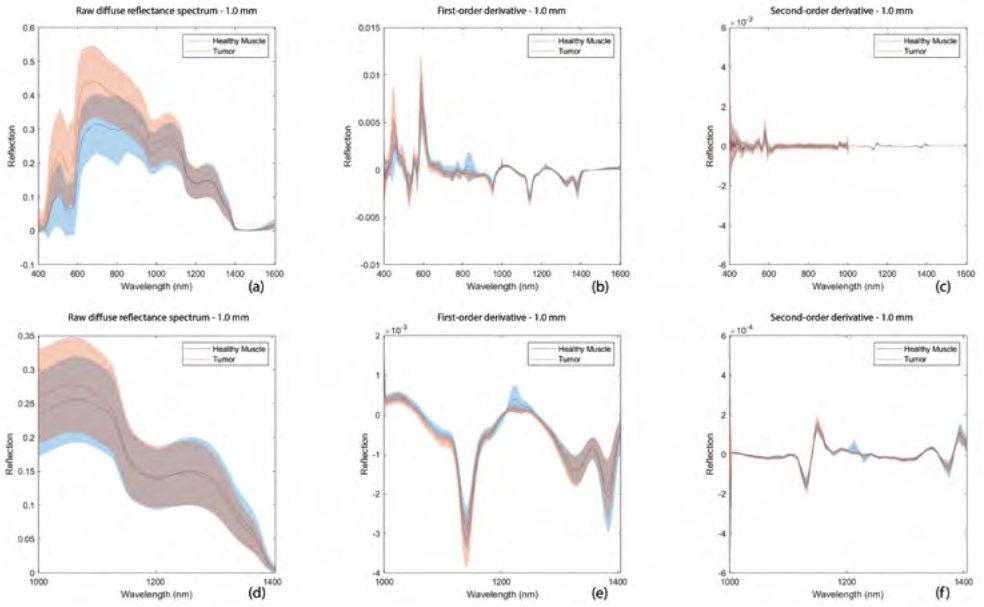

Figure 4 Mean and standard deviation of the diffuse reflectance spectra of tumor and healthy muscle for the 1 mm source-detector distance, plotted as raw data (a), first order derivative (b) and second order derivative (c). (d), (e) and (f) show the raw data, first-order derivative and second-order derivative for the wavelenght band 1000 to 1400 nm, respectively.

Figure 4 shows the original reflectance measurement, the slope of the original reflectance measurement (first-order derivative) and slope of the first-order derivative (the second-order derivative) for the complete spectrum and the wavelengths between 1000 and 1400 nm. The first-derivative shows differences especially around 800 nm, indicating a large difference in slope between the original tumor and healthy reflectance spectra. Figure 4(d), 4(e) and 4(f) show that although the original reflectance spectrum does not necessarily indicate a difference between tumor and healthy measurements for the NIR range, both the first and second-order derivatives do show subtle differences between the two tissue types.

Using the first and the second-order derivatives of the spectra in a linear SVM in the ten times 5-fold cross-validation (CV), MCC ranged from 0.50-0.71 for all fiber distances (Table 2). a 1 mm distance between source and detection fiber resulted in the highest value for the MCC (Figure 5). Mean sensitivity, specificity and accuracy were 89% ± 0.01, 82% ± 0.02, and 86% ± 0.01, respectively, for this distance between source and detection fiber.

Table 2 Classification results of ten times fivefold cross-validation with a linear support vector machine

Distance between source and detection fiber	0.3 mm		0.7 mm		1 mm		2 mm	
	Mean	STD	Mean	STD	Mean	STD	Mean	STD
Sensitivity	0.83	0.01	0.89	0.01	0.89	0.01	0.84	0.01
Specificity	0.66	0.04	0.81	0.02	0.82	0.02	0.76	0.02
ACC	0.76	0.01	0.86	0.01	0.86	0.01	0.81	0.01
AUC	0.81	0.01	0.90	0.01	0.91	0.01	0.86	0.01
MCC	0.50	0.03	0.70	0.02	0.70	0.02	0.60	0.02

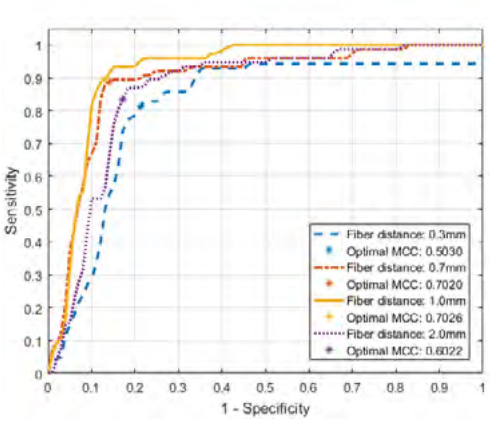

Figure 5 ROC curves of the different distances between source and detection fiber. Cutoff points are chosen based on the maximum MCC value.

Classification outcomes for different factors for data reduction and data processing are shown in Table 3. Reducing the data with a factor 5 did not indicate a significant difference in classification outcomes, it only affected the STD. Thus, using less data, the results were more in line. This shows that by using a factor 5, the data is less subject to overfitting. Also when comparing the different data processing methods, the classification outcomes are not significantly affected. Using the first- and second-order derivatives resulted in a minor increase in sensitivity, which is clinically most valuable. Furthermore, using the derivatives resulted in the smallest STDs.

The results obtained with a 0.7 mm distance are comparable to the results obtained with a 1 mm distance, while the measurements obtained with 0.3 mm and 2 mm distances show less accurate discrimination of tumor from healthy tissue.

Table 3 Classification results of 1-mm distance between source and detection fiber with different factors for data reduction and data processing.

	Variable down-sampling factor used with 1st and 2nd order derivative						Variable processing of diffuse reflectance spectra used with down-sampling factor 5							
	None		Factor 3		Factor 5		None		1st order derivative		2nd order derivative		1st and 2nd order derivative	
	Mean	STD	Mean	STD	Mean	STD	Mean	STD	Mean	STD	Mean	STD	Mean	STD
Sensitivity	0.88	0.01	0.87	0.02	*0.89*	*0.01*	0.88	0.01	0.88	0.01	0.86	0.02	*0.89*	*0.01*
Specificity	0.83	0.04	0.83	0.03	*0.82*	*0.02*	0.84	0.03	0.79	0.06	0.79	0.04	*0.82*	*0.02*
ACC	0.86	0.02	0.85	0.02	*0.86*	*0.01*	0.86	0.01	0.84	0.02	0.84	0.01	*0.86*	*0.01*
AUC	0.91	0.01	0.90	0.01	*0.91*	*0.01*	0.91	0.01	0.89	0.01	0.90	0.01	*0.91*	*0.01*
MCC	0.71	0.03	0.70	0.03	*0.70*	*0.02*	0.72	0.03	0.67	0.06	0.67	0.03	*0.70*	*0.02*

Discussion

Aiming for resection margin assessment of the deep resection margin during oral cavity cancer surgery, we evaluated whether DRS (in the wavelength range of 400-1700 nm) can accurately discriminate tumor from healthy oral muscle tissue, in an *ex vivo* setting. Using a 1 mm distance between source and detection fiber, and a linear SVM, we found a sensitivity, specificity and accuracy of 89%, 82%, and 86%.

The sampling depth of a DRS probe is defined as the depth reached by 50% of the photons. This depth depends on different factors, such as the optical properties of the tissue, the geometry of the probe and the wavelength of the light (15). Hennessy *et al.* (15) used a Monte Carlo model of DRS to investigate the effect of the source-detector distance and the wavelength on the sampling depth of photons collected by a DRS probe. The source-detector distance of 0.25 and 1.0 mm measured sampling depths of up to 0.3 and 0.7 mm, respectively. Thus, with a larger source-detector distance, larger sampling depths can be measured. They also showed that the exact sampling depth was wavelength-dependent: within the visual range of 400-700 nm, the sampling depth varied between 0.4 and 0.7 mm for a source-detector distance of 1.0 mm. According to these data, we estimated that in our study a source-detector distance of 1.0 mm should be able to measure a sampling depth between 0.4 and 0.7 mm and a source-detector distance of 2 mm should at least be able to measure at a depth of > 1 mm.

We looked at 0.3 mm, 0.7 mm, 1.0 mm and 2 mm distances between source and detection fiber. In our study, both the 0.7 mm and 1 mm categories were superior in discriminating tumor from healthy tissue, over the 0.3 mm and 2 mm categories. This could be explained by the methodology we used to validate the data. We labelled the measurements with a tumor or healthy label based on the first histopathological section of the complete surface of the specimen. Due to the direction of the histopathological slices and the orientation of the specimen in the paraffin block, it is not known from what depth this slice originated from. It could have been that the absolute superficial layer, being measured with the 0.3 mm source-detector distance, was not present in our histopathological section, because it was sliced off before the slice including the entire intact surface was reached in the cutting process. On the other hand, in the 2 mm source-detector distance, the category with the largest sampling depth, it could have been the case that besides travelling through a superficial layer of tumor

tissue, the light also could have been travelling through an underlying layer of healthy tissue. Since we did not measure the tumor thickness at the measurement locations we could not accurately validate the data for this larger sampling depth.

The current clinical practice guidelines in head and neck cancer define a close margin as tumor cells found within <5 mm from the resection surface. However, there is no consensus with regard to whether <5 mm is the right definition of 'close'. Ciufielli *et al.* reported in their systematic review that a range of 2-7 mm is considered close (16). Also, specifically for the tongue, Zanoni *et al.* recently suggested to redefine the definition of close margins for patients with squamous cell carcinoma (17). In their study, local recurrence free-survival was significantly affected only with surgical margins of less than or equal to 2.2 mm. Thus, to be able to use DRS in the detection of close margins, the required sampling depth is >2 mm.

In our study, the discriminative power of tumor from healthy tissue was not the strongest for the largest sampling depth obtained with the 2 mm source-detector distance, due to the validation method of this category. Thus, we recommend future work to focus on improving the validation method for larger sampling depths. As an initial approach, US could be used to measure the tumor thickness at the measurement locations. Several studies have shown that the tumor thickness can be accurately measured by using US (18, 19).

As far as we are aware, this is the first study reporting on the use of DRS in discriminating oral cavity tumor from healthy oral muscle tissue, which is essential for the intraoperative application we are aiming at. Other studies have been reporting on the use of DRS for diagnosing oral cavity cancer and are therefore focused on discriminating tumor from healthy mucosa, a completely different tissue type (6-13). Therefore, it is not directly possible to compare our results with these studies. At the moment, oral cavity tumor resection is performed without any intra-operative feedback on the presence of tumor cells at the tumor resection margins. So far, there are only studies reporting on the *in vivo* use of US to obtain tumor free margins in tongue surgery (19-21). In these studies, US was used to position needles as an indication for the safety margin during the resection. Also, Songra *et al.* used a metal retractor into the surgical cut, half-way during resection to evaluate the resection margin with US (18). Other research on this topic focused on *ex vivo* evaluation of the resection margins, e.g. by magnetic resonance (MR). Steens *et al.* reported in six out of seven patients a resection margin within a 2 mm range of the resection margin reported by histopathology (22). Both US and MR provide image guidance during surgery, while we aim to use DRS for tissue characterization. Therefore, DRS and US/MR are not mutually exclusive and could be used complementary to each other.

Clinically, we would like to use DRS as an intra-operative tool to distinguish oral cavity tumor tissue from healthy muscle tissue at the resection plane. The surgeon could position the probe at a suspicious location at the deep resection margin. After measuring the tissue with DRS, the reflectance spectrum will be compared to the data base which was used to train the SVM, and a prediction can be made on the type of the measured tissue, real time. a scale on a monitor will indicate the likelihood of measuring tumor tissue. Detection of tumor tissue at the deep resection margin will allow for direct re-excision and thus reduce the involved margins. Intra-operative use of DRS is feasible, because measurements do not delay the surgery and the results can be made available in real time. With the reported sensitivity and specificity in this *ex vivo* study, it would be interesting to further develop the technology into a surgical instrument which can be sterilized for *in vivo* use.

Conclusion

This *ex vivo* study showed that DRS can discriminate tumor from healthy oral tissue. Using a linear SVM in a ten times 5-fold CV, sensitivity, specificity and accuracy measures of 89%, 82%, and 86% were obtained. Future work should focus on accurate validation methods for larger sampling depths to allow real time guidance during oral cavity tumor excision.

References

1. Smits RW, Koljenovic S, Hardillo JA, Ten Hove I, Meeuwis CA, Sewnaik A, et al. Resection margins in oral cancer surgery: Room for improvement. Head Neck. 2016;38 Suppl 1:E2197-203.
2. Spliethoff JW, Evers DJ, Klomp HM, van Sandick JW, Wouters MW, Nachabe R, et al. Improved identification of peripheral lung tumors by using diffuse reflectance and fluorescence spectroscopy. Lung Cancer. 2013;80(2): 165-71.
3. Spliethoff JW, Tanis E, Evers DJ, Hendriks BH, Prevoo W, Ruers TJ, editors. Monitoring of tumor radio frequency ablation using derivative spectroscopy2014: SPIE.
4. de Boer LL, Molenkamp BG, Bydlon TM, Hendriks BH, Wesseling J, Sterenborg HJ, et al. Fat/water ratios measured with diffuse reflectance spectroscopy to detect breast tumor boundaries. Breast Cancer Res Treat. 2015;152(3):509-18.
5. Baltussen EJM, Snaebjornsson P, de Koning SGB, Sterenborg H, Aalbers AGJ, Kok N, et al. Diffuse reflectance spectroscopy as a tool for real-time tissue assessment during colorectal cancer surgery. J Biomed Opt. 2017;22(10):1-6.
6. Yu C, Lau C, O'Donoghue G, Mirkovic J, McGee S, Galindo L, et al. Quantitative spectroscopic imaging for noninvasive early cancer detection. Opt Express. 2008;16(20):16227-39.
7. Amelink A, Kaspers OP, Sterenborg HJ, van der Wal JE, Roodenburg JL, Witjes MJ. Non-invasive measurement of the morphology and physiology of oral mucosa by use of optical spectroscopy. Oral Oncol. 2008;44(1):65-71.
8. de Veld DC, Skurichina M, Witjes MJ, Duin RP, Sterenborg HJ, Roodenburg JL. Autofluorescence and diffuse reflectance spectroscopy for oral oncology. Lasers Surg Med. 2005;36(5):356-64.
9. Schwarz RA, Gao W, Redden Weber C, Kurachi C, Lee JJ, El-Naggar AK, et al. Noninvasive evaluation of oral lesions using depth-sensitive optical spectroscopy. Cancer. 2009;115(8):1669-79.
10. McGee S, Mardirossian V, Elackattu A, Mirkovic J, Pistey R, Gallagher G, et al. Anatomy-Based Algorithms for Detecting Oral Cancer Using Reflectance and Fluorescence Spectroscopy. Ann Otol Rhinol Laryngol. 2009;118(11):817-26.
11. Jayanthi JL, Nisha GU, Manju S, Philip EK, Jeemon P, Baiju KV, et al. Diffuse reflectance spectroscopy: diagnostic accuracy of a non-invasive screening technique for early detection of malignant changes in the oral cavity. BMJ Open. 2011;1(1):e000071.
12. Stephen mm, Jayanthi JL, Unni NG, Kolady PE, Beena VT, Jeemon P, et al. Diagnostic accuracy of diffuse reflectance imaging for early detection of pre-malignant and malignant changes in the oral cavity: a feasibility study. BMC Cancer. 2013;13:278.
13. Mallia RJ, Narayanan S, Madhavan J, Sebastian P, Kumar R, Methews AT, G. , et al. Diffuse Reflection Spectroscopy: An Alternative to Autofluorescence Spectroscopy in Tongue Cancer Detection. Applied spectroscopy. 2010;64(4).
14. Nachabe R, Hendriks BHW, Van der Voort M, Desjardins AE, Sterenborg HJCM. Estimation of biological chromophores using diffuse optical spectroscopy: benefit of extending the UV-VIS wavelength range to include 1000 to 1600 nm. OPTICS EXPRESS. 2010;18(24).
15. Hennessy R, Goth W, Sharma M, Markey MK, Tunnell JW. Effect of probe geometry and optical properties on the sampling depth for diffuse reflectance spectroscopy. Journal of Biomedical Optics. 2014.
16. Alicandri-Ciufelli M, Bonali M, Piccinini A, Marra L, Ghidini A, Cunsolo EM, et al. Surgical margins in head and neck squamous cell carcinoma: what is 'close'? Eur Arch Otorhinolaryngol. 2013;270(10):2603-9.
17. Zanoni DK, Migliacci JC, Xu B, Katabi N, Montero PH, Ganly I, et al. a Proposal to Redefine Close Surgical Margins in Squamous Cell Carcinoma of the Oral Tongue. JAMA Otolaryngol Head Neck Surg. 2017;143(6):555-60.
18. Songra AK, Ng SY, Farthing P, Hutchison IL, Bradley PF. Observation of tumour thickness and resection margin at surgical excision of primary oral squamous cell carcinoma--assessment by ultrasound. Int J Oral Maxillofac Surg. 2006;35(4):324-31.
19. Kodama M, Khanal A, Habu M, Iwanaga K, Yoshioka I, Tanaka T, et al. Ultrasonography for intraoperative determination of tumor thickness and resection margin in tongue carcinomas. J Oral Maxillofac Surg. 2010;68(8):1746-52.
20. Helbig M, Flechtenmacher C, Hansmann J, Dietz A, Tasman AJ. Intraoperative B-mode endosonography of tongue carcinoma. Head & Neck. 2001;23:233-7.

21. Baek CH, Son YI, Jeong HS, Chung MK, Park KN, Ko YH, et al. To investigate the clinical usefulness of intraoral sonography-assisted resection for securing adequate deep resection margins in T1–2 tongue cancers. Otolaryngology–Head and Neck Surgery. 2008;139(6).
22. Steens SCA, Bekers EM, Weijs WLJ, Litjens GJS, Veltien A, Maat A, et al. Evaluation of tongue squamous cell carcinoma resection margins using ex-vivo MR. Int J Comput Assist Radiol Surg. 2017;12(5):821-8.

Chapter 6

Towards assessment of resection margins using hyperspectral diffuse reflection imaging (400-1,700 nm) during tongue cancer surgery

S.G. Brouwer de Koning

P. Weijtmans

M.B. Karakullukcu

C. Shan

E.J.M. Baltussen

L. A. Smit

R.L.P. van Veen

B.H.W. Hendriks

H.J.C.M. Sterenborg

T.J.M. Ruers

Lasers in Surgery and Medicine (2019) https://doi.org/10.1002/lsm.23161

Abstract

Objectives

There is a clinical need to assess the resection margins of tongue cancer specimens intraoperatively. In the current *ex vivo* study, we evaluated the feasibility of hyperspectral diffuse reflectance imaging (HSI) for distinguishing tumor from healthy tongue tissue.

Materials and Methods

Fresh surgical specimens (n=14) of squamous cell carcinoma of the tongue were scanned with two hyperspectral cameras that cover the visible and near-infrared spectrum (400-1700 nm). Each pixel of the hyperspectral image represents a measure of the diffuse optical reflectance. a neural network was used for tissue type prediction of the hyperspectral images of the visual and near-infrared data sets separately as well as both data sets combined.

Results

HSI was able to distinguish tumor from muscle with a good accuracy. The diagnostic performance of both wavelength ranges (sensitivity/specificity of visual and near- infrared were 84%/80% and 77%/77%, respectively) appears to be comparable and there is no additional benefit of combining the two wavelength ranges (sensitivity and specificity were 83%/76%).

Conclusion

HSI has a strong potential for intra-operative assessment of tumor resection margins of squamous cell carcinoma of the tongue. This may optimize surgery, since the entire resection surface can be scanned in a single run and results can be readily available.

Keywords

resection margin assessment; hyperspectral imaging; tongue cancer; tissue recognition; deep learning.

Introduction

Early stage squamous cell carcinoma of the tongue is generally treated with a partial glossectomy, where the surgeon aims to remove the tumor, while sparing as much healthy tissue as possible. The resected specimen is examined by the pathologist, who reports on the shortest distance between tumor cells and resection plane, postoperatively. It is generally accepted that this margin should be at least 5 mm to ensure local control and good prognosis (1, 2). However, due to the lack of intra-operative feedback, other than palpation, obtaining this 5 mm margin remains challenging. Smits *et al.* reported in a review that in up to 85% of the patients, tumor cells are found at the resection plane (positive margin) or within 5 mm from the resection plane (close margins) (3). These patients may need adjuvant treatment with either additional surgery, radiotherapy or sometimes chemo radiation to minimize the risk for local recurrence. a technology allowing intra-operative evaluation of the resection planes for the presence of tumor cells is therefore highly desired, as it would enable the surgeon to perform surgery more accurately.

In this study, we evaluated whether we can use hyperspectral diffuse reflectance imaging (HSI) for intra-operative resection margin assessment of tongue cancers. a diffuse reflectance spectrum is acquired for each pixel of the hyperspectral image, while illuminating the tissue with a broadband white light source (4). The measured reflectance is related to the absorption and scattering properties of the illuminated tissue. Tissue composition affects the absorption and scattering properties, and thus, the diffuse reflection spectrum can be interpreted as an 'optical fingerprint' of the tissue.

Diffuse reflectance spectroscopy (DRS) and related technologies have been evaluated for diagnostic purposes, in which the discrimination between healthy mucosal tissue and tumor is required (5-13). However, the extent of tumor growth below the mucosa, into the tongue tissue, is difficult to identify. Thus, tumor clearance of the so called deep margin challenges radical tongue tumor surgery (Figure 1). Our long-term objective is to enable optical evaluation of the deep resection margin of oral cavity tumors. Hence, in this study, we aim to differentiate tumor tissue from healthy muscle tissue at this deep resection plane.

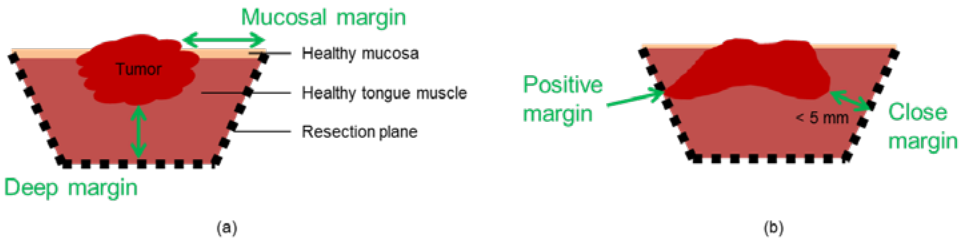

Figure 1 (a) Cross section of a tongue tumor specimen with the definitions of the two different margins used in tongue cancer surgery. (b) Definition of a positive and close margin.

In a previous study, we have shown that we could discriminate tongue tumor from healthy tongue muscle tissue using point measurements acquired with a fiber optic DRS probe (400-1600 nm, accuracy of 86%) (14). In the present study, we focus on the use of the image-based technique HSI (400-1700 nm) to discriminate tumor from healthy tongue muscle tissue at the entire resection surface. An imaging technique like HSI may have the advantage over a point based technique by giving an overview of the resection margin in one view.

The group of Fei *et al.* also evaluated HSI for tissue-labeling of surgical specimen of head and neck cancer (15-17). Using leave-one-patient out cross-validation in a cohort of 20 patients with squamous cell carcinoma from oral cavity, larynx, pharynx, and paranasal and nasal cavity, a sensitivity and a specificity of 85% ± 9% and 84% ± 12%, respectively, were reported (15). In contrast to the spectral range of 450-900 nm used by the group of Fei *et al.*, we are using a broader spectral range of 400-1700 nm. The extension of the spectral range towards the infrared, where absorption of light by blood is negligible, should make the technology more applicable for use in a surgical environment where blood is present.

Materials and methods

Patient population

Specimens from patients undergoing surgery for the removal of squamous cell carcinoma of the tongue were considered for this study. All patients were treated in the Netherlands Cancer Institute-Antoni van Leeuwenhoek Hospital, Amsterdam. All ethical guidelines required for *ex vivo* human studies were followed.

Hyperspectral imaging

Two hyperspectral cameras (Spectral Imaging Ltd., Oulu, Finland) operating in different wavelength regions were used in this study (Table 1). Both cameras were push broom cameras, i.e. line sensors creating images by moving the specimen on a translation stage under the camera through the scanning line, thus acquiring 3D data cubes. The scanning speed was set so that the spatial resolution along the direction of the translational stage was matched to the spatial resolution of the scanned line. The tissue was illuminated with three broadband halogen lamps during the acquisition of the hyperspectral data cubes. Acquisition of the images took less than five seconds per image.

Table 1 Specifications of the two hyperspectral cameras.

	Wavelength range	Spectral resolution (FWHM)	Spatial resolution	Sensor
VIS camera (PFD-CL-65-V10E)	400-950 nm	3.0 nm	0.16 mm/pixel	CMOS 1312x384 pixels
NIR camera (VLNIR CL-350-N17E)	950-1700 nm	5.0 nm	0.5 mm/pixel	InGaAs 320x256 pixels

VIS = visible, NIR = near infrared

Measurement workflow

Directly after resection, the tongue specimen was brought to the pathology department, where the resection margins were inked according to the routine clinical workflow. The pathologist localized the tumor by palpation, and subsequently cut the specimen through the middle of the tumor. First, an RGB image was taken from the cut surface with a regular photo camera. Immediately after and without touching the specimen, the cut surface of the specimen was imaged with the hyperspectral visible wavelength range (VIS) camera and the near-infrared wavelength range (NIR) camera. Thereafter, the specimen was subjected to further routine pathological processing. The specimen was fixed, the imaged surface was sectioned, stained with hematoxylin and eosin (H&E) and mounted on a histopathology slide. The H&E slide was evaluated microscopically by the pathologist, who annotated different tissue types on the slide.

Pathology to HSI registration

The hyperspectral data cubes were matched with the corresponding histopathology slides, in order to be able to link each pixel in the hyperspectral image to the tissue type determined by the pathologist on the H&E slide. For this, a digital scan was made of the H&E slide and this was registered to the hyperspectral image (Figure 2). The registration was done in two steps: the H&E slide was transformed to the RGB image (transformation T1) first and subsequently underwent the transformation from the RGB to the hyperspectral image (transformation T2). Choosing the RGB image for correlation with histopathology, eliminates a potential bias in correlation that could occur if the histopathology would be registered with the hyperspectral data cube directly.

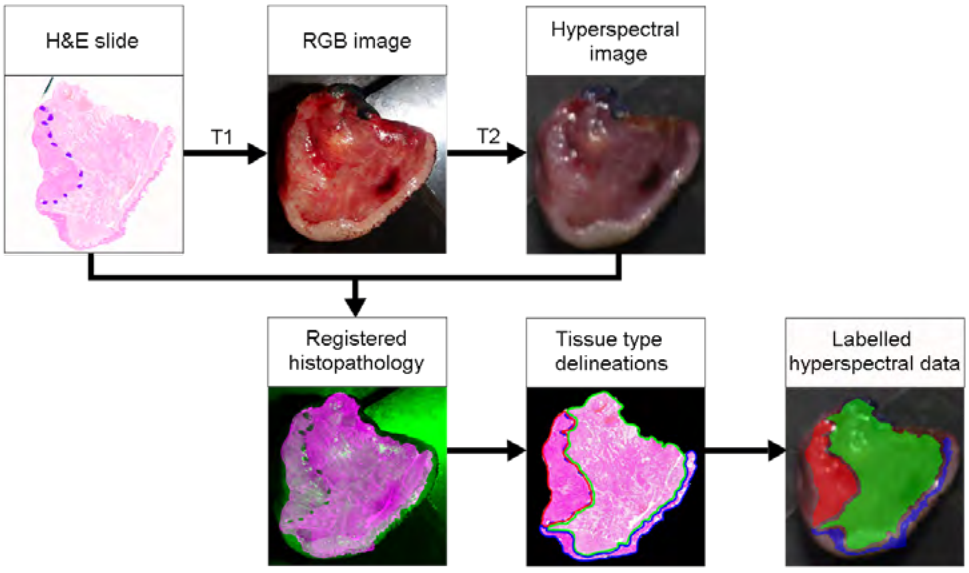

Figure 2 Annotation of the hyperspectral data: tumor (red), healthy tongue muscle (green) and healthy mucosa (blue). The transformation between pathology and HSI is calculated in two steps: the transformation between H&E slide and RGB (transformation T1) and the transformation between RGB and hyperspectral image (transformation T2).

Due to deformation of the specimen during the histopathological processing, a non-rigid registration algorithm was used for both the T1 and T2 transformations. The transformations were based on a set of ±15 matching points, which were obviously identifiable in both images. The VIS and NIR data were also registered to each other using the same registration points that were used in the pathology to HSI registration process.

On the H&E slide, the pathologist delineated three tissue types: tumor, healthy muscle tissue and healthy mucosa. Both the transformations T1 and T2 were then applied to these annotated images. The annotation of each pixel was used as a tissue type label for each spectrum from the matching pixel from the hyperspectral image.

Hyperspectral data preprocessing

The InGaAs sensor of the NIR camera did not show a perfectly linear behavior between the amount of incident light and the number of counts generated. As a first step, a correction was done for this, as published previously (18). Subsequently, the data cubes acquired were calibrated with dark and white reference images according to equation 1. In this equation, $I_{reflect}$ is the calibrated reflectance spectrum, I_{raw} is the raw measured spectrum on the sample, I_{dark} is the dark reference and I_{white} is the white reference. Values outside the (0, 1) domain were clipped as they were caused by noise or specular reflection. The calibrated data was then manually cropped to a region of interest.

$$I_{reflect} = \frac{I_{raw} - I_{dark}}{I_{white} - I_{dark}} \qquad (1)$$

VIS, NIR and combined hyperspectral data sets

The VIS and NIR hyperspectral data sets were analyzed as two separate data sets. In addition, the data of both the VIS and NIR hyperspectral cameras were combined in a third data set and analyzed.
Both the spatial and spectral resolutions of the VIS camera were higher than the NIR camera (Table 1), making the VIS data set larger in size.

Hyperspectral data analysis

A neural network was trained for the discrimination between tumor tissue and healthy muscle tissue. This neural network was built in Keras, a Python deep learning library that is used on top of TensorFlow 1.12 in a Python 3.5 environment. The networks were trained using a NVIDIA Titan Xp GPU. The networks had several fully connected dense layers before coming to a two-class output. Table 2 shows details of the architectures of the neural networks.

Specimens were different in size. To ensure that a large specimen did not dominate in the training of the neural network because of its larger input, an equal number of pixels was selected from each specimen for training. Furthermore, to have balanced classes, an equal number of pixels was selected from each tissue type. If not enough pixels were available to reach this number in a class (tumor/healthy) from one patient, the same pixels were used more often so that the amount of data used for both classes, for all patients, was equal in the training stage of the neural network.

In contrast to the training of the data, all the pixels from tumor tissue and healthy muscle tissue were considered for testing the data.

Table 2 The architecture of the neural networks trained on the visible hyperspectral data set, the near infrared hyperspectral data set and the neural network trained on the data set in which both the visible and near infrared hyperspectral data were combined.

	Visible	Near infrared	Combined
Number of input wavelengths	384	256	585
First dense layer	384	256	585
Second dense layer	128	128	320
Third dense layer	64	64	160
Fourth dense layer	-	-	80
Output classes	2	2	2
Total number parameters	205,506	107,074	594,732

To evaluate the performance of the neural network, the network was tested on the patients in a cross-validation. The metrics used to quantify the performance were the mean and standard deviation of the area under the receiver operating curve (AUC), accuracy, sensitivity and specificity of the outcomes of each fold of the cross-validation. To calculate the accuracy, sensitivity and specificity, a global cutoff was determined using the Youden's index (defined as J = sensitivity + specificity – 1, ranging from 0 to 1), based on the classification results on all the patients in cross-validation experiments. The selected cutoffs were 0.40, 0.44 and 0.45, for the VIS, NIR and combined dataset, respectively.

Results

Data set

Freshly excised specimens were imaged from fourteen patients with squamous cell carcinoma in the tongue. The tumors were radiologically staged as T1-T3.

The total number of VIS pixels annotated as tumor and healthy tissue were 65,565 and 144,903, respectively. The total number of NIR pixels annotated as such were 7,445 and 16,071, respectively.

Each pixel of the hyperspectral image contained a diffuse reflectance spectrum. Figure 3 shows the average spectral shape of tumor and healthy muscle tissue of all patients with the standard deviation per pixel.

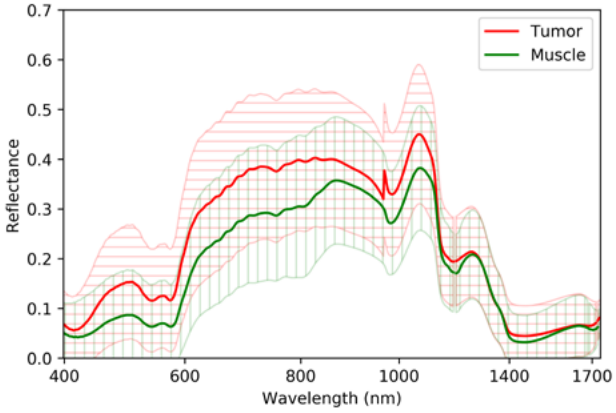

Figure 3 Mean and standard deviation of the spectra of tumor and healthy muscle of all fourteen patients. Differences in the VIS and NIR measurement setups in combination with the rough surface of the specimen, resulted in an inexact merge between the VIS and NIR spectra around 950 nm. This is further elaborated in previous work of our group (24).

Classification results

The neural network was trained and evaluated for the VIS and NIR datasets separately, as well as for both data sets combined. a seven-fold leave-two-patients-out cross-validation was performed, meaning that the fourteen patients were divided into 7 pairs of two patients. During each fold, six groups were used for training and the remaining pair was used for testing. Figure 4 shows the mean receiver operating curves (ROC) of the classification of the data from all patients, using the VIS, NIR and combined HSI data. In Table 3, the AUC, accuracy, sensitivity and specificity of the VIS, NIR and combined data set are shown for quantitative comparison.

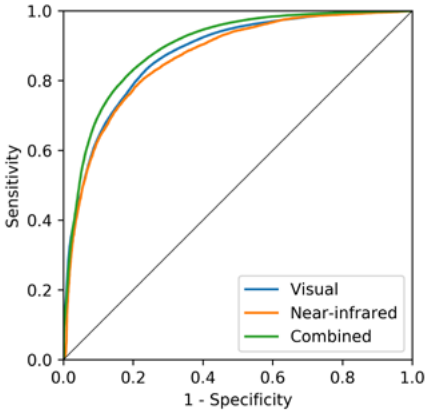

Figure 4 The receiver operating curves (ROC) of the three different types of hyperspectral data sets.

Table 3 Classification results of testing the neural network on fourteen patients (mean ± std) in the cross-validation using the three different types of hyperspectral data sets (visible, near infrared and combined).

	Visible	Near infrared	Combined
AUC	93.2% ± 3.8	88.6% ± 8.5	91.7% ± 4.6
Accuracy	82.4% ± 11.1	77.9% ± 13.8	82.3% ± 8.7
Sensitivity	83.6% ± 15.4	76.6% ± 23.3	82.8% ± 14
Specificity	80.3% ± 17.9	77.4% ± 25.6	75.7% ± 21.8

The results in Table 3 show that it is feasible to distinguish tongue tumor tissue from tongue muscle tissue using all combinations, with a high accuracy. The confidence intervals given were calculated from the leave-two-patients out analysis. Table 3 also clearly shows that there is only a slight difference between the performance of the VIS and NIR cameras and that there is no large additional benefit of combining the two cameras. The standard deviations obtained suggest that there is no difference between any of them.

Figure 5 shows some example tissue predictions of hyperspectral images acquired from three patients.

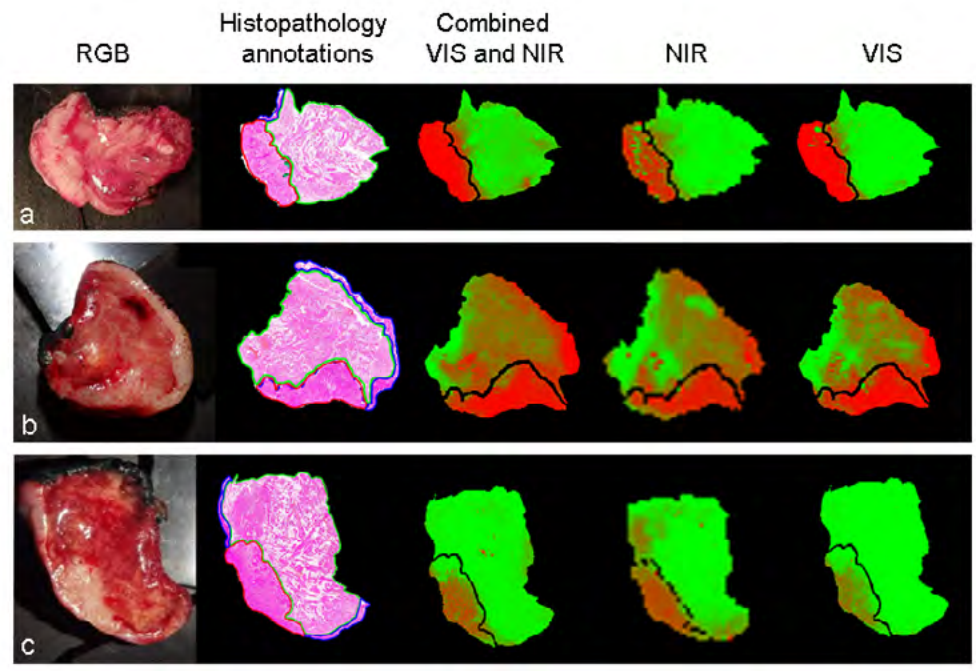

Figure 5 The tumor (red) and healthy muscle tissue (green) predictions of the neural network using the VIS, NIR and combined data sets for patient 9 (a), patient 2 (b) and patient 12 (c). Predictions were performed with a high sensitivity and specificity for patient 9 (a). However, in patient 2 (b), high sensitivity and low specificity are demonstrated. Patient 12 (c) is an example of prediction with a low sensitivity and high specificity. The healthy mucosa (delineated on the H&E slices in blue) was not classified and therefore not shown in the predictions (i.e. indicated as background).

Discussion

We evaluated whether hyperspectral diffuse reflectance imaging (with two cameras: one in the visible wavelength range of 400-1000 nm and one in the near-infrared wavelength range of 950-1700 nm) can accurately discriminate tumor from healthy tongue muscle tissue for intra-operative assessment of the deep resection margin. The results indicate that both cameras can do so with a good accuracy. The performance in tissue type prediction of both cameras is comparable and there is a no additional benefit of combining the VIS and NIR regions. Thus, with regard to the differentiation of healthy and tumor tissue, there seems no preferred wavelength range (VIS, NIR or the VIS and NIR combined). Nevertheless, the selection of any wavelength range may depend on the clinical application.

The clinical guidelines in head and neck cancer define a close margin as tumor cells found within <5 mm from the resection surface and a positive margin as tumor cells at the resection plane (19). This study was performed with the aim to contribute to the development of a technology that can be used to detect such close and positive margins at the deep resection plane during oral cavity cancer surgery. Therefore, two challenges for intra-operative use are: whether tumor cells at the resection plane (positive margins) can be detected and whether we can detect the presence of tumor cells within a sampling depth up to 5 mm (close margins). With the wavelengths accessed by the NIR camera, spectral information of the more superficial layers of the specimen is obtained, which is promising for the detection of positive margins. On the basis of the current results, it can be deduced that the VIS camera would be the preferred camera to detect close margins, as it comprises the wavelength region with the largest optical sampling depth (650-900 nm) (20).

Depending on the wavelength, the diffuse reflectance spectra imaged with the hyperspectral cameras contain information of an imaged volume, from the surface up to several millimeters into the tissue. We registered the data to the first histopathological section of the complete surface of the specimen and used that as the gold standard. And thus, the tissue types that were above and below the slice of which the histopathological section was taken, may have varied, but did contribute to the hyperspectral images. We expect that classification results can be improved when future studies that evaluate HSI for tissue characterization, take the imaging depth into account in the design of the validation method.

We were the first group that evaluated the use of the entire 400-1700 nm range with HSI for tongue tumor and healthy tongue muscle discrimination. Therefore, we started with imaging tongue cancer specimens in a very controlled setting. That is, that the classification results found in this study were obtained from a cross section through the tumor. This enabled imaging of pure tumor and pure healthy muscle tissue. However, in case this technology will be used for intra-operative deep margin assessment, in which the resection plane would be imaged, the amount of tumor tissue in the imaged volume will be much less than what we see in the cross sections in our current studies. The value of HSI in this setting still has to be determined.

Halicek *et al.* recently published a study in which they used a hyperspectral camera (450-900 nm) with convolutional neural networks to discriminate normal tissue from head and neck squamous cell carcinoma in six patients with tumors located in the tongue, larynx, pharynx and mandible (21). They found an AUC of 82% ± 13, accuracy of 81% ± 11, sensitivity of 81% ± 15 and a specificity of 80% ± 16. In terms of sensitivity and specificity, these results are comparable to the classification results obtained

from our visible hyperspectral camera. However, their data set contained squamous cell carcinoma of different tumor sites and the normal tissue contained epithelium, skeletal muscle and glandular tissue. Since our data set included twice as many patients and only contained squamous cell carcinoma of the tongue compared to muscle tissue of the tongue, the classification results cannot be compared directly to the results of Haliceks study. Still, they also looked into a sub-classification of the normal tissue into epithelium, skeletal muscle and glandular mucosa. This sub-classification was performed with an AUC of 94% ± 8, accuracy of 90% ± 9, sensitivity of 93% ± 6 and a specificity of 89% ± 13.

Intraoperative evaluation of the resection margin in real time during surgery might lower the number of close and positive margins. Currently, only frozen section technology is often used for this purpose. However, this approach is time-consuming and has the limitations that it is only possible to evaluate the resection plane superficially, and thus, cannot detect close margins (22). Steens *et al.* evaluated the use of ex-vivo magnetic resonance (MR) to evaluate resection margins of tongue specimens (23). However, *ex vivo* MR needs optimization in reducing the scanning time to be able to give an outcome on the resection margins during surgery. Our technique has more potential for intra-operative use, because compared to frozen section, HSI enables to image the whole resection surface of the specimen, and compared to MRI, the HSI images could be made available in real time.

Our long term objective is to enable optical evaluation of the deep resection plane of resected oral cavity tumors. In the current study, we have shown that it is possible to distinguish relatively large tongue tumor areas at the surface of the resected specimen from healthy tongue muscle tissue, using HSI (400-1700 nm). However, for use in an intra-operative setting, two more challenges need to be overcome: whether it is possible to detect smaller tumor pockets at the deep resection margin (to detect positive margins) and whether it is possible to detect small tumor pockets up to 5 mm deep below the margin (to detect close margins). For the latter, we recommend further studies to focus on the wavelength range of 650-900 nm, since these wavelengths are known to have the largest optical sampling depth.

Conclusion

This *ex vivo* study showed that HSI of diffuse reflection (400-1700 nm) was able to distinguish tumor from muscle with a good accuracy. The performance in tissue type prediction of both the VIS and NIR wavelength ranges is comparable and there is no additional benefit of combining both. HSI has potential for intra-operative feedback on the status of the deep resection margin in tongue cancer surgery.

References

1. Sutton, D.N., et al., The prognostic implications of the surgical margin in oral squamous cell carcinoma. Int J Oral Maxillofac Surg, 2003. 32(1): p. 30-4.
2. Dillon, J.K., et al., How does the close surgical margin impact recurrence and survival when treating oral squamous cell carcinoma? J Oral Maxillofac Surg, 2015. 73(6): p. 1182-8.
3. Smits, R.W., et al., Resection margins in oral cancer surgery: Room for improvement. Head Neck, 2016. 38 Suppl 1: p. E2197-203.
4. Lu, G. and B. Fei, Medical hyperspectral imaging: a review. Journal of Biomedical Optics, 2014. 19(1).
5. Yu, C., et al., Quantitative spectroscopic imaging for noninvasive early cancer detection. Opt Express, 2008. 16(20).
6. Amelink, A., et al., Non-invasive measurement of the morphology and physiology of oral mucosa by use of optical spectroscopy. Oral Oncol, 2008. 44(1): p. 65-71.
7. de Veld, D.C., et al., Autofluorescence and diffuse reflectance spectroscopy for oral oncology. Lasers Surg Med, 2005. 36(5): p. 356-64.
8. Schwarz, R.A., et al., Noninvasive evaluation of oral lesions using depth-sensitive optical spectroscopy. Cancer, 2009. 115(8): p. 1669-79.
9. McGee, S., et al., Anatomy-Based Algorithms for Detecting Oral Cancer Using Reflectance and Fluorescence Spectroscopy. Ann Otol Rhinol Laryngol, 2009. 118(11).
10. Jayanthi, J.L., et al., Diffuse reflectance spectroscopy: diagnostic accuracy of a non-invasive screening technique for early detection of malignant changes in the oral cavity. BMJ Open, 2011. 1(1): p. e000071.
11. Stephen, M.M., et al., Diagnostic accuracy of diffuse reflectance imaging for early detection of pre-malignant and malignant changes in the oral cavity: a feasibility study. BMC Cancer, 2013. 13: p. 278.
12. Grillone, G.A., et al., The color of cancer: Margin guidance for oral cancer resection using elastic scattering spectroscopy. Laryngoscope, 2017. 127 Suppl 4: p. S1-S9.
13. Mascharak, S., B.J. Baird, and F.C. Holsinger, Detecting oropharyngeal carcinoma using multispectral, narrow-band imaging and machine learning. The Laryngoscope, 2018. 128(11): p. 2514-2520.
14. Brouwer de Koning, S.G., et al., Toward complete oral cavity cancer resection using a handheld diffuse reflectance spectroscopy probe. J Biomed Opt, 2018. 23(12): p. 1-8.
15. Lu, G., et al., Detection of Head and Neck Cancer in Surgical Specimens Using Quantitative Hyperspectral Imaging. Clin Cancer Res, 2017. 23(18): p. 5426-5436.
16. Halicek, M., et al., Deep convolutional neural networks for classifying head and neck cancer using hyperspectral imaging. J Biomed Opt, 2017. 22(6): p. 60503.
17. Fei, B., et al., Label-free reflectance hyperspectral imaging for tumor margin assessment: a pilot study on surgical specimens of cancer patients. J Biomed Opt, 2017. 22(8): p. 1-7.
18. Kho, E., et al., Hyperspectral imaging for resection margin assessment during surgery. Clinical Cancer Research, 2019.
19. NCCN Guidelines Version 1.2018 Head and Neck cancers. National Comprehensive Cancer Network, 2018.
20. Kho, E., et al., Classification method for resection margin assessment with hyperspectral imaging that considers imaging depth variations 2019.
21. Halicek, M., et al., Optical biopsy of head and neck cancer using hyperspectral imaging and convolutional neural networks. Proceedings of SPIE, 2018.
22. Miyawaki, A., et al., Intraoperative frozen section histological analysis of resection samples is useful for the control of primary lesions in patients with oral squamous cell carcinoma. Mol Clin Oncol, 2015. 3(1): p. 55-62.
23. Steens, S.C.A., et al., Evaluation of tongue squamous cell carcinoma resection margins using ex-vivo MR. Int J Comput Assist Radiol Surg, 2017. 12(5): p. 821-828.
24. Kho, E., et al., Broadband Hyperspectral Imaging for Breast Tumor Detection using Spectral and Spatial Information. Not yet available, 2019.

Part II

Surgical guidance for mandibular osteotomies

Chapter 7

Evaluating the accuracy of resection planes in mandibular surgery using a preoperative, intraoperative and postoperative approach

S.G. Brouwer de Koning,

T.P. ter Braak,

F. Geldof,

R.L.P. van Veen,

M.J.A. van Alphen,

L.H.E. Karssemakers,

W.H. Schreuder,

M.B. Karakullukcu

International Journal of Oral and Maxillofacial Surgery (2020) https://doi.org/10.1016/j.ijom.2020.06.013

Abstract

To translate the preoperatively virtually planned resection planes to the operating room, 3D printed patient-specific cutting guides are used in mandibular surgery. This study evaluated whether cutting guides are positioned according to the virtual plan and compared the intra-operative position of the cutting guide with the performed resection.

Exact positions of the resection planes were virtually planned and a patient-specific cutting guide was designed and printed. After surgical placement of the cutting guide, a cone beam CT (CBCT) was acquired intraoperatively, in nine patients. a postoperative CT scan was used to obtain the final resection planes. Distances, yaw and pitch angles were calculated between preoperative, intraoperative and postoperative resection planes.

Cutting guides were positioned on the mandible with a millimeter accuracy. Anterior osteotomies were performed more accurately than posterior osteotomies (intraoperatively positioned and final resection planes differed with 1.2±1.0 mm, 4.9±6.6° and 1.8±1.5°, respectively and 2.2±0.9 mm, 9.3±9° and 8.3±6.5° respectively). Differences between intraoperatively planned and final resection planes imply a directional freedom of the saw through the saw slots.

Since cutting guides are positioned with a millimeter accuracy compared to the virtual plan, the design of the sawing slots of cutting guides needs improvement to allow more accurate resections.

Keywords

mandibulectomy; virtual surgical planning; patient-specific cutting guides; intra-operative CBCT; tumor resection margin.

Introduction

Patients with malignant and benign disease abutting or invading the mandible often undergo segmental resection of the mandible. To restore continuity of the mandible and associated function and esthetics, a reconstruction with a titanium plate in combination with an osseous free flap is performed in the majority of the cases (i.e. osteomyocutaneous fibular flap (FFF) or deep circumflex iliac artery flap (DCIA)) (1, 2). The resection planes of the involved part of the mandible must be accurately determined to ensure adequate and free margins, but also to allow precise placement of bone segments enabling the contour of the neomandible to match the native resected mandible.

The exact location of the resection planes, as well as the reconstruction after resection, can be prepared with virtual surgical planning (VSP)(3). Using this technique, 3D rendered models of the mandible and graft are constructed from a preoperative computed tomography (CT) scan. The 3D models are used to perform a virtual (segmental) mandibulectomy and to virtually segment the graft to match the defect. To translate the position of the resection planes from the VSP to the clinical situation in the operating room, patient-specific cutting guides and fixation plates are designed and manufactured using computer-aided-design/computer-aided-manufacturing (CAD/CAM) techniques. These cutting guides enable the surgeon to perform the surgical procedure more accurately, while significantly shortening operating time (4-6).

Post-operative CT imaging has been used to verify how precise the VSP has been translated during surgery. Several studies have evaluated the accuracy of translation by comparing the location and orientation of the planned resection plane with the plane of the actual performed osteotomy. Kraeima *et al.* used the difference between landmarks on the planned and actual resection planes to define the deviation from the preoperative planning (7). These landmarks were identified on both the buccal and lingual sides of the proximal and distal mandibular segments, as well as the center points of the resection planes, identified by two independent observers. Both Maesschalck *et al.* and Roser *et al.* used a slightly different method and measured the maximum distance between the planned and actual resection planes, rather than landmarks (8, 9). Mean deviations of 2-2.3 mm between preoperatively planned and postoperative resection planes were reported (7-9).

The studies mentioned compare the preoperative planning with the postoperative outcome assuming that the patient-specific cutting guide is placed according to plan and the sawing through the saw slots happens along the planned direction. To improve clinical outcome, also these critical variables have to be considered. Therefore, in the current study, an intraoperative CBCT scan was acquired directly after fixation of the cutting guide. This scan was used to evaluate whether the mandibular cutting guide was positioned according to the virtual surgical plan. Using the intraoperative position of the cutting guide, we evaluated the accuracy of the translation of the preoperative plan to the intraoperative situation and secondly, whether the cutting guide provided enough directional guidance during the performed resection.

Materials and Methods

A prospective cohort study was designed including patients undergoing a continuity resection of the mandible for malignant diseases abutting or invading the mandible, or for osteoradionecrosis of the mandible at the department of Head and Neck Surgery & Oncology of the Netherlands Cancer Institute/ Antoni van Leeuwenhoek (NKI-AVL). The study was approved by the local Medical Ethics Committee and all patients signed an informed consent for participation.

Per patient, three 3D models were created: the mandible with the planned position of the cutting guide and resection planes (preoperative model), the mandible with the cutting guide in its position during surgery (intraoperative model), and the reconstructed mandible (postoperative model) (Figure 1).

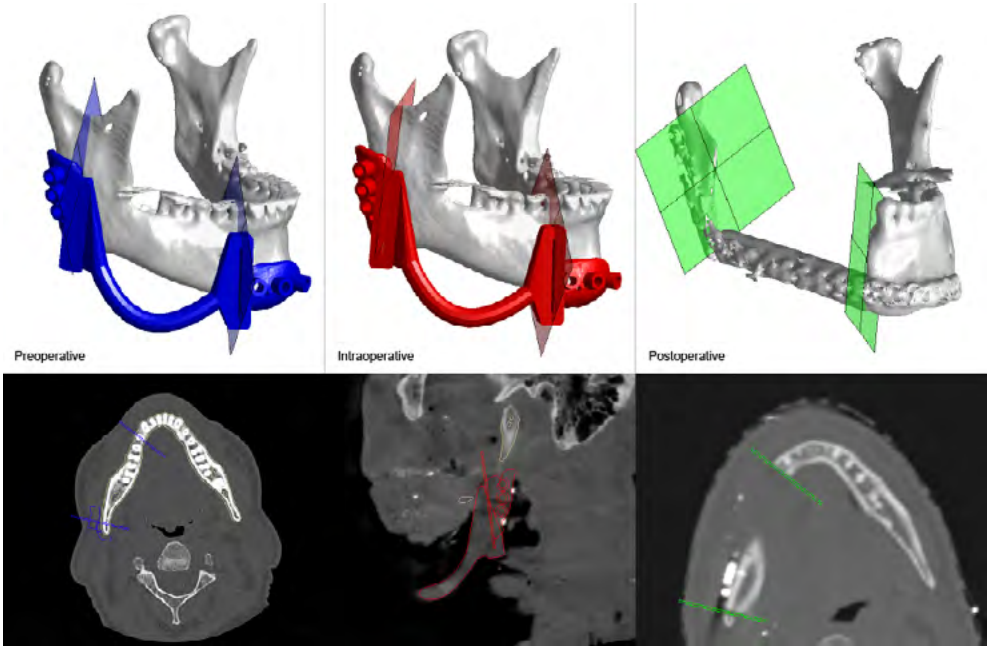

Figure 1 Preoperative model of the mandible with the cutting guide and the virtually planned resection planes, the cutting guide in its position during surgery, and the final resection planes in the postoperative model of the mandible with the reconstruction.

Pre-operative model

All patients underwent a preoperative conventional diagnostic CT scan (Toshiba Aquilion high resolution helical CT scanner, 0.468x0.468x1.0 mm voxel size). Automatic segmentation of the mandible was performed to create a virtual 3D model (3D Slicer, http://www.slicer.org, (10)). The surgeon planned the location and orientation of the resection planes on this virtual model. a custom cutting guide was designed to fit around the mandible and guide the saw to the planned resection planes. The cutting guide consisted of one part where two sawing slots were connected by an arch (Figure 1). We design

the cutting guides with an arch to provide a better fit to the mandible and hereby minimize the degrees of freedom in placement. Since the distance between the resection planes on the mandible have to correspond exactly with the lengths of the graft segments, the cutting guides of the mandible and the graft segments are carefully designed with respect to each other. For patients undergoing a hemi mandibulectomy, the cutting guide had one sawing slot. After approval of the surgeon, the cutting guides were printed in 3D (KLS Martin Group, Tutlingen, Germany) using CAD/CAM technique in order to accurately translate the virtual plan to the operating room.

Intra-operative model

During surgery, the mandibular bone was exposed by a combined transoral-transcervical approach and lifting the periosteum from the bone. The 3D printed cutting guide was manually positioned and fixated to the mandible with monocortical screws using non-locking 2.3 screws (KLS Martin Group, Tutlingen, Germany). After fixation of the cutting guide, a cone beam CT (CBCT) was acquired at the hybrid operating room (Philips Allura XpertCT CBCT scanner, Philips Medical Systems, 0.688 mm isotropic voxels). After resection, the cutting guide was removed, and the defect was reconstructed with a customized 3D printed titanium reconstruction plate which was fixated with 2.7 locking screws (KLS Martin Group, Tutlingen, Germany). Depending of the vascular status of the patient, a free vascularized osseous or osseo-fascio-cutaneous fibular flap, free vascularized osseo-myo-cutaneous deep circumflex iliac artery bone flap or myo-fascio-cutaneous pectoralis major flap was used to bridge the bony and soft tissue defect.

To obtain the model of the intraoperatively placed cutting guide and the associated resection planes, the planned cutting guide was copied from the preoperative model to the intraoperative CBCT scan and its location was matched to the intraoperative position by using parts of the cutting guide that were clearly identifiable on the CBCT (e.g. the saw slots that were not surrounded by soft tissue, 3D Slicer, http://www.slicer.org, (10)). The transformation that could be calculated from the preoperative and intraoperative positions of the cutting guide was applied to the preoperative resection planes to obtain the intraoperative position of the resection planes.

Post-operative model

The remaining distal and proximal segments of the mandible and bone segments used for reconstruction could be segmented from a CT scan acquired postoperatively (Siemens CT scanner, 1.5 mm/3.0 mm slice thickness and 0.977 x 0.977 mm voxel size; usually acquired 1-3 months after surgery). From this segmentation, the bone segments used for reconstruction, and the titanium reconstruction plate, were erased manually on each slice, so that the actual resection planes of the mandible were exposed. a single point was manually selected at the 3D resection surface of the mandible. The outward facing normal vector was calculated, and all neighboring points with normal vectors deviating less than 10 degrees were deemed to belong to the resection surface. The postoperative resection plane was determined by fitting a plane through these points in Matlab (Matlab R2018b, The MathWorks, Inc).

Registration of the pre-operative, intra-operative and post-operative resection planes

In order to compare the exact locations of the resection planes between the different pre-operative, intra-operative and post-operative models, the segmentations of the mandibles were registered using the surface registration algorithm in Matlab. The transformation that could be calculated from the registration was used to transform the resection planes, so that the pre-, intra- and post-operative resection planes could be projected onto the same mandible and the differences could be calculated.

Since the remaining mandible in the postoperative model consisted of two parts after the resection, the surface registration was done two times: for analysis of the distal (most anteriorly located) osteotomy, the registration was done on the remaining contralateral part of the mandible, and for the analysis of the proximal (most posterior) osteotomy, the registration was done on the ipsilateral condyle.

Outcome measures

For each planned, intraoperative and postoperative resection plane, a delineation was constructed from the points where the plane sliced the mandible. The points for this delineation were found by intersecting the resection planes with the preoperative model. Per delineation, the center of gravity was determined. Distances between the center of gravity of the planned, intraoperative and postoperative resection planes were used to compare the positions of the different planes (Figure 2).

The difference between the orientation of the resection planes was expressed as the angles along the cranial-caudal axis (yaw) and the angle along the lateral-medial axis (pitch) (Figure 2).

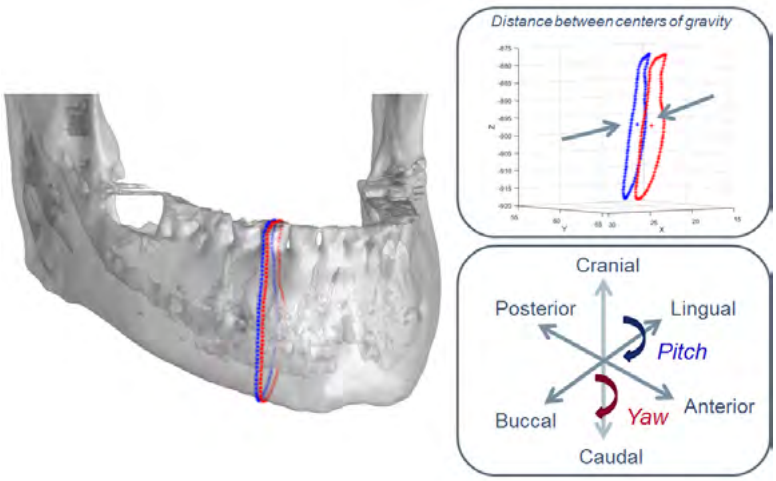

Figure 2 Delineation of the resection plane through the mandible. The distance between the centers of gravity of the resection planes was used as the study outcome, together with the yaw and pitch angles. There is no roll angle, since the resection is performed all the way through the mandibular bone, along one plane; rotations around the anterior-posterior axis do not change the position of the resection plane.

Results

Patients

A total of nine patients were included in this study. These patients underwent a segmental (n=8) or hemimandibulectomy (n=1) with a free fibular flap reconstruction (n=7), pectoralis major flap reconstruction (n=1) or a free deep circumflex iliac artery bone flap reconstruction (n=1), between December 2017 and February 2019 (Table 1). In this analysis 9 anterior resection planes were evaluated, and 8 posterior resection planes (as a result of the hemimandibulectomy).

Patient 7 was excluded from the analysis, because it was impossible to position the cutting guide according to the virtual planning due to the fact that the cutting guide interfered too much with the tumor infiltrated soft tissue surrounding the mandible (Figure 3). In addition, the posterior plane from patient 8 was excluded, due to a pathological fracture that occurred after the preoperative diagnostic CT scan. Patient 9 was also partially excluded from the analysis: due to tumor progression in the interval between virtual planning and surgery, the surgeons decided to extend the tumor margin at the medial site and therefore adjusted the position of the cutting guide as such after the acquisition of the intraoperative CBCT.

Table 1 Specifications and pathology outcomes of the surgeries of the patients included in the study.

Case	Gender	Age	Mandibulectomy	Reconstruction	Tumor type / Osteoradionecrosis	Pathology
1	M	74	Segmental	Free fibular flap	T4aN0M0 SCC retromolar trigone right	Tumor positive posterior bone resection plane
2	M	48	Segmental	Free fibular flap	T4aN1M0 intraosseous mucoepidermoid carcinoma right	Tumor free bone resection planes
3	M	53	Segmental	Free fibular flap	Osteoradionecrosis	No malignancy
4	M	42	Segmental	Free fibular flap	Osteoradionecrosis	No malignancy
5	M	50	Hemi	Free fibular flap	T4N0M0 SCC retromolar left	Tumor free bone resection planes
6	F	58	Segmental	Free fibular flap	T4aN0M0 alveolar process region 42-37	Tumor free bone resection planes
7	M	65	Segmental	Free fibular flap	T4aN1M0 SCC retromolar trigone right	Tumor free bone resection planes
8	M	64	Segmental	Pectoralis major flap	Osteoradionecrosis	No malignancy
9	M	67	Segmental	Deep circumflex iliac artery (DCIA) bone flap	T4aN2bM0 SCC floor of mouth right	Tumor free bone resection planes

F = female, M = male, SCC = squamous cell carcinoma

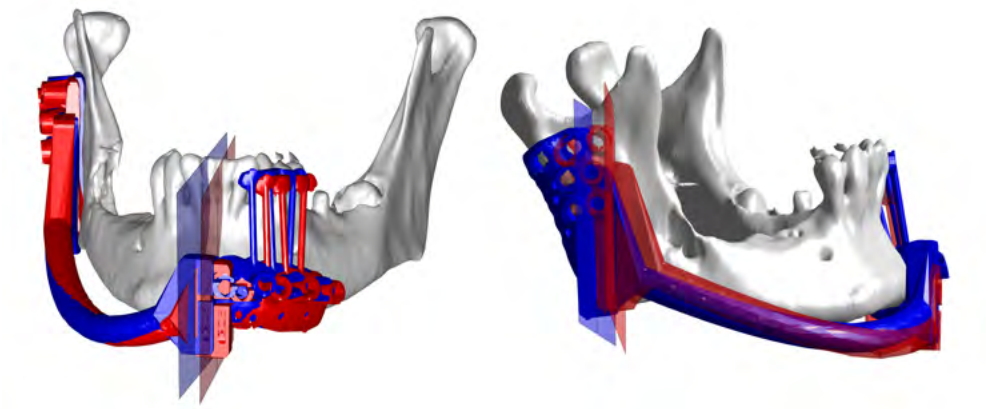

Figure 3 Superimposition of the preoperative (blue) and intraoperative (red) cutting guides in patient 7.

Preoperative, intraoperative and postoperative comparisons

Table 2 shows the differences between the centers of gravities of the resection planes, with the differences in angles for the preoperative and intraoperative comparison, intraoperative and postoperative comparison and the preoperative and postoperative comparison, for the anterior and posterior osteotomies.

Resection margins

The current study shows that, compared to the planned location of the resection planes, the postoperative margins decreased (e.g. closer to the disease) in four out of seven anterior osteotomies with a maximum distance of 1.3 mm (Table 2). For the posterior plane, margins decreased for four out of five osteotomies, with a maximum distance of 3.7 mm. In the one patient, for whom a positive tumor resection margin of the posterior bone resection plane was reported, the margin reduced with 1.8 mm according to our analysis comparing the preoperative planning with the postoperative outcome (Table 1).

Since the difference between preoperative planning and postoperative resection of the anterior resection plane is negligible (absolute mean of 0.9 mm), only the effect of the placement of the cutting guide on the margin at the posterior resection plane will be discussed here. In four out of five posterior osteotomies, less bone was resected when comparing preoperative planning with postoperative outcome. In three of these cases, the cutting guide was positioned with a smaller margin relatively to the tumor/ORN (-0.8 mm on average). In two of these cases, the margin reduced further by the sawing (-1.8 mm on average). In the other two cases, the positioning of the cutting guide would have resulted in a larger resection of 0.8 mm on average. However, the actual sawing shifted the osteotomy with a mean distance of 2.3 mm towards the tumor/ORN.

The bone resection increased in three out of seven anterior osteotomies (1.0 mm on average), and one out of five resections in the posterior mandible (2.2 mm).

Table 2 Differences between preoperative, intraoperative and postoperative resection planes for the anterior and posterior osteotomies. Patient 7 was excluded from the analysis. In addition, the posterior plane of patient 8 and the postoperative analysis of patient 9 were excluded.

	Distal (anterior) resection plane								
	Preoperative vs intraoperative			Intraoperative vs postoperative			Preoperative vs postoperative		
	distance (mm)	yaw (°)	pitch (°)	distance (mm)	yaw (°)	pitch (°)	distance (mm)	yaw (°)	pitch (°)
1	-1,3	0,2	0,1	0,8	0,9	3,5	-0,5	0,7	3,6
2	2,4	1,7	0,2	-3,6	2,6	4,4	-1,3	0,6	4,8
3	2	5,7	1,4	-0,5	2,3	0,1	1,5	7,9	1,6
4	-0,1	0,8	0,1	1,5	0,1	1,1	1,4	0,6	1,2
5	-1,4	0	0	0,7	2,5	1,1	-0,7	2,5	0,9
6	-1,2	0,6	0,1	0,8	20,6	0,4	-0,5	21	3,6
8	-0,4	2,7	0,9	0,4	5,2	2,2	0,1	2,6	2,8
9	0,2	0,4	0	NA	NA	NA	NA	NA	NA
Absolute mean	1.1	1.5	0.4	1.2	4.9	1.8	0.9	5.1	2.6
Std	0.8	1.8	0.5	1.0	6.6	1.5	0,5	6.9	1.4

	Proximal (posterior) resection plane								
	Preoperative vs intraoperative			Intraoperative vs postoperative			Preoperative vs postoperative		
	distance (mm)	yaw (°)	pitch (°)	distance (mm)	yaw (°)	pitch (°)	distance (mm)	yaw (°)	pitch (°)
1	0,8	0,2	1	-2,8	17,2	20,6	-1,8	14,8	4,6
2	-0,7	2,1	1,9	-0,6	2,5	3,2	-1,3	4,6	5
3	-0,9	4,3	3	-2,9	22,8	7,6	-3,7	19,4	4,9
4	-0,7	0	0	2,9	2,7	7,6	2,2	6,6	4,7
5	NA	NA	NA	NA	NA	NA	NA	NA	NA
6	0,8	0	0	-1,8	1,1	2,5	-0,9	2	1,9
9	0,8	0	0	NA	NA	NA	NA	NA	NA
Absolute mean	0.8	1.1	1.0	2.2	9.3	8.3	2.0	9.5	4.2
Std	0.1	1.6	1.1	0.9	9.0	6.5	1.0	6.6	1.2

Std = standard deviation, NA = not applicable, +/- more/less mandible resected compared to the planning

Discussion

In mandibular surgery, the position of the resection planes affects both complete tumor resection and accurate reconstruction. Virtual surgical planning is used to plan the exact positions of the resection planes preoperatively. To translate the virtual plan to the surgery, patient-specific cutting guides are designed. In this study, the positioning of the cutting guide was evaluated with an intraoperative CBCT scan. The virtual surgical plan, the intraoperative position of the cutting guide and the postoperative outcome were evaluated. We found that cutting guides were positioned with a millimeter accuracy. Anterior osteotomies were performed more accurately through the saw slots compared to posterior osteotomies. The relatively large yaw angle between the resection planes (up to 21°) indicates a directional freedom of the saw through the resection slots (i.e. clearance between the saw slot and saw blade) that is responsible for the difference between the planned/intraoperative resection planes with the postoperative resection planes. Resection margins were affected in the majority of the resection planes in such a way that less bone was resected than planned, and thus the resection margin was reduced.

A millimeter accuracy in the execution of the virtual surgical planning is of importance for accurate reconstruction of the mandible; even more when the virtual planning also includes placement of dental implants. With an accurate reconstruction, the aesthetics of the face can be re-established, the ability of mastication and occlusion can be restored, and speech could be maintained. To allow accurate reconstruction of the mandible, the reconstruction segments need to fit the mandibular defect as precisely as possible. When, as shown in our study, less or more mandibular bone is resected, the segments used for reconstruction will not fit precisely. To achieve an accurate reconstruction nevertheless, the graft segments have to be adjusted manually during surgery. This increases the operational time and affects the accuracy of reconstruction.

Besides accurate reconstruction, a precise execution of the preoperative plan is also of importance to ensure complete tumor resection with adequate margins. The location of the resection plane is usually planned with a 10 mm margin between the tumor and the resection. The clinical practice guidelines (NCCN) recommend adequate tumor-free margins; as well as the Royal College of Pathologists, who recommend to record the presence or absence of carcinoma at the bone margins (11, 12). Tumor positive margins are an important prognostic factor, as the 5-year overall survival was significantly lower in this group. In order to lower the number of positive bone resection margins, improvements in the accuracy of the execution of the virtual surgery plan are needed.

In line with the literature, the current study reported on differences up to 2 mm between preoperatively planned and postoperatively found resection planes (7-9, 13, 14). Van Baar *et al.* published a review on the accuracy of computer-assisted surgery in mandibular reconstruction (15). Although, a meta-analysis could not be conducted due to the lack of uniformity in planning and evaluation methods among the studies, they do report on accuracy deviations in the pre- and postoperative situations. They mention that possible factors responsible for inaccuracies include image acquisition, segmentation, 3D printing, surgery and/or the method used to evaluate the postoperative result. Recently, Goormans *et al.* added an extra factor to this list: the methods that are used for fixation of the segments used for reconstruction (16). They found that fibular segments can be prepared very accurately according to the planning, but that inaccuracies in reconstruction occur due to the method of fixation of the

segments. Compared to the latter study, the current study did not evaluate the fixation method of the several segments that were used for reconstruction, but focused merely on the resection planes on the remaining mandibular bone instead, with the main focus to the evaluate the accuracy of resection planes in the mandible.

Our study is the first study that acquired an intraoperative CBCT scan after fixation of the cutting guide to the mandible. This allowed evaluation whether the deviation is caused by the positioning of the cutting guide or by the sawing process after positioning of the guide. Our results suggest that inaccuracies occur predominantly after positioning of the cutting guide, since the preoperative comparison with the intraoperative situation is very precise. The sawing procedure itself seems a cause for inaccuracies found in the intra- and postoperative comparison. Another reason for these inaccuracies could be the bone remodeling process, since most of the postoperative CT scans were acquired within 1-3 months after surgery.

The cutting guide consists of two saw slots, one for the distal (anterior) osteotomy and one for the proximal (posterior) osteotomy, that are connected by an arch. This is meant to provide a better fit of the cutting guide to the mandible and less degree of freedom. However, our results suggest that the directions of the resection planes are affected by each other due to this arch connection between the saw slots. This is shown in the yaw angle: where the angle is small comparing the pre/intraoperative resection plane with the postoperative plane of the anterior osteotomy, this angle is large in the same comparison of the posterior osteotomy (patient 1 and 3). For patient 6, the yaw angle is very large for the anterior osteotomy, where it is very precise for the posterior osteotomy. The yaw angle represents the angle along the caudal-cranial axis. This suggests that when one osteotomy is performed, the second osteotomy starts according to plan, but deviates from the plan during the sawing process. To prevent the slots from affecting each other, it might be an option to design the cutting guides without the connecting arch. However, this approach requires the use of other technologies to ensure a millimeter accurate positioning.

For the posterior plane, the difference between preoperative and postoperative planes is relatively large (2.0 mm, yaw 9.5° and pitch 4.2°) compared to the difference between preoperative and intraoperative planes (0.8 mm, yaw 1.1° and pitch 1.0°). This could be explained by the fact that the posterior saw slot only provides guidance during the caudal part of the posterior osteotomy (Figure 1) and the cranial part is sawed free hand. Since the postoperative resection plane is fitted through the whole height of the mandible for evaluation of accuracy, thus including both cranial and caudal parts, a few degrees in angular deviation and thus a shift between the centers of gravity of the planes could have occurred. From both oncological, and reconstruction point of view, a millimeter accuracy is of less value for the upper part of the posterior resection plane, since the tumour does not usually impinge in the subsigmoid region and the graft segments are usually fixated to the lower border of the remaining mandible. However, the more extensive elevated soft tissue overlying the mandibular ramus and condyle (e.g. parotid gland and masseter muscle) may hamper the surgeon's accessibility and overview while performing the posterior osteotomy. Even more, the pressure of the elevated soft tissues could increase the deviation of a non-rigid hand hold sawblade. This could be an explanation for the difference in accuracy between the posterior and anterior resection planes, since the anterior mandible is frequently easy and well exposed.

This study has several limitations. First of all, care should be taken in interpretation of the results due to the limited number of patients included in the study. Second, inaccuracies could have occurred in the comparison between the intraoperative and postoperative 3D models. The fact that the cutting guide presented with similar grey values on the intra-operative CBCT scan challenged the construction of the intraoperative 3D model in some cases. An inaccurate segmentation of the cutting guide affects the position of the intraoperative resection plane.

Future studies could focus on optimization of the cutting guides. In order to reduce the directional freedom of the saw within the saw slots, the design of the saw slot could be improved. Possible ways are to enlarge the thickness of the saw slot, to extend the length of the slot along the whole mandible for the posterior osteotomy or to use a titanium slit that fits into the saw slot of the guide.

In conclusion, deviations are found between the position and direction of the resection plane that is planned during virtual surgery, and the postoperative outcome. Using an intraoperatively acquired CBCT scan, we evaluated whether this deviation can be caused by the positioning of the patient-specific cutting guide. We found that cutting guides are positioned with a millimeter accuracy compared to the virtual plan. And thus, the deviation must be caused by the fact that the cutting guide does not provide enough guidance during the sawing, especially for posterior osteotomies.

References

1. Brown, J.S., et al., Mandibular reconstruction with vascularised bone flaps: a systematic review over 25 years. Br J Oral Maxillofac Surg, 2017. 55(2): p. 113-126.
2. Hurvitz, K.A., M. Kobayashi, and G.R. Evans, Current options in head and neck reconstruction. Plast Reconstr Surg, 2006. 118(5): p. 122e-133e.
3. Rodby, K.A., et al., Advances in oncologic head and neck reconstruction: systematic review and future considerations of virtual surgical planning and computer aided design/computer aided modeling. J Plast Reconstr Aesthet Surg, 2014. 67(9): p. 1171-85.
4. Liu, Y., et al., Technical procedures for template-guided surgery for mandibular reconstruction based on digital design and manufacturing. Biomedical Engineering Online, 2014. 13(63).
5. Chang, E.I., et al., Long-Term Operative Outcomes of Preoperative Computed Tomography-Guided Virtual Surgical Planning for Osteocutaneous Free Flap Mandible Reconstruction. Plast Reconstr Surg, 2016. 137(2): p. 619-23.
6. Ren, W., et al., Virtual Planning and 3D printing modeling for mandibular reconstruction with fibula free flap. Med Oral Patol Oral Cir Bucal, 2018. 23(3): p. e359-e366.
7. Kraeima, J., et al., Multi-modality 3D mandibular resection planning in head and neck cancer using CT and MRI data fusion: a clinical series. Oral Oncol, 2018. 81: p. 22-28.
8. De Maesschalck, T., D.S. Courvoisier, and P. Scolozzi, Computer-assisted versus traditional freehand technique in fibular free flap mandibular reconstruction: a morphological comparative study. Eur Arch Otorhinolaryngol, 2017. 274(1): p. 517-526.
9. Roser, S.M., et al., The accuracy of virtual surgical planning in free fibula mandibular reconstruction: comparison of planned and final results. J Oral Maxillofac Surg, 2010. 68(11): p. 2824-32.
10. Fedorov, A., et al., 3D Slicer as an Image Computing Platform for the Quantitative Imaging Network. Magnetic Resonance Imaging, 2012. Nov;30(9):1323-41.
11. NCCN Clinical Practice Guidelines in Oncology (NCCN Guidelines) Head and Neck Cancers. 2018.
12. Helliwell, T. and J. Woolgar, Dataset for histopathology reporting of mucosal malignancies of the oral cavity. The Royal College of Pathologists, 2013.
13. Schepers, R.H., et al., Accuracy of fibula reconstruction using patient-specific CAD/CAM reconstruction plates and dental implants: a new modality for functional reconstruction of mandibular defects. J Craniomaxillofac Surg, 2015. 43(5): p. 649-57.
14. Pietruski, P., et al., Supporting mandibular resection with intraoperative navigation utilizing augmented reality technology- a proof of concept study. J Craniomaxillofac Surg, 2019. 47(6): p. 854-859.
15. van Baar, G.J.C., et al., Accuracy of computer-assisted surgery in mandibular reconstruction: a systematic review. Oral Oncol, 2018. 84: p. 52-60.
16. Goormans, F., et al., Accuracy of computer-assisted mandibular reconstructions with free fibula flap: Results of a single-center series. Oral Oncol, 2019. 97s.

Chapter 8

Electromagnetic surgical navigation in patients undergoing mandibular surgery

S.G. Brouwer de Koning

F. Geldof

R.L.P. van Veen

M.J.A. van Alphen

L.H.E. Karssemakers

J. Nijkamp

W.H. Schreuder

T.J.M. Ruers

M.B. Karakullukcu

Scientific Reports (2021) https://doi.org/10.1038/s41598-021-84129-5

Abstract

The purpose of this study was to evaluate the feasibility of electromagnetic (EM) navigation for guidance on osteotomies in patients undergoing oncologic mandibular surgery.

Preoperatively, a 3D rendered model of the mandible was constructed from diagnostic computed tomography (CT) images. Cutting guides and patient specific reconstruction plates were designed and printed for intraoperative use. Intraoperative patient registration was performed using a cone beam CT scan (CBCT). The location of the mandible was tracked with an EM sensor fixated to the mandible. The real-time location of both the mandible and a pointer were displayed on the navigation system. Accuracy measurements were performed by pinpointing four anatomical landmarks and four landmarks on the cutting guide using the pointer on the patient and comparing these locations to the corresponding locations on the CBCT. Differences between actual and virtual locations were expressed as target registration error (TRE).

The procedure was performed in eleven patients. TREs were 3.2±1.1 mm and 2.6±1.5 mm using anatomical landmarks and landmarks on the cutting guide, respectively. The navigation procedure added on average half an hour to the duration of the surgery.

This is the first study that reports on the accuracy of EM navigation in patients undergoing mandibular surgery.

Keywords

Mandibular surgery; image-guided surgery; computer-assisted surgery; electro-magnetic navigation; bone cutting guides.

Introduction

Computer-aided-design/computer-aided-manufacturing (CAD/CAM) techniques have become routine use in mandibular surgery. In this, a 3D rendered model of the mandible, constructed from a preoperative computed tomography (CT) scan, is used to plan the exact positions of the osteotomies virtually, in advance of the surgery. In this way, adequate tumor resection and an accurate fit of bone segments that will be used for reconstruction after resection can be planned. In order to convert the virtual plan to the patient in the operating room, patient-specific cutting guides and fixation plates are designed. This procedure is costly and time-consuming. In the meantime, there is a change in the tumor size, for which the cutting guide cannot account for during surgery. Therefore, there is a need for a technology that saves preparation time, money and provides flexibility during surgery.

Surgical navigation has been used increasingly and we hypothesize that this technology fulfills the requirements mentioned above. Surgical navigation provides real-time visual feedback about the position of surgical instruments in relation to the patient's anatomy. This could potentially be used to translate the preoperative planning to the operating room, thereby eliminating the use of cutting guides.

Electromagnetic (EM) navigation is used routinely in neurosurgery or surgery of the sinonasal cavity, but not in mandibular surgery so far: the fact that the mandible is mobile challenges accurate navigational tracking. However, there are studies that evaluated the technology in phantoms and cadavers. In these studies, accuracy measures mostly involve the comparison between the planned and performed osteotomy or the position of the mandibular condyle before and after the osteotomy (1, 2). For example, Peacock *et al.* report on a <2mm difference between preoperatively planned osteotomy and navigated osteotomy and Nova *et al.* found a difference between navigated condyle position and preoperative condyle position that was also within 2mm. Bouchard *et al.* evaluated the target registration error (TRE) of EM navigation on a dissected mandible with a reference sensor secured to a tooth with composite dental material (3). The tip of the tracked surgical instrument was placed at different locations on the mandible and the difference between the actual and virtual location was measured (TRE was 2.10 +- 0.88 mm). Seeberger *et al.* evaluated the usability of an EM tracking device in maxillofacial surgery through testing on a phantom skull under operating room conditions. They report on a TRE of 2.1 +- 0.86 mm (4). With regards to patient studies, there are only a few reports published on studies that use EM navigation in mandibular surgery (5, 6). These studies were focused on condylar repositioning after osteotomies and did not focus on the TRE of the EM navigation. Thus, the accuracy of EM navigation used in patients undergoing mandibular surgery has not been reported so far. Therefore, as a first step of utilizing intraoperative EM navigation, we conducted a study investigating the accuracy of EM navigation in eleven patients undergoing mandibular surgery.

Methods

Patients that were planned for a segmental or hemi-mandibulectomy at the Netherlands Cancer Institute – Antoni van Leeuwenhoek Hospital were included. These patients were treated for malignant and benign tumors invading the mandible, or for osteoradionecrosis of the mandible. The study was approved by the Medical Ethics Committee of the Antoni van Leeuwenhoek hospital and the institutional research ethics board, and all patients signed an informed consent for participation (NL60004.031.17). An overview of the pre-, intra- and post-operative steps of the procedure is shown in Figure 1.

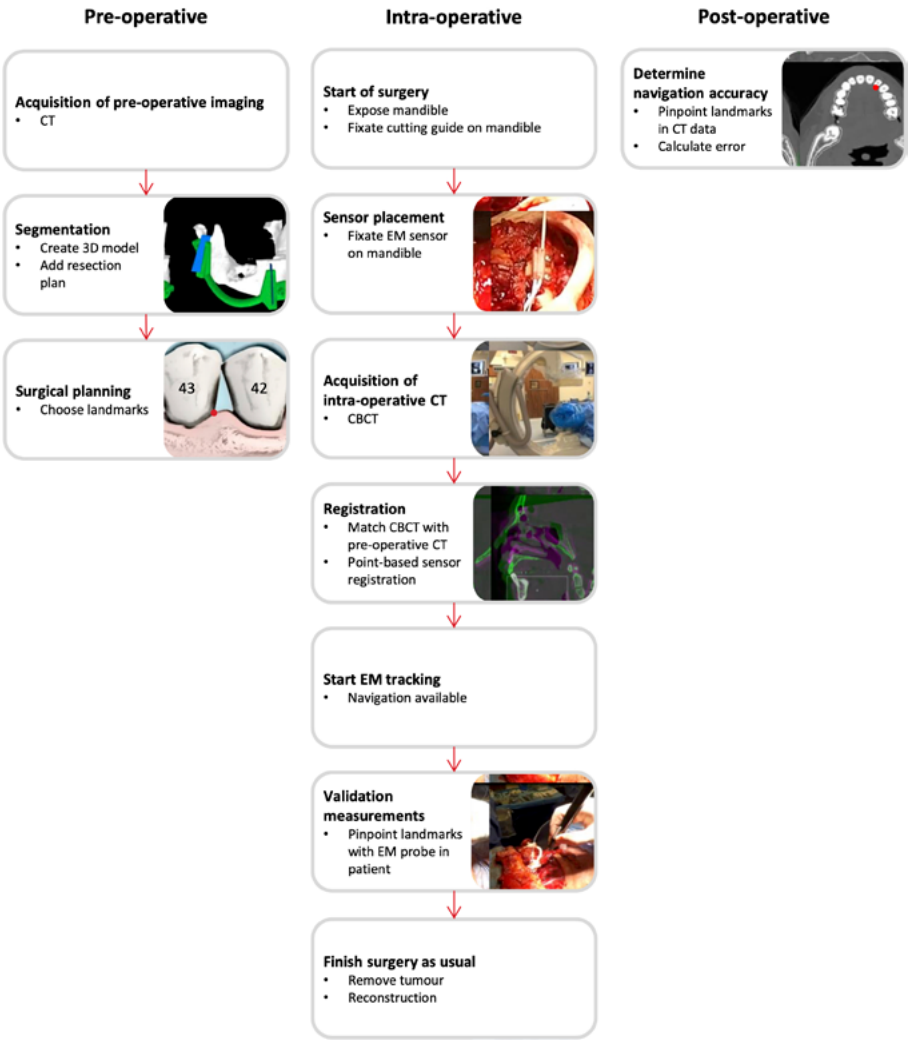

Figure 1 Overview of pre-, intra- and post-operative steps of the surgical navigation procedure.

EM navigation system

The tracking system (NDI Aurora, Northern Digital Inc., Waterloo, Canada) consists of a field generator, a six degrees of freedom (6DOF) EM-tracked probe and a shielded 6DOF cable sensor. The in-house developed navigation software *SurgNav* (7), holds the registration procedure and a four-display mode (axial, sagittal, frontal and 3D) where the position and orientation of the tracked probe and sensor are visualized relative to the imaging data and the virtual model.

Pre-operative model

All patients underwent a preoperative conventional diagnostic CT scan (Toshiba Aquilion high resolution helical CT scanner, 1.0 mm slice thickness and 0.468 x 0.468 mm voxel size). Automatic segmentation of the mandible was performed to create a virtual 3D model (8). The surgeon planned the location and orientation of the resection planes on this virtual model. a patient tailored cutting guide was designed to fit on the mandible and guide the saw to the planned resection planes. After approval of the design of the cutting guide by the surgeon, the cutting guides were printed in 3D (KLS Martin Group, Tutlingen, Germany) in order to accurately translate the virtual plan to the operating room.

Surgical approach

During the surgery, the mandibular bone was exposed, and the 3D printed cutting guide was positioned and fixated to the mandible with screws. a dedicated sensor housing module for the 6DOF EM-sensor was fixated to the part of the mandibular bone that was planned for resection (Figure 2).

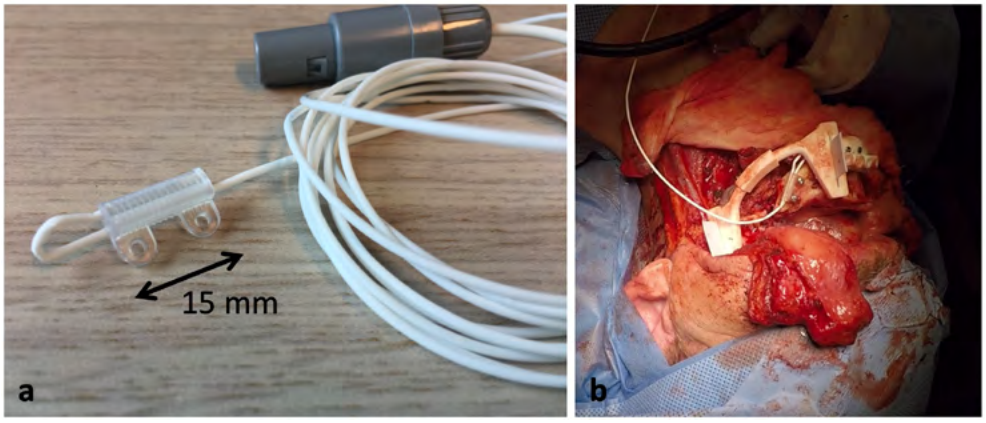

Figure 2 (a) EM sensor placed in a sensor housing module that was designed for this study. (b) The sensor housing module with EM sensor fixated to the mandible with screws.

Intra-operative procedure

To register the real-time situation in the operation room with the virtual 3D model, landmarks that are precisely localizable on both the patient and the 3D model are matched. Usually, e.g., in neurosurgery, these landmarks are placed prior to the preoperative CT scan so that they are present in the 3D model. In the current study, the screws of the cutting guide are used as landmarks for registration as a substitute for screws that can be placed before the surgery and intraoperative CBCT is the substitute for preoperative CT with screws *in situ*. With this approach, we could test if a CT with preoperatively

placed mandibular screws can be used accurately for navigation purposes. Therefore, directly after positioning and fixation of the cutting guide and EM-sensor at the mandible, a cone beam CT scan (CBCT) was acquired. This was done in the hybrid operation room, equipped with an Allura FD20 CBCT system (Philips Medical Systems, Best, the Netherlands), with 0.688 mm isotropic voxels. The CBCT scan could be superimposed on the diagnostic CT scan that was used to construct the 3D model, using bone registration in an in-house developed software program. This bone registration was performed using an automatic rigid gray-value registration with mutual information as a cost function, within a user-defined region of interest (ROI) including only the mandible. This way the screws that were visible on the CBCT could be matched with the 3D model to allow registration of the 3D model with the patient in the operation room. Thus, the CBCT scan was only used to register the 3D model with the real-time situation in the operation room, and as a surrogate for preoperative CT with screws planted. An intraoperative CBCT is not compulsory for utilization of the proposed method.

The EM field generator was positioned near the patient's head. The location of the mandible was tracked by the 6DOF EM tracked sensor that was fixated to the mandible with the sensor housing module. a rigid point-based registration was performed by pinpointing four landmarks (screws of the cutting guide and screws of the sensor housing module) using an EM tracked pointer in the patient and simultaneously indicating the corresponding points in the CBCT scan (that was superimposed on the 3D model). The error of the point-based registration was expressed as fiducial registration error (FRE), which is the root mean squared distance among corresponding landmarks used in registration.

Accuracy measurements were performed by pinpointing four anatomical landmarks (e.g. mental foramina, cusps mandibular teeth) and four landmarks on the cutting guide (the end points of the sawing slots) (Figure 3, Figure 4) with the trackable pointer.

Post-operative evaluation

Two observers indicated the anatomical landmarks, and the landmarks on the cutting guide, in the intraoperative CBCT data. Inter-observer variability was calculated as the intraclass coefficient (ICC). The mean position of the points indicated by the two observers was used as the virtual location of the landmark in the CBCT data. The accuracy of the system was determined by comparing the pinpointed location of the landmarks on the patient with the location of the corresponding landmarks on the CBCT data. The location of the landmarks (in x,y,z-coordinates) that are pinpointed by the trackable pointer on the patient (x_1,y_1,z_1) were saved into the same coordinate system as the locations of the corresponding landmarks on the CBCT (x_2,y_2,z_2). The distance between these two points (one originating from the landmark on the patient (x_1,y_1,z_1) and one originating from the corresponding landmark on the CBCT (x_2,y_2,z_2)) was expressed as the target registration error (TRE), meaning the Euclidean distance between a pair of corresponding landmarks.

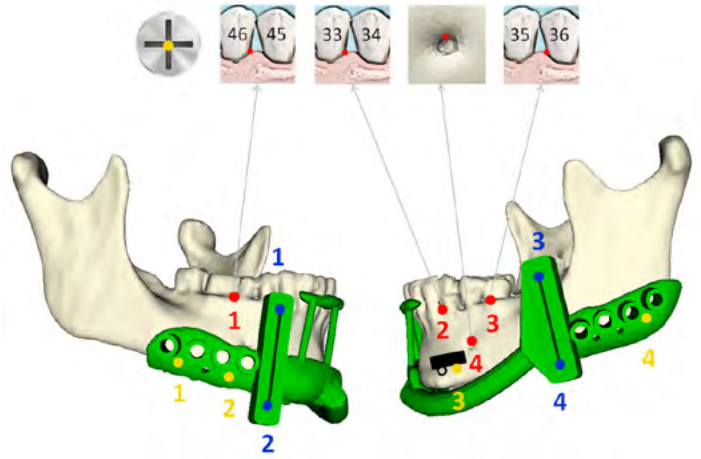

Figure 3 Schematic model of a mandible with the cutting guide (green). The sensor housing module (black) is fixated on the part of the mandible that will be resected. The yellow landmarks are used for fiducial registration. The anatomical landmarks (red) are located on teeth and mental foramen. The landmarks at the cutting guide (blue) are located in the upper and lower ends of the sawing slots. Dental numbering according to the FDI World Dental Federation (ISO 3950).

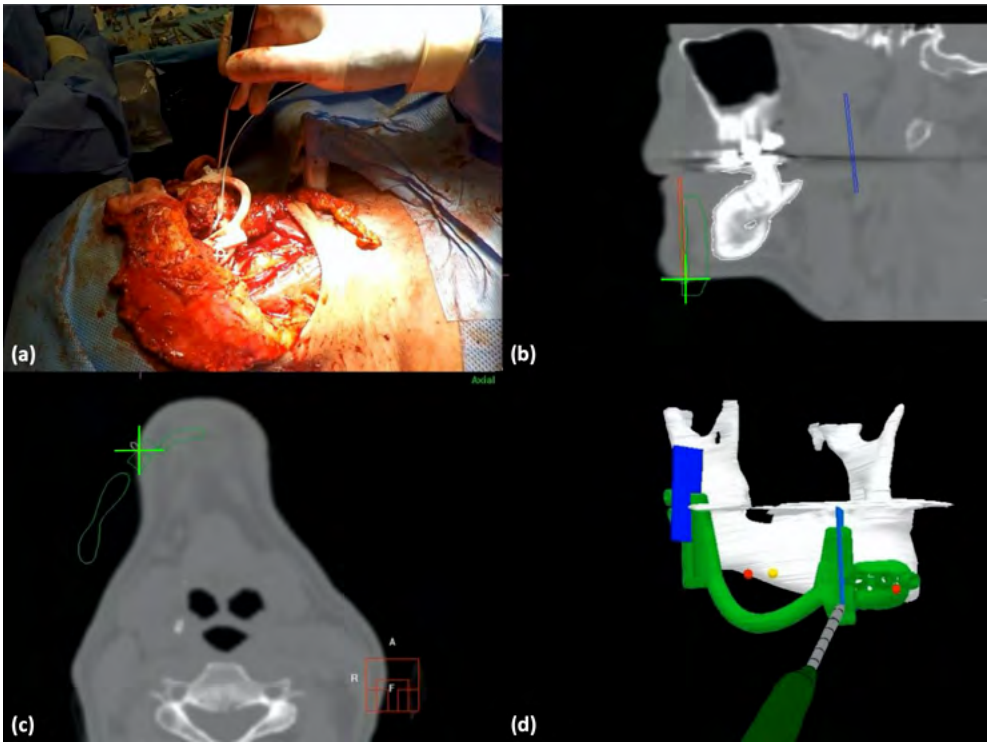

Figure 4 The surgeon points at the resection plane with the tracked pointer (a). The position of the pointer in relation to the mandible (white), the cutting guide (green), and the resection planes (blue) are shown in the sagittal and axial sections (b, c) and the 3D model (d).

Results

Patients

A total of eleven patients were included in this study. These patients underwent a segmental (*n*=9) or hemimandibulectomy (*n*=2) with a free fibula flap reconstruction (1=9), pectoralis major flap reconstruction (*n*=1) or a deep circumflex iliac artery bone flap reconstruction (1=1), at the NKI-AVL, between December 2017 and September 2019 (Table 1).

Table 1 Specifications and pathology outcomes of the surgeries of the patients included in the study.

Case	Gender	Age	Mandibulectomy	Reconstruction	Tumour type / Osteoradionecrosis
1	M	74	Segmental	Free fibular flap	T4aN0M0 SCC retromolar trigone right
2	M	48	Segmental	Free fibular flap	T4aN1M0 intraosseous mucoepidermoid carcinoma right
3	M	53	Segmental	Free fibular flap	Osteoradionecrosis
4	M	42	Segmental	Free fibular flap	Osteoradionecrosis
5	M	50	Hemi	Free fibular flap	T4N0M0 SCC retromolar trigone left
6	F	58	Segmental	Free fibular flap	T4aN0M0 alveolar process region 42-37
7	M	65	Segmental	Free fibular flap	T4aN1M0 SCC retromolar trigone right
8	M	64	Segmental	Pectoralis major flap	Osteoradionecrosis
9	M	67	Segmental	Deep circumflex iliac artery bone flap	T4aN2bM0 SCC floor of mouth right
10	M	58	Segmental	Free fibular flap	T4N0M0 SCC midline floor of mouth midline
11	F	76	Hemi	Free fibular flap	T4N0M0 SCC alveolar process right

F = female, M = male, SCC = squamous cell carcinoma

Accuracy of the EM navigation system

In seven out of eleven patients, the FRE of the EM navigation was <1 mm, indicating a very high accuracy of the ready-to-use technology (Table 2). The deviating FRE of patient five was caused by the fact that the sensor was not properly fixated in the sensor housing module.

Mean TREs measured on anatomical landmarks and on landmarks on the cutting guide were 3.2 ± 1.1 mm and 2.6 ± 1.5 mm, respectively.

Inter-observer variability

In order to account for the variability of pinpointing the landmarks on the CBCT, the inter-observer variability was measured. The ICC of the anatomical landmarks, and the landmarks on the cutting guide were for both subsets 1.0, meaning that the landmarks pinpointed on the CBCT by the two different observers resemble each other. This indicates that landmarks were evident on the CBCT.

Table 2 The accuracy measures for the registration (fiducial registration errors, FRE) and the navigation procedure (target registration errors (TRE)).

Case	FRE (mm)	TRE (mm)	
		Anatomical landmarks	cutting guide landmarks
		2.0	1.4
2	0.5	2.6	1.6
3	1.5	3.3	2.7
4	0.6	2.0	1.2
5	4.1	4.6	3.7
6	0.6	2.2	1.7
7	1.9	4.4	3.1
8	1.6	3.6	1.7
9	0.8	3.2	5.8
10	0.7	4.9	4.8
11	0.7	1.9	1.3
Mean (STD)	**1.2 ± 1.1**	**3.2 ± 1.1**	**2.6 ± 1.5**

FRE = fiducial registration error, TRE = target registration error, STD = standard deviation

Surgical workflow

The total time that was needed to prepare the EM navigation for use, and to perform the accuracy measurements, was on average 32 minutes (Figure 5). Registration of the sensor was most time consuming. This step was often redone in order to improve the accuracy of the system.

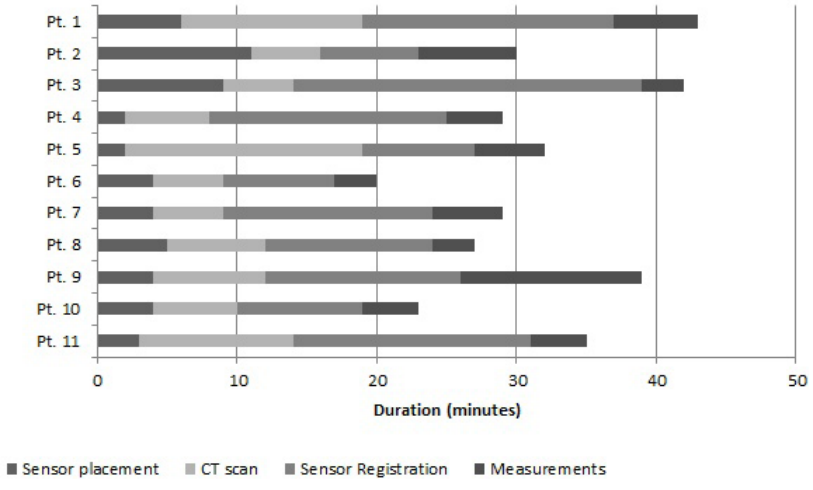

Figure 5 Surgical delay due to navigation workflow.

Discussion

This study tested EM navigation in eleven patients undergoing mandibular surgery, with the aim to evaluate whether this technology could provide accurate guidance for localization purposes, e.g. tumour margins and planned cutting planes for accurate mandible reconstructions. The accuracy of the EM navigation system was evaluated by measuring the deviation between the location of a landmark that was pinpointed on the patient with a tracked pointer and the location of the corresponding point in the 3D virtual model of the surgical navigation system. The deviation was 2.6 ± 1.5 mm and 3.2 ± 1.1 mm for landmarks located on the cutting guide and for anatomical landmarks, respectively. The navigation procedure added half an hour to the duration of the surgery.

The use of surgical navigation during mandibular surgery could optimize the clinical workflow in several ways. First of all, the surgical navigation can shorten preoperative preparation time. Preparation of the virtual model for surgical navigation takes one day maximally, and only depends on the date of the preoperative CT scan. Thus, if radiology planning allows, preparation can be performed very near to the day of surgery. This procedure eliminates the factor of tumor growth in the time between virtual surgery planning, printing of the patient specific cutting guides, and the surgery. As a result, the virtual model provides a more accurate representation of the real-time situation, which can affect the number of positive bone resection margins. Besides the shorter time needed for preparation, the surgical procedure itself could also be performed faster when reconstruction segments fit the mandibular defect precisely. Accurate guidance for localization of the resection planes could lower the number of cases in which reconstruction segments have to be adjusted manually to fit the mandibular defect, which is a time-consuming process.

In surgical navigation, the real-time position of the patient and the surgeon's instrument are tracked by the navigation system and registered with a patient-specific anatomical 3D model. Most commercially available surgical navigation technologies use optical tracking technologies to track the patient and the surgical instruments (9). However, electromagnetic (EM) navigation has practical advances over optical navigation for use during mandibular surgery: patient reference sensors and instrument sensors are small (less than 2 mm in diameter and 1 cm length), and no line-of-sight is required for application in a small surgical field (9). In addition, the EM field generator can be positioned near the patient's head, e.g. underneath the operating table.

For mandibular/maxillofacial surgeries specifically, optical or EM navigation has been evaluated in patients or phantoms (Table 3). The different studies use different definitions for the outcome measures. However, all provide some insight in the accuracy that was obtained by using the technology. The table shows that the current study is the first study reporting on accuracies of EM navigation in a group of patients, instead of cadavers/phantoms and that accuracies are comparable to the accuracies obtained with optical navigation that was used in patients undergoing mandibular surgery. This also applies for the accuracies reached in the phantom/model studies. Compared to other applications of the navigation system that was used in this study, the application in mandibular surgery seems quite accurate. For example in malignancies in the pelvis, TREs of 4.0-6.3 mm were reported (10).

Table 3 Overview of studies evaluating surgical navigation for use in mandibular/maxillofacial surgeries.

Author	Year	Navigation	Number of patients	Phantom/ model	Outcome	Definition
Hasan *et al.* (13)	2019	Optical	5	-	1.7 ± 0.8 mm, 5.4 ± 1.5° and 6.7 ± 4.6°, respectively	Difference in distance, pitch, and roll between planned resection plane and performed resection planes
Naujokat *et al.* (12)	2017	Optical	6	-	1.52 mm	Mean difference between planned osteotomy line and performed osteotomy line.
Naujokat *et al.* (12)	2017	Optical	-	3 skull models	1.03 mm (1), 0.98 mm (2) and 1,7 mm (3)	FRE: based on metal points on the mandibles (1), metal points on a splint based on the occlusal surface of the mandible teeth (2) and anatomical landmarks that were located interdental on the alveolar bone.
Shan *et al.* (14)	2016	Optical	20	-	79% < 1 mm; 87% < 2 mm; 92% < 3mm	Difference between preoperative plan and postoperative outcome
Lee *et al.* (6)	2019	EM with real-time augmented model	1	-	1.71 ± 0.63 mm	TRE measured on three condylar landmarks
Berger *et al.* (5)	2018	EM	10	-	No significant difference	Position of condyles after high oblique sagittal split osteotomy, manually or EM guided; no TRE reported
Nova *et al.* (2)	2017	EM	-	6 plastic skull models	± 2 mm	Displacement of the condyle between preoperative CT and postoperative CT
Peacock *et al.* (1)	2015	EM	-	Human cadavers and live minipig	< 2 mm	Differences between the navigation's prediction of the location of the osteotomy and the virtual planning
Bouchard *et al.* (3)	2012	EM	-	3 minipig cadavers	2.35 ± 1.35 mm	Mean difference in width mandibular rami after osteotomy and in the 3D model.
Bouchard *et al.* (3)	2012	EM	-	1 dissected mandible	2.10 ± 0.88 mm	TRE: The pencil tip was placed in different holes on the mandible and the difference between the actual and virtual location was measured in millimeters (n=11 measurements)
Seeberger *et al.* (4)	2012	EM	-	Plastic skull phantom (maxilla)	2.1 mm ± 0.68	TRE
The current study	*2019*	*EM*	*11*		*1.2 ± 1.1 mm* *2.6 ± 1.5 mm* *3.2 ± 1.1 mm*	*FRE* *TRE measured on cutting guide landmarks* *TRE measured on anatomical guide landmarks*

EM = electromagnetic; TRE = target registration error; FRE = fiducial registration error

Sun *et al.* argued that inaccuracies of 1.5 mm can be considered as clinically acceptable (14). Thus, with inaccuracies of 2.6 and 3.2 mm (TRE) as reached in the current study, there is still room for improvement. The TRE is a result of a couple of factors: the FRE, the variability in pinpointing the validation landmarks on the patient and selecting the corresponding landmarks on the CBCT and, an inadequate fixation of the sensor onto the mandible. Within the following paragraphs, these different factors will be discussed on how the inaccuracy was minimized in the current study and suggestions will be done on how to minimize the inaccuracies further for future research.

The accuracy of the registration between the patient during surgery with the virtual model, is expressed as the FRE (1.2 ± 1.1 mm). This value depends on several factors: the accuracy of the NDI Aurora EM tracking system, the accuracy of the CBCT-CT registration and the variability in pinpointing the landmarks used for fiducial registration (both on the patient and on the CBCT). According to the manufacturer, the used NDI system had a tracking accuracy of 0.8 mm in a laboratory setting. This inaccuracy can increase in the presence of any metal distortions in the EM field. However, Seeberger *et al.* showed that electromagnetic interference due to metallic instruments was significant, but that the effect on the TRE was still acceptable in comparison to optical navigation devices (4). Inaccuracies of the CBCT-CT registration could be a result of a change in bone anatomy in the time between the pre- and intra-operative CT. However, since this registration is automated on bone contours and the result is checked visually, no large inaccuracies are expected in this step of the procedure. For fiducial registration, the head of the screws used for the cutting guide were used. These were clearly identifiable on the patient and also on the CBCT. The slice thickness of the CBCT was 0.7 mm, which could have contributed to the inaccuracy of this particular step in the procedure.

With regards to the landmarks used for fiducial registration, instead of using screws on the cutting guide as was done in this study, Lee *et al.* used an, especially for this purpose designed, registration body. This registration body was made as a symmetrical arch that could be fixated to the mandible. It had 24 holes of different depths and in different positions, containing 1 mm in diameter ceramic balls for use as fiducial points for registration. Using this registration body, they obtained a registration accuracy of less than one mm (6). This is most likely caused by the fact that a registration body allows an optimal configuration, i.e. a larger distance between the locations of the fiducial registration landmarks. It is shown that a larger distance between fiducial registration landmarks increases the registration accuracy (15). Also in optical navigation, the use of a splint resulted in an increase in accuracy: Naujokat *et al.* evaluated different registration methods for the mandible by using three skull models and infrared navigation (12). Registration was performed with metal points on the mandibles (1), metal points on a splint based on the occlusal surface of the mandible teeth (2) and anatomical landmarks that were located interdental on the alveolar bone. The FREs found were 1.03 mm, 0.98 mm and 1,7 mm, respectively. Although, the results of these studies were obtained in one patient and in models, respectively, we can still learn from these studies. In seven out of the eleven patients, our FREs were also smaller than 1 mm, and thus, a very accurate registration of the 3D model with the situation in the OR was obtained. However, the FRE could potentially reduce further by using a registration body that increases the distance between fiducial registration landmarks.

The FRE should be as small as possible in order to obtain a small TRE. Therefore, in case the point-based registration resulted in a large FRE, it was advised to redo the registration procedure. The difference between the TRE measured with the anatomical landmarks and the landmarks on the cutting guide can be explained by the variability in pinpointing the anatomical landmarks. Apart from the mental foramen

and teeth, there are no precise landmarks identifiable on the mandible. Still, also these anatomical landmarks are multi-interpretable when aiming for a <1 mm accuracy. Variability in pinpointing the landmarks on the CBCT was minimal, since the ICC for the two observers in selecting both the anatomical and cutting guide landmarks on the CBCT were 1.0. The TRE can also be a result of inadequate fixation of the sensor to the mandible. Rotational movements of the sensor can occur within the sensor housing module, when the mandible was repositioned during pinpointing the landmarks. We are currently working on a new housing module that provides a better fixation and that is smaller (max 10 mm in length). As this was a study reporting on the first results obtained in using surgical EM navigation in a small group of patients, this will be taken into account for improvements in future research.

As the first results on accuracy were promising, we are currently working on methods to optimize the workflow, e.g., to eliminate the need for an intraoperative CBCT for registration, or preoperative CT with screws *in situ*. The first results for an alternative method for registration are recently published (16) and with the final aim to use a navigated cutting guide for optimal positioning and guidance during sawing we recently published a paper on a prototype of a navigated cutting guide (17).

This study evaluated the accuracy of an in-house developed EM navigation system, as a first step towards EM navigated assisted bone resection in mandibular tumour surgery. In a total of eleven patients, EM navigation approaches clinically acceptable accuracies to guide resections in mandibular surgery. Future studies will aim to improve accuracy and practical workflow further. Our group is currently working on an improvement of the registration method and on the implementation of the angle of the resection plane, besides the position of the osteotomy only.

References

1. Peacock ZS, Magill JC, Tricomi BJ, Murphy BA, Nikonovskiy V, Hata N, et al. Assessment of the OsteoMark-Navigation System for Oral and Maxillofacial Surgery. J Oral Maxillofac Surg. 2015;73(10):2005-16.
2. Nova I, Kallus S, Berger M, Ristow O, Eisenmann U, Freudlsperger C, et al. Computer assisted positioning of the proximal segment after sagittal split osteotomy of the mandible: Preclinical investigation of a novel electromagnetic navigation system. J Craniomaxillofac Surg. 2017;45(5):748-54.
3. Bouchard C, Magill JC, Nikonovskiy V, Byl M, Murphy BA, Kaban LB, et al. Osteomark: a surgical navigation system for oral and maxillofacial surgery. Int J Oral Maxillofac Surg. 2012;41(2):265-70.
4. Seeberger R, Kane G, Hoffmann J, Eggers G. Accuracy assessment for navigated maxillo-facial surgery using an electromagnetic tracking device. Journal of Cranio-Maxillofacial Surgery. 2012;40(2).
5. Berger M, Nova I, Kallus S, Ristow O, Eisenmann U, Dickhaus H, et al. Electromagnetic navigated condylar positioning after high oblique sagittal split osteotomy of the mandible: a guided method to attain pristine temporomandibular joint conditions. Oral Surg Oral Med Oral Pathol Oral Radiol. 2018;125(5):407-14 e1.
6. Lee SJ, Yang HJ, Choi MH, Woo SY, Huh KH, Lee SS, et al. Real-time augmented model guidance for mandibular proximal segment repositioning in orthognathic surgery, using electromagnetic tracking. J Craniomaxillofac Surg. 2019;47(1):127-37.
7. Nijkamp J, Kuhlmann KFD, Ivashchenko O, Pouw B, Hoetjes N, Lindenberg MA, et al. Prospective study on image-guided navigation surgery for pelvic malignancies. J Surg Oncol. 2019;119(4):510-7.
8. Fedorov A., Beichel R., Kalpathy-Cramer J., Finet J., Fillion-Robin J-C., Pujol S., et al. 3D Slicer as an Image Computing Platform for the Quantitative Imaging Network. Magn Reson Imaging. 2012;30.
9. Liu TJ, Ko AT, Tang YB, Lai HS, Chien HF, Hsieh TM. Clinical Application of Different Surgical Navigation Systems in Complex Craniomaxillofacial Surgery: The Use of Multisurface 3-Dimensional Images and a 2-Plane Reference System. Ann Plast Surg. 2016;76(4):411-9.
10. Nijkamp J, Kuhlmann KFD, Ivashchenko O, Pouw B, Hoetjes N, Lindenberg MA, et al. Prospective study on image-guided navigation surgery for pelvic malignancies. Journal of Surgical Oncology. 2019;119(4):510-7.
11. Hasan W, Daly MJ, Chan HHL, Qiu J, Irish JC. Intraoperative cone-beam CT-guided osteotomy navigation in mandible and maxilla surgery. Laryngoscope. 2019.
12. Naujokat H, Rohnen M, Lichtenstein J, Birkenfeld F, Gerle M, Florke C, et al. Computer-assisted orthognathic surgery: evaluation of mandible registration accuracy and report of the first clinical cases of navigated sagittal split ramus osteotomy. Int J Oral Maxillofac Surg. 2017;46(10):1291-7.
13. Shan XF, Chen HM, Liang J, Huang JW, Zhang L, Cai ZG, et al. Surgical navigation-assisted mandibular reconstruction with fibula flaps. Int J Oral Maxillofac Surg. 2016;45(4):448-53.
14. Sun Y, Luebbers HT, Agbaje JO, Schepers S, Vrielinck L, Lambrichts I, et al. Evaluation of 3 different registration techniques in image-guided bimaxillary surgery. J Craniofac Surg. 2013;24(4):1095-9.
15. Soteriou E, Grauvogel J, Laszig R, Grauvogel TD. Prospects and limitations of different registration modalities in electromagnetic ENT navigation. Eur Arch Otorhinolaryngol. 2016;273(11):3979-86.
16. Brouwer de Koning SG, Riksen JJM, Ter Braak TP, van Alphen MJA, van der Heijden F, Schreuder WH, et al. Utilization of a 3D printed dental splint for registration during electromagnetically navigated mandibular surgery. Int J Comput Assist Radiol Surg. 2020;15(12):1997-2003.
17. Ter Braak TP, Brouwer de Koning SG, van Alphen MJA, van der Heijden F, Schreuder WH, van Veen RLP, et al. a surgical navigated cutting guide for mandibular osteotomies: accuracy and reproducibility of an image-guided mandibular osteotomy. Int J Comput Assist Radiol Surg. 2020;15(10):1719-25.

Chapter 9

Utilization of a 3D printed dental splint for registration during electromagnetically navigated mandibular surgery

S.G. Brouwer de Koning

J.J.M. Riksen

T. P. ter Braak

M.J.A. van Alphen

F. van der Heijden

W.H. Schreuder

L.H.E. Karssemakers

M.B. Karakullukcu

R.L.P. van Veen

International Journal of Computer Assisted Radiology and Surgery (2020)
https://doi.org/10.1007/s11548-020-02271-3

Abstract

Purpose

A dental splint was developed for non-invasive rigid point-based registration in electromagnetically (EM) navigated mandibular surgery. Navigational accuracies of the dental splint were compared with the common approach, that is, using screws as landmarks.

Methods

A dental splint that includes reference registration notches was 3D printed. Different sets of three points were used for rigid point-based registration on a mandibular phantom: notches on the dental splint only, screws on the mandible, contralateral screws (the side of the mandible where the sensor is not fixated), and a combination of screws on the mandible and notches on the dental splint. The accuracy of each registration method was calculated using 45 notches at one side of the mandible and expressed as the target registration error (TRE).

Results

Average TREs of 0.83 mm (range: 0.7-1.39 mm), 1.28 mm (1.03-1.7 mm), 2.62 mm (1.91-4.0 mm), and 1.34 mm (1.30-1.39 mm) were found respectively for point-based registration based on the splint only, screws on the mandible, screws on the contralateral side only, and screws combined with the splint.

Conclusion

For dentate patients, rigid point-based registration performs best utilizing a dental splint with notches. The dental splint is easy to implement in the surgical, and navigational, workflow, and the notches can be pinpointed and designated on the CT scan with high accuracy. For edentate patients, screws can be used for rigid point-based registration. However, a new design of the screws is recommended to improve the accuracy of designation on the CT scan.

Keywords

Mandibular surgery, electromagnetic surgical navigation, rigid point-based registration, dental splint, target registration error.

Introduction

Computer-aided-design/computer-aided-manufacturing (CAD/CAM) techniques are routinely used in mandibular surgery. To prepare for surgery, the surgeon uses a 3D rendered model of the mandible, that is constructed from a preoperative computed tomography (CT) scan. The exact positions of the osteotomies are planned virtually, in order to achieve adequate tumor margins and to ensure an accurate fit of the bone segments that will be used for reconstruction after resection. To translate the positions of the osteotomies to the clinical situation in the operating room, patient-specific cutting guides and bone segment fixation plates are designed and manufactured by a certified producer. Besides the fact that this is a costly procedure, the preparation time can take up to several weeks before surgery. If tumor progression occurred in the meantime, the cutting guide cannot be adapted during surgery. Therefore, there is a need for a technology that is more adaptable than the patient specific 3D printed cutting guides (1).

Surgical navigation provides real-time visual feedback regarding the position and orientation of surgical instruments in relation to the patient's anatomy. This could potentially be used to translate the preoperative planning to the operating room, thereby eliminating the use of cutting guides. Electromagnetic (EM) navigation is used routinely in neurosurgery or surgery of the sinonasal cavity, but not in mandibular surgery so far: the fact that the mandible is mobile challenges accurate navigational tracking. In a previous study we evaluated the accuracy of an in-house developed EM navigation system, as a first step towards EM navigated assisted bone resection in mandibular tumour surgery (2). In a total of eleven patients, EM navigation approached clinically acceptable accuracies to guide resections in mandibular surgery. However, we hypothesize that the accuracy could be improved further. One possible improvement could be achieved in the registration procedure: the method on how the virtual 3D rendered model is registered to the actual patient's mandible at the OR table.

In rigid point-based registration, or fiducial registration, the rotation and translation between the virtual model and the real-time situation is determined by pinpointing at least three points on the patient's mandible with an EM trackable instrument and matching those tracked locations with the corresponding points on the CT scan that is used for the virtual 3D model. This is challenging for the mandible, due to the lack of clear and precise anatomical landmarks on the mandibular surface: Naujokat *et al.* evaluated rigid point-based registration using interdental bone structures as anatomical landmarks, but found that the use of anatomical landmarks does not provide sufficient accuracy (error of 1.7 mm) (3). As an alternative to anatomical landmarks, several studies have reported on the use of titanium screws fixated to the bone for rigid point-based registration (4-6). Fixated screws would offer maximum accuracy due to the fixation, and in addition, screws are easily detectable on a CT scan and on the patient. However, the method is invasive: the screws have to be implanted prior to the acquisition of the preoperative CT and are subject to causing discomfort.

In order to improve the accuracy of EM navigated mandibular surgery, a dental splint was developed for rigid point-based registration in this study. The TRE obtained after registration based on the dental splint, was compared to the TRE obtained with the use of fixated screws in different configurations.

Materials and methods

A mandible phantom was printed with a Form 2 3D printer (Formlabs, Sommerville, Massachusetts, USA) and the standard Formlabs material, using a clear resin. Along the complete outer surface of the mandible, notches are located (Figure 1). These notches are designed in such a way that they fit the EM trackable pointer of the navigation system exactly: the notches are cone shaped with a maximum diameter of 3 mm that equals the largest diameter of the pointer. In addition, five titanium 1.5x5mm Drill-Free maxDrive® (KLS Martin, Freiburg, Germany) screws were drilled into the mandible at various locations along the body and the ramus of the mandible.

A 3D printed dental splint was designed to exactly fit the teeth of the mandible phantom, using Meshmixer (2017 Autodesk, Inc. version 3.5.474). The spacing between the teeth's surface and the splint was 0.1 mm. The dental splint fits the teeth on the mandible and the upper jaw, however, only the mandible side was used for this study. Five notches (3 mm diameter) were added to the mandibular side of the 3D dental splint for registration purposes.

A computed tomography (CT) scan was acquired of the mandible phantom with the dental splint in position (pixel spacing of 0.68mm and a 1mm slice thickness, Siemens Somatom Confidence® (Siemens Healthineers, Erlangen, Germany)). On this CT scan, the notches and the screws were visible to allow rigid point-based registration (Figure 2).

A 6 DOF EM tracked sensor was used to track the position of the mandible (Figure 1). The sensor remains fixed to the mandible phantom during, and after, the registration procedure, so that the position of the mandible is tracked throughout the whole procedure. The positions of both the sensor and a trackable pointer were tracked by a planar EM field generator of NDI Aurora (Northern Digital Inc., Waterloo, Ontario, Canada). The distance between the sensor and the field generator was approximately 25 cm during the measurements, to simulate an intraoperative situation.

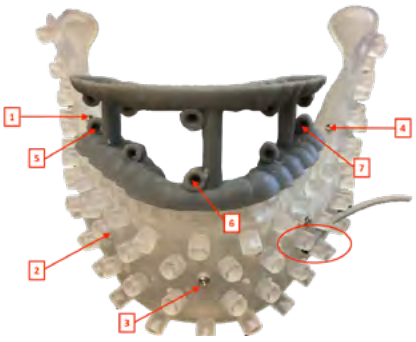

Figure 1 The mandible model with the dental splint in position and a 6DOF sensor (in grey, circle) attached. The numbers indicate the points used for registration (1,2,3 and 4 indicate screws, 5,6,7 indicate notches on the dental splint).

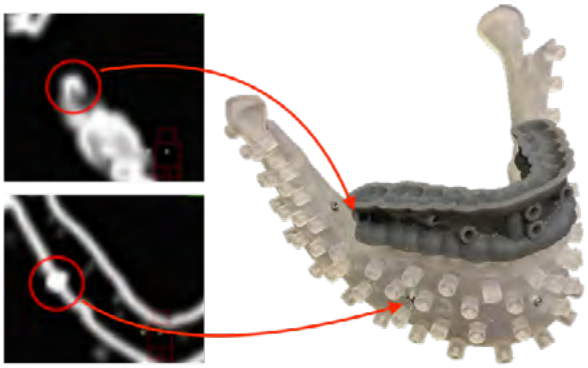

Figure 2 Axial CT slices of the phantom. The upper CT image shows a notch, the lower CT image shows a screw.

Rigid point-based registrations

Several configurations of registration points were used for different methods of rigid point-based registration, i.e. screws on the mandible, and notches on the dental splint (Table 1, Figure 1): screws on the mandible, contralateral screws (the side of the mandible where the sensor is not fixated), a combination of screws on the mandible and notches on the dental splint, and notches on the dental splint only. The registration points were pinpointed using an EM tracked pointer on the mandible phantom with the dental splint. Corresponding points on the CT scan were manually indicated simultaneously, using coronal, sagittal and axial views in an in-house developed software program. The root mean squared error of the Euclidean distance between the pinpointed registration points on the mandible and the virtual registration points was calculated as the fiducial registration error (FRE).

Table 1 The sets of points that were used for the different point-based registration procedures

Registration method	**Registration points** (see Figure 1)
Screws	1-3-4
Contralateral screws	1-2-3
Screws and notches on the dental splint	1-3-7
Notches on the dental splint	5-6-7

Accuracy measurement

The accuracy of each registration method was calculated using 45 notches at one side of the mandible, assuming that when the tumor is located on that side of the mandible, this is the side where the technique is of clinical value. The 45 notches were virtually indicated on the CT scan (Figure 3) and pinpointed with the trackable pointer at the actual mandible phantom. The location of the notches in the CT data was compared to the pinpointed location of the corresponding notches on the mandible phantom. The resulting difference was expressed as the target registration error (TRE), meaning the Euclidean distance between the virtual and pinpointed location.

Each registration method was repeated five times, and for each time, the TRE was calculated for all 45 notches. The average TRE of the five repetitions was calculated for each of the 45 notches. This average TRE was mapped onto a 3D surface model of the mandible using color coding. For the latter, Matlab 2017b (MathWorks, Natick, Massachusetts, USA) was used. The 3D surface model, consisting of small polygons, was colored using triangulation-based nearest neighbor interpolation, where each polygon received a color corresponding to the average TRE of the nearest notches. This results in small single-colored areas around the notches, indicating their corresponding average TRE (Figure 4).

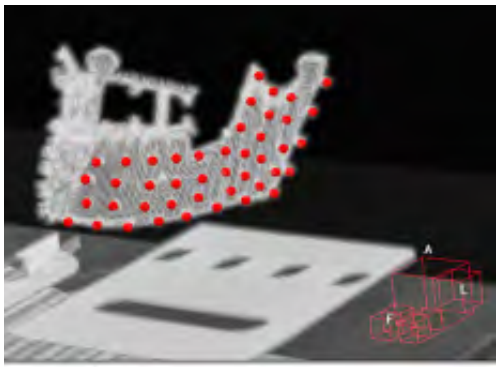

Figure 3 The 45 points at the affected side of the mandible that are used to calculate the TRE, shown on the CT scan.

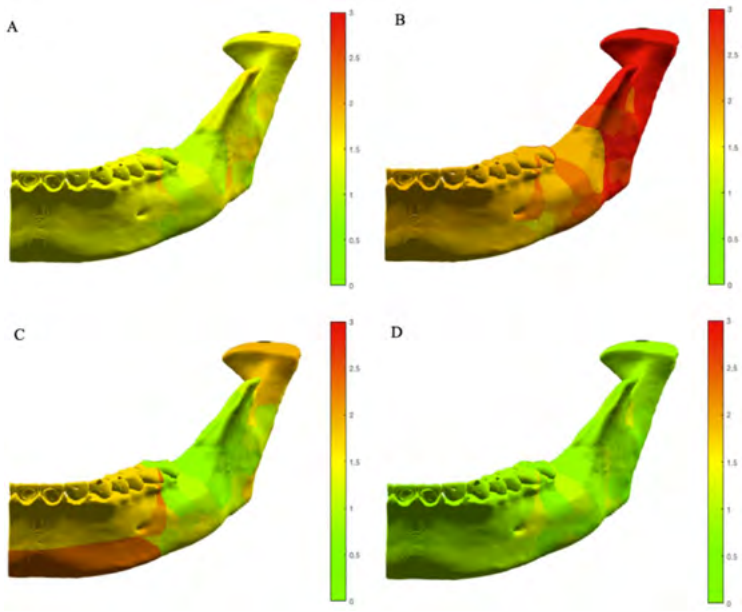

Figure 4 Colourmaps indicating the TRE (in mm) for the affected side of the mandible after point based registration using the screws (a), only the contralateral screws (b), using a combination of the screws and the notch on the dental splint (c) and using the notches on the dental splint only (d).

Repeatability in designating the registration points (screws and notches) on the CT data

During the different registration methods, the registration points were repeatedly pinpointed on the phantom and designated on the CT data. To evaluate the reproducibility of the registration methods, the repeatability of designating the screws on the CT data was compared to the repeatability of designating the notches on the CT data.

There were a total of four screws that were designated as a registration point for forty times (over all methods and all repetitions). Whereas three notches were designated as a registration point for twenty times. The centroid was calculated for each of the four screws and three notches individually, using their designations on the CT data. Then, the centroids of all screw registration points were superimposed on each other and standard deviation (STD) of all screw designations with respect to the centroid was calculated. This was also done for the notches. The STD in Euclidean distance between the designation and the centroid, was used as a measure to compare the repeatability of marking the screws and notches on the CT data.

Results

The FREs and TREs calculated from the outcomes of the five repetitions of accuracy measurements are shown in Table 2. Figure 4 provides insight into the areas of the affected mandible where high accuracies of the EM navigation technique can be achieved for each different type of registration method used. The use of a 3D printed dental splint demonstrated the smallest error and thus resulted into the most accurate method for EM navigational mandible tracking.

Regarding the repeatability of designating notches and screws on the CT scan, designating the notches on CT was more consistent (STD = 0.27 mm), compared to the screws (STD = 0.39 mm).

Table 2 FRE and TRE calculated after point-based registration using the different registration methods.

Registration method	Average FRE (mm)	Average TRE (mm)	Minimum TRE (mm)	Maximum TRE (mm)
Screws	0.73	1.28	1.03	1.70
Contralateral screws	0.59	2.62	1.91	4.00
Screws and notches on the dental splint	0.74	1.34	1.30	1.39
notches on the dental splint	0.36	0.83	0.70	1.39

Discussion

In this phantom study, different variants of rigid point-based registration were evaluated, in order to investigate the accuracy of EM navigation for mandibular surgery. With a mean error of 0.83 mm, measured over the target surface of the mandibular phantom, the use of a dental splint has shown to achieve the highest accuracy.

The design, production and intra-operative use of a dental splint shows high potential for implementation within the EM navigation workflow. For the design of the dental splint, a non-invasive intra oral scan of the mandibular teeth can be acquired during the first visit of the patient in the outpatient clinic. Using a handheld scanner, the physician or the dentist can acquire the scan within a few minutes. The intra oral scanner acquires a 3D surface map of the mandibular teeth that can be inverted to design the dental splint. Subsequently, the dental splint can be printed using a sterilizable resin. The 3D virtual model of the dental splint can be added to the 3D reconstructed model of the mandible using two approaches, (a) the dental splint can be positioned on the patients teeth during the acquisition of the preoperative CT scan, or (b) the digital version of the dental splint can be added to the 3D model virtually. In the latter, the transformation found after surface registration of the intra oral scan with the preoperative CT can be used to position the splint accurately. In the intraoperative setting, the 6 DOF reference sensor is fixated to the mandible and the dental splint can be placed on top of the patient's teeth. Rigid point-based registration can be performed by pinpointing the notches on the dental splint on the patient with the trackable pointer and linking them with the corresponding points on the virtual model which includes the surgical plan, e.g. cutting planes. After the registration procedure, the dental splint can be removed, and the EM navigation would be ready for use. Because the splint only has to be in place during the registration procedure to set up the surgical navigation, it will not hinder the use of other surgical instruments that are needed to perform the resection for example. The sensor remains in place and allows tracking of the position of the mandible throughout the whole procedure, thereby eliminating the need for immobilization of the mandible.

The described method could be used for different types of mandibular procedures for which surgical navigation is indicated, such as tumour resection surgery and reconstructive surgery, as long as the patients are dentate so that a splint can be designed, and there is an area on the mandible that allows fixation of the sensor. The dental splint is easy to implement in the EM navigation workflow, and it is a non-invasive method. However, its employment requires a patient specific preparation (the splint can be designed in less than 30 minutes, and printing time is approximately 60 minutes).

The use of screws would be a possibility for point-based registration in edentate patients. With the design of this study, we hypothesized that the screws would show a high accuracy due to the fact that they are fixated to the mandibular bone and clearly visible on the CT scan. The registration accuracy of the screws only method however was not superior, and our analysis on the variability of indicating the screws on the CT data confirms that the exact screw heads visible on the CT scan could be interpreted with a high variety (i.e. high STD). To perform rigid point-based registration using screws, special screws should be designed with e.g. an attachable notch so that similar accuracies can be achieved as reported with the dental splint. Concerning the position of the screws, the current study implies that the smallest errors are reached when screws are positioned on the anterior surface and on both lateral surfaces of the mandible, making the methods accuracy dependent on the location of the tumor. Regarding the

workflow for edentate patients, one should keep in mind that the screws need to be positioned prior to the acquisition of the preoperative CT scan and must remain in the mandible until the surgery.

In 2001, West *et al.* described four guidelines to achieve optimal TRE with rigid point-based registration: 1) avoid (near) linear configurations, 2) arrange the registration points so that the center of their configuration (centroid) is as close as possible to the target region, 3) increase the distance between the registration points, and 4) use as many registration points as possible (7). Regarding the latter, they found that the increase in accuracy diminishes after using five or six registration points. However, in 2011, Shamir *et al.* suggested that the TRE would not necessarily improve by adding or deleting registration points, nor does the TRE increase as the target is further away from the center of the registration points (8). In a recent study, Hwang *et al.* also demonstrated that an increase in the number of registration points was not necessarily associated with a decrease in the TRE (9). Using from three up to seven screws as registration points distributed over a mandible phantom, and TREs calculated at various anatomical locations, they found that the minimum number of registration points to achieve optimal TREs, depends on the location of the target site. In the current study, small TREs were achieved with the use of only three registration points that were located near each other, in an almost linear configuration, but with their centroid near the target area. Thus, our results suggest that the position of the centroid of the registration points near the target area, contributes most to the accuracy.

In order to improve accuracy results with a splint by enlarging the distance between the registration points, Lee *et al.* designed a registration body for EM surgical navigation, in such a way that it could be fixated to the mandible as a symmetrical arch (9). The registration body had 24 holes of different depths and in different positions. The holes contained 1 mm in diameter ceramic balls that served as fiducial points for registration. For point-based registration, six points at the registration body were used. TRE was measured on three condylar landmarks. Using the registration body, they found that highest accuracies (~ 0.7 mm) were found when the six registration points were located near the condyle that was used for accuracy measurement. This is comparable with the results obtained for the dental splint in this study and confirms that the position of the registration points is important for the accuracy.

Naujokat *et al.* also used different registration methods for the mandible and reported a superior registration accuracy when a splint manufactured on the occlusal surface was used (3). However, they used an optical navigation system and required large optical markers attached to the splint. This challenges the way the splint is fixated to the mandible. Within the study they fixated the splint with the optical marker using wires around the mandibular bone, which challenges the application and fixation in patients.

Soteriou *et al.* found that after a rigid point-based registration with four titanium screws, a TRE of 0.94 +- 0.06 mm measured at 26 titanium screws was achieved on a skull model using EM navigation (5). Kristin *et al.* also used an EM navigation system and measured an overall accuracy of 0.6 +- 0.3 mm after point-based registration with six titanium screws on a cadaver skull (6). Both studies positioned the screws on the mastoid for navigation purposes on the ENT area or skull base, not the mandible. Our TRE of 1.28 mm, obtained with the screws only registration, needs improvement when compared to these results (< 1 mm). Main differences between our study and those studies are the number of registration points used, and the distance between the registration points. Both studies utilized the whole skull and therefore could extend the distance between the registration points. Due to the fact that the mandible is movable with respect to the skull, registration points are limited to the mandibular

surface, limiting the distance between the registration points. Hwang *et al.* utilized screws positioned at the mandible only and obtained comparable results as our study, however they used optical navigation, which is clinically less practical for use in a small surgical field as the oral cavity due to the required line of sight (9).

According to Wang *et al.*, augmented reality shows great promise for image registration (10). They used an intraoral 3D scanner to acquire the patient's teeth shape intraoperatively. The 3D shape of the teeth is registered with the 3D model obtained from the preoperative CT scan using a custom-made stereo camera system. In jaw phantom experiments they found an average TRE of 0.50 mm.

Future studies will focus on translating this phantom study to a patient study: utilizing patient specific dental splints during EM navigation in patients undergoing mandibular surgery.

Conclusion

In this phantom study, different variants of rigid point-based registration were evaluated, in order to facilitate EM navigation during mandibular surgery. For dentate patients, a method was developed to obtain high navigational accuracies after rigid point-based registration using a dental splint with notches. The dental splint is easy to implement in the surgical, and navigational, workflow, it is non-invasive, and the notches can be pinpointed and designated on the CT scan with high accuracy. For edentate patients, screws can be used for rigid point-based registration. However, a new design of the screws is recommended to improve the accuracy of designation on the CT scan.

References

1. Ter Braak TP, Brouwer de Koning SG, van Alphen MJA, van der Heijden F, van Veen RLP, Karakullukcu MB. a surgical navigated cutting guide for mandibular osteotomies: Accuracy and reproducibility of an image-guided mandibular osteotomy. Int J CARS 15:1719–1725. https://doi.org/10.1007/s11548-020-02234-8
2. Brouwer de Koning SG, Geldof F, van Veen RLP, van Alphen MJA, Karssemakers LHE, Nijkamp J, Schreuder WH, Ruers TJM, Karakullukcu MB. Electromagnetic surgical navigation in patients undergoing mandibular surgery. Submitted to Scientific Reports
3. Naujokat H, Rohnen M, Lichtenstein J, Birkenfeld F, Gerle M, Florke C, Wiltfang J. Computer-assisted orthognathic surgery: evaluation of mandible registration accuracy and report of the first clinical cases of navigated sagittal split ramus osteotomy. Int J Oral Maxillofac Surg. 2017;46(10):1291-7.
4. Eggers G, Muhling J, Marmulla R. Image-to-patient registration techniques in head surgery. Int J Oral Maxillofac Surg. 2006;35(12):1081-95.
5. Soteriou E, Grauvogel J, Laszig R, Grauvogel TD. Prospects and limitations of different registration modalities in electromagnetic ENT navigation. Eur Arch Otorhinolaryngol. 2016;273(11):3979-86.
6. Kristin J, Mucha D, Schipper J, Klenzner T. Registration strategies for the application of the navigation system Fiagon at the lateral scull base. Laryngorhinootologie. 2012;91(5):306-10.
7. Jay B. West PD, J. Michael Fitzpatrick, Ph.D., Steven A. Toms, M.D., Calvin R. Maurer, Jr., Ph.D., Robert J. Maciunas, M.D. Fiducial Point Placement and the Accuracy of Point-based, Rigid Body Registration. Neurosurgery. 2001;48(4).
8. Shamir RR, Joskowicz L. Geometrical analysis of registration errors in point-based rigid-body registration using invariants. Med Image Anal. 2011;15(1):85-95.
9. Lee SJ, Yang HJ, Choi MH, Woo SY, Huh KH, Lee SS, Heo MS, Choi SC, Hwang SJ, Yi WJ. Real-time augmented model guidance for mandibular proximal segment repositioning in orthognathic surgery, using electromagnetic tracking. J Craniomaxillofac Surg. 2019;47(1):127-37.
10. Wang J, Shen Y, Yang S. a practical marker-less image registration method for augmented reality oral and maxillofacial surgery. Int J Comput Assist Radiol Surg. 2019;14(5):763-73.

Chapter 10

A surgical navigated cutting guide for mandibular osteotomies: accuracy and reproducibility of an image-guided mandibular osteotomy

T.P. ter Braak

S.G. Brouwer de Koning

M.J.A. van Alphen

F. van der Heijden

W.H. Schreuder

R.L.P. van Veen

M.B. Karakullukcu

International Journal of Computer Assisted Radiology and Surgery (2020)
https://doi.org/10.1007/s11548-020-02234-8

Abstract

Purpose

3D-printed cutting guides are the current standard to translate the virtual surgery plan to the intra-operative setting. The production of these patient specific cutting guides is time consuming and costly, and therefore alternative approaches are currently subject of research. The aim of this study was to assess the accuracy and reproducibility of using a novel electromagnetic (EM) navigated surgical cutting guide to perform virtually-planned osteotomies in mandible models.

Methods

A novel 3D-navigated cutting guide (dubbed Bladerunner) was designed and evaluated with a total of 20 osteotomies, performed on plaster mandibular models according to preoperative planning using EM navigation. The pre- and postoperative scans were registered and the difference between the preoperatively planned osteotomy and the performed osteotomy was expressed as the distance between the planned and performed cutting planes, and the yaw and roll angles between the planes.

Results

The mean difference in distance between the planned and performed osteotomy was 1.1 mm (STD 0.6 mm), the mean yaw was 1.8° (STD 1.4°) and mean roll was 1.6° (STD 1.3°).

Conclusion

The proposed EM navigated cutting guide for mandibular osteotomies, demonstrated accurate positioning of the cutting plane according to the pre-operative virtual surgical plan with respect to distance, yaw and roll angles. This novel approach has the potential to make the use of 3D printed cutting guides obsolete, thereby decreasing the interval between diagnosis and surgery, reduce cost and allow for adaptation of the virtual plan in case of rapid tumor proliferation or unanticipated in-situ deviations from the pre-operative CT/MR imaging.

Keywords

Surgical Navigation; Electromagnetic; Oral and maxillofacial surgery; Computer-assisted surgery; Intraoperative navigation; Pre-surgical virtual planning; Cutting guide.

Introduction

Computer assisted surgery has become a common tool in head and neck surgery. With the use of 3D planning software in combination with rapid prototyping, a patient specific cutting guide can be created to improve precision and reduce the duration of bone reconstruction during head and neck surgery (1–3). In addition, this approach allows for less experienced surgeons to conduct this type of surgery successfully.

Virtual surgical planning has made the outcome more predictable and accurate compared to the free-hand approach. However, several shortcomings and problems still occur using the virtual surgical planning. The time interval between the planning-CT and the surgery should not exceed two weeks (4), but can take as long as four weeks or more due to production, shipping and designing difficulties. Even a two-week delay may result in serious limitations for patients with rapidly growing tumors or acute trauma (3). Positioning of the 3D-printed cutting guide can be inaccurate due to remaining soft tissue between the mandible and the cutting guide, resulting in aberrant cutting planes. Deviations from the virtual plan can also occur when the shape of the 3D cutting guide is not sufficiently patient specific i.e. after placement on the mandible it still allows for small shifts. If a non-perfect fit is noticed or an unexpected intra-operative finding occurs, the non-flexibility of the cutting guides does not allow for alterations of the original planning. In addition, the printed material lacks robustness, making it possible for the surgical saw to cut through the 3D-printed cutting guide and create a non-straight cut. The dependence on an external medical printing company and the frequently complicated and time-consuming logistics and communication between engineer, surgeon, operating department/nurses and sterilization department results in overall costly 3D-printed cutting guides (5). a novel approach that overcomes the disadvantages of 3D printed cutting guides is therefore required. One potential approach is the use of image guided optical or electromagnetic navigation.

Recently, two research groups have been working on different navigated saws tracked with an optical navigation system, for performing mandibular osteotomies according to a virtual plan. The implementation of the navigated saw can be carried out exclusively by medical team members, thereby eliminating the need for bioengineer services, and the relatively long production and design time of the 3D printed cutting guides (6, 8). In an experimental setting, multiple osteotomies were performed on plaster or polyurethane model mandibles. Pietruski *et al.* (6) let a single operator perform the osteotomies and two observers evaluated the difference in volume, the angular deviations and the differences between preoperative and postoperative marginal point positions. The mean difference between the planned and actual bone resection volumes was 8.55% ± 5.51, the mean angular deviation between planned and actual osteotomy trajectory was 8.08° ± 5.50, and the mean difference between the preoperative and the postoperative marginal point positions was 2.63 mm ± 1.27 (6). The study highlights the potential for image-guided resection, but the method requires further improvement and a comparison with the patient specific cutting guide. In a study by Bernstein *et al.* (7) four surgeons (two attendings and two clinical fellows) performed unnavigated and navigated osteotomies and evaluated the distance and angular deviations (here, pitch and roll) between the planned and the cutting planes. The navigated cuts were significantly better than the unnavigated cuts in all evaluated measures. Mean distance from the virtual planned osteotomy was 2.65 mm ± 2.25 unnavigated and 1.3 mm ± 0.80 3D-navigated; mean pitch was 5.06° ± 4.24 unnavigated and 4.11° ± 2.723 D-navigated; mean roll was 9.4° ± 8.3 unnavigated and 3.5° ± 3.1 3D-navigated. However, no comparison is made with the

patient specific cutting guides. Both of these groups demonstrate the potential of surgical navigation in providing accurate osteotomies, however a free-hand navigated saw requires good eye-hand coordination (6) and without a saw-compelling cutting guide it is challenging to make a non-straight cut. These studies achieved a good accuracy (in general this should be less than 1 mm) in distance, but still have high angular deviations. During reconstruction, this angular and distance errors propagate over the entire length of the defect and can thus result in malocclusion and facial deformation. Navigating the cutting guide instead of the saw itself can overcome these shortcomings. a navigated cutting guide placed at the right position and fixed at the right angle is no longer dependent on the hand stability of the surgeon.

The aim of this study was to assess the accuracy and reproducibility of three-dimensional (3D) virtually-planned osteotomies in mandible models using a novel electromagnetic (EM) image guided navigated surgical cutting guide.

Methods

Bladerunner design

An experimental navigated cutting guide system (dubbed Bladerunner) was designed consisting of three elements; a baseplate for a rigid fixation to the mandible, a navigated cutting guide i.e. a slot with thickness that corresponds to the saw blade thickness and adjustment rods (Figure 1). The baseplate has three equidistant spikes with a screw hole in the center to provide the best kinematic constraint on an irregular surface such as the mandible, and an L-shaped support with three holes for the adjustment rods. The connection and mobility provided by the adjustment rods is derived from a kinematic mirror mount, to provide 5 degrees-of-freedom (DOF) movement. By elongating or shortening the adjustment rods, the navigated cutting guide is able to tilt and translate opposed to the baseplate. This is necessary for providing minute and larger adjustment options to obtain the best cutting plane alignment according to virtual planning. When the optimal position and orientation is obtained the setup can be fixed using opposing nuts along the adjustment rods. The navigated cutting guide has a 30x20x1mm slit to adequately compel the saw, a trench for the EM sensor and fourteen widely spaced indentations on the outer surface which can be used for registration. The prototype was 3D-printed on a Formlabs Form 2 stereolithographic printer (Formlabs, Somerville, USA) using clear resin FLGPCL04. The design and material were approved by the in-house sterilization department for future clinical use.

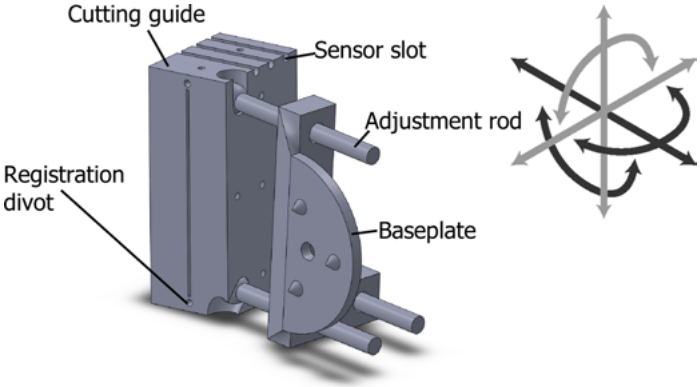

Figure 1 3D model of the navigated cutting guide, dubbed "Bladerunner". In the upper right corner, displayed in black are the 3 degrees of freedom.

3D-navigation system

This study utilized in-house developed navigation software, *SurgNav* (9), in combination with an EM tracking system, NDI Aurora (Northern Digital Inc., Waterloo, Canada). The system allows for real-time tracking of sensor coils locations and orientations inside a 3D measuring EM volume. The software accommodates the registration and a four-display mode (axial, sagittal, frontal, and 3D) where the position and orientation of the tools relative to the imaging data is visualized.

Mandible phantoms

The plaster mandible cutting models were constructed as follows; a mandible model was extracted from a computed tomography (CT) scan of a dentate patient and split along the midsagittal plane, where the (healthy) left half was 3D-printed and used to create a mold. The 3D-printed mandible model was half submerged in silicone (Dragon Skin® 10; Smooth-On, inc.Inc.; Easton, PA 18042; USA) and hardened in a 20-degree oven, thereafter the other half was covered and hardened. After removal of the 3D-printed mandible model this resulted in a reusable silicon mold. Using this mold, ten plaster mandible models were created using generic plaster. All of the plaster models were scanned individually using a CT-scan (Somatom Sensation Open; Siemens Medical Solutions, Erlangen, Germany) with a resolution of 0.59 mm/pixel and a 1.5 mm slice thickness. Image data were saved in Digital Imaging and Communication in Medicine (DICOM) format.

Osteotomy planning

The segmentation of the plaster mandibles was performed with the 3D Slicer software platform (10) using a simple threshold, and converted to a stereolithographic file (STL) format. Using computer-assisted design freeware Meshmixer (Autodesk, Inc., http://meshmixer.com), two osteotomies based on actual cases of osteotomy locations were planned and drawn in 3D for each plaster mandible model (Figure 2).

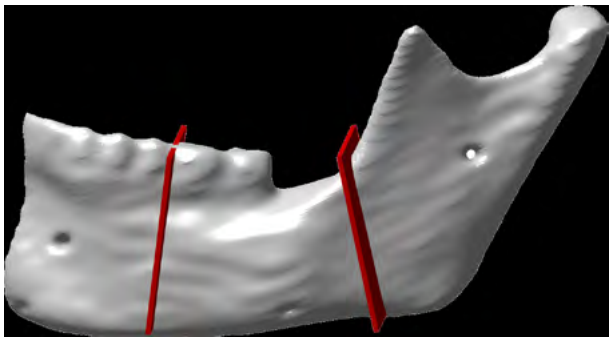

Figure 2 3D model of the plaster mandible with the planned osteotomies indicated in red.

Calibration and registration

EM sensors were attached with tape in between the two osteotomies on the plaster models, and in the specifically designed grooves on top of the Bladerunner as seen in (Figure 1). The Bladerunner and the plaster mandible were both registered using a point match registration. The plaster mandible models were registered to the 3D reconstructions using three widely spaced fiducials (condyle, mental foramen and mental protuberance), that were holes drilled into the models. Image-to-sensor paired-point registration was measured in the root mean square registration error to assess how closely the preoperative CT and physical plaster mandible model were registered. The Bladerunner was registered to the 3D model using fourteen widely spaced fiducials in the small indentations along its surface.

Osteotomies

All surgical procedures were performed in an operating theatre setting, according to the same operating protocol. The baseplate was attached to the plaster mandible in the vicinity of the planned planes using a stainless-steel screw. Next, the Bladerunner with predicted cutting plane was positioned using the 3D views of *SurgNav* in such a way that the predicted plane was superimposed on the virtually planned osteotomy plane (Figure 3). Rigid fixation was attained by securing opposing nuts on the adjustment rods. a 0.1mm thin handheld sawblade was inserted through the Bladerunner and used to perform the osteotomies. All mandibular osteotomy cuts were made approximately 80% of the cut height so that each bone remained intact for the postoperative CT scan to facilitate accurate analysis.

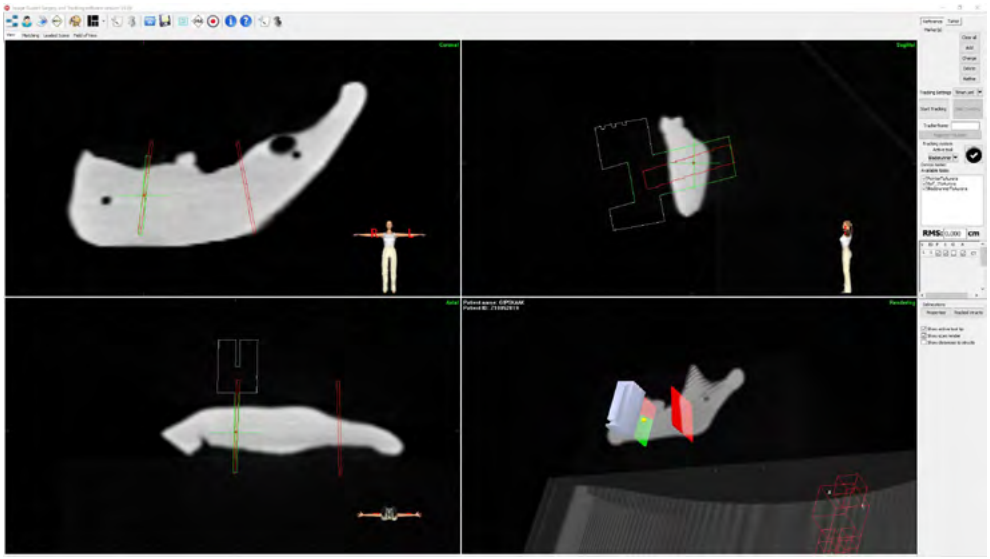

(a) Performing the osteotomy

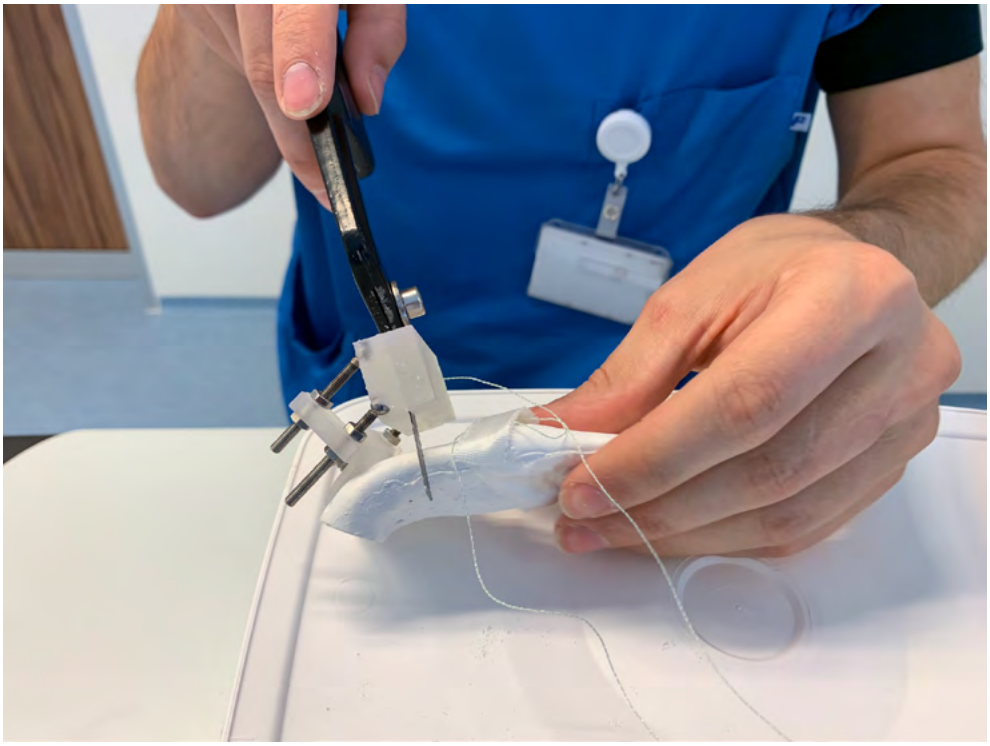

(b) Positioning the Bladerunner using Surgnav

Figure 3 An osteotomy being performed on a plaster mandible model using the 3D navigated cutting guide in combination with Surgnav and a 0.1 mm thin handheld sawblade.

Osteotomy plane analysis

After completing the osteotomies, the mandible models were CT scanned with identical imaging parameters to the preoperative scans and stored in DICOM file format. Segmentations were again performed with 3D Slicer using the same threshold value and stored in STL file format. Both pre- and postoperative STL files were registered in MATLAB R2018b (The MathWorks Inc., Natick, USA) using an Iterative Closest Point (ICP) algorithm. Model-to-model registration error was determined as the root mean square error between the planned and registered models, to confirm the accuracy of the quantitative outcome measures. The osteotomy was found in the model by determining the outward orientated normal vectors which intersected with the model, where the corresponding vertices had an intermediate distance of approximately the thickness of the osteotomy. This resulted in points on both sides of the osteotomy. Resection planes were defined by determining a plane of best fit through these points by minimizing the normal quadratic distance.

In order to quantitatively determine the difference between the planned (virtual) and postoperative (performed) resection planes, the distance and angles (yaw and roll) between the planes were analyzed (mean and standard deviation (STD)). The distance between the planned and postoperative resection plane was defined as the distance between the center of gravities of each plane intersecting with the mandibular bone model. The center of gravity was defined as the average of all 3D points of the cross section between the cutting plane and the jaw model. The postoperative plane was transformed to align the planned resection plane along the Z-axis, before performing a registration to determine the yaw and the roll between the planes.

Results

A total of 20 osteotomies guided with the Bladerunner were performed on ten plaster mandible models. The mean image-to-sensor paired-point registration error was 0.4 mm (STD 0.3 mm) and the mean model-to-model registration error was 1.0 mm (STD 0.1 mm).

The paired-point registration procedure only took 2-3 minutes, the accurate positioning of the 3D-Navigated Bladerunner took about 10-15 minutes. a single measurement including attachment of the sensors and performing the osteotomy lasted between 20-30 minutes.

Table 1 shows the difference between the virtually planned osteotomy and the 3D-navigated performed osteotomy using the Bladerunner for anterior and posterior cutting planes in all 10 plaster mandible models. Mean distance between the planned and performed osteotomy was 1.1 mm (STD 0.6 mm), the mean yaw 1.8° (STD 1.4°) and mean roll 1.6° (STD 1.3°).

Table 1 Distance, yaw and roll between the virtually planned osteotomy and the 3D-navigated osteotomies using the Bladerunner.

Mandible model	Plane	Distance (mm)	Roll (°)	Yaw (°)
1	Anterior	0.69	2.50	3.63
	Posterior	1.04	2.57	0.92
2	Anterior	1.01	1.37	0.84
	Posterior	0.60	1.19	3.02
3	Anterior	1.11	0.35	1.64
	Posterior	0.96	1.06	0.18
4	Anterior	0.36	0.97	1.55
	Posterior	0.86	0.70	1.13
5	Anterior	0.67	4.08	0.62
	Posterior	1.54	0.12	0.14
6	Anterior	2.06	1.05	1.88
	Posterior	1.73	0.23	0.07
7	Anterior	2.28	0.24	0.68
	Posterior	1.45	1.69	2.47
8	Anterior	0.23	2.49	3.28
	Posterior	0.29	0.46	4.82
9	Anterior	0.90	2.73	1.75
	Posterior	1.36	3.94	3.24
10	Anterior	1.33	0.68	3.98
	Posterior	0.76	4.11	0.77
Mean		1.06	1.63	1.83
STD (standard deviation)		0.56	1.33	1.41

Discussion

The current state-of-the-art 3D-printed cutting guides have shown to be a clear improvement on the traditional free-hand techniques(12). However, these cutting guides come with their own shortcomings in the form of inflexibility during surgery, logistics, long production time and cost. Several research groups have started to look for alternative methods in the form of a navigated saw. In this study the concept of a navigated cutting guide is introduced, and multiple navigated osteotomies were performed to evaluate the efficacy.

In this study, the Navigated Bladerunner shows a high accuracy and the small standard deviations suggest that these results are reproducible. An average distance of 1 mm between planned and performed resection planes approaches clinically acceptable values. Furthermore, both the roll and the yaw indicate an accurate osteotomy.

The yaw and roll angles work over the entire length of the reconstruction; a small deviation in the angle can result in a multiple millimetre offset over the length of the bone segment. This is where the Bladerunner could provide the most improvement, the length and the shape of the excised bone segment will be more accurate.

Osteotomies performed with the navigated Bladerunner should at least achieve similar, and preferably better, accuracies compared to the currently used state-of-the-art 3D printed rigid cutting guides. A study that was performed in-house, included seven patients and showed that the distance between preoperatively planned cutting plane and the performed cutting plane was 0.9 mm (STD 0.5 mm) for the anterior osteotomy and 2.0 mm (STD 1.0 mm) for the posterior osteotomy (11). The angles ranged between 2.6° and 9.5°. Due to the difference in study setup, it is not possible to compare these results directly with the results of Bladerunner presented in this study. However, it shows a frame of reference to the order of accuracy that should be achieved when evaluating the use of the Bladerunner in a patient study.

Bernstein *et al.* (7) navigated on maxillary osteotomies in anatomical models, using a 3D-navigated saw. Mean distance from the virtual planned osteotomy was 1.3 mm ± 0.80, mean pitch was 4.11° ± 2.723 and mean roll 3.5° ± 3.1 3D-navigated. This study included 144 osteotomies on the mandible, and it is therefore not possible to compare the results with the results obtained by the Bladerunner. This study also provides an indication of the order of accuracy that should be achieved in our future studies.

Both of the navigated saw groups (6, 7) utilize an optical navigation system as EM navigation has demonstrated to be inaccurate in the vicinity of large metallic instruments such as the saw (13). However, surgical navigation with a navigated cutting guide is only needed during the actual positioning of the Bladerunner, that is manufactured from non-ferrous material (e.g. medical-grade stainless steel or titanium). During the navigated positioning of the Bladerunner no interfering metallic instruments are needed that could affect the accuracy. When the correct position and orientation are obtained, the navigation system can even be turned off before using the metallic saw for the osteotomy. When using optical navigation, the required line-of-sight between the optical tracker and surgical tools limits the surgeons flexibility and this type of navigation is therefore challenging to use in practice, especially in small working areas like in head and neck surgery (14). Therefore, EM navigation is the preferred system for the navigation of the navigated cutting guide.

The benefit of a navigated cutting guide versus a navigated saw is that the saw is compelled by the guide, making a curved cut impossible. The free-hand navigated saw requires good eye-hand coordination during the positioning and performing the osteotomy which could impact the performance (6). The navigated cutting guide only requires this eye-hand coordination during positioning. When the cutting guide is aligned according to planning, the position of the Bladerunner can be fixed so the surgeon can focus on performing the osteotomy. Future studies could also evaluate the use of augmented reality (AR) while positioning the Bladerunner. Pietruski *et al.* recently published a promising study that AR could already be used for presentation of digital navigation data to enhance the surgeon's hand-eye coordination (15).

This is a proof of concept study and thus has some limitations. The Bladerunner setup requires that the baseplate is attached to the mandible at some distance from the planned osteotomy. As it is not feasible to position the baseplate on the tumour site, it is of yet difficult to perform an osteotomy near the

condyle of the mandible. In further studies this could be alleviated by providing multiple baseplates for different attachment locations. The fixation of the Bladerunner after cutting plane alignment is achieved by tightening opposing bolts on the adjustment rods. While this was fine for the proof of concept, this is not feasible during surgery as this is time and labour intensive. Different fixation options are required, which also provides room for improvement.

There are some future improvements planned for the Bladerunner. The 3D-printed material has some minor slack which could affect the osteotomy and is not suitable for an electric saw. Therefore, the next iteration will be from a different material, including millimetre scales for alignment and fixation methods. a quantitative feedback on how well the virtual and actual planes coincide is required, to assist in the alignment and to eliminate possible inaccuracies caused by the hand-eye coordination. There is also future work in translating the angles and distances to a fibula cutting guide or virtual planning.

The focus of subsequent studies is to incorporate the previously stated improvements and asses the technology in a clinical patient study. The end goal would be to also eliminate the fibula 3D-printed Cutting Guide and use the virtual planning with the Bladerunner directly for the operation.

Conclusion

This study demonstrates the potential of image guided EM navigated cutting guides for mandibular osteotomies. The distance, yaw, and roll were accurate, clinically acceptable and had a high reproducibility. The proposed method has the potential to make the use of 3D printed cutting guides obsolete, thereby decreasing the interval between diagnosis and surgery, reduce costs and allow for adaptation of the virtual surgical pre-operative plan in case of rapid tumor proliferation or unanticipated in-situ deviations from the pre-operative CT/MR imaging. Subsequent studies are focused on improvements to the navigated cutting guide setup and on evaluation of this novel approach in a clinical patient study.

References

1. Bao T, He J, Yu C, Zhao W, Lin Y, Wang H, Liu J, Zhu H (2017) Utilization of a pre-bent plate-positioning surgical guide system in precise mandibular reconstruction with a free fibula flap. Oral Oncol 75:133–139. https://doi.org/10.1016/j.oraloncology.2017.11.011
2. Roser SM, Ramachandra S, Blair H, Grist W, Carlson GW, Christensen AM, Weimer KA, Steed MB (2010) The accuracy of virtual surgical planning in free fibula mandibular reconstruction: Comparison of planned and final results. J Oral Maxillofac Surg 68:2824–2832. https://doi.org/10.1016/j.joms.2010.06.177
3. Rodby KA, Turin S, Jacobs RJ, Cruz JF, Hassid VJ, Kolokythas A, Antony AK (2014) Advances in oncologic head and neck reconstruction: Systematic review and future considerations of virtual surgical planning and computer aided design/computer aided modeling. J Plast Reconstr Aesthetic Surg 67:1171–1185. https://doi.org/10.1016/j.bjps.2014.04.038
4. Mazzoni S, Marchetti C, Sgarzani R, Cipriani R, Scotti R, Ciocca L (2013) Prosthetically guided maxillofacial surgery: Evaluation of the accuracy of a surgical guide and custom-made bone plate in oncology patients after mandibular reconstruction. Plast Reconstr Surg 131:1376–1385. https://doi.org/10.1097/PRS.0b013e31828bd6b0
5. Rustemeyer J, Melenberg A, Sari-Rieger a (2014) Costs incurred by applying computer-aided design/computer-aided manufacturing techniques for the reconstruction of maxillofacial defects. J Cranio-Maxillofacial Surg 42:2049–2055. https://doi.org/10.1016/j.jcms.2014.09.014
6. Pietruski P, Majak M, Swiatek-Najwer E, Popek M, Szram D, Zuk M, Jaworowski J (2016) Accuracy of experimental mandibular osteotomy using the image-guided sagittal saw. Int J Oral Maxillofac Surg 45:793–800. https://doi.org/10.1016/j.ijom.2015.12.018
7. Bernstein JM, Daly MJ, Chan H, Qiu J, Goldstein D, Muhanna N, De Almeida JR, Irish JC (2017) Accuracy and reproducibility of virtual cutting guides and 3D-navigation for osteotomies of the mandible and maxilla. PLoS One 12:e0173111. https://doi.org/10.1371/journal.pone.0173111
8. Pietruski P, Majak M, Swiatek-Najwer E, Popek M, Jaworowski J, Zuk M, Nowakowski F (2015) Image-guided bone resection as a prospective alternative to cutting templates- a preliminary study. J Cranio-Maxillofacial Surg 43:1021–1027. https://doi.org/10.1016/j.jcms.2015.06.012
9. Nijkamp J, Kuhlmann KFD, Ivashchenko O, Pouw B, Hoetjes N, Lindenberg MA, Aalbers AGJ, Beets GL, van Coevorden F, KoK N, Ruers TJM (2019) Prospective study on image-guided navigation surgery for pelvic malignancies. J Surg Oncol 119:510–517. https://doi.org/10.1002/jso.25351
10. Fedorov A, Beichel R, Kalpathy-Cramer J, Finet J, Fillion-Robin JC, Pujol S, Bauer C, Jennings D, Fennessy F, Sonka M, Buatti J, Aylward S, Miller J V., Pieper S, Kikinis R (2012) 3D Slicer as an image computing platform for the Quantitative Imaging Network. Magn Reson Imaging 30:1323–1341. https://doi.org/10.1016/j.mri.2012.05.001
11. Brouwer de Koning SG, ter Braak TP, Geldof F, van Veen RLP, van Alphen MJA, Karssemakers LHE, Ruers TJM, Schreuder WH, Karakullukcu MB (2019) Resection planes in mandibular surgery: preoperative planning, intraoperative placement and postoperative evaluation. Unpublished manuscript.
12. Zhu M, Liu F, Zhou C, Lin L, Zhang Y, Chai G, Xie L, Qi F, Li Q (2018) Does intraoperative navigation improve the accuracy of mandibular angle osteotomy: Comparison between augmented reality navigation, individualised templates and free-hand techniques. J Plast Reconstr Aesthetic Surg 71:1188–1195. https://doi.org/10.1016/j.bjps.2018.03.018
13. Wagner A, Schicho K, Birkfellner W, Figl M, Seemann R, König F, Kainberger F, Ewers R (2002) Quantitative analysis of factors affecting intraoperative precision and stability of optoelectronic and electromagnetic tracking systems. Med Phys 29:905–912. https://doi.org/10.1118/1.1469625
14. Seeberger R, Kane G, Hoffmann J, Eggers G (2012) Accuracy assessment for navigated maxillo-facial surgery using an electromagnetic tracking device. J Cranio-Maxillofacial Surg 40:156–161. https://doi.org/10.1016/j.jcms.2011.03.003
15. Pietruski P, Majak M, Świątek-Najwer E, Żuk M, Popek M, Mazurek M, Świecka M, Jaworowski J (2019) Supporting mandibular resection with intraoperative navigation utilizing augmented reality technology – a proof of concept study. J Cranio-Maxillofacial Surg 47:854–859. https://doi.org/10.1016/j.jcms.2019.03.004

Chapter 11

General discussion and future perspectives

Surgery is the foundation of any approach with curative intent in the management of oral cavity cancer. However, there is no guidance on where to cut exactly in order to ensure that the tumor is completely removed, and that healthy tissue is conserved. In this thesis, different technologies were evaluated on their feasibility to provide guidance during oncological oral surgery. Guidance could be considered in two ways: to determine whether the complete tumor has been removed *after* the resection (resection margin assessment) or to indicate where to cut *during* the resection (surgical guidance). In this general discussion, the optimal requirements that a technology for resection margin assessment needs to fulfil will be discussed. The performance of the technologies that were studied in this thesis will be measured against these requirements. Concerning surgical guidance, the accuracy is the main outcome measure and requires a comprehensive discussion. The current methodology involving the patient-specific cutting guides will be measured against the surgical navigation. In addition, factors that jeopardize the accuracy and factors that can improve the accuracy will be discussed.

Part I: Resection margin assessment

Whether a technology for resection margin assessment is cost- and time-effective depends on several factors (Chapter 1). Some of these factors are studied extensively, and can be well defined, while other factors are still unclear. What is sure, is that the technology should especially be able to discriminate tumor from submucosal-, or muscle tissue, tissue that is found at the deep resection margin as this has a prognostic value that is more accurate than the mucosal resection margin. Furthermore, the technology should be feasible for specimen-driven margin assessment, rather than tumor bed sampling, as this has also been shown to predict local recurrences with higher accuracy. The technology should be able to evaluate the complete resection surface of the specimen in an acceptable amount of time.

The required sampling depth of the technology is, despite extensive investigation, not precisely definable. It depends on the desired margin clearance. The current guidelines on what considers an adequate margin are inconsistent and there is no statistical agreement between studies for an optimal margin width that decreases the rate of local recurrence. In addition, the millimetre accurate estimation of the margin, which is indispensable to define a millimetre guideline, is confounded by several factors involved in the post-operative microscopic evaluation by the pathologist, e.g., inconsistency in dissection and sampling methods, and the effect of specimen shrinkage and field cancerization.

The literature study presented in chapter 2, provided an overview of the technologies that are being used or studied for intra-operative deep resection margin assessment so far. Besides the performance in tumor detection, the factors as described above were included in this overview (performance, specimen or tumor bed driven, maximum sampling depth and acquisition time).

The prevailing technique remains frozen section analysis (FSA) (Chapter 2). However, despite the high accuracies achieved with FSA, the technique is subject to false negatives due to the complexity of some surgical specimens. With one frozen section, only a small fraction of the specimen can be evaluated, and the time needed to evaluate one frozen section is 15-30 minutes. Furthermore, margins that were positive based on intraoperative FSA and re-excised into clear margins during the same surgery, did not equate to an initially clear margin in terms of local control (1). As a result, the effectiveness of

intra-operative frozen section analysis was questioned and alternative methods for intraoperative margin assessment are encouraged. According to the literature study presented in chapter 2, the most promising technologies are ultrasound (less than 10 min, sampling depth several cm) for assessment on a macroscopic scale and fluorescence (real-time, sampling depth up to 6 mm) or optical techniques such as hyperspectral imaging (real-time, sampling depth 3 mm) for microscopic margin assessment. Chapter 2 discusses the other available technologies extensively. The use of ultrasound and optical techniques were further evaluated in this thesis and will be discussed here.

The contrast between tumor tissue and healthy tissue is already used in diagnostic imaging: tumor dimensions are reported from ultrasound (US) and magnetic resonance imaging (MRI). In order to obtain a complete representation of how accurate tumor dimensions of oral cavity cancer were measured with US and MRI, a retrospective study was conducted including all oral cavity cancer patients treated in our institute during the last 5 years. The tumor thickness was more reliably measured with US and the greatest dimension was more reliably measured with MRI and thus, the combination of US and MRI is very useful for obtaining information on the tumor dimensions prior to surgery.

Since the contrast between tumor and healthy tissue is clear on the diagnostic images of both modalities, both the MRI and US also hold promise for specimen-driven margin assessment. MRI has been evaluated for intraoperative margin assessment, but requires several improvements to allow use for clinical practice, e.g., acquisition time and ability to identify margins less than 5 mm (2, 3). US on the other hand is available in almost any operation complex and not expensive to use. However, limited studies report on the use of US for intraoperative margin assessment. This was reason to conduct a study to evaluate whether US could be used for intra-operative resection margin assessment (Chapter 4). An easy method to measure the resection margin of the specimen with US was developed: the resected specimen was suspended in US gel and scanned with the US probe. The minimal deep margin measured on the US images was compared to the minimal margin reported by the histopathologist. US seemed a feasible technology for intraoperative estimation of the deep resection margin of a specimen from the tongue: in 19 of 31 patients, the margin measured on US was within a 1 mm range of the margin measured on the histopathological sections, the method did not require extensive training of the operator and the measurement took less than five minutes. However, US underestimated the margin in 12 of 31 patients, meaning that the margin reported from the US images was smaller (maximum 3.5 mm) than the margin reported from the histopathological sections. This could have been a result of microscopic infiltrations that are not visible on US images but were found on microscopic histopathological analysis. Furthermore, the method used in this study is operator-dependent; an operator-independent technology is preferable. Thus, US should be used as a fast and easily applicable technology for macroscopic margin assessment. Improvements of this methodology can be achieved in the development of an operator-independent method.

To evaluate the resection margin on a microscopic scale instead, the feasibility of optical technologies was evaluated in this thesis (Chapter 5 & 6). First, the performance of a hand-held diffuse reflectance spectroscopy (DRS) probe was evaluated, with the aim to develop a surgical instrument that could acquire point-measurements at a suspicious location at the margin. After measuring the tissue with DRS, the acquired reflectance spectrum is compared to a database that was used to train a support vector machine, and a prediction can be made on the type of the measured tissue. a scale on a monitor indicates the likelihood of measured tumor tissue. Based on this real time feedback on tissue type, the surgeon could decide on whether to resect additional tissue.

The best results were obtained by the reflectance measured with a 1-mm source-detector distance (sensitivity, specificity, and accuracy were 89%, 82%, and 86%, respectively). With these performance measures, the technology is not sufficient for accurate margin evaluation. However, it is expected that this can improve after a more accurate correlation of the measurements with histopathology (see below).

With the current set up, DRS can only be used to detect positive resection margins, rather than close margins, due to its limited sampling depth. This depth depends on different factors, such as the optical properties of the tissue, the geometry of the probe, and the wavelength of the light (4). With a larger source-detector distance, larger sampling depths can be measured. Hennessy *et al.* found that within the visual range of 400 to 700 nm, the sampling depth varied between 0.4 and 0.7 mm for a source-detector distance of 1.0 mm. Thus, this sampling depth is sufficient to detect positive margins that are defined as tumor cells found at the margin. However, close margins can only be detected when tumor cells are present within 0.7 mm from the resection surface, and thus a margin assessment of 5 mm seems not possible to measure with DRS. Improvements in sampling depth could be reached by a further increase of the source-detector distance, and this would especially be interesting when guidelines would tend towards a close margin defined as 2 mm (5).

It is recommended that future study on the use of DRS for resection margin assessment should focus on an improvement of the performance measures by using an improved correlation method. In addition, as DRS is limited to the detection of positive margins only, future developments should also focus on an increase of the sampling depth to allow close margin evaluation.

Hyperspectral imaging (HSI) was evaluated as a diffuse reflectance imaging technique that may have the advantage over a point-based technique by giving an overview of the resection margin in one image (Chapter 6). Fresh surgical specimens of squamous cell carcinoma of the tongue were scanned with two hyperspectral cameras that cover the visible and near-infrared spectrum (400-1,700 nm). a diffuse reflectance spectrum is acquired for each pixel of the hyperspectral image, while illuminating the tissue with a broadband white light source. The measured reflectance is related to the absorption and scattering properties of the illuminated tissue and could be used to predict the tissue type. The hyperspectral images could be made available in real-time. When imaging the resection surface of a freshly resected specimen, the diffuse reflectance spectra of the hyperspectral image will be compared to a database of spectra obtained from tumor and healthy tissue. Based on the agreement with the spectra of this database, the pixels of the hyperspectral image can be visualized in a colour coding, e.g., red for tumor and green for healthy tissue.

The imaging depth of HSI varies with wavelength and tissue composition. The broad wavelength covered by the two cameras has the prospect of being able to detect both positive and close margins. Kho *et al.* estimated the imaging depth of the different wavelengths in breast tissue (6, 7). Wavelengths around 1200 nm obtained spectral information of superficial layers of the tissue, while a penetration depth up to 4.5 mm was obtained with wavelengths around 910 nm. Further research is essential to determine whether this is applicable for tongue muscle tissue as well.

The study presented in chapter 6 showed that it is possible to distinguish relatively large tongue tumor areas at the surface of the resected specimen from healthy tongue muscle tissue, using HSI (400-1,700 nm): sensitivity/specificity of visual and near-infrared were 84%/80% and 77%/77%, respectively. It is

expected that classification results can be improved when future studies that evaluate HSI for tissue characterization, consider the imaging depth in the design of the validation method (see below).

In this study, the tongue cancer specimens were imaged in a controlled setting. That is, that the images were acquired from a cross section through the tumor. This enabled imaging of large pockets of pure tumor and pure healthy muscle tissue. However, in case this technology will be used for intra-operative deep margin assessment, the amount of tumor tissue in the imaged volume will be much less than what was present in the cross sections used in this study. Thus, for use in an intra-operative setting, two more challenges need to be overcome: whether it is possible to detect smaller tumor pockets at the deep resection margin and whether it is possible to detect tumor up to 5 mm deep below the margin to detect close margins. In order to overcome the first challenge, a study should be conducted in which hyperspectral images are acquired from the resection surface, rather than a cross section through the tumor. For this, an improved correlation with the histopathology is essential: to determine how deep the tumor is located underneath the resection surface, and to determine the size of the imaged tumor. Since the imaging depth of HSI varies with wavelength and tissue composition, in order to overcome the second challenge, a study should be conducted to find out which wavelengths reach the desired imaging depth in (tongue) muscle tissue. In case specific wavelengths can be selected for an optimal discrimination between tumor and healthy tissue, these wavelengths could be used in a multispectral camera, to save data storage and decrease processing time. This promising imaging technology could also be useful for robotic surgery to build into a laparoscopic camera.

Correlation of study measurements with histopathology as gold standard

The performance of each technology was estimated by comparing the outcome of the technology with the outcome of post-operative histopathological microscopic evaluation. Although this is crucial in the determination of whether a technology is feasible for resection margin assessment, it is a very challenging process to set up accurately. Mainly due to tissue shrinkage and deformation that occurs between the time of measurement and the microscopic evaluation.

This correlation could not optimally be estimated in the study presented in chapter 3 in which the dimensions of the tumor *in situ* measured on US and MRI were compared with the dimensions measured on histopathological sections of the *ex vivo* resected specimen. Besides the tissue shrinkage that occurs during pathological processing, the direction of the sliced histopathology sections is not the same as the slicing direction of MR slices, or the same angle of the US probe positioning.

In chapter 4, the smallest resection margin measured on the US images was compared to the smallest margin reported by histopathology. Although the results did correspond well, there was no methodology applied for an accurate slice-by-slice comparison of US and histopathological specimens. In theory, the cross section with the smallest margin that was imaged by the US probe could have been different from the histopathological section with the smallest margin. To confirm or improve the results, the position and direction of the probe should be marked during image acquisition to allow correlation with the corresponding histopathological section.

In the studies described in chapter 5 and 6, a method for accurate correlation of measurements/images with histopathology was developed. This registration was based on the first histopathological section of the complete surface of the specimen. However, due to the direction of the histopathological sections and the orientation of the specimen in the paraffin block, it is not known from what depth this section

originated. While, depending on the wavelength, the diffuse reflectance spectra measured with the DRS probe or imaged with the hyperspectral cameras contain information of an imaged volume, from the surface up to several millimetres into the tissue.

For the DRS study, the sampling depth also depended on the source-detector distance: the larger the distance, the larger the sampling depth. The measurements acquired with the different source-detector distances were obtained from the same location and were all correlated to the same histopathological section. This section was the first section of the complete surface of the specimen. Therefore, it could have been so that the absolute superficial layer of the specimen, that was measured with the smallest source-detector distance, was not correlated to the right histologically confirmed tissue type: because the measured superficial layer of the specimen was sliced off before the slice including the entire intact surface was reached in the cutting process. On the other hand, in the source-detector distance with the largest sampling depth, it could have been the case that, besides traveling through a superficial layer of tumor tissue, the light also could have been traveling through an underlying layer of healthy tissue. Since we did not measure the tumor thickness at the measurement locations, we could not accurately validate the data for this larger sampling depth. This inaccurate validation could have been an explanation for the lower sensitivity and specificity reported in the 2-mm source-detector distance category. For the HSI study, the tissue types that were above and below the slice of which the histopathological section was taken, may have varied, but did contribute to the hyperspectral images. It is expected that in both studies the classification results can be improved when considering the sampling/imaging depth in the design of the validation method.

Costs

Guidelines recommend re-excision, and if re-excision is not feasible, radiotherapy with or without chemotherapy in case positive or close resection margins are reported after surgery (8). In a rough calculation, Dinardo *et al.* estimated the costs of an additional surgery around $4,000 per patient (9). Intraoperative resection margin assessment could prevent these extra costs and thus decrease the overall costs of treatment. The estimated costs of intraoperative frozen section averaged as much as $3,123 per patient, mainly due to the pathological consult that is required during surgery (9). The technologies for resection margin assessment that are currently under development should be more cost-efficient compared to this current method. Since US is already available at any operation complex, an operator-independent methodology to measure the margin with US would be cost-efficient. In addition, the one-time purchase costs and maintenance costs of a DRS probe or a hyperspectral camera are the only costs for these technologies as the surgeons can make the measurements by themselves.

Intra-operative re-excision after a positive margin

The basis for intraoperative resection margin assessment is to determine whether it is needed to resect additional tissue in response to a positive margin, directly during the initial surgery. This is thought to improve local recurrence and survival rates, maybe even equate the rates obtained with clear margins. However, it has been reported that re-excision of initially positive margins into clear margins did not equate to an initially clear margin and does not significantly improve local control compared to positive margins (1). Besides the method used for intra-operative margin assessment, the imprecision of relocating tissue sites may be a factor contributing to the increased recurrence in initial positive margins that were revised into clear margins. Kerawala *et al.* showed that re-locating the site intended for margin re-excision occurs with a mean error in relocating the origin of a tissue sample site of 12 mm for deep margins (10). In addition, tissue retraction of muscle *in situ* challenges direct correlation from

tumor to patient, since the different tongue muscles that are oriented in various directions retract in different amounts with the result that the tumor bed does not represent the tumor margin (11). This suboptimal re-localization of the area of concern in the tumor bed could explain that in up to 73% of the revised margins, no residual tumor is found (12). Van Lanschot *et al.* recently proposed a method for accurate relocation of inadequate tumor resection margins in the wound bed: the surgeon places numbered tags on both sides of the resection line in a pair-wise manner, so that after the resection, one tag of each pair remains on the specimen and the corresponding tag remains on the wound bed (13). The issue on accurate relocation of the area of concern is an extra motivation to develop the DRS probe (Chapter 5) further for intra-operative use, as this hand-held surgical instrument is a promising technology for real-time detection of tumor cells in the wound bed.

Based on real-time feedback on the status of the resection margin, the surgeon can perform a re-excision to improve the outcome of the surgery directly. The technology that is used for intra-operative resection margin assessment has to fulfil several requirements to be feasible for clinical use and to be cost- and time-effective: it should be feasible for detection of tumor cells at the deep resection margin, from the specimen cutting edge, and should be able to detect tumor cells at a certain sampling depth. Now, the prevailing technique remains frozen section analysis. However, this method is expensive and is time-consuming and thus many alternatives are currently under development. Table 1 presents an overview of the technologies for intraoperative margin assessment that were evaluated in this thesis. Ultrasound works fast, reaches a sampling depth of several centimetres and it is widely available, but it is user dependent and cannot detect microscopic tumor infiltrations. Diffuse reflectance spectroscopy is suitable for microscopic tumor detection of suspicious locations with a surgical instrument, whereas hyperspectral imaging could be used for evaluation of the whole resection surface in one view. However, these optical technologies require more research to increase the robustness. In the end, perhaps a combination of technologies will provide the desired information to guide the initial resection with clear margins or to help in the decision on re-excision or adjuvant treatment. Lastly, clear indications for intra-operative margin assessment should be determined and methods need to be developed for accurate re-location of the site intended for margin re-excision.

Table 1 Overview of factors that determine whether the technologies for resection margin assessment that were evaluated in this thesis, are cost- and time-effective

	Tumor – healthy tissue discrimination at the deep resection margin?	Feasible for specimen-driven margin assessment?	Feasible for intra-operative feedback during resection?	Acquisition time?	Sampling depth	Costs	Disadvantages/ Improvements required
Ultrasound	< 1 mm accurate with histopathological measurements	Yes	Yes (14)	<5 min	Several cm	Minimal (surgeon performs measure-ment; US widely available)	User dependent Macroscopic assessment
Diffuse reflectance spectro-scopy	Sensitivity 89% Specificity 82% Accuracy 86%	Point-measu-rements of suspicious location at the margin	Yes	Real-time	between 0.4 and 0.7 mm	NA	Performance requires improvement
Hyperspec-tral imaging (VIS/NIR)	Sensitivity 84%/77% Specificity 80%/77%	Yes	Yes, if build into a laparoscope	Real-time	< 3 mm	NA	Performance requires improvement

Part II: Surgical guidance for mandibular osteotomies

Osteotomies of the involved part of the mandible must be determined accurately to ensure adequate resection margins, but also to allow precise placement of bone segments for reconstructive surgery. In this thesis, the accuracy of the current procedure involving the patient-specific cutting guides was evaluated (Chapter 7) and surgical navigation was studied as an alternative (Chapter 8). In order to optimise the accuracy and workflow of surgical navigation, a dental splint and a navigated surgical cutting guide were designed and their performance was evaluated on phantoms (Chapter 9 & 10).

In patients undergoing surgery for malignant disease invading the mandible, osteotomies must be determined accurately to ensure clear resection margins. Tumor positive bone resection margins are reported in 21% of the patients and these patients have a significantly lower 5-year overall survival (15). Bone tissue requires an extensive and time-consuming histopathological process before it is possible to determine the status of the bone resection margin (16). Within this period of several weeks, the reconstructed mandible is healing, and thus, in case positive bone margins are found, it is highly undesirable to perform a re-excision. There are currently no methods available to evaluate the bone resection margin during surgery. Few technologies are currently being studied for this application e.g., fluorescent cytology, frozen section analysis (FSA) and specimen radiography (Chapter 2) (17). However, these technologies are yet not optimal for bone resection margin assessment during surgery. High diagnostic values were reported by the use of integrin αvβ6-targeting arginylglycylaspartic acid peptides as a marker for fluorescent cytology but the technique required 40 minutes to use (18). The high density

of bone makes routine FSA of cortical bony margins difficult. Few groups have presented methods for FSA in bone margin assessment but sensitivities found are not sufficient (19, 20). Concerning specimen radiography, convex structures such as the mandible are difficult to interpret on a two-dimensional image (21).

Since there are currently no methods available for intraoperative assessment of bone resection margins, guidance on the precise location of the osteotomy is offered during the resection instead. For this, the location of the osteotomy is planned carefully on a virtual 3D model, in advance of the surgery. To translate the position of the osteotomies from the virtual surgical plan to the clinical situation in the operating room, patient-specific cutting guides and fixation plates are designed and manufactured using computer-aided design/computer-aided manufacturing (CAD/CAM) techniques. The accuracy of this methodology was evaluated in chapter 7. Deviations were found between the location of the resection planes that were planned virtually and the postoperative outcomes. An intraoperative CBCT scan was acquired to determine whether this deviation could be the result of an inaccurate positioning of the patient-specific cutting guide on the patient. The CBCT showed that the cutting guides were positioned with a millimetre accuracy compared to the virtual plan. Thus, the sawing procedure itself appeared to be the cause of the deviations: the resection slots of the cutting guides allow a directional freedom of the saw. In order to reduce the directional freedom of the saw within the saw slots, the design of the saw slots could be improved (to enlarge the thickness of the saw slot in the design, or to use a titanium slit that fits into the saw slot of the guide).

Anterior osteotomies were performed more accurately than posterior osteotomies (intraoperatively positioned and final resection planes differed by 1.2 ± 1.0 mm, yaw angle 4.9 ± 6.6° and pitch angle 1.8 ± 1.5° and 2.2 ± 0.9 mm, yaw angle 9.3 ± 9° and pitch angle of 8.3 ± 6.5° respectively for anterior and posterior). This could be explained by the fact that the posterior saw slot only provided guidance during the caudal part of the posterior osteotomy and the cranial part was sawed free hand. From both an oncological and reconstruction point of view, millimetre accuracy is of less value for the upper part of the posterior resection plane, since the tumor does not usually impinge on the subsigmoid region and the graft segments are usually fixed to the lower border of the remaining mandible. Another explanation for the difference in accuracy between the posterior and anterior resection planes is the accessibility: the anterior mandible is frequently easily accessible and well exposed, whereas the access to the posterior mandible is often hampered by the more extensive elevated soft tissue overlying the mandibular ramus and condyle (e.g., parotid gland and masseter muscle).

Recently, Van Baar *et al.* published a systematic review on the accuracy of computer-assisted surgery in mandibular reconstruction (22). The studies that were included quantitatively assessed the accuracy of mandibular reconstruction compared to virtual planning. However, they concluded that there is a lack of uniformity in planning (e.g., image acquisition, mandibular resection size) and evaluation methods among the studies. Therefore, it was not possible to perform a meta-analysis. This is also the reason that it is not possible to compare the results of chapter 7 with the reported deviations of this systematic review. As an approach to standardize evaluation methods to allow valid comparisons and facilitate meta-analysis in the future, the same authors proposed a guideline (23).

The current methodology is costly and time-consuming. In the meantime, there is a chance for a change in tumor size, for which the cutting guide cannot account during surgery. In this thesis, it is hypothesized that surgical navigation could optimize the workflow in several ways. First, the surgical navigation can

shorten preoperative preparation time. Preparation of the virtual model for surgical navigation takes a few hours maximally, and only depends on the date of the preoperative CT scan. Thus, if radiology planning allows, preparation can be done short before the day of surgery. This procedure eliminates the factor of tumor growth in the time between virtual surgery planning, printing of the patient specific cutting guides, and the surgery. As a result, the virtual model provides a more accurate representation of the real-time situation, which can affect the number of positive bone resection margins. Besides the shorter time needed for preparation, the surgical procedure itself could also be performed faster when reconstruction segments fit the mandibular defect precisely. Accurate guidance for localization of the resection planes could lower the number of cases in which reconstruction segments have to be adjusted manually to fit the mandibular defect, which is a time-consuming process. In short, surgical navigation would save preparation time, would use a virtual model with a more accurate representation of the real-time situation and would decrease the duration of surgery. However, the accuracy of electromagnetic (EM) navigation in patients undergoing mandibular surgery was not studied yet. Therefore, as a first step of utilizing intraoperative EM navigation during head and neck surgery, a study was conducted to investigate the accuracy of EM navigation in eleven patients undergoing mandibular surgery (Chapter 8).

The accuracy of the surgical navigation is judged based on the validation procedure that is expressed as the target registration error (TRE). The locations of anatomical landmarks and landmarks on the cutting guide that were appointed with the navigation pointer on the patient were compared to the corresponding locations on the intra-operatively acquired CBCT scan, to determine the TRE. The TRE's found were 2.6 ± 1.5 mm and 3.2 ± 1.1 mm for landmarks located on the cutting guide and for anatomical landmarks, respectively.

The accuracy depends on both the accuracy of appointing the landmarks on the patient, and the accuracy of identification of the corresponding landmarks on the CBCT scan. The value of the anatomical landmarks is questionable since there are no precise landmarks identifiable on the mandible that can be repeatedly pinpointed with an error of less than a millimetre. The landmarks that were used on the cutting guides were the upper and lower ends of the sawing slots. An inter-observer analysis showed that the variability in identification of these landmarks on the CBCT was minimal.

Inaccuracies can also be a result of the tracking system. The used NDI Aurora EM tracking system had a tracking accuracy of 0.8 mm in a laboratory setting. This inaccuracy can increase in the presence of any metal distortions in the EM field. However, Seeberger *et al.* showed that EM interference due to metallic instruments was significant, but that the effect on the TRE was still acceptable (approximately 0.8 mm added to the TRE without metallic tools) in comparison to optical navigation devices (24).

Furthermore, the way the reference sensor is fixated to the mandible requires revision. a sensor-housing module was especially designed for this study, but within this housing module, rotational movements of the sensor could still occur. An improved sensor-housing module is of indispensable value for further use of surgical navigation. Ultimately, wireless sensors would facilitate easier and more accurate tracking (25).

In order to improve the accuracy of EM navigation further, the registration procedure could be optimized: the method on how the virtual three-dimensional (3D) rendered model is registered to the patient's mandible at the operating room table. Chapter 9 described a study in which a dental splint

was designed to improve the accuracy of registration and to eliminate the use of an intraoperatively acquired CBCT scan.

The design, production and intraoperative use of a dental splint would be promising for implementation within the EM navigation workflow. For the design of the dental splint, a non-invasive intra-oral scan of the mandibular teeth could be acquired during the first visit of the patient in the outpatient clinic. Using a handheld scanner, the physician or the dentist could acquire the scan within a few minutes. The intra-oral scanner acquires a 3D surface map of the mandibular teeth that can be inverted to design the dental splint. Subsequently, the dental splint can be printed using a sterilizable resin. The 3D virtual model of the dental splint can be added to the 3D reconstructed model of the mandible. In the intraoperative setting, the reference sensor is fixated to the mandible and the dental splint can be placed on top of the patient's teeth. Rigid point-based registration can be performed by pinpointing the notches on the dental splint on the patient with the trackable pointer and linking them with the corresponding points on the virtual model. After the registration procedure, the dental splint can be removed, and the EM navigation would be ready for use. Because the splint only has to be in place during the registration procedure to set up the surgical navigation, it will not hinder the use of other surgical instruments that are needed to perform the resection for example. The sensor remains in place and allows tracking of the position of the mandible throughout the whole procedure, thereby eliminating the need for immobilization of the mandible.

For this study, a dental splint that includes reference registration notches was 3D printed. Different sets of three points were used for rigid point-based registration on a mandibular phantom: notches on the dental splint only, screws on the mandible, contralateral screws (the side of the mandible where the sensor is not fixated) and a combination of screws on the mandible and notches on the dental splint. The accuracy of each registration method was expressed as the TRE and calculated using 45 notches at one side of the mandible. With a mean error of 0.83 mm, the use of a dental splint has shown to achieve the highest accuracy. It was concluded that screws could not as precisely be identified on the CBCT as the notches on the dental splint.

This chapter focussed on point-based registration, based on a limited set of landmarks. In maxillary surgery, surface registration is used instead of point-based registration. The navigation pointer is moved on the skin surface of the forehead and around the eyes. These random points on the facial skin surface around the eyes are matched to the corresponding points on the 3D model of the skin that is constructed from CT images. The accuracy of surface registration increases when the included surface increases and curves into various directions. Surface registration on the mandible is more challenging, since the bone surface that is prepared during surgery is limited to the segmental mandibulectomy and often does not include many curves. The advantage of surface registration over point-based registration is that it would eliminate the construction of a patient-specific dental splint, or the use of (invasive) screws as landmarks. However, it is unsure whether this will improve the registration accuracy (26). Therefore, we are currently conducting a study on whether surface registration is applicable in EM navigated mandibular surgery and whether the accuracy of this registration is sufficient.

Finally, to achieve both guidance in localization of the osteotomy as well as guidance during sawing, a navigated cutting guide was developed. In chapter 10, this concept was introduced as an alternative to a navigated surgical pointer or a navigated surgical saw and the efficacy was evaluated in multiple navigated osteotomies on mandible models.

The current methodology using 3D-printed cutting guides comes with its own shortcomings in the form of inflexibility during surgery, logistics, long production time and cost. Therefore, several research groups have started to look for alternative methods in the form of a navigated saw. However, a free-hand navigated saw requires good eye-hand coordination (27), and without a saw compelling cutting guide it is challenging to make a non-straight cut. a navigated cutting guide would only require this eye-hand coordination during positioning. When the cutting guide is aligned according to planning, the position of the cutting guide can be fixed so that the surgeon can focus on performing the osteotomy. In addition, the saw is compelled by the guide, making a curved cut impossible.

In this study, a novel 3D navigated cutting guide was designed and evaluated with 20 osteotomies, performed on plaster mandibular models according to preoperative planning using EM navigation. The pre- and postoperative scans were registered, and the difference between the preoperatively planned osteotomy and the performed osteotomy was expressed as the distance between the planned and performed cutting planes, and the yaw and roll angles between the planes. Using the navigated cutting guide, a high accuracy was achieved with small standard deviations suggesting that these results are reproducible (the mean difference was 1.1 mm ± 0.6 mm, with a yaw angle of 1.8 ± 1.4° and a roll angle of 1.6 ± 1.3°).

Surgical navigation with a navigated cutting guide would only be needed during the actual positioning of the cutting guide that is manufactured from non-ferrous material (e.g., medical-grade stainless steel or titanium). During the navigated positioning of the cutting guide, no interfering metallic instruments are needed that could affect the accuracy. When the correct position and orientation are obtained, the navigation system can even be turned off before using the metallic saw for the osteotomy.

This was a proof-of-concept study and thus some shortcomings have to be addressed before clinical use is possible. The current setup requires the baseplate to be attached to the mandible at some distance from the planned osteotomy. As it is not possible to position the baseplate on the tumor site, it is of yet difficult to perform an osteotomy near the condyle of the mandible. In further studies, this could be alleviated by providing multiple baseplates for different attachment locations. In addition, the way the cutting guide is fixated requires a less labor intensive and time-consuming method. Furthermore, quantitative feedback on how well the virtual and actual planes coincide is required to assist in the alignment and to eliminate possible inaccuracies caused by the hand-eye coordination.

Besides the use of the navigated cutting guide for mandibular osteotomies, these guides also have potential for the fibular osteotomies that are used to reconstruct the mandible. This is currently being studied and has practical challenges e.g., a large EM field generator is needed to generate an EM field both at the site of the mandible and the fibula.

How accurate does the 3D model used for VSP represent the real situation?

The 3D model that is constructed for virtual surgical planning (VSP) and for surgical navigation, is based on a computed tomography (CT) scan. This is usually the imaging modality that is used to interpret bone tissue. However, in contrast to bone tissue, tumor tissue is not clearly visible on the CT images. Only bone deterioration that is caused by a tumor invading the mandible, or by radiation therapy, is recognizable on the CT image. An automated segmentation algorithm is used to extract the mandibular bone from these scans. Depending on the threshold that is set for the grey value of bone tissue used in this algorithm, more or less pixels are added to the 3D representation of the mandible. Especially in

the regions where bone deterioration occurred, the threshold for bone segmentation could introduce an inaccuracy in the construction of the 3D model. Besides the settings of the segmentation algorithm, also dental implants that cause major artefacts on the CT scan can challenge the construction of an accurate 3D virtual model.

Tumor tissue is usually visualized using MRI, or an additional positron emission tomography (PET)-CT. So far, the tumor tissue is not incorporated in the 3D virtual model. This could be easily done by fusion of the MRI with the CT scan based on the mandibular bone (28). This way, the 3D virtual model can be constructed using the bone extracted from the CT scan and the tumor extracted from the MRI or PET scan. This should be implemented as standard practice.

Despite the use of advanced imaging techniques, estimating tumor invading the bone can still be inaccurate, possibly leading to an inadequate 3D model that is used for VSP and ultimately leading to inadequate resection margins or reconstructions.

Electromagnetic tracking as opposed to optical tracking

Two types of tracking systems exist for surgical navigation: EM tracking and optical tracking (29). The studies discussed in this thesis all use EM tracking, in which an EM field is positioned nearby the surgical area and EM sensors as small as 2 mm in diameter and 1 cm in length are used: one built into a surgical navigation pointer and a second sensor fixated to the patient. The sensor and the navigation pointer are wired. In contrast, an optical system uses infrared light in combination with wireless light reflectors/emitters that are fixated to the patient and to a surgical instrument. To track the position of the patient and the surgical instrument, a 'line-of-sight' must be maintained between the reflectors and a detector. Optical tracking systems are often used in maxillofacial surgery, since the rather large patient reference sensor can be attached to the skull.

Optical tracking is not suitable for mandibular surgery, because the optical reference sensor is too large to be attached to the mandible. The optical reference sensor could not be attached to the skull, due to the mobility of the mandible in regard to the skull. EM navigation has advances that are more practical over optical navigation for use during mandibular surgery. The smaller sensor, and navigation pointer are applicable in the small surgical field, and no line-of-sight is required. In addition, the EM field generator can be positioned near the patient's head, e.g., underneath the operating table.

With regard to the accuracy, Strong *et al.* achieved TRE's in the order of one millimetre with various optical tracking systems on maxillofacial surgery of four fresh cadaveric heads (30). This is hard to compare with the TRE of 2.6 millimetre achieved with EM tracking in patients, as discussed in chapter 8, since the registration procedure of the skull can be performed more accurately than the mandible (Chapter 9). It remains that the EM system needs improvement in order to level with the accuracy of optical tracking systems, but the practical advances of EM tracking are allowing surgical navigation for mandibular surgery, where optical navigation is practically not an option.

Osteotomies of the involved part of the mandible must be determined accurately to ensure adequate resection margins, but also to allow precise placement of bone segments for reconstructive surgery. In advance of the surgery, the location of the osteotomy is therefore carefully planned on a virtual 3D model. To translate the position of the osteotomies from the virtual surgical plan to the clinical situation in the operating room, patient-specific cutting guides and fixation plates are designed and manufactured using computer-aided design/computer-aided manufacturing (CAD/CAM) techniques. The cutting guides can be positioned with a millimeter accuracy compared to the virtual plan. However, the sawing procedure itself appeared to cause a difference between the planned and postoperative resection planes. This was attributed to the resection slots of the cutting guides allowing a directional freedom of the saw. Especially the posterior osteotomy deviated with a mean of 2.2 mm from the original plan. This has serious consequences for the extend of the tumor resection margin and the reconstruction segments that need to fit the mandibular defect precisely. Besides this, the current methodology requires weeks for preparation and the cutting guides cannot account for changes in tumor size that occurred recently. In this thesis, it is found that surgical navigation could optimize this workflow in several ways. With the patient study discussed in chapter 8, the accuracy of the surgical navigation system was evaluated and inaccuracies of 2.6 ± 1.5 mm were achieved. This study was the first study that reported on the accuracy of EM navigation in patients undergoing mandibular surgery and as a result, many suggestions for improvement are proposed since (Chapter 9 & 10). Thus, it is likely that after implementation of these, the accuracy will approach the clinical acceptable value of 1.5 mm (31). Therefore, besides improvement on the accuracy, focus of future research should also be on an improved surgical workflow (e.g., eliminate the use of a hybrid operating room by using a dental splint for registration instead), and on larger study populations with more surgeons becoming acquainted with this technology.

References

1. Bulbul, M.G., et al., Does Clearance of Positive Margins Improve Local Control in Oral Cavity Cancer? a Meta-analysis. Otolaryngol Head Neck Surg, 2019. 161(2): p. 235-244.
2. Steens, S.C.A., et al., Evaluation of tongue squamous cell carcinoma resection margins using ex-vivo MR. Int J Comput Assist Radiol Surg, 2017. 12(5): p. 821-828.
3. Heidkamp, J., et al., Assessment of surgical tumor-free resection margins in fresh squamous-cell carcinoma resection specimens of the tongue using a clinical MRI system. Head Neck, 2020. 42(8): p. 2039-2049.
4. Hennessy, R., et al., Effect of probe geometry and optical properties on the sampling depth for diffuse reflectance spectroscopy. J Biomed Opt, 2014. 19(10): p. 107002.
5. Zanoni, D.K., et al., a Proposal to Redefine Close Surgical Margins in Squamous Cell Carcinoma of the Oral Tongue. JAMA Otolaryngol Head Neck Surg, 2017. 143(6): p. 555-560.
6. Kho, E., et al., Feasibility of margin assessment with hyper spectral imaging during breast-conserving surgery: towards intraoperative feedback (Submitted, 2020).
7. Kho, E., et al., Imaging depth variations in hyperspectral imaging: Development of a method to detect tumor up to the required tumor-free margin width. J Biophotonics, 2019. 12(11): p. e201900086.
8. National Comprehensive Cancer Network. Head and neck cancers (Version 1.2018). NCCN clinical practice guidelines in oncology. Available at: https://www.nccn.org/professionals/physician_gls/pdf/head-and-neck.pdf. Accessed April 1, 2018.
9. DiNardo, L.J., et al., Accuracy, utility, and cost of frozen section margins in head and neck cancer surgery. Laryngoscope, 2000. 110(10 Pt 1): p. 1773-6.
10. Kerawala, C.J. and T.K. Ong, Relocating the site of frozen sections- is there room for improvement? Head & Neck, 2001. 23: p. 230-232.
11. Weinstock, Y.E., I. Alava, 3rd, and E.J. Dierks, Pitfalls in determining head and neck surgical margins. Oral Maxillofac Surg Clin North Am, 2014. 26(2): p. 151-62.
12. Scholl, P., et al., Microscopic cut-through of cancer in the surgical treatment of squamous carcinoma of the tongue. Prognostic and therapeutic implications. Am J Surg, 1986. 152(4): p. 354-60.
13. van Lanschot, C.G.F., et al., Relocation of inadequate resection margins in the wound bed during oral cavity oncological surgery: a feasibility study. Head Neck, 2019. 41(7): p. 2159-2166.
14. Songra, A.K., et al., Observation of tumour thickness and resection margin at surgical excision of primary oral squamous cell carcinoma--assessment by ultrasound. Int J Oral Maxillofac Surg, 2006. 35(4): p. 324-31.
15. Smits, R.W.H., et al., Evaluation of bone resection margins of segmental mandibulectomy for oral squamous cell carcinoma. Int J Oral Maxillofac Surg, 2018. 47(8): p. 959-964.
16. Bauer, T.W. and D. Mahovlic, Cutting and Grinding Methods for Hard-Tissue Histology, in Handbook of Histology Methods for Bone and Cartilage, Y.H. An and K.L. Martin, Editors. 2003, Humana Press, Totowa, NJ. .
17. Lubek, J.E. and K.R. Magliocca, Evaluation of the Bone Margin in Oral Squamous Cell Carcinoma. Oral Maxillofac Surg Clin North Am, 2017. 29(3): p. 281-292.
18. Nieberler, M., et al., Fluorescence imaging of invasive head and neck carcinoma cells with integrin alphavbeta6-targeting RGD-peptides: an approach to a fluorescence-assisted intraoperative cytological assessment of bony resection margins. Br J Oral Maxillofac Surg, 2018. 56(10): p. 972-978.
19. Oxford, L.E. and Y. Ducic, Intraoperative evaluation of cortical bony margins with frozen-section analysis. Otolaryngol Head Neck Surg, 2006. 134(1): p. 138-41.
20. Wysluch, A., et al., Intraoperative evaluation of bony margins with frozen-section analysis and trephine drill extraction technique: a preliminary study. Head Neck, 2010. 32(11): p. 1473-8.
21. Ntomouchtsis, A., et al., Pilot study of intraoperative digital imaging with the use of a mammograph for assessment of bone surgical margins in the head and neck region. Clin Radiol, 2013. 68(3): p. e136-42.
22. van Baar, G.J.C., et al., Accuracy of computer-assisted surgery in mandibular reconstruction: a systematic review. Oral Oncol, 2018. 84: p. 52-60.
23. van Baar, G.J.C., et al., Accuracy of computer-assisted surgery in mandibular reconstruction: a postoperative evaluation guideline. Oral Oncol, 2019. 88: p. 1-8.
24. Seeberger, R., et al., Accuracy assessment for navigated maxillo-facial surgery using an electromagnetic tracking device. J Craniomaxillofac Surg, 2012. 40(2): p. 156-61.

25. Eppenga, R., et al., Accuracy assessment of target tracking using two 5-degrees-of-freedom wireless transponders. Int J Comput Assist Radiol Surg, 2020. 15(2): p. 369-377.
26. Runge, A., et al., Accuracy of surface registration in cranial electromagnetic navigation. Otorhinolaryngology-Head and Neck Surgery, 2018. 3(2).
27. Pietruski, P., et al., Accuracy of experimental mandibular osteotomy using the image-guided sagittal saw. Int J Oral Maxillofac Surg, 2016. 45(6): p. 793-800.
28. Kraeima, J., et al., Multi-modality 3D mandibular resection planning in head and neck cancer using CT and MRI data fusion: a clinical series. Oral Oncol, 2018. 81: p. 22-28.
29. Sukegawa, S., T. Kanno, and Y. Furuki, Application of computer-assisted navigation systems in oral and maxillofacial surgery. Jpn Dent Sci Rev, 2018. 54(3): p. 139-149.
30. Strong, E.B., et al., Comparison of 3 Optical Navigation Systems for Computer-Aided Maxillofacial Surgery. Arch Otolaryngol Head Neck Surg, 2008. 134(10): p. 1080-1084.
31. Sun, Y., et al., Evaluation of 3 different registration techniques in image-guided bimaxillary surgery. J Craniofac Surg, 2013. 24(4): p. 1095-9.

Appendices

Summary

In this thesis, different technologies are evaluated on their feasibility to provide guidance during oncological oral surgery. Guidance can be considered in two ways: to determine whether the complete tumor has been removed *after* the resection (resection margin assessment) or to indicate where to cut *during* the resection (surgical guidance).

To determine whether the tumor is completely excised during surgery, there is a need for technologies that provide intra-operative feedback on the status of the resection margin. Surgeons aim to remove the tumor with a margin of healthy tissue to ensure complete tumor removal. In case the margin of healthy tissue is found inadequate after microscopic evaluation by the histopathologist post-operatively, the disease is more likely to recur and further therapy is recommended, e.g., reoperation or radiotherapy. Intra-operative margin assessment could prevent this: based on feedback on the status of the resection margin during surgery, the surgeon could decide on whether to resect additional tissue directly. At the moment, many technologies are being studied for feasibility to assess the resection margin during surgery. The requirements that such a technology needs to fulfil strongly depend on a few uncertainties around the prognostic value and its related definition of a positive or close margin, and the method of how the status of the resection margin is estimated currently (**Chapter 1**).

The literature study presented in **Chapter 2**, provided an overview of the technologies that are currently used or investigated for intra-operative resection margin assessment. The technology should especially be able to discriminate tumor from submucosal-, or muscle tissue, tissue that is found at the deep resection margin as this has a prognostic value that is more accurate than the mucosal resection margin. The results were categorized according to the type of technique: 'Frozen Section Analysis', 'Fluorescence', 'Optical Imaging', 'Conventional imaging techniques', and 'Cytological assessment'. For each technology, an overview is given of the reported performance in discriminating tumor from healthy tissue, acquisition time and sampling depth. At the moment, the technique used in routine practice is frozen section analysis. However, other technologies are very promising for future use when effectiveness has been shown in larger trials.

The contrast between tumor tissue and healthy tissue is already used in diagnostic imaging. Tumor dimensions are reported from *ultrasound* and *magnetic resonance imaging* (MRI). In **Chapter 3**, a retrospective study was conducted to estimate how accurate these tumor dimensions could be measured on preoperative imaging techniques. These dimensions were compared to the corresponding measures reported from microscopic evaluation by the histopathologist. Tumor thickness was more reliably measured with ultrasound and greatest dimension was more reliably measured with MRI.

The contrast found between tumor and healthy tissue on ultrasound images was reason to conduct a study to evaluate whether ultrasound could be used for intra-operative resection margin assessment (**Chapter 4**). The resected tongue specimens of 31 patients were suspended in ultrasound gel and scanned with a small 5-10 MHz ultrasound probe. The tumor was readily visible and ultrasound could differentiate it from muscle tissue. The minimal deep margin measured on the ultrasound images was compared to the minimal margin reported by the histopathologist. The mean difference was 1.1 mm. The method did not require extensive training of the operator and the measurement took less than five minutes. Hence, the method is easy to incorporate into surgical routine.

Ultrasound is an imaging technique that could be used for macroscopic evaluation of the margin. To evaluate the resection margin on a microscopic scale, the feasibility of optical technologies was studied. First, the performance of a hand-held *diffuse reflectance spectroscopy* (DRS) probe was evaluated, with the aim to develop a surgical instrument that could acquire point-measurements at a suspicious location at the margin (**Chapter 5**). Diffuse reflectance spectra (400-1,600 nm) were acquired on fresh surgical specimens from 28 patients with oral cavity squamous cell carcinoma. a total of 76 spectra were obtained from tumor tissue and 110 spectra from healthy muscle tissue. In this study, an algorithm was used to classify spectra obtained from tumor or healthy tissue. DRS, combined with the classification algorithm, could discriminate tumor from healthy tissue with a sensitivity of 89% and a specificity of 82%.

Hyperspectral imaging (HSI) was evaluated as a diffuse reflectance imaging technique that may have the advantage over a point-based technique by giving an overview of the resection margin in one image (**Chapter 6**). Fourteen fresh surgical specimens of squamous cell carcinoma of the tongue were scanned with two hyperspectral cameras that cover the visible and near-infrared spectrum (400-1,700 nm). a diffuse reflectance spectrum is acquired for each pixel of the hyperspectral image, while illuminating the tissue with a broadband white light source. a neural network was used for tissue-type prediction. The diagnostic performance of both wavelength ranges (sensitivity/specificity were 84%/80% and 77%/77% for visual and near-infrared, respectively) appears to be comparable and there is no additional benefit of combining the two wavelength ranges (83%/76%).

While resection margin assessment occurs *after* the resection, surgical guidance indicates where to cut *during* the resection. This is amongst others relevant in patients with malignant disease abutting or invading the mandible. The osteotomies (i.e., the resection through bone) of the involved part of the mandible must be determined accurately to ensure clear resection margins, but also to allow precise placement of bone segments, enabling the contour of the fibular graft to match the native resected mandible. At the moment, these surgeries are prepared virtually, and patient-specific cutting guides are used to translate the position of the osteotomies from the virtual surgical plan to the clinical situation in the operating room. It is hypothesised that the use of surgical navigation could expedite the preparation of the procedure and improve the accuracy.

The exact location of the osteotomy is prepared through virtual surgical planning in which three-dimensional (3D) rendered models of the mandible are used to perform a virtual (segmental) mandibulectomy. a cutting guide is constructed for each patient, so that the osteotomy could be performed according to the virtual planning. The accuracy of this procedure was evaluated in **Chapter 7**. The positions of the resection planes were registered from three moments: the virtually planned resection plane, the resection plane indicated by the cutting guide during surgery (measured from an intra-operatively acquired computed tomography (CT) scan) and the final resection plane (measured from a postoperative CT scan). Cutting guides were positioned on the mandible with millimetre accuracy. Anterior osteotomies were performed more accurately than posterior osteotomies (intraoperatively positioned and final resection planes differed by 1.2 ± 1.0 mm, yaw angle 4.9 ± 6.6° and pitch angle 1.8 ± 1.5° and 2.2 ± 0.9 mm, yaw angle 9.3 ± 9° and pitch angle of 8.3 ± 6.5° respectively for anterior and posterior). Differences between intraoperatively planned and final resection planes imply a directional freedom of the saw through the saw slots. Since cutting guides are positioned with millimetre accuracy compared to the virtual plan, the design of the saw slots in the cutting guides needs improvement to allow more accurate resections.

The accuracy of surgical navigation was evaluated in eleven patients undergoing mandibular surgery (**Chapter 8**). An electromagnetic (EM) navigation system was used. Preoperatively, a 3D rendered model of the mandible was constructed from diagnostic CT images. During the surgery, the virtual 3D model was registered to the patient using an intraoperatively acquired cone beam CT (CBCT) scan and a point-based registration procedure. The location of the mandible was tracked with an EM sensor fixated to the mandible. The surgeon could pinpoint landmarks on the mandible using a tracked surgical pointer. The real-time location of both the mandible and the surgical pointer were displayed on the navigation system. Accuracy measurements were performed by pinpointing four anatomical landmarks and four landmarks on the cutting guide using the pointer on the patient and comparing these locations to the corresponding locations on the CBCT. The system had errors of 3.2 ± 1.1 mm and 2.6 ± 1.5 mm for anatomical landmarks and landmarks on the cutting guide, respectively.

In order to improve the accuracy of EM navigation further, the registration procedure could be optimized: the method on how the virtual 3D model is registered to the actual patient's mandible at the operating room table. An accurate rigid point-based registration procedure requires landmarks that are clearly localizable on both the virtual 3D model and the mandible of the patient. Anatomical landmarks on the mandible, such as the teeth, are not accurate enough for this procedure. **Chapter 9** describes a phantom study in which a dental splint was designed to improve the accuracy of registration. The accuracy reached with the landmarks on the dental splint was compared to amongst others, the accuracy reached by using screws fixated to the mandible. After the registration procedure, the location of landmarks pinpointed on the phantom was compared to the corresponding virtual location and the difference between these locations was measured. The use of the dental splint for registration was most accurate with an average difference of 0.83 mm. For edentate patients, screws can be used as an alternative (1.28 mm).

In **Chapter 10**, a navigated cutting guide was introduced as an alternative to a navigated surgical pointer or a navigated surgical saw. The efficacy was evaluated in twenty navigated osteotomies on mandible models. The planned osteotomy on the preoperative CT scan was compared to the performed osteotomy on the post-operative CT scan. The mean difference was 1.1 mm ± 0.6 mm, with a yaw angle of 1.8 ± 1.4° and a roll angle of 1.6 ± 1.3°. The navigated cutting guide for mandibular osteotomies demonstrated accurate positioning of the cutting plane according to the preoperative virtual surgical plan and is therefore a promising development.

The subjects and results of this thesis are discussed in **Chapter 11**. Suggestions are offered for future studies.

Samenvatting

In dit proefschrift worden verschillende geavanceerde technologieën voor oncologische hoofd-hals chirurgie besproken. Deze technologieën hebben als doel om de huidige chirurgie te verbeteren.

In het eerste deel van dit proefschrift wordt de focus gelegd op technologieën die tijdens de operatie kunnen bepalen of de snijranden schoon zijn. Chirurgen willen de tumor met een marge van gezond weefsel weghalen om er zeker van te zijn dat de tumor helemaal verwijderd is. Wanneer na de operatie door microscopisch onderzoek wordt vastgesteld dat dit niet gelukt is, dat de zogenoemde snijranden niet schoon zijn, is er een grotere kans dat de ziekte terugkomt en wordt de patiënt geadviseerd om aanvullende therapie, zoals bijvoorbeeld een nieuwe operatie of radiotherapie te ondergaan. Om dit te voorkomen zouden we tijdens de operatie graag al willen weten of de snijranden schoon zijn. Dan kan de chirurg namelijk direct ingrijpen door een extra stukje weefsel weg te nemen. Op dit moment worden er veel technieken onderzocht die tijdens de operatie de status van de snijraden zouden kunnen bepalen. De eisen waaraan deze techniek moet voldoen, hangen sterk af van een aantal onzekerheden die nog bestaan over de prognostische waarde en de daaraan gerelateerde definitie van de snijranden, en de manier waarop de status van de snijranden op dit moment vastgesteld wordt (**Hoofdstuk 1**).

Het literatuuronderzoek dat gepresenteerd wordt in **Hoofdstuk 2** laat zien welke technieken er op dit moment ontwikkeld en onderzocht worden om tijdens de operatie de status van het snijvlak te kunnen bepalen. De nadruk is daarbij gelegd op het onderzoeken van het 'diepe snijvlak' oftewel het snijvlak van waar de tumor diep in het weefsel doorgegroeid was, in plaats van het 'mucosale snijvlak', het snijvlak rondom de tumor wat zichtbaar is aan het oppervlak van het weefsel. De gevonden technieken zijn opgedeeld in categorieën: analyse op basis van vriescoupes, fluorescentie, optische beeldvorming, traditionele beeldvormende technieken en cytologische technieken. Voor elk van de technieken is een overzicht gemaakt over hoe goed de techniek onderscheid kan maken tussen tumor en gezond weefsel, hoeveel tijd er nodig is voordat de techniek de status van het snijvlak heeft bepaald en hoe diep in het weefsel de techniek tumor kan detecteren. Op dit moment wordt er nog het meest gebruik gemaakt van analyse op basis van vriescoupes. Toch zijn andere technieken veelbelovend, maar deze moeten hun waarde nog bewijzen in grote klinische onderzoeken.

Om de status van de snijrand te bepalen moet de techniek het onderscheid kunnen maken tussen tumor en gezond weefsel. In de diagnostiek wordt dit gebruikt om de aanwezigheid van een tumor vast te stellen: de dimensies van de tumor worden bepaald op basis van *ultrasound* en *magnetic resonance imaging* (MRI). **Hoofdstuk 3** beschrijft een studie waarbij wordt gekeken hoe precies die tumor dimensies worden bepaald aan de hand van deze twee technieken. Dit werd vergeleken met de dimensies die gerapporteerd waren aan de hand van de microscopische evaluatie door de patholoog. De dikte van de tumor is het beste vast te stellen met ultrasound, terwijl de grootste dimensie het meest precies bepaald kon worden aan de hand van de MRI-beelden.

Het duidelijke contrast tussen tumor en gezond weefsel op ultrasound beelden was aanleiding om onderzoek te doen naar het gebruik van ultrasound voor het bepalen van de status van het snijvlak tijdens de operatie (**Hoofdstuk 4**). Preparaten van 31 patiënten met tongkanker werden onderzocht in een bakje met ultrasound gel en een kleine 5-10MHz ultrasound probe. De tumor was goed zichtbaar en kon goed onderscheiden worden van het gezonde tongspierweefsel. De kortste afstand tussen

de tumor en het snijvlak werd gemeten op de ultrasound beelden en vergeleken met de afstand die gevonden werd bij het microscopisch onderzoek van de patholoog. Het gemiddelde verschil was 1.1 mm. De metingen kostten maximaal vijf minuten en waren makkelijk uit te voeren. Daarmee is het een techniek voor een macroscopische bepaling van de status van de snijvlakken, die makkelijk in te bouwen is in de chirurgische workflow.

Ultrasound kan gebruikt worden om de status van het snijvlak macroscopisch te bepalen. Om ook op microscopisch niveau het snijvlak te bekijken wordt in **Hoofdstuk 5** het onderzoek naar *diffuse reflectie spectroscopie* (DRS) besproken. Een handzame DRS probe zou kunnen functioneren als chirurgisch instrument dat punt-metingen kan doen op een voor tumor verdachte locatie op het snijvlak. Met preparaten van 28 patiënten met mondholtekanker werden 76 spectra (400 tot 1600 nm) verzameld op tumorweefsel en 110 spectra op gezond weefsel. In deze studie is een algoritme gebruikt welke de spectra classificeert als zijnde afkomstig van tumor of gezond weefsel. DRS, gecombineerd met het classificatie algoritme, kan tumor van gezond onderscheiden met een sensitiviteit van 89% en een specificiteit van 82%.

Met *Hyperspectrale imaging* (HSI) kunnen de optische eigenschappen van het hele snijvlak in beeld gebracht worden, in plaats van een enkel punt op het snijvlak zoals bij de DRS probe. In het onderzoek dat staat beschreven in **Hoofdstuk 6** zijn 14 preparaten van tongkankerpatiënten gescand met twee HSI-camera's, zodat zowel het licht dat weerkaatst werd met golflengtes uit het visuele spectrum, als het nabij-infrarode spectrum konden worden gedetecteerd (400-1700 nm). Elke pixel van het HSI-beeld bevat een meting van de diffuse reflectie. Een neuraal netwerk werd gebruikt voor weefsel-type voorspelling. Het bleek dat beide camera's tumor van gezond weefsel konden onderscheiden met vergelijkbare sensitiviteit (84%/80%) en specificiteit (77%/77%). Deze getallen konden niet verbeterd worden door de data van beide camera's te combineren in een analyse (83%/76%).

Het tweede deel van dit proefschrift gaat over chirurgische navigatie, een techniek die ondersteuning kan bieden tijdens het precies bepalen van de plaats voor de osteotomie (doorname van het bot) bij patiënten die een tumor hebben die doorgroeit tot in de mandibula (onderkaak). De plaats van de osteotomie wordt nauwkeurig bepaald om er allereerst voor te zorgen dat de tumor volledig verwijderd wordt, maar ook om ervoor te zorgen dat de botsegmenten van de fibula (het kuitbeen) precies zullen passen voor de reconstructie van de mandibula. Op dit moment wordt de planning van de operaties digitaal voorbereid en d.m.v. zaagmallen uitgevoerd tijdens de operatie. De verwachting is om door het gebruik van chirurgische navigatie het planningsproces te versnellen en de nauwkeurigheid van de procedure te verbeteren.

Operaties waarbij de mandibula betrokken is worden voorbereid aan de hand van een virtueel operatieplan. Daarbij wordt op een 3D model op de computer gepland waar de mandibula doorgenomen zal worden. Voor elke patiënt worden er zaagmallen gemaakt zodat de osteotomie uitgevoerd wordt volgens de planning. **Hoofdstuk 7** beschrijft het onderzoek waarbij de nauwkeurigheid van deze procedure wordt gekwantificeerd. De positie van de zaagvlakken werd op drie momenten geregistreerd: het digitale geplande vlak, het vlak zoals aangegeven door de zaagmal nadat deze op de patiënt bevestigd is tijdens de operatie (te meten op een intra-operatieve CT-scan) en het vlak waarlangs uiteindelijk gezaagd is (te meten op postoperatieve CT-scan). Er werd geconcludeerd dat de zaagmallen op de millimeter nauwkeurig geplaats werden tijdens de operatie t.o.v. de virtuele planning. Bij de vergelijking tussen de intra-operatieve, door de zaagmal aangegeven zaagvlakken, met hoe er

uiteindelijk gezaagd is postoperatief, werden wel verschillen gevonden: de anterieure osteotomie werd nauwkeuriger uitgevoerd dan de posterieure osteotomie (het verschil tussen het zaagvlak intra-operatief en postoperatief was respectievelijk voor anterieur en posterieur 1,2 ± 1,0 mm, 'yaw' hoek van 4,9 ± 6,6° en 'roll' hoek van 1,8 ± 1,5° en 2,2 ± 0,9 mm, 'yaw' hoek van 9,3 ± 9° en 'roll' hoek van 8,3 ± 6,5°). Deze verschillen kunnen verklaard worden door een zekere vrijheid waarbinnen de zaag kan bewegen in de sleuven op de zaagmal. Omdat de plaatsing van de zaagmallen zo nauwkeurig gebeurt, is winst in nauwkeurigheid voornamelijk te behalen in het design van de zaagmallen.

Hoofdstuk 8 beschrijft het onderzoek naar de nauwkeurigheid van het gebruik van chirurgische navigatie bij elf patiënten die een operatie aan de mandibula hebben ondergaan. Hierbij werd gebruik gemaakt van een elektromagnetisch (EM) navigatiesysteem. Voorafgaand aan de operatie werd op basis van een CT-scan een 3D model gemaakt van de mandibula van de patiënt. Tijdens de operatie werd dit digitale model gekoppeld aan de patiënt op de operatietafel d.m.v. een intra-operatieve CT-scan met een, op een aantal aanwijspunten gebaseerde, registratie ('point-based registration'). De locatie van de mandibula kon worden bijgehouden door bevestiging van een EM sensor. Met een genavigeerde chirurgische aanwijspen kon de chirurg punten aanwijzen op de mandibula van de patiënt. De bewegingen van de aanwijspen t.o.v. de mandibula werden overeenkomstig afgebeeld op het navigatie beeldscherm. Om de nauwkeurigheid van het systeem te kwantificeren werden vier anatomische oriëntatiepunten en vier punten op de geplaatste zaagmal aangewezen. De locaties van deze aanwijspunten op de patiënt werden vergeleken met de bijbehorende virtuele locaties. Het systeem toonde een afwijking van 3,2 ± 1,1 mm voor het aanwijzen van de anatomische oriëntatiepunten en 2,6 ± 1,5 mm voor het aanwijzen van de punten op de zaagmal.

Een manier om de nauwkeurigheid van het navigatiesysteem te verbeteren is het optimaliseren van de registratie procedure: de manier waarop het virtuele 3D model gekoppeld wordt aan de patiënt in de operatiekamer. Voor deze registratie wordt gebruik gemaakt van aanwijspunten die duidelijk te lokaliseren zijn in het virtuele 3D model en op de mandibula van de patiënt. De anatomische aanwijspunten op de mandibula, zoals bijvoorbeeld tanden, zijn niet nauwkeurig genoeg hiervoor. Daarom is in het fantoom onderzoek dat beschreven staat in **Hoofdstuk 9**, een bitje ontwikkeld met duidelijke aanwijspunten. De nauwkeurigheid die behaald werd door het gebruik van aanwijspunten op het bitje is vergeleken met o.a. het gebruik van schroeven op de mandibula. Met een verschil van 0,83 mm tussen punten die na de registratie aangewezen werden op het fantoom en de overeenkomstige punten in het virtuele model was het bitje het meest nauwkeurig. Voor edentate patiënten zijn de schroeven een goed alternatief (1,28 mm).

In **Hoofdstuk 10** wordt de genavigeerde zaagmal geïntroduceerd als alternatief voor de genavigeerde chirurgische aanwijspen of een genavigeerde chirurgische zaag. De effectiviteit van deze genavigeerde zaagmal werd getest met 20 verschillende osteotomieën op modellen van de mandibula. De geplande osteotomie op de preoperatieve CT-scan werd vergeleken met de uiteindelijke osteotomie op de postoperatieve CT-scan. Het gemiddelde verschil was 1,1 mm ± 0,6 mm en de 'yaw' hoek van 1,8 ± 1,4° en 'roll' hoek van 1,6 ± 1,3°. De genavigeerde zaagmal kan dus zeer nauwkeurig geplaatst worden voor mandibulaire osteotomieën en is daarmee een veelbelovende ontwikkeling voor de toekomst.

De onderwerpen en resultaten die besproken zijn in dit proefschrift worden bediscussieerd in **Hoofdstuk 11**. Daarnaast worden suggesties gedaan voor mogelijkheden voor toekomstig onderzoek.

Authors and affiliations

AS A.W.M.A. Schaeffers, Medical student, University of Groningen; Department of Head and Neck Surgery and Oncology, The Netherlands Cancer Institute, Antoni van Leeuwenhoek, Amsterdam, The Netherlands

BD B. Dashtbozorg, Department of Surgical Oncology, The Netherlands Cancer Institute, Antoni van Leeuwenhoek, Amsterdam, The Netherlands

BH B.H.W. Hendriks, Department of In-body Systems, Philips Research, Eindhoven, The Netherlands; Department of Biomechanical Engineering, Delft University of Technology, Delft, The Netherlands

BK M.B. Karakullukcu, Department of Head and Neck Surgery and Oncology, Verwelius 3D Lab, The Netherlands Cancer Institute, Antoni van Leeuwenhoek, Amsterdam, The Netherlands

CL C.A.H. Lange, Department of Radiology, The Netherlands Cancer Institute, Antoni van Leeuwenhoek, Amsterdam, the Netherlands

CS C. Shan, Department of In-body Systems, Philips Research, Eindhoven, The Netherlands

EB E.J.M. Baltussen, Department of Surgical Oncology, The Netherlands Cancer Institute, Antoni van Leeuwenhoek, Amsterdam, The Netherlands

FG F. Geldof, student Technical Medicine, University of Twente; Department of Surgical Oncology, The Netherlands Cancer Institute, Antoni van Leeuwenhoek, Amsterdam, The Netherlands

FH F. van der Heijden, Faculty of Science and Technology, University of Twente, Enschede, The Netherlands

HS H.J.C.M. Sterenborg, Department of Surgical Oncology, The Netherlands Cancer Institute, Antoni van Leeuwenhoek, Amsterdam, The Netherlands; Department of Biomedical Engineering and Physics, Academic Medical Center, Amsterdam, The Netherlands

JN J. Nijkamp, Department of Surgical Oncology, The Netherlands Cancer Institute, Antoni van Leeuwenhoek, Amsterdam, The Netherlands

JR J. J. M. Riksen, student Technical Medicine, University of Twente; Department of Head and Neck Surgery and Oncology, The Netherlands Cancer Institute, Antoni van Leeuwenhoek, Amsterdam, The Netherlands

LK L.H.E. Karssemakers, Department of Head and Neck Surgery and Oncology, Verwelius 3D Lab, The Netherlands Cancer Institute, Antoni van Leeuwenhoek, Amsterdam, The Netherlands

LS L.A. Smit, Department of Pathology, The Netherlands Cancer Institute, Antoni van Leeuwenhoek, Amsterdam, the Netherlands

MA M.J.A. van Alphen, Department of Head and Neck Surgery and Oncology, Verwelius 3D Lab, The Netherlands Cancer Institute, Antoni van Leeuwenhoek, Amsterdam, The Netherlands

MB M.W.M. van den Brekel, Department of Head and Neck Surgery and Oncology, The Netherlands Cancer Institute, Antoni van Leeuwenhoek, Amsterdam, The Netherlands

PW P.J.C. Weijtmans, Department of In-body Systems, Philips Research, Eindhoven, The Netherlands

RD R. Dirven, Department of Head and Neck Surgery and Oncology, The Netherlands Cancer Institute, Antoni van Leeuwenhoek, Amsterdam, The Netherlands

RV R.L.P. van Veen, Department of Head and Neck Surgery and Oncology, Verwelius 3D Lab, The Netherlands Cancer Institute, Antoni van Leeuwenhoek, Amsterdam, The Netherlands

TB T.P. ter Braak, student Technical Medicine, University of Twente; Department of Head and Neck Surgery and Oncology, The Netherlands Cancer Institute, Antoni van Leeuwenhoek, Amsterdam, The Netherlands

TR T.J.M. Ruers, Department of Surgical Oncology, The Netherlands Cancer Institute, Antoni van Leeuwenhoek, Amsterdam, The Netherlands; Faculty of Science and Technology, University of Twente, Enschede, The Netherlands

WH W.H. Schreuder, Department of Head and Neck Surgery and Oncology, Verwelius 3D Lab, The Netherlands Cancer Institute, Antoni van Leeuwenhoek, Amsterdam, The Netherlands

WS W. Schats, Scientific Information Service, The Netherlands Cancer Institute, Antoni van Leeuwenhoek, Amsterdam, The Netherlands

Author contributions

Chapter 2

Assessment of the deep resection margin during oral cancer surgery: a systematic review

Study concepts and design | SB, AS, BK
Data acquisition | SB, AS, WS
Data analysis and interpretation | SB, AS
Manuscript preparation | SB, AS
Manuscript editing and review | SB, AS, WS, MB, TR, BK

Chapter 3

The oral cavity tumor thickness: measurement accuracy and consequences for tumor staging

Study concepts and design | SB, BK
Data acquisition | SB, CL
Data analysis and interpretation | SB, BK
Statistical analysis | SB
Manuscript preparation | SB
Manuscript editing and review | SB, BK, CL, TR

Chapter 4

Ultrasound aids in intra-operative deep resection margin assessment of squamous cell carcinoma of the tongue

Study concepts and design | SB, BK
Data acquisition | SB, BK, CL, WH, LK
Data analysis and interpretation | SB, BK
Statistical analysis | SB
Manuscript preparation | SB
Manuscript editing and review | SB, BK, CL, WH, LK, TR

Chapter 5

Toward complete oral cavity cancer resection using a handheld diffuse reflectance spectroscopy probe

Study concepts and design | SB, BK, TR
Data acquisition | SB, EB, LS
Data analysis and interpretation | SB, EB, BD
Manuscript preparation | SB, EB
Manuscript editing and review | SB, EB, BK, BD, LA, RD, BH, HS, TR

Chapter 6

Toward assessment of resection margins using hyperspectral diffuse reflection imaging (400-1,700 nm) during tongue cancer surgery

Study concepts and design | SB, BK, TR
Data acquisition | SB, EB, LS
Data analysis and interpretation | SB, PW, CS
Manuscript preparation | SB
Manuscript editing and review | SB, PW, BK, CS, EB, LS, RV, BH, HS, TR

Chapter 7

Evaluating the accuracy of resection planes in mandibular surgery using a preoperative, intraoperative and postoperative approach

Study concepts and design | SB, RV, BK
Data acquisition | SB, TB, LK, WH, BK
Data analysis and interpretation | SB, TB, FG, RV, MA
Manuscript preparation | SB, TB
Manuscript editing and review | SB, TB, FG, RV, MA, LK, WH, BK

Chapter 8

Accuracy of electromagnetic surgical navigation in patients undergoing mandibular surgery

Study concepts and design | SB, FG, JN, TR, BK
Data acquisition | SB, FG, LK, WH, BK
Data analysis and interpretation | SB, FG
Manuscript preparation | SB, FG
Manuscript editing and review | SB, FG, RV, MA, LK, JN, WH, TR, BK

Chapter 9

Utilization of a 3D printed dental splint for registration during electromagnetically navigated mandibular surgery

Study concepts and design | SB, JR, TB, MA, WH, BK, RV
Data acquisition | JR, TB
Data analysis and interpretation | SB, JR, TB, MA, RV
Manuscript preparation | SB, JR
Manuscript editing and review | SB, JR, TB, MA, FH, WH, LK, BK, RV

Chapter 10

A surgical navigated cutting guide for mandibular osteotomies: accuracy and reproducibility of an image-guided mandibular osteotomy

Study concepts and design | SB, TB, WH, BK, RV
Data acquisition | TB
Data analysis and interpretation | TB, SB, MA, WH, RV, BK
Manuscript preparation | TB, SB
Manuscript editing and review | TB, SB, MA, FH, WH, RV, BK

Scientific Portfolio

List of publications

Assessment of the deep resection margin during oral cancer surgery: a systematic review
S.G. Brouwer de Koning, A.W.M.A. Schaeffers, W. Schats, T.J.M. Ruers, M.B. Karakullukcu
Submitted for publication in European Journal of Surgical Oncology (March 2021)

Electromagnetic surgical navigation in patients undergoing mandibular surgery
S.G. Brouwer de Koning, F. Geldof, R.L.P. van Veen, M.J.A. van Alphen, L.H.E. Karssemakers, T.J.M. Ruers, J. Nijkamp, W.H. Schreuder, M.B. Karakullukcu
Scientific Reports (2021) https://doi.org/10.1038/s41598-021-84129-5

Utilization of a 3D printed dental splint for registration during electromagnetically navigated mandibular surgery
S.G. Brouwer de Koning, J.J.M. Riksen, T. P. ter Braak, M.J.A. van Alphen, F. Van der Heijden, M.B. Karakullukcu, R.L.P. van Veen
International Journal of Computer Assisted Radiology and Surgery (2020)
https://doi.org/10.1007/s11548-020-02271-3

Tongue tumor detection in hyperspectral images using deep learning semantic segmentation
S. Trajanovski, C. Shan, P.J.C. Weijtmans, **S.G. Brouwer de Koning**, T.J.M. Ruers
IEEE Transactions on Biomedical Engineering (2020) https://doi.org/10.1109/TBME.2020.3026683

A surgical navigated cutting guide for mandibular osteotomies: Accuracy and reproducibility of an image-guided mandibular osteotomy
T.P. ter Braak, **S.G. Brouwer de Koning**, M.J.A. van Alphen, F. Van der Heijden, W.H. Schreuder, R.L.P. Van Veen, M.B. Karakullukcu
International Journal of Computer Assisted Radiology and Surgery (2020)
https://doi.org/10.1007/s11548-020-02234-8

Evaluating the accuracy of resection planes in mandibular surgery using a preoperative, intraoperative and postoperative approach
S.G. Brouwer de Koning, T.P. ter Braak, F. Geldof, R.L.P. van Veen, M.J.A. van Alphen, L.H.E. Karssemakers, W.H. Schreuder, M.B. Karakullukcu
International Journal of Oral and Maxillofacial Surgery (2020) https://doi.org/10.1016/j.ijom.2020.06.013

Ultrasound aids in intra-operative deep resection margin assessment of squamous cell carcinoma of the tongue
S.G. Brouwer de Koning, M.B. Karakullukcu, C.A.H. Lange, W.H. Schreuder, L.H.E. Karssemakers, T.J.M. Ruers
British Journal of Oral & Maxillofacial Surgery (2020) https://doi.org/10.1016/j.bjoms.2019.11.013

Using diffuse reflectance spectroscopy to distinguish tumor tissue from fibrosis in rectal cancer patients as a guide to surgery
E.J.M. Baltussen, **S.G. Brouwer de Koning**, J. Sanders, A.G.J. Aalbers, N.F.M. Kok, G.L. Beets, B.H.W. Hendriks, H.J.C.M. Sterenborg, K.F.D. Kuhlmann, T.J.M. Ruers
Lasers in Surgery and Medicine (2019) https://doi.org/10.1002/lsm.23196

Comparing in vivo and ex vivo fiberoptic diffuse reflectance spectroscopy in colorectal cancer
E.J.M. Baltussen, **S.G. Brouwer de Koning**, B.H.W. Hendriks, K. Jozwiak, H.J.C.M. Sterenborg, T.J.M. Ruers
Translational Biophotonics (2019) https://doi.org/10.1002/tbio.201900008

Tissue diagnosis during colorectal cancer surgery using optical sensing: an in vivo study
E.J.M. Baltussen, **S.G. Brouwer de Koning**, J. Sanders, A.G.J. Aalbers, N.F.M. Kok, G.L. Beets, B.H.W. Hendriks, H.J.C.M. Sterenborg, K.F.D. Kuhlmann, T.J.M. Ruers
Journal of Translational Medicine (2019) https://doi.org/10.1186/s12967-019-2083-0

Toward assessment of resection margins using hyperspectral diffuse reflection imaging (400-1,700nm) during tongue cancer surgery
S.G. Brouwer de Koning, P.J.C. Weijtmans, M.B. Karakullukcu, C. Shan, E.J.M. Baltussen, L.A. Smit, R.L.P. van Veen, B.H.W. Hendriks, H.J.C.M. Sterenborg, T.J.M. Ruers
Lasers in Surgery and Medicine (2019) https://doi.org/10.1002/lsm.23161

The oral cavity tumor thickness: measurement accuracy and consequences for tumor staging
S.G. Brouwer de Koning, M.B. Karakullukcu, C.A.H. Lange, T.J.M. Ruers
European Journal of Surgical Oncology (2019) https://doi.org/10.1016/j.ejso.2019.06.005

Hyperspectral imaging for tissue classification, a way toward smart laparoscopic colorectal surgery
E.J.M. Baltussen, E.N.D. Kok, **S.G. Brouwer de Koning**, J. Sanders, A.G. J. Aalbers, N.F.M. Kok, G.L. Beets, C.C. Flohil, S.C. Bruin, K.F.D. Kuhlmann, H.J.C.M. Sterenborg, T.J.M. Ruers
Journal of Biomedical Optics (2019) https://doi.org/10.1117/1.JBO.24.1.016002

Automated tumor assessment of squamous cell carcinoma on tongue cancer patients with hyperspectral imaging
F. Manni, F. van der Sommen, S. Zinger, E. Kho, **S.G. Brouwer de Koning**, T.J.M. Ruers, C. Shan, J. Schleipen, P.H.N. de With
Proceedings Volume 10951, Medical Imaging: Image-Guided Procedures, Robotic Interventions, and Modeling (2019) https://doi.org/10.1117/12.2512238

Toward complete oral cavity cancer resection using a handheld diffuse reflectance spectroscopy probe
S.G. Brouwer de Koning, E.J.M. Baltussen, M.B. Karakullukcu, B. Dashtbozorg, L.A. Smit, R. Dirven, B.H.W. Hendriks, H.J.C.M. Sterenborg, T.J.M. Ruers
Journal of Biomedical Optics (2018) https://doi.org/10.1117/1.JBO.23.12.121611

Tumor Resection Margin Definitions in Breast-Conserving Surgery: Systematic Review and Meta-analysis of the Current Literature
S.G. Brouwer de Koning, M.T.F.D. Vrancken Peeters, K. Jozwiak, P.A. Bhairosing, T.J.M. Ruers
Clinical Breast Cancer (2018) https://doi.org/10.1016/j.clbc.2018.04.004

Optimal endobronchial tool sizes for targeting lung lesions based on 3D modeling
T.M. Bydlon, G.C. Langhout, F. Lalezari, K.J. Hartemink, J. Nijkamp, **S.G. Brouwer de Koning**, S. Burgers, B.H.W. Hendriks, T.J.M. Ruers
PLOSone (2017) https://doi.org/10.1371/journal.pone.0189963

Diffuse reflectance spectroscopy as a tool for real-time tissue assessment during colorectal cancer surgery
EJ.M. Baltussen, P. Snæbjörnsson, **S.G. Brouwer de Koning**, H.J.C.M. Sterenborg, A.G.J. Aalbers, N. Kok, G.L. Beets, B.H.W. Hendriks, K.F.D. Kuhlmann, T.J.M. Ruers
Journal of Biomedical Optics (2017) https://doi.org/10.1117/1.JBO.22.10.106014

Use of a handheld terahertz pulsed imaging device to differentiate benign and malignant breast tissue
M.R. Grootendorst, A.J. Fitzgerald, **S.G. Brouwer de Koning**, A. Santaolalla, A. Portieri, M. van Hemelrijck, M.R. Young, J. Owen, M. Cariati, M. Pepper, V.P. Wallace, S.E. Pinder, A. Purushotham
Biomedical Optics Express (2017) https://doi.org/10.1364/BOE.8.002932

Oral presentations

Clinical demands for intra-operative imaging in breast cancer
S.G. Brouwer de Koning
European Photonics Industry Consortium (EPIC), Meeting on Photonics for Cancer Diagnostics and Treatment, Amsterdam, The Netherlands, December 2019

Adjuvante behandeling tongcarcinoom mogelijk voorkomen door intra-operatieve echografische beoordeling van de resectiemarges
S.G. Brouwer de Koning, M.B. Karakullukcu, C.A.H. Lange, W.H. Schreuder, T.J.M. Ruers
234e Wetenschappelijke Vergadering van de Nederlandse Vereniging voor Keel-Neus-Oorheelkunde en Heelkunde van het Hoofd-Halsgebied, Nieuwegein, The Netherlands, April 2019

Near infrared hyperspectral imaging to evaluate tongue tumor resection margins intraoperatively
S.G. Brouwer de Koning, M.B. Karakullukcu, L.Smit, E.J.M. Baltussen, H.J.C.M. Sterenborg, T.J.M. Ruers
SPIE Photonics West, San Francisco, USA, January 2018 https://doi.org/10.1117/12.2289166

Diffuse reflectance spectroscopy to discriminate tumor from healthy tongue tissue
S.G. Brouwer de Koning, E.J.M. Baltussen, M.B. Karakullukcu, L. Smit, R.L.P. van Veen, B.H.W. Hendriks, H.J.C.M. Sterenborg, T.J.M. Ruers
SPIE Photonics West, San Francisco, USA, January 2018

Using diffuse reflectance for tumor margin assessment in head and neck surgery
S.G. Brouwer de Koning, E.J.M. Baltussen, L. Smit, R.L.P. van Veen, B.H.W. Hendriks, H.J.C.M. Sterenborg, M.B. Karakullukcu, T.J.M. Ruers
European Photonics Industry Consortium (EPIC), Meeting Towards *in vivo* imaging, Amsterdam, The Netherlands, December 2017

Diffuse reflectance spectroscopy from 400-1600 nm to evaluate tumor resection margins during head and neck surgery
S.G. Brouwer de Koning, E.J.M. Baltussen, M.B. Karakullukcu, L. Smit, R.L.P. van Veen, B.H.W. Hendriks, H.J.C.M. Sterenborg, T.J.M. Ruers
SPIE Photonics West, San Francisco, USA, January 2017 https://doi.org/10.1117/12.2251460

Terahertz pulsed imaging to differentiate benign and malignant breast tissue
S.G. Brouwer de Koning, M.R. Grootendorst, A.J. Fitzgerald, A. Portieri, A. Santaolalla, M. Cariati, M. Pepper, V.P. Wallace, S.E. Pinder, A. Purushotham
The Royal College of Surgeons of England, The Society of Academic and Research Surgery Annual Meeting, London, UK, January 2016

Poster presentations

3D technology at the department of Head and Neck Surgery & Oncology – 3D visualization, planning and guidance of surgical interventions to improve surgical outcome and quality of surgery
S.G. Brouwer de Koning, T.P. ter Braak, J.T. Ubbink, N.P.M. Wassenaar, M.J.A. van Alphen, R.L.P. van Veen, F. Van der Heijden, J. Nijkamp, T.J.M. Ruers, L.H.E. Karssemakers, W.H. Schreuder, M.B. Karakullukcu
14th International Netherlands Cancer Institute Head & Neck Cancer Symposium, Amsterdam, The Netherlands, April 2019

Towards intra-operative resection margin assessment using near infrared hyperspectral imaging in squamous cell carcinoma of the tongue (award winning poster, poster pitch)
S.G. Brouwer de Koning, M.B. Karakullukcu, L. Smit, E.J.M. Baltussen, H.J.C.M. Sterenborg, T.J.M. Ruers
ESSO European Society of Surgical Oncology, Budapest, Hungary, October 2018

Terahertz pulsed imaging to evaluate tumour margins during breast-conserving surgery (poster pitch)
S.G. Brouwer de Koning, M.R. Grootendorst, A.J. Fitzgerald, A. Santaolalla, A.C.C. Coolen, A. Portieri, M. Cariati, M. Pepper, V.P. Wallace, S.E. Pinder, A. Purushotham
NVvTG Nederlandse Vereniging voor Technische Geneeskunde, Amsterdam, The Netherlands, January 2016

Supervision of students

Surgical navigation to guide tumor resections in oncological head and neck surgery
F. Geldof, Master student Technical Medicine (12-month graduation internship)

Real-time tissue classification during oncological surgery
S. Romeijn, Master student Technical Medicine (12-month graduation internship)

Courses

Basiscursus Regelgeving en Organisatie voor Klinisch onderzoekers (eBROK)
VUmc Academie, Amsterdam, The Netherlands, January 2021

The Medical Image Computing Summer School (MedICSS)
University College London (UCL), London, UK, June 2018

iQ Winterschool on Machine Learning Applied to Quantitative Analysis of Medical Images
Institute QuantiVision, Noordwijk, The Netherlands, March 2018

Chirurgenweek Antoni van Leeuwenhoek
De Nederlandse Vereniging voor Heelkunde, Amsterdam, The Netherlands, February 2018

Basic Medical Statistics
Antoni van Leeuwenhoek Academy, Oncology Graduate School Amsterdam, Amsterdam, The Netherlands, November 2017

Taste of Teaching bootcamp
University of Twente, Enschede, The Netherlands, May 2017

Machine Learning for Medical Applications
University of Twente, Enschede, The Netherlands, August 2016

Good Clinical Practice (GCP)
Antoni van Leeuwenhoek, Amsterdam, The Netherlands, July 2016, updated July 2019

About the author

Susan G. Brouwer de Koning was born in Gouda, The Netherlands, on February 17, 1991. During high school, she researched the variables affecting the distance travelled by a deflating balloon (with an extensive research proposal including a solution for the main challenge in this study: how to ensure that the balloon travels in a straight line). With mathematics as her favourite course, she explored fractals, of which the Pythagoras tree is the most well-known. Due to these interests in physics and mathematics, together with the wish to study medicine, she entered the Bachelor and Master programs of Technical Medicine at the University of Twente. During the first internship of the master program, the knowledge on the Pythagoras tree appeared to be very useful and served as a mathematical model to estimate the distance between the smallest branches of the bronchial tree. She graduated with distinction from the master track 'Medical imaging and interventions' after spending a year in London, UK, for her graduation project at the Research Oncology (Breast Cancer) department of Guy's and St Thomas' hospital in association with King's College London.

Due to her interest in intra-operative imaging technologies, she began working at the Netherlands Cancer Institute, Antoni van Leeuwenhoek, as a PhD student and as a member of the Clinical Implementation Team of the operation room. To be more involved with the patient rather than a role solely as a researcher, she entered the 'Zij-instroomprogramma Geneeskunde', a graduate entry program in medicine with a strong focus on research, at the VU University, Amsterdam, during the last years of her PhD. She finished the premaster of this program in July 2020 and is planning to start her clinical rotations in 2021.

With the combination of courses in both Technical Medicine and Medicine, together with a very enthusiastic, open, friendly but critical attitude, Susan hopes to add a unique contribution to our health care!

Nawoord

Op het scherp van de snede

Bij de behandeling van kanker valt op te merken dat niet of vrijwel niet kan worden vertrouwd op een inwendige remedie, en dat de enige handelswijze bestaat uit volledige verwijdering van het aangetaste lichaamsdeel. – a Dictionary of Practical Surgery, 1836

Over een marge van gezond weefsel gesproken. Nu bijna 200 jaar later, hebben we het over millimeters weefsel in plaats van hele lichaamsdelen die verwijderd worden om er zeker van te zijn dat de tumor in zijn geheel verwijderd is.

Gedurende mijn eerste stage in het Antoni van Leeuwenhoek ziekenhuis kreeg ik van professor Ruers het boek '*De Keizer aller Ziektes*', geschreven door Siddhartha Mukherjee. Dit boek beschrijft de ontdekkingen die gedaan zijn over kanker, maar ook alle overwinningen die door arts-onderzoekers en wetenschappers zijn geboekt, dankzij een enorme dosis aan vindingrijkheid, veerkracht en doorzettingsvermogen. Het fundament van kennis waarop ons huidige handelen is gebaseerd, en wat zo mooi uiteengezet is door Mukherjee in zijn boek, biedt ons vertrouwen om deze specifieke patiënt naar ons beste weten te kunnen behandelen.

We weten dus al heel veel, als we alleen al naar de dikte van dat boek kijken en heel PubMed nog achterwege laten. Maar '*de ware wijze onder u is degene die weet dat hij niet weet*' (*Socrates*). Alle kennis is beperkt. En het probleem is dat we niet weten *wat* we niet weten, en ook niet *hoeveel* we niet weten (*Steenbergen*). En dus duik je als onderzoeker in een onderwerp, wil je alles weten wat er tot nu toe over bekend is, en ga je met die basis verder, op zoek naar nieuwe inzichten. Je gaat tot het uiterste, met maximale inzet, je werkt op het scherp van de snede. Die drie bovenstaande ingrediënten van vindingrijkheid, veerkracht en doorzettingsvermogen zijn daarvoor onmisbaar. Alles loopt in het onderzoek altijd anders dan verwacht (zoals verwacht). En als we ons niet aan die veranderingen kunnen aanpassen 'overleven' we het niet, dat heeft Darwin al lang geleden voor ons uitgezocht. De kunst als onderzoeker is om ervoor te waken je enthousiasme niet te verliezen.

Met dit proefschrift heb ik getracht een bijdrage te kunnen leveren aan het vergroten van de kennis van wat we *wel* weten. Maar de waarde van kennis is ook beperkt. Kennis moet in praktijk gebracht worden door handen van professionals. Een sterke samenwerking tussen de zorg en het onderzoek is daarvoor een vereiste.

En juist dit is mogelijk in het Antoni van Leeuwenhoek ziekenhuis,
waar medisch wetenschappelijk onderzoek in de klinische praktijk kan worden gebracht;
waar initiatieven als een klinisch implementatie team op het operatiekamercomplex en waar een 3D lab kunnen worden gerealiseerd;
en waar *cutting-edge* technologie ook toegankelijk kan worden gemaakt voor de kleinere patiëntenpopulatie, welke misschien in eerste instantie minder kosteneffectief leek;
waar je deel uitmaakt van een team met zoveel kennis, maar ook zoveel goede mensen;
en het belangrijkste, waar patiënten aan onderzoek mee durven doen. Daar is echt moed voor nodig en een sterk vertrouwen in het medisch- en onderzoeksteam.

ISBN 978-90-365-5130-4